Model-based design of optimal chemical reactors

Dissertation
zur Erlangung des akademischen Grades

Doktor-Ingenieur
(Dr.-Ing.)

von: Dipl.-Ing. Andreas Peschel
geb. am: 17. August 1982
in: Braunschweig

genehmigt durch die Fakultät für Verfahrens- und Systemtechnik
der Otto-von-Guericke-Universität Magdeburg

Gutachter: Prof. Dr.-Ing. Kai Sundmacher
Prof. Dr.-Ing. Hannsjörg Freund
Prof. Dr.-Ing. Günter Wozny

eingereicht am: 10. Januar 2012
Promotionskolloquium am: 27. März 2012

Forschungsberichte aus dem Max-Planck-Institut
für Dynamik komplexer technischer Systeme

Band 34

Andreas Peschel

Model-based design of optimal chemical reactors

Shaker Verlag
Aachen 2012

Bibliographic information published by the Deutsche Nationalbibliothek
The Deutsche Nationalbibliothek lists this publication in the Deutsche Nationalbibliografie; detailed bibliographic data are available in the Internet at http://dnb.d-nb.de.

Zugl.: Magdeburg, Univ., Diss., 2012

Printed in Germany.

ISBN 978-3-8440-1108-1
ISSN 1439-4804

Shaker Verlag GmbH • P.O. BOX 101818 • D-52018 Aachen
Phone: 0049/2407/9596-0 • Telefax: 0049/2407/9596-9
Internet: www.shaker.de • e-mail: info@shaker.de

Kurzzusammenfassung

Da der Reaktor den Kern vieler chemischer Prozesse darstellt, liegt ein großes Potential für die Verbesserung der Energie- und Rohstoffeffizienz heutiger chemischer Prozesse im Design optimaler chemischer Reaktoren. Um einen Durchbruch in der Reaktionstechnik zu erlangen und die Grenzen bestehender Apparate zu überwinden, müssen Aspekte der Prozessintensivierung (PI) in den Reaktorentwurf Eingang finden. Daher ist es Ziel der vorliegenden Arbeit, eine neue modellbasierte Entwurfsmethodik zu entwickeln, die Ansätze der PI berücksichtigt und es ermöglicht, innovative chemische Reaktoren zu entwerfen.

Im ersten Teil der Arbeit werden die erforderlichen theoretischen Grundlagen erläutert und die generelle Entwurfsmethodik skizziert. Basierend auf dem Konzept der elementaren Prozessfunktionen wird ein Fluidelement auf seinem Weg durch den Prozess bilanziert und durch optimale Flussprofile so manipuliert, dass zu jedem Zeitpunkt die optimalen Reaktionsbedingungen vorliegen. Davon ausgehend wird eine dreistufige Methode zum Entwurf optimaler Reaktoren entwickelt. Auf dem ersten Level wird die Apparate-unabhängige optimale Route im thermodynamischen Zustandsraum berechnet, indem die optimalen Flussprofile ermittelt werden. Auf dem zweiten Level wird untersucht, ob und wie diese Flüsse realisierbar sind. Dazu wird das beste prinzipielle Reaktorkonzept einschließlich der Katalysatorträgergeometrie, der Austauschflächen und der Steuervariablen für die Flüsse identifiziert. Auf dem dritten Level wird eine technische Approximation der optimalen Reaktionsroute abgeleitet und so ein optimaler technischer Reaktor entworfen. Die Methodik basiert hierbei auf Bilanzgleichungen, Thermodynamik und Reaktionskinetiken, wobei das Potential von PI-Maßnahmen durch die Modellierung der zugrunde liegenden physikalisch-chemischen Zusammenhänge untersucht wird.

Im zweiten Teil werden verschiedene, industriell bedeutsame Prozesse mit ansteigender Komplexität behandelt. Die Anwendbarkeit der Methode wird anhand der SO_2-Oxidation, der Luft- und Sauerstoff-basierten Ethylenoxid-Synthese (EO) und der Hydroformylierung langkettiger Alkene gezeigt. Für die SO_2-Oxidation wird ein neuer Reaktor mit einer 69% geringeren Verweilzeit entwickelt. Dieses Beispiel unterstreicht das große Potential der Methode und kann qualitativ auf weitere exotherme Gleichgewichtsreaktionen übertragen werden. Für den Luft-basierten EO-Prozess wurden verschiedene Dosierungs- und Abzugsstrategien untersucht und dabei das Screening unterschiedlichster Reaktionskonzepte mit der Methode verdeutlicht. Die Nichtidealitäten im Konzentrations-, Temperatur- und im Strömungsfeld des entwickelten Reaktors wurden mit einem zweidimensionalen Reaktormodell untersucht. Für den Sauerstoff-basierten EO-Prozess wurde das beste Reaktionskonzept für die Gesamtanlage ermittelt. Bezüglich der kritischen Modellannahmen wurde eine Sensitivitätsstudie mit Blick auf die Robustheit des ermittelten Reaktionskonzeptes durchgeführt. An Hand der Hydroformylierung wurde die Methodik auf Mehrphasensysteme erweitert. Hier wurde ein innovatives Reaktorkonzept mit statischen Mischern, Kühlung und verteilter Dosierung von Alken und Synthesegas entwickelt – mit einer Selektivitätssteigerung von 9.1% gegenüber dem optimierten Referenzfall.

Die entwickelte Methodik ermöglicht den Entwurf optimaler chemischer Reaktoren und liefert dadurch einen ersten Schritt auf den Weg zu verbesserten chemischen Prozessen der nächsten Generation. Die Anwendbarkeit und das Potential der Methode wurden dabei an drei industriellen Prozessen aufgezeigt.

Abstract

The core of most chemical processes is the reactor, and therefore optimal reactor design has a large potential to enhance the energy and raw material efficiency of today's chemical processes. In order to make breakthroughs in chemical reactor technology and to overcome the limitations of existing reactors, process intensification (PI) needs to be applied systematically in the reactor design task. Hence, the scope of this thesis is to create a model-based design methodology which includes PI options and enables the design of innovative tailor-made reactors.

In the first part of this work, the fundamentals for the reactor design task are provided and the design framework is explained. The general idea of the design method is based on the conceptual framework of elementary process functions; a fluid element is tracked on its way through the reactor and manipulated by optimal flux profiles to obtain the best reaction conditions over the entire residence time. In order to resolve the complex reactor design task, a three step methodology is developed. On the first level, the optimal heat and mass flux profiles, which provide the best route in the thermodynamic state space, are determined independent of existing apparatuses. On the second level, it is investigated if the desired flux profiles are attainable. For this purpose, the best principle reactor set-up including the catalyst support, the exchange areas and the control variables which can be manipulated by the reactor design are identified. On the third level, a technical approximation of the best reaction route is developed giving rise to superior chemical reactors. The approach is rigorously based on the equations of change, thermodynamic relationships, and the reaction kinetics including PI options by modeling their physico-chemical effects.

In the second part of this thesis, several industrially important examples of increasing complexity are considered. The SO_2 oxidation, the air and oxygen based ethylene oxide (EO) process, and the hydroformylation of long chain linear alkenes are investigated demonstrating the wide applicability of the method. For the SO_2 oxidation, a new reactor design is proposed based on the optimal heat flux profile reducing the residence time in the reactor by 69% compared to an optimized reference case. This result illustrates the large potential of realizing the optimal reaction route and is an example for exothermic equilibrium reactions. For the air based EO process several dosing and removal concepts were investigated showing the potential of the method for screening complex reaction concepts. In addition, the derived reactor is investigated in detail using a two-dimensional reactor model taking non-idealities in the flow, temperature, and concentration field into account. For the oxygen based EO process the overall process is modeled and simultaneously optimized giving rise to the best reaction concept from the overall process point of view. Furthermore, a sensitivity analysis for the critical model assumptions is performed investigating the robustness of the derived optimal reaction concept. For the hydroformylation of long chain linear alkenes the design approach is extended for the design of optimal multiphase reactors. Here, an innovative reactor design including static mixers, advanced cooling, and distributed dosing of alkene and synthesis gas is developed giving rise to a selectivity increase of 9.1% based on an optimized reference case.

In summary, the developed reactor design methodology enables the design of optimal tailor-made chemical reactors, which is a first step on the way to more economical, greener, and more sustainable chemical processes. The potential of the method is exemplified on three industrially important processes.

Preface

The work presented within this thesis was conducted during my time as scientific employee at the Max Planck Institute for Dynamics of Complex Technical Systems and Ph.D. student within the International Max Planck Research School in Magdeburg from November 2007 until March 2012.

My special thanks is directed to Prof. Dr.-Ing. Kai Sundmacher (Max Planck Institute for Dynamics of Complex Technical Systems and Otto-von-Guericke University Magdeburg) for the interesting and challenging topic as well as for the granted trust and scientific freedom. I am very grateful for the supervision, the support, and the possibility to participate at numerous national and international conferences. In addition, special thanks go to Prof. Dr.-Ing. Hannsjörg Freund (Friedrich-Alexander University Erlangen-Nuremberg) for the supervision, the fruitful discussions, and your advice. Additional thanks I owe to Prof. Dr.-Ing. Wozny (Technical University Berlin) for reviewing and evaluating my thesis as external referee.

In completing this work I have benefited from the help of many students which conducted their study research and/or diploma thesis within my supervision, namely Dipl.-Ing. Fabian Futh, Dipl.-Ing. Nadine Novotny, Dipl.-Ing. Florian Karst, Dipl.-Ing. Frank Päßler, and Dipl.-Ing. Andreas Jörke. I like to thank all of you for your good work and like to say that it was a pleasure to work with you.

I greatly value the time I could spend with my colleagues and friends from the Max Planck Institute and the Process Systems Engineering group at the Otto-von-Guericke University Magdeburg, in particular to Dr.-Ing. Peter Heidebrecht, Dr.-Ing. Richard Hanke-Rauschenbach, Dr.-Ing. Sascha Rollié, Dr. rer. nat. Andreas Voigt, Dipl.-Ing. Christian Borchert, Dipl.-Ing. Michael Fricke, and Dipl.-Phys. Robert Flassig. I also like to thank Dipl.-Ing. Kevin McBride and M.Sc. Ali El-Sibai for the help in finishing this thesis. Furthermore, I owe special thanks to my colleagues Dipl.-Ing. Benjamin Hentschel and Dipl.-Ing. Florian Karst for the excellent teamwork within the SFB/Transregio 63 on "Integrated Chemical Processes in Liquid Multiphase Systems" (InPROMPT) and the ethylene oxide project, respectively, as well as for their help on the home straight of this thesis.

I also gratefully acknowledge the discussion with Dr. R. Benfer, Dr. C. Großmann, and Dr. G. Theis (all BASF SE, Ludwigshafen, Germany) within the ethylene oxide project.

Finally, I am truly grateful for the support and encouragement of my parents, my brother, and dear friends throughout the course of the thesis. Although the last, but not least I like to thank Britta simply for your encouragement, love, and presence in my life.

Andreas Peschel Magdeburg, March 2012

Contents

List of symbols

Symbols that are only of local interest are explained on the spot and are not included in the list of symbols. The meaning of all ambivalent symbols can be concluded from the context. The units are stated as used in all equations. In case different units are used for better readability in tables and figures, these units are given in the according table or figure.

Latin symbols

A	Cross sectional area	$\left[m^2\right]$
a	Specific exchange area for flux	$\left[\frac{m^2}{m^3}\right]$
C	Concentration, or relative costs	$\left[\frac{mol}{m^3}\right]$, $\left[\frac{\$}{mol}\right]$, $\left[\frac{\$}{J}\right]$, $\left[\frac{\$}{s}\right]$
c_p	Heat capacity	$\left[\frac{J}{mol \cdot K}\right]$
D	Diameter, or diffusion coefficient	$[m]$, $\left[\frac{m^2}{s}\right]$
E_A	Activation energy	$\left[\frac{J}{mol}\right]$
GHSV	Gaseous hourly space velocity	$\left[h^{-1}\right]$
h	Specific enthalpy	$\left[\frac{J}{mol}\right]$
H	Henry coefficient	$[Pa]$, $\left[\frac{Pa \cdot m^3}{mol}\right]$
j	Molar flux	$\left[\frac{mol}{m^2 s}\right]$
j_{tot}	Molar flux into/out of fluid element	$\left[\frac{mol}{s}\right]$
k	Effective heat transfer coefficient	$\left[\frac{W}{m^2 \cdot K}\right]$
k_j	Reaction rate constant	various
K	Equilibrium constant, or adsorption constant, or heat capacity flow rate	various, $\left[\frac{m \cdot K}{W}\right]$
$(k_L a)$	Product of mass transfer coefficient and specific exchange area based on total reactor volume (no index) or on liquid phase volume (liq)	$\left[s^{-1}\right]$
L	Reactor length	$[m]$
$\dot{m}$	Mass flow	$\left[\frac{kg}{s}\right]$
m	Molality	$\left[\frac{mol_i}{kg_{solvent}}\right]$
M	Molecular weight	$\left[\frac{kg}{mol}\right]$
n	Molar amount in fluid element, or reaction order	$[mol]$, $[-]$

Latin symbols (continued)

$\dot{n}$	Mole flow	$\left[\frac{mol}{s}\right]$
p	Pressure	$[Pa]$
P	Power	$[W]$
Per	Permeance	$\left[\frac{mol}{Pa \cdot m^2 \cdot s}\right]$
q	Heat flux	$\left[\frac{W}{m^2}\right]$
q_{tot}	Total heat flux into/out of fluid element	$[W]$
$\dot{Q}$	Heat duty (of a process unit)	$[W]$
R	Radius, or gas constant	$[m]$, $\left[\frac{J}{mol \cdot K}\right]$
r	Reaction rate, or radial coordinate	$\left[\frac{mol}{m^3_{IL} \cdot s}\right]$, $\left[\frac{mol}{kg_{cat} \cdot s}\right]$, $[m]$
s	Selection variable	$[-]$
S	Selectivity	$[-]$
STY	Space time yield	$\left[\frac{mol}{m^3 s}\right]$
T	Temperature	$[K]$
t	Residence time	$[s]$
v_s	Superficial velocity of gas or liquid	$\left[\frac{m}{s}\right]$
v_i	Interstitial velocity	$\left[\frac{m}{s}\right]$
V	Volume	$[m^3]$
w	Mass fraction	$[-]$
x	Mole fraction (in case of hydroformylation: liquid phase)	$[-]$
X	Conversion	$[-]$
y	Mole fraction (in case of hydroformylation: gas phase, else: phase composition)	$[-]$
z	Axial coordinate	$[m]$

Greek symbols

α	Heat transfer coefficient	$\left[\frac{W}{m^2 K}\right]$
β	Mass transfer coefficient	$\left[\frac{m}{s}\right]$
Δh_r	Enthalpy of reaction	$\left[\frac{J}{mol}\right]$
ϵ	Phase fraction, or catalyst void fraction	$[-]$
λ	Thermal conductivity	$\left[\frac{W}{m \cdot K}\right]$
Λ	Effective thermal conductivity	$\left[\frac{W}{m \cdot K}\right]$
μ	Dynamic viscosity	$\left[\frac{kg}{m \cdot s}\right]$
ν	Stoichiometric coefficient	$[-]$
ρ	Density	$\left[\frac{kg}{m^3}\right]$
τ	Total residence time	$[s]$
Θ	Temperature	$[^\circ C]$
ξ	Split fraction	$[-]$

Dimensionless numbers

Da	Damköhler number	[−]
Nu	Nusselt number	[−]
Pe	Péclet number	[−]
Pr	Prandtl number	[−]
Re	Reynolds number	[−]

Sets

COM	Set of components (gas + liquid)
COMG	Set of gas components
COML	Set of liquid components
CP	Set of collocation points
DIS	Set of distributors
FE	Set of finite elements
FG	Set of flammable gases
ISC	Intermediate species in CO_2 absorption reactions
PH	Set of phases
RE	Set of reactions
STR	Set of streams with CO_2 absorption equilibrium

Subscripts

ads	Adsorption
bed	Catalyst bed
c	Coolant phase or coolant side
cat	Catalyst
d	Dosing points
e	Environmental phase
ef	Effective
eq	Equilibrium
f	Final/outlet value
i	Component index, or inner boundary
IL	Ionic liquid phase
j	Reaction index
g	Gas phase
k	Phase index
liq	Total liquid phase
m	Molecular
M	Service phase on other side of membrane/membrane side
o	Outer boundary
org	Organic phase
p	Catalyst particle
ref	Reference value

Subscripts (continued)

rel	Relative value/scaled variable
s	Surface conditions, solid phase, or segment index
0	Inlet value

Superscripts

L	Lower boundary value
s	Saturation value
U	Upper boundary value

Abbreviations

AR	Attainable region
C	Column
Cond	Condenser
CP	Compressor
CSTR	Continuous stirred tank reactor
CW	Cooling water
DAE	Differential algebraic equation
DoF	Degree of freedom
DOP	Dynamic optimization problem
DSR	Differential side stream reactor
El	Electricity
EPF	Elementary process functions
H	Heat exchanger
IL	Ionic liquid
KKT	Karush-Kuhn-Tucker
LEL	Lower explosion limit
LPS	Low pressure steam
M	Mixer
MINLP	Mixed integer nonlinear programming
NLP	Nonlinear programming
ODE	Ordinary differential equation
P	Pump
PFTR	Plug flow tubular reactor
PI	Process intensification
PDE	Partial differential equation
PSE	Process systems engineering
R	Reactor
Reb	Reboiler
S	Splitter
UEL	Upper explosion limit
UOP	Unit operation
V	Valve

Components

SO_2 oxidation	
SO_2	Sulfur dioxide
SO_3	Sulfur trioxide
O_2	Oxygen
N_2	Nitrogen
Ethylene oxide synthesis	
E	Ethylene
O_2	Oxygen
EO	Ethylene oxide
H_2O	Water
N_2	Nitrogen
Ar	Argon (used as pseudo inert component)
CO_2	Carbon dioxide
CH_4	Methane
Hydroformylation	
tAlk	1-Octene
inAlk	2-Octene
nAld	n-Nonanal
isoAld	iso-Nonanal
nAlc	n-Nonanol
isoAlc	iso-Nonanol
Dec	Decane
IL	[Bmim][PF_6]
syngas	Synthesis gas with composition $H_2 : CO = 1$

Part I

Fundamentals

Chapter 1
Introduction

Motivation and scope

Improving the reactor of a chemical process offers large potential for reducing the energy and raw material consumption since reactors constitute the core of most chemical processes. Thereby, the economics of the process can be improved and these processes become greener and more sustainable at the same time.

In order to obtain drastic improvements for existing processes, innovative process intensification (PI) options need be be considered in the reactor design task. So far, process intensification was mainly driven by examples whereas model-based design methodologies for reactors including innovative Pi concepts are still missing. However, a design method rigorously based on the physical and chemical insights is necessary for the reactor design due to the strong nonlinear effects arising from the reaction kinetics, complex reaction networks, and the interplay between the reactor and the process which cannot be handled using heuristic approaches. In addition, the well established concept of unit operations (UOPs) is not suited to include all PI approaches since it is limited to existing apparatuses. Thereby, the design space is limited a priori and detailed physical and chemical insights can hardly be included into the reactor design.

Here, the elementary process functions (EPF) framework developed by Freund and Sundmacher [1–6] gives rise to a new perspective on the design of efficient chemical processes. Within this concept, each chemical process can be considered as a travel route of a fluid element from an initial point to a final point within the thermodynamic state space. The optimal route is obtained by tracking this fluid element and manipulating the fluxes into and out of this element in such a way that a certain objective is optimized. In order to overcome the limitations of existing apparatuses, Freund and Sundmacher [1] proposed the decomposition of the process into functional modules. The purpose of a functional module is to realize a specific task, and the functional module itself is not initially associated with a specific apparatus.

The scope of this thesis is to create a design methodology for optimal chemical reactors based on the conceptual framework of the EPF. This method is rigorously based on the equations of change, thermodynamic relationships, and the reaction kinetics of a system. Within this design method, fruitful combinations of phenomena are identified and a deep understanding of the physical and chemical insights of the reactor design tasks is gained. Process intensification options are systematically included, and innovative tailor-made reactors are derived. The method is illustrated on technically important processes to validate its applicability and illustrate its potential.

Content and structure of the thesis

The thesis is divided into two main parts. Part one deals with the fundamentals of process intensification and process systems engineering (PSE), which are necessary to understand the developed methodology. In addition, the general methodological approach is explained. In the second part of the thesis, several industrially important processes are considered.

In Chapter 2, the fundamental basis for the derived reactor design approach is explained. This includes a review on the elementary process functions framework and systematic treatment of process intensification approaches in Section 2.1. In addition, established reactor selection and design approaches are discussed in Section 2.3. At the end of Chapter 2, the requirements for a new design method are derived.

In Chapter 3, the design method is explained in detail. First, the scope of the method is defined by placing the method within the elementary process functions framework and by deriving the challenges and tasks for a new design method. Afterwards, the main idea of the method is illustrated, followed by a detailed explanation of the design levels and of the sequential order of the design approach. At the end of Chapter 3, the method is compared to the existing design approaches and its unique features are highlighted.

The design method explained in Chapter 3 constitutes the methodological background for the investigated process examples and thereby it is the theoretical basis of the thesis. The examples are the litmus test for the method and proof the practical value. The considered processes are all of large industrial importance and were chosen in such a way that the most important classes of chemical reactions are covered. The aspects of the method illustrated by the individual examples are explained at the beginning of the second part.

In this thesis, the SO_2 oxidation, the ethylene oxide synthesis, and the hydroformylation of long chain linear alkenes are investigated as examples. Each of these processes is discussed in an individual chapter from the SO_2 oxidation in Chapter 4 to the hydroformylation in Chapter 6. These examples clarify the application of the method and give details on the modeling and the sequential order of the decisions which need to be taken. In addition, they clearly show the potential of the method and motivate its further application. All of these examples are of major industrial importance and require a high modeling effort due to their complexity. In addition, problems of data availability arising from real world examples need to be handled within the design method.

In Chapter 7, the results are summarized, an outlook on how the method can be extended is given, and a conclusion is drawn.

Chapter 2
Background

This chapter deals with the systematic treatment of process intensification options and established reactor design methods. It is intended to provide the reader with the required basic knowledge to understand the proposed design approach in Chapter 3. The numerical solution approach which is used to solve the arising optimization problems is explained in Appendix A.4, after the optimization problems are introduced in the examples. In addition, further required basics in the field of chemical reaction engineering are introduced on the spot whenever required.

In general, process intensification can be regarded as drastic enhancement of the existing process and as the design of new processes yielding major improvement. In this context, PI is often described using striking, but vague phrases such as "cheaper, smaller, cleaner". Here, Ramshaw's concept of higee can be regarded as first example of PI in a modern sense [7]. So far, PI was mostly driven by examples and the systematization of PI as well as the model-based approach to PI are quite new research fields.

The elementary process functions framework is one of the recently published concepts considering both aspects. In addition to process intensification approaches for the reactor design task, also reactor design methods were developed in the field of process systems engineering. In order to capture all aspects of PI and PSE regarding the reactor design, this chapter is partitioned into four sections.

In Section 2.1, the elementary process functions framework is illustrated. Afterwards, alternative classifications of PI options and a systematic framework for PI are discussed in Section 2.2. In Section 2.3, established reactor design methods developed in the process systems engineering community are illustrated. Based on these fundamentals, the scope of the design methodology proposed in this thesis is defined in Section 3.1.2. Here, the method is placed within the EPF framework and the requirements for the design of optimal chemical reactors are defined.

2.1 The elementary process functions framework

In this section, the general idea of the elementary process functions approach and the systematic treatment of PI approaches within this framework is illustrated. The EPF concept is based on the equations of change and thereby it is a rigorous model-based approach. It is intended to design better processes in a systematic manner by gaining physical and chemical insights on how to improve the process and how to shift

existing technological limits. The general idea of the elementary process functions framework consists of three main aspects, which are:

1. Obtain the optimal route of a fluid element by using tailor-made functional modules instead of pre-defined unit operations.
2. Decomposition of chemical processes into different levels reaching from the molecular level to the plant level.
3. Systematic classification of the possibilities of manipulating the process route.

These aspects will be covered individually in Section 2.1.1 – Section 2.1.3. In the next sections, the terms *optimal route*, *functional module*, *unit operation*, *reaction concept*, *reactor*, and *service phase* will be defined.

2.1.1 Optimal route of a fluid element

Each chemical process can be considered as a travel route of fluid elements from an initial point to a final point within the thermodynamic state space. The *optimal route* can be obtained by tracking such a fluid element and manipulating the internal and external fluxes in such a way that a certain objective is optimized. This objective might be minimum residence time of the fluid element in the process or an optimal path with respect to minimal energy or raw material consumption.

In general, the optimal route can only be obtained if the fluxes are optimized along the entire residence time giving rise to a dynamic optimization problem. This dynamic adaption of the fluxes (Lagrangian tracking of the fluid element) cannot be realized with conventional apparatuses. Pre-defined apparatuses can only manipulate the fluid element within certain technical limits giving rise to suboptimal solutions.

In order to overcome the limitations of existing apparatuses, Freund and Sundmacher [1] proposed to divide the process into *functional modules*. The purpose of a functional module is to realize a specific task, and the functional module itself is not associated with an apparatus at the beginning. This constitutes the main difference to the *unit operation* approach, where the operations are associated with pre-defined apparatuses.

Most processes consist of functional modules for preprocessing, contacting, activation, reaction, heat management, separation, and product formulation. In each functional module different fluxes such as the heat and reaction flux can be integrated depending on the purpose of the module. In addition, some of these modules can be integrated as it is done, for example, in reactive distillation. Therefore, Fig. 2.1 presents only one possible process design in terms of functional modules.

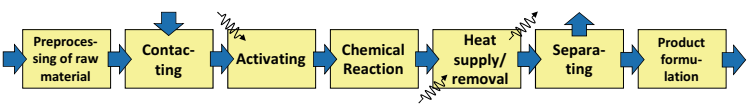

Figure 2.1: Representation of a process in functional modules (reprinted with permission from Elsevier [1])

Within the functional module *chemical reaction*, the *reaction concept* defines which fluxes are integrated and manipulated. The reaction concept is not yet the *reactor*, which is the concrete apparatus. In many cases, a reaction concept might be realized by several reactors. However, for some reaction concepts no reactor exists which puts the reaction concept into practice.

In each module a dynamic optimization problem is solved. For this optimization, a certain set of fluxes is adapted in an optimal manner along the path of the fluid element as illustrated in Fig. 2.2. The inlet and outlet conditions of individual modules are connected according to the flowsheet, and within the functional modules the evolution of the states are subject to the equations of change, thermodynamic state equations, and kinetic expressions.

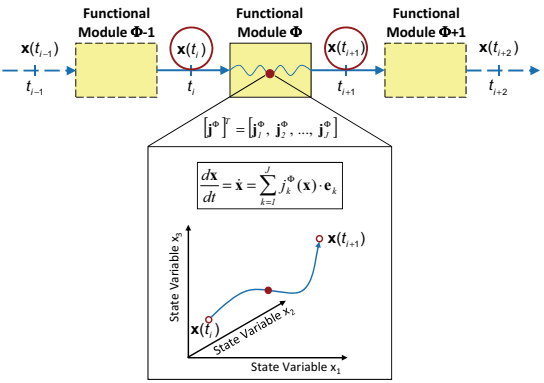

Figure 2.2: Optimal route within a functional module (reprinted with permission from Elsevier [1])

2.1.2 Hierarchical classification of a process

In addition to partitioning a process into functional modules instead of UOPs, Freund and Sundmacher [3–6] proposed a hierarchy how a chemical process can be classified into different levels (refer to Fig. 2.3).

Within this hierarchy, a chemical process consists of a molecular, a phase, a process unit, and a plant level. Process intensification approaches can be classified according to the level where they have the largest impact or induce the largest change. In addition, this classification helps to understand for which purpose the design methodology is developed as will be explained in Section 3.1.1.

For example, a new catalyst acts on the molecular level. Changing the solvent or using innovative solvents such as thermoregulated solvent systems is a modification on the phase level of the process. In addition, using a membrane reactor for the distributed dosing of a reactant changes the phase composition, and thereby it can be regarded as process intensification on the phase level as well. Switching from a semi-batch reactor for temperature control of a strongly exothermic reaction to a continuously operated micro reactor is a change on the process unit level.

Redirecting a recycle without changing the equipment is an alteration on the plant level. Most often modifications in the subjacent levels stir changes in the levels above. For example, if the solvent for the chemical reaction is changed, most often the downstream process and thereby the overall process structure is different. Modifications in the above levels might also lead to changes in the levels below. For example, if the downstream section is changed, this leads to a different composition of the recycle and the phase composition in the reactor is affected.

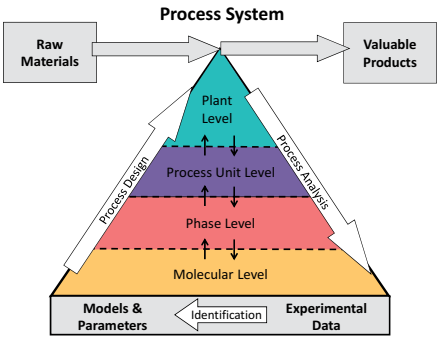

Figure 2.3: Hierarchical structure of a process (adapted from [3])

Beside the just proposed process hierarchy, alternative hierarchies in the field of chemical reaction engineering and in the field of PSE exist. Here, the relevant hierarchies are shortly reviewed in order to distinguish between these approaches and the hierarchy presented in the EPF framework.

Dautzenberg and Mukherjee [8] developed a classification of multi-functionality to achieve intensified reactors. Their levels of multi-functionality act on the catalyst level, the reaction inter-phase level, the intra-reactor level, or the inter-reactor level. Within their work, they present interesting options to design intensified reactors and one of their proposed reactors is discussed in the ethylene oxide example in Section 5.2.

Lerou and Ng [9] proposed a multiscale approach in chemical reaction engineering. In every chemical reactor, phenomena occur at different scales with respect to time and space. They classify the occurring phenomena into molecular, fluid dynamics and transport, catalyst, reactor, as well as plant level and attribute time and length scales to each phenomenon.

Beside these hierarchies, which are proposed in the field of reaction engineering, different modeling hierarchies can be found in the field of process systems engineering (e.g. [10–13]). These approaches deal with the question on how models can be arranged in a structured manner in order to enable a systematic description and implementation (object-oriented) of chemical processes, but do not deal with process intensification or design of innovative apparatuses.

2.1.3 Possibilities for controlling the process route direction

Within the elementary process functions concept it is proposed that an optimal process consists of a sequence of optimal manipulations of a fluid element. These manipulations can be separated into functional modules where in each functional module a dynamic optimization problem is solved. In addition, the manipulation options to obtain the optimal route in state space can be classified into measures acting on the capacity matrix **C**, the flux-weighting matrix **F**, the kinetic matrix **K**, and the flux vector **j** according to Fig. 2.4 [2].

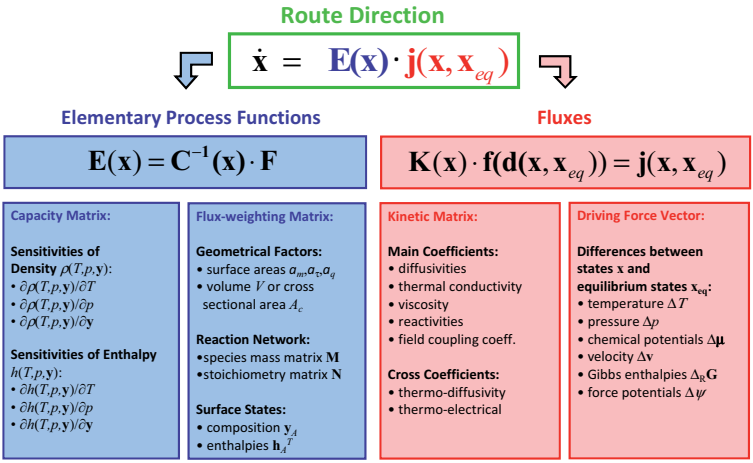

Figure 2.4: Possibilities for controlling the process route direction (adapted from [2])

In general, the state of the fluid element evolves according to the equations of change. The balance equations are reformulated yielding the direct change of the states of the fluid element according to eq. (2.1.1) [2] giving rise to the elementary process functions matrix $\mathbf{E}(\mathbf{x})$.

$$\dot{\mathbf{x}} = \mathbf{E}(\mathbf{x}) \cdot \mathbf{j}(\mathbf{x}, \mathbf{x}_{eq}) \tag{2.1.1}$$

The elementary process functions matrix is composed of the inverse capacity matrix times the flux-weighting matrix. The rate of change is defined by the inner and outer fluxes acting on the fluid element. According to the theory of non-equilibrium thermodynamics, these fluxes depend on the kinetic matrix and the driving force vector. The driving forces itself are dependent on the state of the fluid and its equilibrium state.

This concept is used to classify process intensification approaches according to their physical effect. For example, certain entries of the capacity matrix are changed if a solvent or an inert gas is substituted in the process.

By applying micro reactors, the surface-to-volume ratio is changed and this alteration is reflected within the flux-weighting matrix. In case a different catalyst gives

rise to a new reaction route, the new reaction network induces also a change in the flux-weighting matrix.

By operating the process in a different temperature region mainly the kinetic matrix is influenced, for example both the reactivity and diffusivity change.

The driving forces of the external fluxes such as the heat flux can be increased by changing the state of the environment which is in exchange with the fluid element. The external system can be composed of different *service phases* each associated with a specific outer flux which is integrated in the problem formulation. In addition, internal fluxes such as the reaction flux are dependent on the inner state of the fluid element. Therefore, the reaction flux can be manipulated by operating at a different reactant concentration, pressure, or temperature. Thereby, the difference in the chemical potential can be increased and the reaction accelerated.

While some process intensification approaches are clearly associated with only one of the fields shown in Fig. 2.4, other options affect several fields. For example, applying gas-expanded liquids changes the solubility of gases in a solvent. In addition, the diffusivity of the gases rises which causes changes in the kinetic matrix.

Summing up, the elementary process functions framework yields a definition for optimal chemical processes (optimal travel route of the fluid element), the decomposition of this route into single functional modules, and the classification of PI approaches according to influenced levels in the process hierarchy and their physical effects. The classification according to changes in the capacity matrix, in the flux-weighting matrix, in the kinetic matrix, and in the flux vector gives rise to a deeper understanding of the physical effect associated with the according PI measure.

2.2 Alternative approaches towards intensified processes

Besides the elementary process functions framework, also different classifications of process intensification options and approaches to improve the process design exist. In this section, existing classifications of PI options, design procedures taking PI measures into account, and task-based approaches are discussed.

Different hierarchies in the field of chemical reaction engineering were already illustrated and compared to the process structure proposed by Freund and Sundmacher [3] in Section 2.1.2.

Classifications

From the existing classifications in the field of process intensification, the systematization approaches of Strohrmann [14], Stankiewicz and Moulijn [15], and Van Gerven and Stankiewicz [16] are shortly reviewed.

According to Strohrmann, process intensification measures can be classified into integration and enhancement [14]. Here, reactive distillation is an example for integration of reaction and separation. Micro-reactors enhance the heat and mass transfer, but in that case no integration is achieved.

Stankiewicz and Moulijn [15] proposed a classification into process-intensifying equipment and process-intensifying methods. Examples for the process-intensifying equipment are micro reactors, spinning disk reactors, and static mixers. Hybrid separation, membrane absorption, and reactive extraction are regarded as examples for process-intensifying methods.

Later on, Van Gerven and Stankiewicz [16] suggested that the fundamentals of PI can be classified into effects on the spatial, thermodynamic, functional, or temporal domain. Here, the spatial domain refers to changes in the structure of the reactor, e.g. giving rise to a better flow distribution. How to transfer energy to where it is required is the central question of the thermodynamic domain. Using synergistic effects is the focus of the functional domain. The changes in the temporal domain are either changes in the time scales of different processes or using dynamic operation to achieve process improvements.

The classifications might help to understand the different aspects how a process can be improved, but in contrast to the concept of elementary process functions these classifications do neither define the optimality of a process nor give a modeling framework how to systematically model and apply PI approaches.

From these classifications it can be concluded that a design method for innovative apparatuses should be able to investigate different integration and enhancement concepts. This approach should give rise to quantitative and qualitative improvements of the process. Furthermore, the intensification may be on the spatial, thermodynamic, functional, or temporal domain of a process and a design method should cover all of these domains. In addition, the design method should be able to yield innovative, tailor-made apparatuses, which then can be referred to as process-intensifying equipment.

Process design

Besides the classifications of PI options, several authors worked on process design procedures which take intensified equipment into account. These process synthesis approaches extend the well known combination of unit operations by using intensified apparatuses in order to improve the overall process performance. Here, the methods of Rong et al. [17] and Lutze et al. [18] are shortly reviewed.

Rong et al. [17] proposed a methodology of conceptual process synthesis for process intensification. Within their approach, the limiting steps of the process are identified and afterwards better suited equipment is used to overcome the limitations of this step. It is intended as phenomena-based approach trying to use more physical and chemical insights. The production of peracetic acid is presented as an example. Here, a batch reactor is exchanged by a micro reactor in order to solve the problem of limited heat transfer. However, the discussed example indicates that the approach is still based on existing apparatuses.

Lutze et al. [18] presented process intensification as a perspective on process synthesis. In this approach, PI options are generated by identifying a set of feasible equipment. This set includes innovative apparatuses and is used to built a superstructure of the process including intensified equipment. Hence, this approach can be taken directly as an extension of the classical superstructure optimization approach for process design.

Task-based approaches

Within the elementary process functions framework, functional modules were defined. These functional modules are associated to tasks rather than to equipment. In this context also other task-based approaches were developed which try to understand chemical processes in terms of physical phenomena and model the process accordingly. In the field of process intensification two approaches are discussed here.

Arizmendi-Sánchez and Sharratt [19] structured the process description in a task level, a phase level, and a phenomena level. However, their approach is more a multilevel modeling approach and does not describe the modeling of multiple physical scales and so far it is not defined where process intensification measures are included.

Menon et al. [20] and Lakerveld et al. [21] developed a task-based synthesis approach for industrial crystallizers. This approach yields insights into the complex interplay of different phenomena occurring during crystallization. In addition, this method is based on dynamic optimization similar to defining the optimal route of a fluid element. Therefore, this approach can also be regarded as a design approach based on dynamic optimization, a concept which will be discussed in the next section.

So far, the elementary process functions concept and different approaches towards process intensification were discussed. However, several reactor design methods were also developed within the field of PSE. These reactor design methods are described in the next chapter before the derived method is placed within the EPF framework and the requirements for the design of innovative optimal chemical reactors are defined.

2.3 State-of-the-art reactor selection and design methods

The state-of-the-art reactor selection methods can be classified into heuristics, attainable region (AR) methods, or rigorous optimization approaches as shown in Fig. 2.5. The fundamental idea of each method will be discussed in this section. In Section 3.3 these approaches will be compared to the developed methodology in order to illuminate similarities and differences.

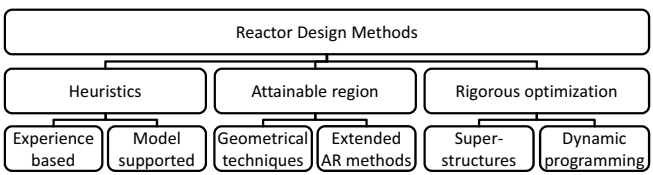

Figure 2.5: Classification of reactor design methods

Heuristics

Reactor selection heuristics can be classified into criteria based on experience reviewed in many textbooks on chemical reaction engineering and on reactor design

(e.g. [22, 23]) and model supported heuristic approaches [24, 25]. In many cases, these heuristics can result in a good reactor selection, are easy to apply, and fast to use. However, these criteria do not hold for any arbitrary reaction network and the application for complex systems is limited. Therefore, it is hard to find the best reactor using such criteria. In addition, these heuristics are made to choose from existing reactors, but not for the design of new apparatuses. After having chosen a reactor type, the reactor can only be adjusted to the special requirements of the reaction system within certain limits by parameter optimization.

Attainable region concepts

In order to define performance targets of a complete family of reactor networks, the concept of the attainable region was developed. It yields the best possible performance of any reactor network consisting of a set of pre-defined ideal reactors, which are usually a plug flow tubular reactor (PFTR) and a continuous stirred-tank reactor (CSTR).

The concept was first introduced by Horn [26] and most of the further work was done by Glasser, Hildebrandt and Feinberg (e.g. [27–30]). Since a convex hull of the feasible region is derived graphically, the classical AR approach can only be applied easily to problems which can be reduced to at most three dimensions. In order to overcome this limitation, techniques to apply the AR concept to higher dimensional problems were developed [31]. However, reducing the dimension of the problem is limited and therefore the application of the classical AR approach is restrained.

In addition, the AR method is hard to apply if the reactor network is embedded into the complete process design problem since the initial conditions for composition and temperature must be known for the attainable region analysis a priori. Every time the boundary conditions for the reactor problem change, the AR must be recalculated.

In order to overcome the limitations with respect to dimensionality and integration within the overall process, Biegler and co-workers developed hybrid methods, which combine the AR approach with rigorous optimization [32–35]. They introduced the so-called differential side stream reactor (DSR), which can be used to investigate distributed dosing and removal from the reactor. However, the dosing/removal concepts are limited to dosing of initial feed and removal of the overall product mixture at the according location in the reactor. In addition, optimal temperature profiles can be obtained by cold shot or external cooling. The new model formulation and the use of rigorous optimization gave rise to the possibility of an automated generation of the AR in high dimensional state space.

Furthermore, the AR concept was extended to reaction-separation networks (e.g. [36, 37]) and to certain cases of reactive distillation [38, 39].

Summing up, the AR method yields the best performance of the optimal network of pre-defined reactor types. The limitations of using only PFTR and CSTR are partly overcome by the use of the DSR. However, the AR concept does not allow to develop new reactor concepts directly or even design innovative apparatuses.

Superstructure approaches

Beside the AR approach, rigorous optimization methods for the reactor synthesis problem were derived. The rigorous optimization methods can be classified into superstructure approaches and techniques based on dynamic programming. In this

paragraph superstructure approaches are reviewed, while the next paragraph deals with methods based on dynamic optimization.

Superstructure approaches for the reactor network synthesis problem were developed by several authors (e.g. [40–44]). In this context, a superstructure is composed of a set of redundant pre-defined reactor types. In contrast to the AR, the possible connections between the reactors must be specified a priori and the best connection is identified as a result of the optimization.

The interaction between several parts of the plant can easily be taken into account by adding further flowsheet equations. However, the possible connections between the units often give rise to integer variables in the model. In case the reaction kinetics are nonlinear, complex mixed integer nonlinear programming (MINLP) problems arise. This can lead to many local optima and finding the global optimum cannot be guaranteed using conventional MINLP solvers.

In addition, the characteristics of many reaction networks are similar, e.g. a cascade of CSTRs approximates a PFTR. Hence, finding the best combination from a technical and economical point of view becomes very difficult. This problem can be reduced by using simple superstructures, which only include the most promising combinations. However, these simplifications may lead to the loss of a potentially better reactor network in the superstructure and a high experience in modeling and reaction engineering is required.

In summary, the advantage of the superstructure approach is that it yields the best combination of reactors and that a multitude of possible reactor type can be investigated. On the downside, with increasing number of reactor types the modeling effort and the complexity increase. Thereby the solvability drastically reduces. Hence, superstructure modeling requires always a trade-off between the number of combinations included in the superstructure, the solvability of the problem, and the uniqueness of the solution.

Methods based on dynamic optimization

The dynamic programming approach for the reactor optimization can be traced back to Aris [45], Horn [46], and Bilous and Amundson [47, 48]. The optimal design of chemical reactors is given, if the optimal temperature and concentration profiles are achieved along the entire reaction coordinate [49, 50]. This holds for batch reactors as well as for continuous plug flow reactors. The nature of these optimal profiles were already investigated by analytical and – as far as possible in those days – by numerical methods. Since the number of reaction rate equations and the calculation power were very limited, only some examples were evaluated. In addition, it was not investigated how these optimal profiles could be obtained by an adequate reactor design. As a result, these innovative approaches were not used to design new reactors at that time. Nowadays, solving optimal control problems for the class of semi-batch reactors is state-of-the-art. The problem of optimal control variable profiles (feed, temperature, pressure) is considered for batch and semi-batch reactors by several authors (e.g. [51, 52]).

Further examples for the use of dynamic optimization to design reactors are the works of Kjelstrup and co-workers [53–55], Hillestad [56], and Lakerveld et al. [21], where the latter were already discussed in Section 2.2.

Kjelstrup and co-workers solved the minimum entropy production problem as dynamic optimization problem for the SO_2 oxidation [53, 54] and for several other processes (e.g. [55]). The main focus of their work is to show that the entropy production can be significantly reduced by applying a distributed cooling strategy.

Hillestad [56] developed a method for the systematic staging of reactors. Here, design functions like catalyst density, cooling, dosing of fresh feed, and back-mixing are taken into account. The problems are constrained by the equations of change. Therefore, this method is also based on solving dynamically constrained optimization problems. However, no control functions to obtain optimal profiles for temperature and concentration are investigated, but rather the reactor is segmented and on every segment constant values for the design functions are chosen. Hence, this method can approximate optimal profiles for either a very high number of segments or in the special case where the optimal control profiles are piecewise constant (e.g. in case of a bang-bang solution of a minimal time problem). While this approach includes many interesting PI options, it hinders the design of new reactors by segmentation of the reactor a priori.

Multiphase systems

All of the reactor design approaches discussed in this section have been developed for homogeneous systems. For multiphase systems only heuristics and superstructure approaches were developed so far. These methods will be shortly reviewed at the beginning of Chapter 6 and then compared to the approach used for the hydroformylation example in this work.

Chapter 3
Design of optimal chemical reactors

The scope of this chapter is to explain the general idea of the design method, its general modeling approach, and the sequential order of the decisions which need to be taken. At the beginning of the chapter, the scope of the method is defined in Section 3.1 and the requirements for a new design methodology for optimal chemical reactors are derived.

In Section 3.2, the methodological approach is explained in detail. Here, the main idea and overall picture on the method is given first. Afterwards, the details of level 1 to level 3 are discussed and the sequential order of the approach is illustrated in form of a flowchart. All the modeling details such as the required equations, thermodynamic data, reaction kinetics, and further intrinsic bound as well as the formal statement of the arising optimization problems will be given in the examples in part two.

In Section 3.3, the method is compared to established reactor design approaches discussed in Section 2.3 and the unique features of the proposed method are discussed.

3.1 Scope of the reactor design method

3.1.1 Placement within the elementary process functions framework

The scope of this thesis is to create a method, which enables the design of innovative reactors based on the optimal reaction route in state space. Thereby, the method accounts for the analysis of the chemical reaction process using an apparatus independent functional module in the beginning. With respect to the process hierarchy shown in Section 2.1.2 the method transforms the optimal reaction route determined on the phase level to the process unit level.

The method is focused on the reaction module and not intended for the design of entire processes using functional modules for all tasks. However, the reaction module is placed within an overall process exemplified on the ethylene oxide process in Section 5.4 in order to illustrate the potential of the EPF approach for plant wide process intensification.

The modeling based on the equations of change enables to consider all PI options whether they act on the capacity matrix, the flux-weighting matrix, the kinetic matrix, or the driving force vector as shown in Section 2.1.3. The systematic placement of dif-

ferent process intensification options according to this classification will be illustrated on the examples in part two of the thesis.

3.1.2 Requirements for the design of optimal chemical reactors

In this section, the requirements for a reactor design method, which is able to yield optimal chemical reactors taking process intensification options into account, are defined. Within the elementary process functions the general guideline is followed: *The optimal route of a fluid element is given if the internal and external fluxes of this element are optimized along the entire reaction coordinate in order to manipulate the states in such a way that a certain objective is optimized.*

In order to create a design method which is able to yield the best technical reactor based on this idea, the following criteria must be met:

1. In order to obtain the optimal route, the method must start independent of existing apparatuses. The method should work for batch as well as continuously operated reactors in order to allow the technical realization of the optimal route in time or space.
2. It must be possible to investigate different integration concepts in order to be able to yield different types of reactors at the end. The method must include existing reactor concepts and be able to give rise to innovative reactors.
3. The maximum potential of the reaction system should be obtained as soon as possible to be able to exclude certain reaction concepts in an early stage and to benchmark the derived technical reactor at the end. The different reaction concepts and their potential must be compared on an early stage in order to allow for fast screening of different concepts and avoid extensive enumeration of all possible reactor types.
4. System inherent limitations as imposed by the reaction kinetics of a catalyst must be considered at all stages of the design method. Therefore, the method must be rigorously based on the equations of change, thermodynamics, and system inherent limitations of the investigated system. In addition, limitations arising from the validity of the used models and the operation range of the catalyst need to be taken care of.
5. The modeling framework must be adequate to investigate process intensification options as shown in Fig. 2.4. It must be able to include all relevant of physico-chemical phenomena.
6. A general and fundamental modeling framework must be ensured to be able to extend the method to a wide field of processes.
7. In order to come from the optimal route in state space to a technical reactor, it must be possible to use different control variables to enforce the desired fluxes.
8. On the way to the best technical reactor, the losses due to the technical limitations must be quantified.

A new design methodology, which is able to meet the above criteria, is developed in this work and is explained in the next chapter. In part two, the approach is illustrated on several examples focusing on different aspects of the method.

3.2 Methodological approach

Along the reaction coordinate the composition of a fluid element changes and this gives rise to different optimal reaction conditions along the reaction coordinate. Consequently, a reactor can be regarded as optimal if the optimal temperature, pressure, and concentration profiles are obtained over the entire residence time. Since the states are subject to the equations of change, only the fluxes such as heat, component, and reaction flux can be used to manipulate the states. In order to calculate the optimal profiles for the fluxes, a fluid element is tracked on its way through the reactor and the external fluxes are control functions of a dynamic optimization problem. Since a detailed discussion of the numerical solution approach is only possible when the optimization problems are known in their full complexity, the numerical solution approach is explained in Appendix A.4.

In order to come from the idea of tracking a fluid element to an optimal technical reactor, a three step methodology is developed within this work. The general idea and procedure of the method is shown in Fig. 3.1.

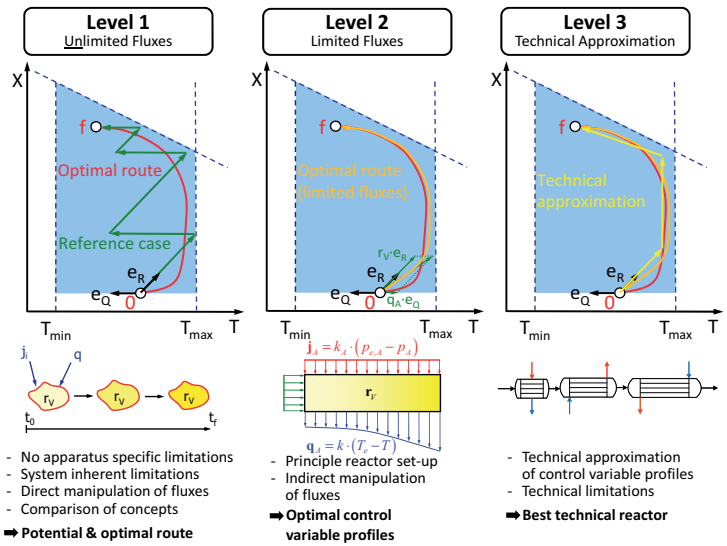

Figure 3.1: General methodological approach

Referring to Fig. 3.1, the optimal route (red curve) in state space is calculated by solving a dynamic optimization problem with unconstrained fluxes in the first design level. The *integration concept* defines, which fluxes are integrated in the design problem, and the *enhancement concept* determines, which fluxes are optimized. The cases, where the fluxes are optimized as control functions, are referred to as *intensified reaction concepts* or *intensified cases*, in contrast to the *reference case*. In addition, a

comparison to an optimized reference case (green curve) is performed to determine the potential of the intensified case.

In the second design level, the attainability of the desired flux profiles is investigated. For this purpose, the transport kinetics are added to the problem and control variables which can be manipulated by changing the reactor design are chosen as control functions. This gives rise to a more constrained optimization problem and the optimal route which can be obtained with the constrained fluxes (orange curve) might be different to the optimal route in state space.

Based on the optimal control variable profiles of level 2, a technical approximation on the third design level is developed (yellow curve). The result of level 3 is the best technical reactor. The different levels will be explained in detail below in Section 3.2.1 to Section 3.2.3.

3.2.1 Design level 1 – Integration and enhancement concept

The purpose of level 1 is to determine the best route in state space without any technical limitations imposed by existing reactors. In addition, different integration and enhancement concepts are investigated and compared to an optimized technical reference case in order to determine the best reaction concept and its potential with respect to the technical established reaction concept. Here, integration refers to the simultaneous integration of several fluxes in the balance equations. For example, within a cooled tube bundle reactor the reaction and heat flux are integrated. Enhancement refers to the fluxes which are controlled in an optimal manner over the entire residence time. While the outer fluxes can be manipulated, the reaction flux cannot be chosen freely since it is subject to the state of the fluid and to the chosen catalyst in case of a catalyzed reaction. However, the reaction fluxes can be scaled by optimizing the catalyst density profile if desired.

In order to limit the number of investigated cases, preliminary considerations regarding the investigated system and chemical engineering knowledge is used in a first step. The reaction concept used in industry is usually chosen as reference concept. The reference case is optimized using the same model with respect to the reaction kinetics, thermodynamic relationships, and equation of change, but the fluxes are constrained according to the general technical set-up and not optimized as profiles. The comparison with the reference case yields the potential of the intensified cases and answers the question whether a further investigation of these cases is worthwhile. The best intensified case of level 1 determines the optimal performance of the investigated system and is used as benchmark for the technical approximation on the subsequent levels.

On the first level, a fluid element is tracked considering the balance equations for energy and mass, thermodynamic relationships, reaction kinetics, and further system inherent limitations. The model does not include technical limitations and also the flow field is assumed to refer to an ideally distributed system. Thereby, the flow field is decoupled from the design problem in the first stage. The influence of the flow field on the reactor performance is investigated later. With respect to the flow field, this assumption is similar to the approach of Mangold and Gilles [11] who divided the distributed phases into fluid dynamic and a thermodynamic subsystem and considered both systems individually. This simplification is made, because the

best profiles for the fluxes are unique in case all important fluxes are optimized in an ideally distributed system. Only if not all significant fluxes are optimized, effects like back-mixing (arising from a non-ideal flow field) might lead to superior solutions. This aspect will be clarified on the examples later in the second part of this thesis. Hence, the influence of the flow field will not be further considered on level 1 for the intensified cases.

With respect to Fig. 3.1, the results of the first level are presented on the left hand side of the figure. Within this example, the heat and reaction flux are integrated and the states are the conversion (X) and the temperature (T). The optimal route in state space (red curve) is obtained by an optimal heat flux profile, while the reference case refers to an adiabatic reaction with intermediate cooling (green curve). Here, the system inherent limitations are illustrated by dotted lines. The vertical lines are the minimum and maximum allowed temperatures, and the diagonal curve represents system inherent limitations such as an equilibrium conversion. The initial point at the beginning of the reaction is indicated by 0 and the final point at the end of the reaction by f.

In general, the reactor with the lowest investment and running costs from the overall process point of view is desired. However, quantifying the investment and running expenses is not always possible. Therefore, different objective functions capturing the most significant aspects of the investigated system might be of interest. For example, either the fastest route, the route with the highest energy efficiency (similar to [53]), or the final point in state space can be chosen as objective function. Here, the final point within the state space might be the maximum conversion achievable within a specified reaction time, or the maximum selectivity in case of a reaction network. In case the intensified reaction concept is promising, it is further investigated on level 2.

3.2.2 Design level 2 – Attainability of desired fluxes

On level 2 of the design approach, it is investigated whether the desired fluxes are attainable. For this purpose, the principle reactor set-up and the principle composition of service phases must be defined. In this context, service phases are in mass and/or heat exchange with the reaction phase and thereby provide the desired fluxes. For example, a cooling phase can be defined to remove or supply heat. A reactant supply phase can be established in order to allow for distributed dosing. These service phases are assumed to be ideal and can still be manipulated along the residence time of the fluid element.

The choice of the reactor set-up and service phases provides the number of exchange areas, transport mechanisms, and transport kinetics. Once the transport kinetics are known, control variables which can be manipulated by reactor design can be identified. The optimal profiles of these design variables are obtained by solving a dynamic optimization problem which is now additionally constrained by the transport kinetics.

In addition to the principle reactor set-up, the catalyst support geometry must be chosen in case of heterogeneously catalyzed reaction. For example, this might be a fixed bed of catalyst particles, monolithic honeycombs, or foam like catalyst supports.

The catalyst support geometry defines the catalyst fraction and the possible exchange areas of the fluxes since it is associated with a minimum and maximum tube diameter.

On this level, it is answered which catalyst support geometries are suited, which principle reactor set-up is reasonable, and which different control variables can yield the desired flux profiles. If the optimal flux profiles cannot be obtained, a sensitivity analysis can be performed to determine which bound need to be shifted in order to obtain a better solution. The decision loops which can be applied to identify a better principle reactor set-up and combination of control variables is explained using a flowchart in Section 3.2.4.

Referring to Fig. 3.1, the second design level is illustrated in the middle of the figure. The principle reactor set-up provides the exchange areas and transport kinetics. The control variable for the heat flux might be the cooling temperature. In state space, the change of the fluid is then constrained by the vector e_Q, which gives the direction achievable by cooling without reaction, and the vector e_R, which represents the state space direction of the adiabatic chemical reaction. The optimal route which is obtained by the combination of both constrained fluxes (orange curve) is compared to level 1; if the differences in the objective functions of level 1 and level 2 are acceptable, the optimal control variable profiles are approximated on level 3 giving rise to the best possible technical reactor.

3.2.3 Design level 3 – Technical approximation

On level 3, the optimal control variable profiles of level 2 are approximated by a tailor-made technical reactor. This technical approximation can consist of one or several segments. In each segment the full toolbox of existing reactors can be used or the segment can be constructed in a new manner following the catalog of requirements defined by the principle reactor set-up and optimal flux profiles determined on level 2. It should be noted that the reactor is not segmented a priori, but the segments are derived based on the optimal profiles. In addition, the technical approximation depends on the experience and know-how of the reaction engineer.

In the technical approximation, the service phases of level 2 are also subject to the equation of change and cannot be manipulated freely anymore. This leads to a parameter optimization problem on level 3, where design variables of the reactor in addition to the inlet conditions and capacities of the service phases are optimized.

In a first step, it is investigated if the technical approximation is in principle suited to approximate the optimal route. This can be done by using relatively simple models. In a second step, the influence of non-idealities in the flow, concentration, and temperature field are analyzed using a detailed reactor model.

Referring to Fig. 3.1, the technical approximation might consist of a reactor with several segments (right hand side of the figure, yellow curve in the state space diagram). In each of these segments, a different cooling strategy is applied giving rise to a good approximation of the optimal cooling profile.

In summary, specific decisions must be made and the model must be extended on each level. By applying this methodological approach, the complex reactor design task is divided into smaller subproblems, which are solved by a sequence of specific

optimization problems with increasing complexity regarding the constraints. The decisions, modeling aspects, and results of each level are summarized in Fig. 3.2.

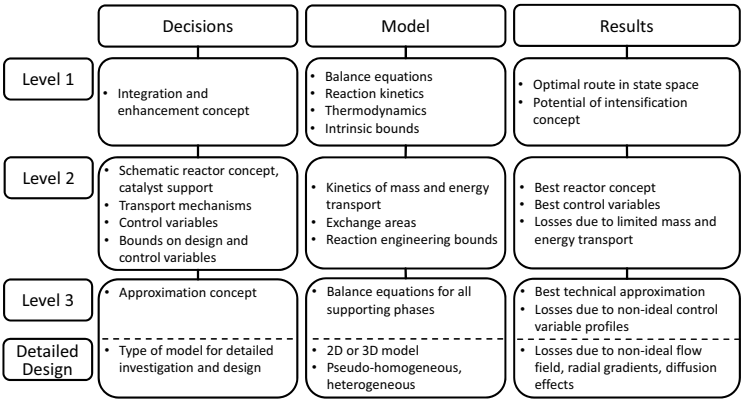

Figure 3.2: General decision structure

3.2.4 Sequential order of the design approach

In order to illustrate the sequential arrangement of all aspects, the interfaces between the different levels, and the decision loops which may be necessary between the levels, a flowchart of the methodological approach is shown in Fig. 3.3.

In the beginning, the scope of the analysis is defined. This includes specifying the envelope for the mass and energy balances, for example either the single reactor or the total plant with an intensified reaction module is considered. This choice determines which inlet and outlet conditions must be defined. In addition, the objective function is chosen. For example, either the selectivity or residence time can be optimized in case of a single reactor, while the running expenses are usually optimized in case of a total plant.

Afterwards, the catalyst is selected. This choice has a major influence on the reaction network and determines the reaction kinetics. In addition, the integration and enhancement concepts are chosen and the reference case is defined. By solving the arising optimization problems the potential of each case is calculated. If the difference in the objective function compared to the reference case is worthwhile, the most promising case can be further investigated on level 2. Otherwise, the reference case sufficiently approximates the best reaction route and the existing reaction concept cannot be further improved from a technical point of view.

Level 1 offers the possibility to investigate whether the manipulation of a certain flux is worthwhile regardless the possible technical realization of the concept. For example, in situ removal concepts of an intermediate product can be easily investigated and thereby the maximum potential of such a concept is determined.

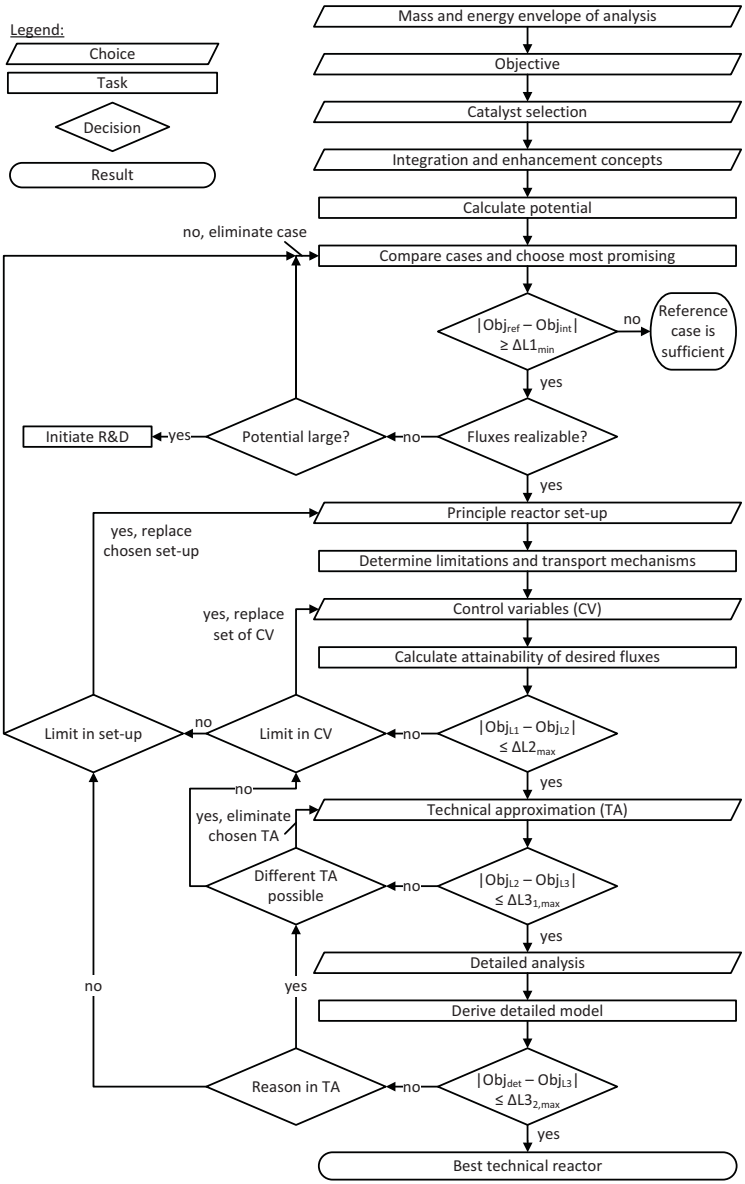

Figure 3.3: Detailed flowchart of the methodological approach

If the flux concept cannot be realized by existing technological means, the potential of this case determines whether further research and development efforts are worthwhile in order to realize this concept. In case of the successful development of a possible realization, this concept can be further investigated. However, such a development might take a long time and is connected to major uncertainty. Hence, an easier intensified reaction concept may be further investigated on the subsequent levels, if this concept offers a large potential compared to the reference case. For the sake of clarity, the further decisions and tasks associated with the research and development step are not illustrated in the flowchart.

At the end of this first decision loop, either an interesting case for further analysis on level 2 is obtained or the existing technological set-up is found to be optimal since no optimization potential using other integration and enhancement concepts exists.

For the most promising case, a principle reactor set-up is chosen at the beginning of level 2. This includes the definition of the exchange areas, service phases, and transport kinetics describing the fluxes. In addition, the catalyst support geometry is chosen and suitable control variables for the fluxes are identified. Then, the attainability of the fluxes is determined by solving the arising optimization problem.

In case the fluxes are fully attainable or the difference in the objective compared to level 1 is small, the optimal profiles of the control variables are approximated on level 3. If the fluxes are not satisfactorily attainable, either different control variables or a different principle reactor set-up must be chosen (decision loop 2). In case all available reactor set-ups and control variable combinations do not yield a solution close enough to the objective function value obtained on level 1 for this case, a different integration and enhancement concept should be further evaluated. Alternatively, if the objective value obtained on level 2 is still better than all other cases of level 1 which were not excluded in the first decision loop, this case can be further investigated on level 3.

On the third level, a technical approximation of the optimal design profiles is derived and an optimization problem considering all technical constraints is solved. In case the technical approximation exhibits significant losses in the objective function, a different technical approximation should be investigated. If no further approximation of the optimal control variable profile exists, an alternative principle reactor set-up and/or control variable profile should be tested on level 2.

In case the technical approximation of level 3 is sufficient, the proposed reactor set-up is investigated in detail to determine the influence of non-idealities in the flow, concentration, and temperature fields. If the losses due to the non-idealities are small, the best technical reactor is derived. Otherwise, a different technical approximation, or a different principle reactor set-up should be investigated depending on whether the losses arise from the technical approximation or from the principle reactor set-up.

It should be noted that the difference in the objective functions $\Delta L2_{max}$, $\Delta L3_{1,max}$, and $\Delta L3_{2,max}$ do not have to be specified a priori. All meaningful options on level 2 and level 3 can be evaluated simultaneously if desired and the best option can be chosen for further analysis. However, the minimum required potential on level 1 $\Delta L1_{min}$ between the intensified case and the reference case should be defined since it refers to the potential overall savings of the intensified case. At the end, the savings of the derived reactor compared to the reference case should still be large enough to

cover for the arising costs for the detailed design of the reactor and for the possible larger investment costs.

3.3 Comparison to established design methods

After stating the new reactor design methodology and providing an overview on existing reactor selection and design method in Section 2.3, the different approaches are compared in this section.

In general, the scope of heuristics, classical AR concepts, and superstructure approaches is different from the scope of the proposed design method. Heuristics are used to choose the best reactor from a given set. The scope of the AR concept is to identify the maximum potential of a combination of pre-defined reactors and the superstructure approach yield the best combination of such a pre-defined set of reactors. These approaches are not made for the development and design of new apparatuses.

The proposed methodology can rather be compared to approaches based on dynamic programming and to the extended AR concept of Biegler and co-workers [32–35]. With respect to the work of Johannessen et al. [53, 54], Hillestad [56], and Lakerveld et al. [21], all of these methods are based on the idea of Aris [45], Horn [46], and Bilous and Amundson [47, 48]; in order to obtain an optimal reactor, optimal profiles for the concentrations and the temperature must be achieved along the entire reaction coordinate. With respect to the optimal profiles for the states, the idea of Freund and Sundmacher [1] is quite similar to the just mentioned pioneering works. However, the states can only be manipulated by fluxes and the EPF approach is rigorously based on the consideration of the equations of change and optimal dynamic manipulation of the available fluxes. All of these methods are based on the solution of dynamically constrained optimization problems, but the model formulations and the individual scopes of the methods differ.

In general, the main difference between the proposed method based on the EPF concept and the earlier approaches based on dynamic programming is that the derived reactor design method gives a framework from the evaluation of all concepts on level 1 to the concrete technical realization on level 3. The second level of the design approach, where it is investigated which catalyst support geometry is required and how the desired fluxes can be realized, is not included in any other method published so far. In addition, level 3, which deals with the selection of an appropriate technical approximation, is not taken into account by the existing approaches. In addition, several differences between the available methods and the first level of the proposed design methodology exist and are discussed below.

In detail, the original proposals of Aris [45], Horn [46], and Bilous and Amundson [47, 48] did not account for a general description in terms of all possible fluxes. Furthermore, complex thermodynamic relationships as imposed by equations of state or from the description of explosion limits were not rigorously considered in the original works.

The extended AR method includes options for dosing, removal, and cooling. However, not all fluxes can be controlled and selective removal of individual components is not taken into consideration.

The focus of the method proposed by Johannessen et al. [53, 54] is to minimize the entropy production within a chemical reactor. For example, they optimize the cooling temperature profile of a continuously operated plug flow reactor in order to obtain a temperature profile which minimizes the accumulated entropy production of heat transfer, chemical reaction, and pressure loss. For this reason, they start directly at the unit operation level and are restricted by all the associated technical limitations.

The method of Hillestad [56] starts with a pre-defined number of reactor segments. Within each segment the design functions catalyst density, cooling, adding of feed, and back-mixing are optimized as constant parameters. Since continuous (and not piecewise constant) functions are optimal in general, this method limits the solution space. In addition, concepts such as the selective removal of products are not included in this method and all design functions are directly restricted by technical limitations. The back mixing function is obtained by a combination of PFTR and CSTR. However, if all relevant fluxes are optimized as control functions, back mixing is not required, but a CSTR may constitute an adequate technical approximation of constant state space profiles. This will be demonstrated on the hydroformylation example in Chapter 6.

Based on the idea of elementary process functions, Lakerveld et al. [21] proposed a task-based approach for crystallizers. The method is not flux-based, but based on certain task such as cooling, pressure change, or mixing that are combined in one apparatus in order to design better crystallizers. This approach might give rise to more physical and chemical insights into crystallization and also to a modularization of crystallizer design.

Concluding the comparison of the reactor design method, the scope of the proposed design methodology compared to the scope of heuristics, AR, and superstructure approaches is different. In addition to the evaluation of different reaction concepts, the proposed design method is made for the conceptual design of innovative and optimal chemical reactors. Furthermore, the method extends the earlier approaches based on dynamic programming in the following aspects:

- It is rigorously based on the equations of change, thermodynamic relationships, system inherent limitations, and reaction kinetics. The optimal route is obtained by optimal manipulation of the fluxes. Thereby, the physico-chemical principles of PI approaches can easily be included.
- All kind of reaction concepts referring to different integration and enhancement options can be screened without restrictions on level 1.
- The attainability of the desired flux profiles are investigated on level 2 and the best control variables, catalyst support, and exchange areas are identified.
- On level 3, the derivation of a technical approximation gives rise to the best technical reactor.
- In addition to the determination of the best reaction concept, process parameters can be optimized simultaneously and complex objective functions can be optimized.
- The design method is also extended towards multiphase systems.

Part II

Applications

The scope of the second part of this thesis is to illustrate the method on industrially important process examples. In addition, part two provides detailed insights into the modeling associated with the proposed design methodology. Furthermore, the method is extended towards multiphase systems and plant wide optimization.

The structure of the second part follows that of the chosen process examples. First, the method is presented by means of the SO_2 oxidation. Afterwards, the ethylene oxide synthesis is considered. Here, additional fluxes, reactor design criteria, and plant wide optimization are taken into account. At last, a new reactor for the hydroformylation of long chain linear aldehydes in a multiphase system is derived.

The examples are chosen with increasing complexity regarding the reaction network, the number of integrated fluxes, and the phase behavior. In addition, different aspects of the methodology are covered by the examples and the different examples demonstrate the wide applicability of the method. The characteristics and investigated aspects of each example are summarized in the table below.

Overview on the features of the investigated processes

System	**SO_2**	**EO synthesis**		**Hydroformylation of higher alkenes**
		Air based	**O_2 based**	
Type of reactions	exothermic equilibrium	parallel reaction network		complex reaction network
Fluxes integrated	r, q	r, q, j_i		r, q, j_i
Phases	pseudo hom.	pseudo homogeneous		multiphase
Level 1	✓	✓	✓	✓
Level 2	✓	✓	–	✓
Level 3	✓	✓	–	✓
Detailed analysis	–	✓	–	–
Recycle	not existent	not cons.	considered	considered

The SO_2 oxidation represents the class of exothermic equilibrium reactions without selectivity issues. Due to the good data availability and the restricted complexity, it is best suited to exemplify the modeling and the sequential order of the design method. In order to focus on the methodological aspects, only an optimal heat flux profile in addition to the reaction is considered on level 1. On the second level, different options on how the fluxes can be realized are investigated. Level 3 demonstrates how a technical approximation based on the optimal control variable profiles is derived yielding an optimal technical reactor at the end.

The ethylene oxide synthesis is one of the most important partial oxidation reactions, and even small process enhancements give rise to significant improvements with respect to the economical and ecological performance of the process. For the production of ethylene oxide two industrially applied processes exist, namely the air based process and the oxygen based process. The names of the processes refer to the oxidizing agent used, either air or pure oxygen. From the process intensification point of view a shift in the concentration region is performed from the air to the oxygen based process towards higher reactant concentrations. This shift leads to higher

selectivities and space time yields, but safety issues become more important. Hence, it is interesting to investigate how the optimal reaction concept changes and whether the change in concentration space is beneficial. The reaction network of the ethylene oxide synthesis gives rise to a selectivity problem. In case of selectivity issues, dosing and removal concepts become more interesting, and hence several combinations of component fluxes are investigated in this example.

For the air based process, all levels of the design method are applied giving rise to an innovative reactor design. On level 2 of this example, criteria for external and internal heat and mass transport are considered in order to investigate if the chosen catalyst support geometry is suitable. In addition, the derived reactor is analyzed in detail using a two-dimensional model accounting for non-idealities in the flow, concentration, and temperature field.

In the oxygen based process, the interplay between the optimal reaction module and the overall process is investigated. For this purpose, the reactor is considered as a functional module and for the additional process units conventional apparatuses are used. Thereby, the effect of the process on the reactor is considered and an optimal reaction concept from an overall process point of view is determined. Additionally, the impact of the superior performance of the reaction module on the process is determined and the process operation is simultaneously optimized. By considering the overall process, the total production costs of ethylene oxide can be minimized. Here, only the first level of the methodology is investigated since the reactor design will be similar to the air based process, and hence these steps are straight forward. This example constitutes a first extension towards the optimal design of entire processes based on optimal functional modules as proposed by Freund and Sundmacher [1]. In addition, the overall process is intensified by using an optimized reaction module.

The hydroformylation is one of the most important homogeneously catalyzed reactions, and an example for multiphase processes. From the investigated examples, the hydroformylation features the most complex reaction network and phase behavior. Here, a reaction network consisting of parallel and consecutive reactions is considered giving rise to a complex interplay between the different side reactions along the reaction coordinate. In addition, the hydroformylation of long chain linear aldehydes is a multiphase process consisting of at least an organic liquid phase and a gas phase. In order to design optimal multiphase reactors, the second level of the design methodology is extended.

In summary, three different industrially important processes are investigated including the class of exothermic equilibrium reactions, parallel reaction networks, and complex reaction networks. In addition, extensions of the method towards overall process design and towards multiphase reactors are proposed.

Chapter 4
SO_2 oxidation

In order to demonstrate the proposed methodology, the development of a SO_2 oxidation reactor is presented as a first example [57].

At the beginning of each example, the according process will be comprehensively described. In this description, the general objective and the balance envelope considered in the optimization will be explained. Afterwards, the design methodology is applied. For the SO_2 oxidation the levels 1 to 3 are presented. On each level, it is explained

- which reaction concepts are investigated,
- which decisions are taken,
- which model equations are required,
- how the arising optimization problems are formulated,
- which results are obtained and what can be concluded from the optimization results,
- and which information are transferred on to the next design level.

4.1 Process description

The SO_2 oxidation is an exothermic equilibrium reaction and therefore it is representative for a whole class of industrially important reactions. The chemical equation of the SO_2 oxidation is given by

$$SO_2 + \frac{1}{2}O_2 \rightleftharpoons SO_3 \quad \text{with} \quad \Delta h_r = -99\,\frac{kJ}{mol}$$

Depending on the sulfur source different process configurations exist [58]. In this example elementary sulfur is considered as source for the SO_2 and the state-of-the-art process for this sulfur source is the double contact process with intermediate absorption. In this process, five adiabatic fixed bed reactors with intermediate cooling and intermediate absorption after the third bed are used in order to achieve almost complete conversion (referred to as $3+2$ configuration). In this example, only the reactor section up to the third bed are considered according to Fig. 4.1.

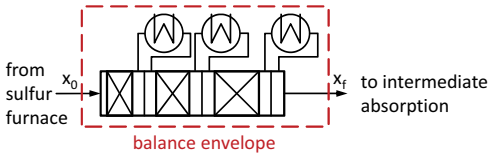

Figure 4.1: Balance envelope of the SO_2 oxidation

Since no side reactions occur, the objective is to minimize the residence time for a given catalyst and given initial and outlet conditions. The given inlet conditions are typical for a plant based on a sulfur furnace ($T_0 = 710\,K$, $p_0 = 2\,bar$, $y_{SO_2,0} = 0.11$, $y_{O_2,0} = 0.10$, $y_{SO_3,0} = 0.01$, $y_{N_2,0} = 0.078$). The outlet conditions are typical values upstream the intermediate absorption ($T_0 = 740\,K$, $p_0 \geq 1.5\,bar$, $X \geq 0.95$).

4.2 Design of an optimal SO_2 oxidation reactor

4.2.1 Level 1 - Integration and enhancement concept

Investigated integration and enhancement concepts

On level 1, different integration and enhancement concepts are investigated. In this example, the reaction flux and the heat flux are the only fluxes considered. At the start, it has to be determined how to combine these fluxes and which fluxes should be controlled (referred to as enhanced fluxes). Here, three reaction concepts are of major interest:

Case 1: Adiabatic reaction with intermediate cooling
This is the ideal case of an adiabatic staged reactor, which is regarded as the technical reference case. Reaction and cooling are applied in series. No flux is controlled in a strict manner.

Case 2: Polytropic reaction with constant cooling temperature
Reaction and cooling are integrated. This case represents a conventional tube bundle reactor. No flux is controlled in a strict manner.

Case 3: Optimal control of heat flux
Reaction and cooling are integrated and the heat flux is controlled to investigate the potential of distributed cooling.

In principle, several fluxes such as component mass fluxes can be integrated and controlled simultaneously. However, in this example, the discussion is limited to the heat flux in order to focus on the basics principles of the design methodology.

The applied decision structure is summarized in Fig. 4.2. In anticipation of the following levels, also the decisions taken on level 2 and level 3 are shown in this figure.

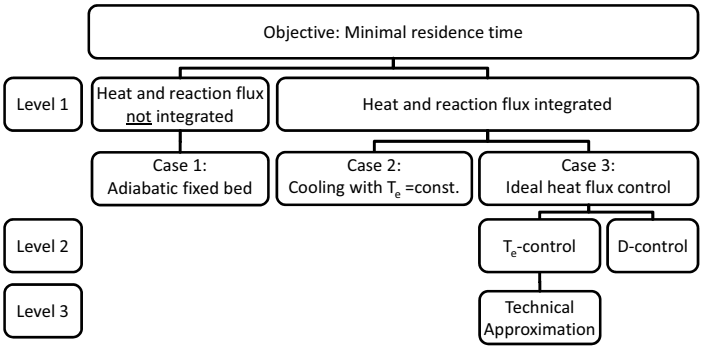

Figure 4.2: Decision structure for the SO_2 oxidation reactor design task

Model

On level 1, a pseudo-homogeneous, one-dimensional model is used to represent the gas solid reaction system. The reasons for the choice of this model are that an ideal catalyst support geometry and an ideal flow field is assumed on this level.

The assumption of an ideal catalyst support results in a gradient-free system with respect to temperature and concentration between the fluid and the catalyst as well as inside the catalyst pellets. In addition, it is assumed that the lowest catalyst void fraction of industrial reactors can be used on level 1 giving rise to the highest volume related reaction rate. This lower limit for the catalyst void fraction is associated with a packed bed of equally sized spherical catalyst particles ($\epsilon = 0.4$). Furthermore, no pressure drop is considered on level 1. The losses due to the pressure drop are associated with the principle reactor set-up and catalyst support geometry and hence considered on the subsequent levels.

Furthermore, it is assumed that the flow field can be represented by tracking a fluid element on its way through the reactor. If mass exchange due to diffusion between the individual fluid elements is neglected, the chosen substantial formulation of the balance equations holds for a batch or a continuous reactor. The non-idealities in the flow field are considered in the detailed analysis of level 3 as will be shown for the ethylene oxide synthesis in Section 5.3.

In case of the SO_2 oxidation, the dimension of the model is reduced by considering the conversion X. Since no side reactions occur, no individual component mass balances are required and only a conversion balance is considered (eq. (4.2.2)). Assuming an initial amount of SO_2 in the tracked fluid element, the conversion is defined according to eq. (4.2.1).

$$X := \frac{n_{SO_2,0} - n_{SO_2}}{n_{SO_2,0}} \tag{4.2.1}$$

$$\frac{dX}{dt} = \frac{r \cdot \rho_p \cdot V_{gas}}{n_{SO_2,0}} \cdot \frac{1-\epsilon}{\epsilon} = \frac{r \cdot \rho_p \cdot R \cdot T}{p} \cdot \left(\frac{1}{y_{SO_2,0}} - \frac{1}{2} X \right) \cdot \frac{1-\epsilon}{\epsilon} \tag{4.2.2}$$

The reaction rate model is based on the catalyst investigated by Eklund [59] and thermodynamic data presented in the literature [60]. Here, a conventional vanadium pentoxide catalyst is used and the possibility to account for different catalyst systems is not investigated. A lower catalyst activation temperature of $633\,K$, which is the melting temperature of an industrially used promoted vanadium pentoxide catalyst, is included in the model. An upper catalyst temperature of $923\,K$ due to the catalyst stability is also considered [61]. A full bodied catalyst density of $\rho_p = 1330\,\frac{kg}{m^3}$ is used. Using eq. (4.2.3) to express the individual mole fractions, the reaction rate is written in terms of conversion, temperature, pressure, and initial composition (eq. (4.2.4)).

$$y_i = \frac{y_{i,0} + \frac{\nu_i}{|\nu_{SO_2}|} \cdot X \cdot y_{SO_2,0}}{1 - 1/2 \cdot X \cdot y_{SO_2,0}} \tag{4.2.3}$$

$$r = k_r \sqrt{\frac{y_{SO_2,0}(1-X)}{y_{SO_3,0} + y_{SO_2,0}X}} \cdot \left[\frac{(y_{O_2,0} - \frac{1}{2} y_{SO_2,0} X)p}{1 - \frac{1}{2} y_{SO_2,0} X} - \left(\frac{y_{SO_3,0} + y_{SO_2,0}X}{y_{SO_2,0}(1-X)K_p} \right)^2 \right] \tag{4.2.4}$$

$$k_r = 9.8692 \cdot 10^{-3} \exp\left(\frac{-97\,782}{T} - 110.1 \ln(T) + 848.1 \right) \tag{4.2.5}$$

$$K_p = 3.142 \cdot 10^{-3} \exp\left(\frac{98\,359}{RT} - 11.24 \right) \tag{4.2.6}$$

The energy balance in terms of temperature (eq. (4.2.7)) is simplified by assuming no technical work, no dosing or removal of components, and negligible influence of the pressure change on the temperature change.

$$\frac{\mathrm{d}T}{\mathrm{d}t} = -\left(a_q \cdot q + \Delta_r H \cdot r \cdot \rho_p \cdot \frac{1-\epsilon}{\epsilon} \right) \frac{M}{\rho \cdot c_p} \tag{4.2.7}$$

A linear mixing rule for the heat capacity is assumed (eq. (4.2.8)) using heat capacity correlations for the individual components (eq. (4.2.9)) obtained from the literature [60].

$$c_p = \sum_{i \in COM} y_i \cdot c_{p,i} \tag{4.2.8}$$

$$c_{p,i} = A_{cp,i} + B_{cp,i} \cdot T + C_{cp,i} \cdot T^2 \tag{4.2.9}$$

Assuming ideal gas behavior, the density is given by eq. (4.2.10).

$$\rho = \sum_{i \in COM} \frac{y_i \cdot M_i \cdot p}{R \cdot T} \tag{4.2.10}$$

For the adiabatic fixed bed (case 1) and polytropic PFTR (case 2) further assumptions considering the heat removal must be made since the heat flux is not an optimization function.

The heat flux is given by eq. (4.2.11) and the bounds for the temperature of the cooling media (in general: environment phase which is responsible for the according flux) are chosen to be $700\,K \leq T_e \leq 740\,K$. The upper limit for T_e is given by the outlet

temperature and the lower limit is chosen in order to limit the temperature gradients. In addition, a tubular geometry for the heat exchanger tubes with a minimum required diameter of $D = 5\,cm$ is considered. The heat transfer coefficient is assumed to be constant with a value of $k = 40\,\frac{W}{m^2K}$. The heat flux is modeled according to eq. (4.2.11) with the specific surface area for the heat exchange of the gas according to eq. (4.2.13) or eq. (4.2.12), respectively.

$$q = k \cdot (T - T_e) \tag{4.2.11}$$

$$a_q = \frac{4}{D \cdot \epsilon} \quad \text{(packed bed)} \tag{4.2.12}$$

$$a_q = \frac{4}{D} \quad \text{(empty tube)} \tag{4.2.13}$$

Optimization problems of level 1

The full optimization problems of case 1 to case 3 are stated in a comprehensive manner (DOP1-1) – (DOP1-3), respectively. In order not to loose track in the multitude of equations, the constraints of the optimization problems on level 1 are grouped into component balances, reaction kinetics, energy balance, transport kinetics, thermodynamic relationships, initial and final conditions, as well as intrinsic bounds.

The adiabatic staged reactor (case 1) consists of three reaction ($s = 1, 3, 5$) and three cooling segments ($s = 2, 4, 6$). The exchange area of the heat exchangers (via an associated tube diameter D), the cooling temperature T_e, and the individual residence time in each segment τ_s are degrees of freedom. Since the heat and reaction flux are not integrated, the component mass balance reduces to $\frac{dX}{d\tau} = 0$ in the cooling sections. In addition, there is no heat flux in the reaction sections and special connectivity equations for X and T must be enforced in the optimization.

$$\text{Obj} = \min_{D, T_e, \tau_s} \tau \tag{DOP1-1}$$

s.t.

Component balances: eq. (4.2.2) for $s = 1, 3, 5$. $\frac{dX}{d\tau} = 0$ for $s = 2, 4, 6$

Reaction kinetics: eq. (4.2.4) – eq. (4.2.6) for $s = 1, 3, 5$

Energy balance: eq. (4.2.7) with $q = 0$ for $s = 1, 3, 5$ and $r = 0$ for $s = 2, 4, 6$

Connectivity equations: $T_{0,s} = T_{f,s-1}$ and $X_{0,s} = X_{f,s-1}$ for $s = 2 - 6$

Transport kinetics: eq. (4.2.11), eq. (4.2.13), $k = 40\,\frac{W}{m^2K}$, $D \geq D^L$, $T_e^L \leq T_e \leq T_e^U$

Thermodynamic properties: eq. (4.2.8) – eq. (4.2.10)

Initial conditions: $y_{i,0,1} = y_{i,0}$, $T_{0,1} = T_0$, $X_{0,1} = 0$

Final conditions: $X_{f,6} \geq 0.95$

Total residence time: $\tau = \sum_{s=1}^{6} \tau_s$

Intrinsic bounds: $T^L \leq T_s \leq T^U$ for $s = 1 - 6$

In case 2, a polytropic reaction system with constant cooling temperature is optimized. The exchange area (via an associated tube diameter) and the cooling temperature are degrees of freedom.

$$\text{Obj} = \min_{D,T_e} \tau \qquad \text{(DOP1-2)}$$

s.t.

Component balance: eq. (4.2.2)

Reaction kinetics: eq. (4.2.4) – eq. (4.2.6)

Energy balance: eq. (4.2.7)

Transport kinetics: eq. (4.2.11) – eq. (4.2.12), $k = 40\ \frac{W}{m^2 K}$, $D \geq D^L$, $T_e^L \leq T_e \leq T_e^U$

Thermodynamic properties: eq. (4.2.8) – eq. (4.2.10)

Initial conditions: $y_i\,(t=0) = y_{i,0}$, $T\,(t=0) = T_0$, $X_0 = 0$

Final conditions: $X_f \geq 0.95$

Intrinsic bounds: $T^L \leq T \leq T^U$

Case 3 refers to the intensified reaction concept with optimal heat flux profile. Since the heat flux profile is not limited, no constraints on the transport kinetics arise. In addition to the heat flux, the inlet temperature can be optimized in order to avoid a temperature jump at the beginning and the numerical problems due to the associated infinite heat flux.

In order to avoid an ill formulated optimization problem, the inlet temperature is only limited by $T^L \leq T_0 \leq T^U$, and thereby the heat flux can be bounded by numerical meaningful values. In principle, the inlet temperature could be regarded as optimization parameter for any reaction concept, but in this example it is assumed that the inlet temperature is fixed. Only for the ideal heat flux case, the inlet temperature is free in order to avoid numerical problems.

$$\text{Obj} = \min_{(a_q \cdot q(t)),T_0} \tau \qquad \text{(DOP1-3)}$$

s.t.

Component balance: eq. (4.2.2)

Reaction kinetics: eq. (4.2.4) – eq. (4.2.6)

Energy balance: eq. (4.2.7)

Thermodynamic properties: eq. (4.2.8) – eq. (4.2.10)

Initial conditions: $y_i\,(t=0) = y_{i,0}$, $X_0 = 0$

Final conditions: $X_f \geq 0.95$

Intrinsic bounds: $T^L \leq T \leq T^U$

Results

In Fig. 4.3 the trajectories of the different reaction concepts are shown in state space representation. The minimum residence time of an adiabatic staged reactor is about

2010 ms, for the polytropic reaction concept with environmental temperature (case 2) 714 ms, and for the intensified reaction concept 591 ms.

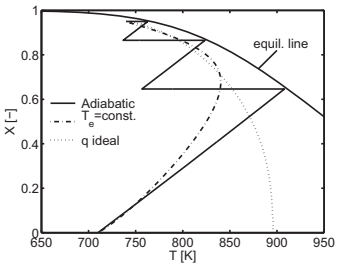

Figure 4.3: Results level 1: State space representation

In case of the staged reaction concept (case 1), the total residence time is composed of 955 ms in the reaction and 1055 ms in the cooling sections. Since a minimal residence time problem is considered, the lower bounds for the cooling temperature and the tube diameter are chosen by the optimizer. A similar design was already proposed by Aris [62], who analyzed the SO_2 oxidation with further simplifying assumptions by analytical methods.

The optimal values for the degrees of freedom of the polytropic reaction concepts (case 2) are $D_{opt} = 5\,cm$ and $T_{e,opt} = 727.9\,K$. The temperature of the environment phase (here, the environment phase is not referred to as cooling phase since the environment phase can also be used to heat the fluid) is above the inlet temperature and the fluid is heated up in the first part of the reactor. The residence time is reduced by 64.5% compared to the optimized technical reference (case 1).

If the heat flux is optimized along the entire reaction coordinate (case 3), the residence time is reduced by 70.6% compared to case 1. This case quantifies the potential of ideal heat flux control. Here, the fluid is directly heated up to the optimal reaction inlet temperature. Afterwards, the optimal temperature trajectory is followed until the outlet temperature is reached.

These results show that integration of cooling and reaction will yield a significant residence time reduction – even for a constant cooling temperature. The perfect control of the heat flux reduces the residence time even further. How this heat flux profile can be obtained is investigated on the second level. In addition, the losses due to limited heat transfer are quantified. At this early point, the methodology indicates which reaction concept is best suited for the reaction system. If the savings by optimizing the heat flux along the reactor are considered to be not sufficient, the investigations can be stopped and the tube bundle reactor with constant cooling temperature can be developed further.

4.2.2 Level 2 – Best control variables

Principle reactor set-up and investigated heat transfer options

On the second level, it is investigated if the desired fluxes are attainable. For this purpose, it is necessary to choose the principle reactor set-up and the associated control variables. This principle reactor set-up determines which transport mechanisms for the desired fluxes exist and how the transport kinetics behave.

Here, a fixed bed reactor with spherical catalyst particles of uniform size is chosen. Cooling and heating is provided by a service phase. For this set-up either the cooling temperature or the tube diameter can be used to control the heat flux.

In the first case considered on level 2 (Fig. 4.2), the temperature of the environment phase is taken as control function while the tube diameter and the initial velocity are optimization parameters. In the second case, the tube diameter is the control function while the temperature of the environment phase and the initial velocity are optimization parameters.

Additional model equations of level 2

On level 2, additional equations describing the transport kinetics of the fluxes and the momentum balance are required.

In packed beds different models can be used to describe the heat transfer resulting from convection and conduction. For this purpose, either a simple one-dimensional model (α-model), a two-dimensional model with one parameter (λ_r-model), or a two-dimensional model with two parameters (λ_r, α-model) are used [63, 64]. The more detailed models describe the radial temperature profile, which cannot be calculated by a one-dimensional model. However, the one-dimensional model can still yield very accurate solutions; for the examples investigated by De Wasch and Froment [63] the mean deviation of the fitted one-dimensional models was only 3.75%.

Since the flow field and the temperature field are still assumed to be ideal on level 2, no radial gradients are considered and hence only the α-model is applicable within the modeling framework of this level. Here, the correlation for the heat transfer obtained from De Wasch and Froment [63] is used (eq. (4.2.18)) since the parameters are fitted for the investigated catalyst system. However, the validity of the model is limited within the stated Re-number range (eq. (4.2.19)).

$$q = k \cdot \Delta T = k \cdot (T - T_e) \tag{4.2.17}$$

$$k = k_0 + 0.024 \frac{\lambda \cdot \mathrm{Re}}{D_p} = k_0 + 0.024 \frac{\lambda \cdot \rho \cdot v_s}{\mu} \tag{4.2.18}$$

$$30 \leq \mathrm{Re} = \frac{\rho \cdot v_s \cdot D_p}{\mu} \leq 1000 \tag{4.2.19}$$

In case of the SO_2 oxidation catalyst, the range for the static contribution of the catalyst packing is approximately $6 \frac{W}{m^2 K} \leq k_0 \leq 16 \frac{W}{m^2 K}$ [63]. For reasons of simplicity, a mean value for the static contribution of $k_0 = 11 \frac{W}{m^2 K}$ is chosen. At typical SO_2 oxidation conditions, the contribution of the Re-term is between $17 \frac{W}{m^2 K}$ and $35 \frac{W}{m^2 K}$. Hence, both terms are important for the modeling of the heat transport coefficient.

The thermal conductivity and viscosity of the gas are assumed to be constant ($\lambda = 0.0476\ \frac{W}{mK}$, $\mu = 3.322 \cdot 10^{-5}\ \frac{kg}{m \cdot s}$). These values are calculated at the inlet conditions using temperature dependent correlations for both the pure component thermal conductivity and viscosity, and the model of Wassiljewa and Wilke, respectively, to calculate the mixture properties [65]. The heat conductivity, the viscosity, and the density influence the heat transfer, but they are not suited to control the heat transfer in this example.

In addition, bounds for the design variables (here: T_e and D) must be chosen on level 2. The bounds for the environment phase temperature are chosen to be $T_e^L = 600\,K$ and $T_e^U = 900\,K$.

For the tube diameter no direct bounds are imposed since the interaction between velocity, particle diameter, and tube diameter is complicated and better to be imposed by indirect bounds. In order to use the heat transfer correlation, bounds for the Re-number must be kept according to eq. (4.2.19). The Re-number depends on the density, velocity, and viscosity of the fluid as well as on the particle diameter. Additionally, a minimal tube-to-particle diameter ratio according to eq. (4.2.20) with a lower value obtained from the literature [66] is defined to limit the effect of bypassing.

$$\frac{D}{D_p} \geq 10 \tag{4.2.20}$$

Eq. (4.2.19) connects the velocity with the particle diameter and eq. (4.2.20) the tube diameter to the particle diameter in certain limits. In addition, an indirect lower bound for the particle diameter in combination with the velocity is given by including the maximum allowed pressure drop. Using these design limits on T_e, D/D_p, Re, Δp and include physical bounds on the tube and particle diameter ($D > 0$, $D_p > 0$) yields a reasonable reactor design.

The upper limit of the catalyst particle diameter is also given by the onset of pore diffusion limitation. This can be considered keeping the Thiele modulus or Damköhler number of the reaction below a certain value at every point along the reaction coordinate as will be shown for the ethylene oxide example in Section 5.3.2.

Instead of solving the rigorous momentum balance, the Ergun equation for spherical particles given by eq. (4.2.21) is used to estimate the pressure drop [67].

$$\frac{\partial p}{\partial z} = -\left(150\frac{\mu\,(1-\epsilon)^2}{D_p^2\epsilon^2} + 1.75\frac{v_s\rho\,(1-\epsilon)}{D_p\epsilon^3}\right)v_s \tag{4.2.21}$$

Under steady state conditions eq. (4.2.22) is used to convert the Ergun equation eq. (4.2.21) into its substantial formulation eq. (4.2.23).

$$\frac{\mathrm{d}p}{\mathrm{d}t} = v_i\frac{\partial p}{\partial z} \tag{4.2.22}$$

$$\frac{\mathrm{d}p}{\mathrm{d}t} = -\left(150\frac{\mu\,(1-\epsilon)^2}{D_p^2\epsilon^3} + 1.75\frac{v_s\rho\,(1-\epsilon)}{D_p\epsilon^3}\right)\frac{v_s^2}{\epsilon} \tag{4.2.23}$$

The velocity for a constant mass flux can be expressed as function of the initial velocity $v_{s,0}$, the cross sectional area, and the fluid density according to eq. (4.2.24). The initial velocity is taken as optimization parameter.

$$v_s = v_{s,0} \frac{A_0}{A} \frac{\rho_0}{\rho} \tag{4.2.24}$$

Optimization problems of level 2

The arising optimization problems of level 2 are summarized in (DOP2). Both investigated cases differ only in the degrees of freedom. In the first case, the environmental temperature is controlled along the entire reaction coordinate as a control function. In addition, the tube diameter, the particle diameter, and the inlet velocity are degrees of freedom ($u = T_e(t), D, D_p, v_{s,0}$). In the second case, the tube diameter is the control function and the environment phase temperature, the particle diameter, and the inlet velocity are additional degrees of freedom ($u = D(t), T_e, D_p, v_{s,0}$).

$$\text{Obj} = \min_u \tau \tag{DOP2}$$

s.t.

Component balance: eq. (4.2.2)

Reaction kinetics: eq. (4.2.4) – eq. (4.2.6)

Energy balance: eq. (4.2.7)

Transport kinetics: eq. (4.2.11) – eq. (4.2.12), eq. (4.2.17) – eq. (4.2.19)

Momentum balances: eq. (4.2.23) – eq. (4.2.24)

Thermodynamic properties: eq. (4.2.8) – eq. (4.2.10)

Initial conditions: $y_i(t=0) = y_{i,0}$, $T(t=0) = T_0$, $p(t=0) = p_0$, $X_0 = 0$

Final conditions: $X_f \geq 0.95$, $p_f \geq 1.5\,bar$

Intrinsic bounds: $T^L \leq T \leq T^U$

Design bounds: $T_e^L \leq T_e(t) \leq T_e^U$, eq. (4.2.20), $D > 0$, $D_p > 0$

Results

Fig. 4.4(a) and Fig. 4.4(b) illustrate the profiles for the temperature of the environment phase and the tube diameter as control functions. In case of the environment phase temperature control, the residence time is 620 ms. In case of the diameter control, the residence time is 677 ms. Both state space trajectories are compared with the ideal case in Fig. 4.4(c).

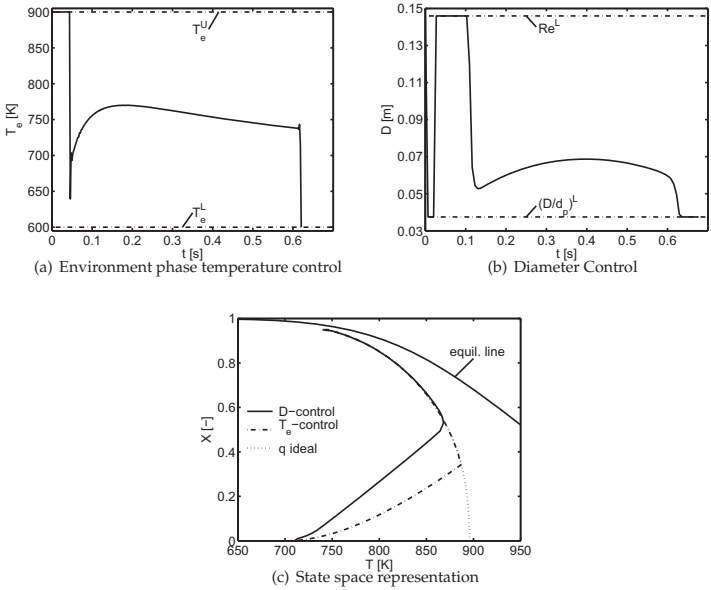

(a) Environment phase temperature control

(b) Diameter Control

(c) State space representation

Figure 4.4: Results level 2

As can be seen in Fig. 4.4(a) the temperature of the environment phase is at its maximum at the beginning of the reaction. As soon as the state space trajectory of the ideal heat flux case is reached (the dash dotted line hits the dotted line in Fig. 4.4(c)), the environment phase temperature switches from heating to cooling. The environment phase temperature jumps to 640 K and then increases to 770 K. Afterwards, it decreases slowly to 736 K. As soon as the required conversion is reached, the environment phase temperature is at its minimum in order to reduce the gas temperature as fast as possible to the required outlet temperature of 740 K. Even though it is hardly visible in Fig. 4.4(c), it should be noted that the outlet temperature is not on the optimal trajectory.

In Fig. 4.4(b) the optimal profile for the tube diameter is shown. The optimum constant temperature of the environment phase is 738 K. For the first finite element the tube diameter is at its maximum before it jumps to its minimum in the second finite element. Since the temperature of the environment phase is above the inlet temperature, the section with the minimal tube diameter heats up the fluid to the environment phase temperature as fast as possible. The boundaries for the minimum and maximum tube and catalyst particle diameter are indirectly defined by the the Re-number range, the pressure drop, and the D/D_p-ratio. Since a tube diameter of 0.0375 m is at the lower limit defined by the minimum D/D_p-ratio, the tube diameter can only be further reduced if the catalyst particle diameter is decreased. In addition, a tube diameter of 0.146 m is at the lower limit of the Re-number constraint. Hence, the tube diameter can only be increased above 0.146 m by raising the initial velocity

further in case of a constant catalyst particle diameter. However, both increasing the inlet velocity and decreasing the catalyst particle add to the pressure drop, which reduces the reaction rate. The negative effect of a lower pressure is more severe than the positive effect of using a larger range for the tube diameter.

As soon as the fluid temperature reaches the environment phase temperature, the diameter jumps to its maximum in order to approximate a quasi adiabatic section. Shortly before the optimal temperature profile is reached (the solid line hits the dotted line in Fig. 4.4(c)), the diameter reduces in order to avoid a temperature overshoot. Afterwards, the diameter follows a specific profile to keep the state space trajectory as optimal as possible. At the end a minimal tube diameter is used to decrease the fluid temperature as fast as possible.

Even for this well known example, the control variable profiles were not known a priori. This underlines the necessity of rigorous optimization for the reactor design instead of using heuristics.

Summing up, it can be observed that for both investigated cases, the desired heat flux profile is not fully attainable. As can be seen from the comparison of the results of level 1 and level 2, an overall potential for further improvement of 29 ms (temperature control case) and 86 ms (diameter control case) exists. The limitations in the flux control can also be observed in the control variable profiles (refer to Fig. 4.4(a) and Fig. 4.4(b)). In case the environment phase temperature is controlled, the temperature for heating up at the beginning and the temperature for cooling down at the end limit the heat flux. In case the tube diameter is controlled, limitations by the minimum Re-number and the minimum D/D_p-ratio become active at some points.

Both set-ups can be further intensified by increasing the range of the design bounds. For example, this can be done by allowing a lower cooling temperature at the end of the temperature control case or by using a different catalyst support geometry which does not impose a bound on the D/D_p-ratio in case of the diameter control. Such a shift of the constraints comes along with applying different principle reactor set-ups and service phases. In order to determine which constraints are most worthwhile to be shifted, a sensitivity analysis can be used.

Since the overall potential for further improvement is small (less than 5% if the environment phase temperature is controlled), it can be concluded that the chosen principle reactor set-up, the catalyst support geometry, and environment phase temperature as control function are suited to approximate the ideal heat flux profile. Hence, different principle reactor set-ups and catalyst support geometries are not investigated in this example. Since controlling the environment phase temperature yields a much better objective function value than controlling the tube diameter, only the former case is further investigated on the third level.

4.2.3 Level 3 – Technical approximation

Derivation of a technical approximation

Based on the results of level 2, three reactor segments with different cooling strategies seem to be well suited to approximate the optimal environment phase temperature profile (refer to Fig. 4.4(a)). In the first segment, a constant maximum temperature of the environment phase is optimal. In the second segment, a cooling temperature

which increases along the path of the fluid element is required. This can be realized with a co-current heat exchanger. The third segment can be approximated either by constant cooling temperature or by slightly decreasing cooling temperature. The former can be realized by an evaporating fluid and the latter by a counter-current heat exchanger.

For the simplicity of manufacturing, the number of tubes is the same in all segments and only one tube diameter D and one catalyst particle diameter D_p for all segments are used as optimization parameters.

On level 3, a simple model is used first to investigate if the chosen technical reactor can approximate the desired control variable profiles. Afterwards, more detailed models such as a two-dimensional reactor model can be applied to further investigate the chosen reactor set-up as it will be done for the ethylene oxide process in Section 5.3.3.

Model equations of level 3

Since a continuously operated reactor is chosen, the local form of the balance equations is used on level 3. This allows to directly determine the dimensions of the reactor and to be able to investigate non-idealities in the flow, temperature, and concentration fields.

The balance for the conversion, the energy balance, and the pressure drop equation are given under steady state conditions by eq. (4.2.26) – eq. (4.2.28). Here, s is the segment index ($s = 1, 2, 3$) for the chosen technical approximation.

$$\frac{\mathrm{d}X_s}{\mathrm{d}z_s} = \frac{r_s \cdot \rho_p \cdot R \cdot T_s \cdot (1-\epsilon)}{(p \cdot v_s)_s} \cdot \left(\frac{1}{y_{SO_2,0}} - \frac{1}{2} X_s \right) \tag{4.2.26}$$

$$\frac{\mathrm{d}T_s}{\mathrm{d}z_s} = -\left(\frac{4}{D} \cdot q_s + \Delta_r H \cdot r_s \cdot \rho_p \cdot (1-\epsilon) \right) \frac{M_s}{(\rho \cdot c_p \cdot v_s)_s} \tag{4.2.27}$$

$$\frac{\mathrm{d}p_s}{\mathrm{d}z_s} = -\left(150 \frac{\mu (1-\epsilon)^2}{D_p^2 \epsilon^2} + 1.75 \frac{(v_s \rho)_s (1-\epsilon)}{D_p \epsilon^3} \right) v_{s,s} \tag{4.2.28}$$

The overall residence time is described by using eq. (4.2.29).

$$\tau = \sum_{s=1}^{3} \int_0^{L_s} \frac{\epsilon}{v_{s,s}} \mathrm{d}z_s \tag{4.2.29}$$

The co- and counter-current heat exchangers are modeled using a simplified energy balance for the cooling (heating) shell. It is assumed that the flow of the environment fluid is constant in each individual segment. In addition, constant density, no axial diffusion of heat and mass, no radial gradients, constant pressure, no evaporation, no reaction, no technical work, constant heat capacity, and steady state operation for the environment fluid are assumed. The energy balance of the environment phase is reduced to a one-dimensional energy balance in terms of temperature using the above simplifications and by introducing the cross sectional area of the environment channel A_e.

$$\frac{\left(v_{i,e} \cdot \rho_e \cdot c_{p,e}\right)_s}{M_e} \frac{\mathrm{d}T_{e,s}}{\mathrm{d}z_s} = q_s \frac{\pi \cdot D}{A_{e,s}} \tag{4.2.30}$$

The energy balance for the environment phase is further simplified by merging all constants into a heat capacity constant K_e according to eq. (4.2.31).

$$K_{e,s} = \frac{\pi \cdot D \cdot M_e}{\left(A_e \cdot v_{i,e} \cdot \rho_e \cdot c_{p,e}\right)_s} \tag{4.2.31}$$

$$\frac{\mathrm{d}T_{e,s}}{\mathrm{d}z} = K_{e,s} \cdot q_s \tag{4.2.32}$$

Eq. (4.2.32) is used to describe co-current cooling (i.e. $K_e > 0$), counter-current cooling (i.e. $K_e < 0$), and cooling at constant temperature (i.e. $K_e = 0$) without defining the type of cooling in each segment a priori. The design bounds for the heat capacity constant arise from the properties and the flow rate of the chosen cooling/heating media. Without specifying further design details of the shell and the cooling/heating media, the limits of the heat capacity constant are chosen according to eq. (4.2.33).

$$-1 \frac{m \cdot K}{W} \leq K_e \leq 1 \frac{m \cdot K}{W} \tag{4.2.33}$$

Optimization problem of level 3

The optimization problem of level 3 is summarized in (DOP3). Of course, the balance equations as well as the intrinsic and design bounds apply in all segments and connectivity equations for X, T, and p need to be specified. The degrees of freedom of this problem are the coolant constant in each segment $K_{e,s}$, the inlet temperature of cooling media in each segment $T_{e,s,0}$, the length of each segment L_s, the tube diameter D, the particle diameter D_p, and the inlet velocity $v_{s,0}$.

Due to the additional balance equations for the service phase, the degrees of freedom of the optimization problem are reduced and no flux or design variable profiles, i.e. control function, can be optimized anymore. Only the design variables arising from the chosen technical approximation are degrees of freedom giving rise to a parameter optimization problem.

$$\text{Obj} = \min_{K_{e,s}, T_{e,s,0}, L_s, D, D_p, v_{s,0}} \tau \tag{DOP3}$$

s.t.

Component balances: eq. (4.2.26)

Reaction kinetics: eq. (4.2.4) – eq. (4.2.6)

Energy balances: eq. (4.2.27)

Transport kinetics: eq. (4.2.12), eq. (4.2.17) – eq. (4.2.19)

Momentum balances: eq. (4.2.28), eq. (4.2.24)

Connectivity equations: $X_{0,s} = X_{f,s-1}$, $T_{0,s} = T_{f,s-1}$, $p_{0,s} = p_{f,s-1}$ for $s = 2, 3$

Initial conditions: $y_{i,0,1} = y_{i,0}$, $T_{0,1} = T_0$, $p_{0,1} = p_0$, $X_{0,1} = 0$

Final conditions: $X_{f,3} \geq 0.95$, $p_{f,3} \geq 1.5\,bar$

Total residence time: eq. (4.2.29)

Intrinsic bounds: $T^L \leq T_s \leq T^U$

Design bounds: $K_e^L \leq K_e \leq K_e^U$, $T_e^L \leq T_{e,s,0} \leq T_e^U$, eq. (4.2.20), $D > 0$, $D_p > 0$

Results

A design drawing of the technical approximation with the optimal values for the heat capacity constant of each segment and the according inlet and outlet temperatures is shown in Fig. 4.5.

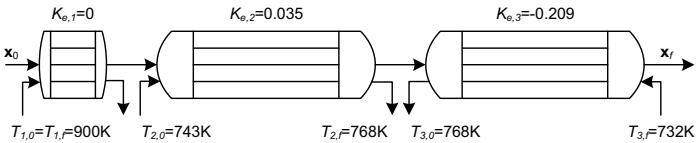

Figure 4.5: Technical approximation of the optimal process route

The total length of the reactor is $0.83\,m$ with a total residence time of $623\,ms$. This is a reduction of 69% compared to the optimized reference case. In addition, the losses due to the technical approximation of the environment phase temperature profile (determined by comparing the results of level 2 and level 3) are merely $3\,ms$.

By examining the environment phase temperature profile of level 3 (Fig. 4.6(a)) and the state space representation of level 1 to level 3 (Fig. 4.6(b)), one can conclude that the technical approximation is well suited to approximate the optimal reaction route.

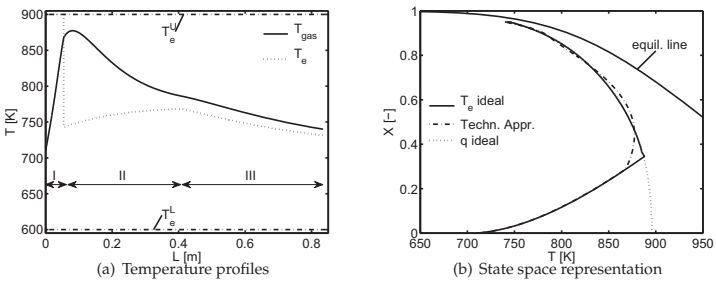

(a) Temperature profiles (b) State space representation

Figure 4.6: Results level 3

4.3 Summary

In this chapter, the developed reactor design method was exemplified by the SO_2 oxidation. The example and the objective function were chosen in order to demonstrate

the methodological approach. Furthermore, this reaction represents the important class of exothermic equilibrium reactions and the results can be qualitatively projected to other processes.

Within this example, all three levels for the design of an optimal technical SO_2 oxidation reactor were presented. For the sake of clarity, the investigated process intensification options were limited and some assumptions were made.

On the first level, different integration and enhancement concepts with respect to the heat and reaction flux were compared. The concept of adiabatic reaction with intermediate cooling was chosen as the technical reference case. As advanced cases, integrated reaction with cooling at a constant cooling temperature and an intensified reaction concept, where the heat flux is ideally controlled, were investigated. Here, the intensified reaction concept with the ideal heat flux profile showed a potential of reducing the residence time of about 70.6% compared to the optimized technical concept.

On level 2, it was investigated if the desired heat flux profile is attainable. It was chosen that cooling is achieved by a service phase (separated from the reacting phase with respect to mass exchange). The heat flux was controlled either by an environment phase temperature profile or by controlling the tube diameter. In addition, a packed bed of uniform sized catalyst particles was chosen as catalyst support. Both concepts for controlling the heat flux cannot realize the ideal heat flux profile and hence suffer losses due to limitations in the design variables. It was discussed that the bounds on the design variables can be shifted by further process intensification. In case of controlling the environment phase temperature, the increase in residence time was small compared to the ideal flux case investigated on level 1. Therefore, no further principle reactor set-ups such as micro reactors were investigated and this case was chosen for a technical approximation.

Based on the optimal control variable profile of level 2, a technical approximation of this profile was developed on the third level of the design approach. Here, the reactor is staged in three segments each applying a different cooling strategy. This technical approximation proved to approximate the optimal temperature profile very well – the losses due to a non-ideal T_e-profile were only $3\,ms$. In addition, such a technical approximation is possible by clever combination of existing apparatuses and gives rise to a new reactor set-up for the SO_2 oxidation, which reduces the residence time compared to an optimized technical reference by 69%.

In general, it was shown that the method yields innovative technical reactors. In the case of the SO_2 oxidation, an appropriate combination of existing apparatuses seems to be well suited to obtain a good technical approximation.

Chapter 5
Ethylene oxide synthesis

The production of ethylene oxide (EO) is one of the most important partial oxidation reactions in the chemical industry. Due to the large annual production rate (estimated worldwide capacity of about 19 million tons in 2010 [68]), cost efficient production is very important and even small process improvements have a big impact on the economics of the process. Since the costs for ethylene dominate the production costs, a high efficiency in the reactor gives rise to major process improvements. In addition, the EO process is a main producer of CO_2 in the chemical industry due to the undesired total combustion of ethylene (E) in the reactor. Hence, the CO_2 emissions of the EO production may also be significantly reduced by a better reaction concept giving rise to a more sustainable process.

At the beginning of the chapter, a general introduction to the ethylene oxide process technology is given and process intensification aspects for EO reactors are discussed. In Section 5.3, an optimal reactor for the air based process is derived using the proposed design methodology [69]. Here, all design levels of the approach are executed with special focus on the screening level 1, choosing a suitable catalyst support geometry by considering reactor design criteria on level 2, and on the validation of the technical approximation using detailed models on level 3.

In Section 5.4, the reactor design method is extended towards the simultaneous identification of the best reaction concept and optimization of the plant operation exemplified on the oxygen based EO process [70]. Here, the interaction between the reaction module and the process are rigorously taken into account by modeling the complete process and by applying the design approach to the reaction module. Thereby, the impact of the optimized reaction concept on the overall process performance is determined. In case a recycle exists in the process, the reactor design and best reaction concept are not independent of the downstream process, and therefore the coupled problem of reactor design and downstream process operation needs to be solved.

In Section 5.5, a short summary of both ethylene oxide processes is given with special focus on the methodological and modeling aspects considered in this chapter.

5.1 General process description

The reaction network of the silver catalyzed ethylene oxide production by partial oxidation of ethylene is shown in Fig. 5.1. It consists of the desired partial oxidation of ethylene to ethylene oxide (reaction 1), the total oxidation of ethylene to carbon diox-

ide (reaction 2), and the consecutive oxidation of EO to carbon dioxide (reaction 3). The total oxidation is the main heat producer in the reactor and hence a high selectivity simplifies the heat removal from the reactor and helps to avoid the formation of a hot spot.

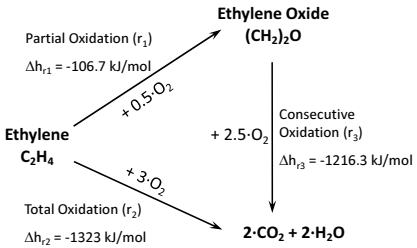

Figure 5.1: Simplified macroscopic reaction scheme of the EO synthesis

Usually, ethylene is oxidized over a promoted Ag-catalyst either using air or pure oxygen. The air based process operates at lower ethylene and oxygen concentrations but at higher conversion (refer to Tab. 5.1).

Table 5.1: Operation parameters of both the air and oxygen based ethylene oxide process [71]

Parameter	Air based process	Oxygen based process
Composition $[vol.-\%]$		
Ethylene	$2-10$	$15-40$
Oxygen	$4-8$	$5-9$
Carbon dioxide	$5-10$	$5-15$
Methane		$1-60$
Ethane	$0-1$	$0-2$
Argon		$5-15$
Temperature $[K]$	$493-550$	$493-548$
Pressure $[bar]$	$10-30$	$10-22$
GHSV $[h^{-1}]$	$2000-4500$	$2000-4000$
Pressure drop $[kPa]$	$40-200$	not stated
Ethylene conversion $[\%]$	$20-65$	$7-15$
Selectivity $[\%]$	80	$80-90$

In addition to the different process technologies, different types of Ag-catalysts can be used. So far, the development of promoted catalysts focused on selectivity rather than activity.

In both processes, tube bundle reactors with a constant cooling temperature are commonly used. Due to explosion hazards, the E, O_2, and EO concentrations as well as the conversion are limited. In addition, the used reactor types cannot provide optimal component concentration and temperature profiles along the reactor length.

This may give rise to problems with an axial hot spot and the depletion of reactants along the channel, which results in a lower reactor productivity.

The different operation regions of the air and oxygen based process are shown in Fig. 5.2. This change in the operation conditions is also an interesting process intensification option, which may lead to higher selectivities and space time yields (STY) in the reactor.

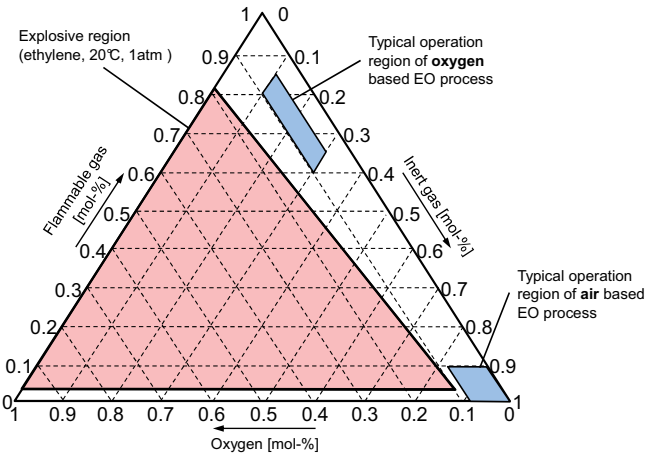

Figure 5.2: Explosive region and typical operation window

In this figure, the explosive region of ethylene is qualitatively given. In general, the explosive region of the mixture depends on the composition, temperature, and pressure. It can be noticed that the oxygen based process operates in the oxygen limited region (rich mixture, above the upper explosion limit (UEL)). In the air based process, the gas mixture is limited by an upper value for the oxygen and the ethylene mole fraction. Thereby, the process operates mostly in lean mixture regime (below the lower explosion limit (LEL)).

Considering the explosion limits during the reaction is of major importance for the process safety. Several explosions of EO plants are reported in the literature (e.g. [72]). Even though most of these explosions occurred in the ethylene oxide purification steps, the reactor might be subject to explosion, and therefore the reaction mixture must never lie in the explosive region.

5.2 Process intensification aspects for ethylene oxide reactors

In order to increase the selectivity of the EO reactor, many experimental and theoretical studies were performed. The selectivity depends on the temperature, pressure, concentration of all components, the catalyst composition, and 1,2-dichloroethane (DCE) which is added to the feed as a promoter.

Different process intensification methods such as membrane reactors or micro reactors were successfully demonstrated for the EO production process in order to increase the reactor selectivity.

The influence of different dosing options for the air based process was experimentally studied by Lafarga et al. [73] using a fixed bed membrane reactor. In their study, distributed dosing of ethylene via a membrane increased the selectivity compared to the performance of a classical fixed bed reactor, while distributed dosing of oxygen decreased the selectivity. However, the obtained selectivities of up to 67% do not reach the selectivities of the industrial processes, probably due to the use of an unpromoted catalyst. These results indicate that concentration manipulation inside the reactor is important for the selectivity. However, the results are specific for the catalyst system and the amount of converted ethylene differs in all three investigated cases.

Dautzenberg and Mukherjee [8] proposed a catalytic membrane reactor for the EO synthesis. Within this reactor set-up, the catalyst is located within the membrane and ethylene and O_2 are supplied at different sides of the membrane. Thereby, the reaction can be performed at higher ethylene and oxygen concentrations which are not possible in the conventional process due to the explosion hazard. However, the set-up was not investigated experimentally or by simulation for the ethylene oxide production. Hence, problems arising from cross diffusion or limited cooling are not yet solved. In addition, the reaction rate laws of the ethylene oxide synthesis are not known for this concentration region (even though a conventional catalyst is used). Hence, no proof of principle either by experiment or by simulation was performed so far. Furthermore, the economics of such a reactor set-up may suffer from a small STY. However, the idea of integrated reaction and separation is of major importance for process intensification and it was shown for other reactions (e.g. dehydrogenation of ethylbenzene [74]) that catalytic wall reactors can have superior performance compared to standard reactors.

In order to investigate the potential of micro reactors for the EO process, Kestenbaum et al. [75] constructed several micro reactors and compared their performance to the industrial EO reactors. The ethylene inlet concentration was lower, while the oxygen concentration was increased in the micro reactors compared to the industrial process. The space time yield was in the same range or higher for some channel geometries and the conversion was also in the same range compared to the industrial process. However, the selectivity – which is the major factor for the economics of any EO plant – was always less than 69%, and hence the micro reactors with the used catalyst were not competitive to the industrial process.

An important aspect when using micro reactors is that the reaction mixture can lie in the explosive region, which may allow for higher ethylene and oxygen inlet and higher EO outlet concentrations. Increasing the EO outlet concentration can improve

the productivity of the plant. However, in the connecting pipes the composition will also be in the explosive region and hence such a reactor will require additional safety measures in the plant. In addition, even in a micro reactor the maximum safe diameter might be exceeded as shown by Fischer et al. [76]. Therefore, the gas mixture must never be within the explosive region for the EO process.

Besides these approaches to design new micro or membrane reactors or to enhance the performance of existing EO reactors, Berndt and Bräsel [77] worked on a completely new reaction route. Here, the epoxidation of olefins is performed using ozone in the gas phase. This concept features extremely low residence times ($8\,ms - 38\,ms$) and a selectivity of about 90 % for $C_2 - C_6$ olefins. A major disadvantage of the concept is that the reaction is performed at a pressure of $0.25\,bar$ and requires ozone as oxidizing agent.

Lee et al. [68] presented a concept for the EO production based on gas-expanded liquids similar to the HPPO process. Here, EO is produced in the liquid phase, which enables a better control of the explosive region of the gas and allows a higher ethylene conversion. For this reaction concept, hydrogen peroxide is required as oxidizing agent and the economic efficiency is not yet known.

To sum up, selectivity optimization for the EO reactor is of major industrial importance. Different trends for temperature, pressure, and component concentrations on the selectivity can be observed depending on the used catalyst. As shown by various authors, process intensification concepts such as membrane reactors or micro reactors seem to be an interesting option for the production of EO. However, no study was performed which considers all PI measures in a systematic manner. Hence, it can be concluded that the question on how an optimal EO reactor has to be designed and what would be the benefit compared to the standard design has not yet been answered satisfactorily.

Therefore, it is intended to design an optimal EO reactor for the air based process with respect to the selectivity taking component dosing and removal concepts, advanced temperature control, the dimensioning of specific exchange areas for heat and mass transport, the choice of catalyst, and the choice of the catalyst packing into account. Compared to the SO_2 oxidation, this example demonstrates successfully the extension of the reactor design methodology to a selectivity problem taking more advanced process intensification options, more complex thermodynamic relationships, and reactor design criteria on level 2 into account.

In addition, the shift to a different operation region is investigated by considering also the oxygen based process. Here, the method is extended to simultaneously determining the optimal reaction concept and optimizing the process operation.

5.3 Air based EO process – Optimal reactor design

Catalyst selection

Before the best reaction concept for the air based EO process can be derived a suitable catalyst must be chosen. The choice of the catalyst has a major influence on the performance of the reaction system and determines how the selectivity changes with temperature, pressure, and concentration of reactants and reaction products. The catalyst is selected mainly based on its selectivity, activity, and on the experimental conditions for which the reaction rate laws are determined.

Under industrial conditions the consecutive oxidation of EO is usually much slower than r_1 and r_2. The measurements of Mueller and Walters [78] indicate that the homogeneous decomposition of EO at reaction conditions can be neglected. The heterogeneously catalyzed consecutive oxidation of EO is also assumed to be much slower than the formation of EO. Hence, most authors fit their data to a simplified reaction network consisting of r_1 and r_2. Since r_3 and r_2 are hard to determine independently by conventional kinetic measurements, the consecutive oxidation of EO r_3 is lumped into r_2 using this approach.

From the many investigated catalysts for the EO process, the kinetics published by Petrov et al. [79], Stoukides et al. [80], Al-Saleh et al. [81], Borman and Westerterp [82], Schouten et al. [83], and Lafarga et al. [84] are compared in order to identify the best catalyst from this selection (refer to Fig. 5.3). The temperature range for this comparison and for the reactor design task are chosen a bit higher compared to the values stated in Tab. 5.1 in order to ensure a reasonable STY later.

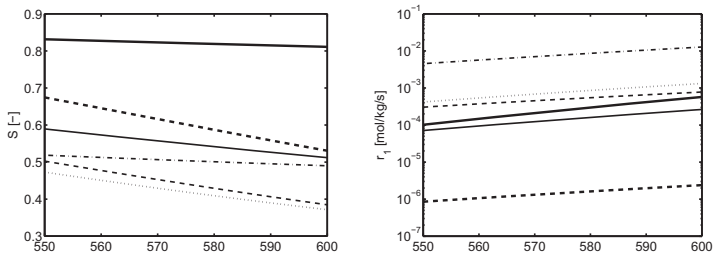

(a) Differential selectivity (b) Reaction rate r_1

Figure 5.3: Catalyst comparison (Al-Saleh et al. 1988 [81]: ——, Stoukides and Pavlou 1986 [80]: – –, Borman and Westerterp 1995 [82] (model 2 including long time deactivation factors): ——, Lafarga et al. 2000 [84]: · · · ·, Schouten et al. 1996 [83] (model 3, tubular reactor): — —, Petrov et al. 1986 [79]: – · –).

For all of the investigated catalysts, the ethylene and oxygen partial pressure are considered as the driving forces for the reactions, sometimes with different reaction orders depending if molecular or atomic oxygen is assumed to be the oxidizing agent. However, the components considered in the adsorption term vary in all the publications. The influence of the components on the selectivity and the qualitative trends are also different.

The selectivities of the investigated systems are quite different and also the reaction rates (only r_1 shown) vary strongly. The comparison is performed at typical inlet conditions for the component partial pressures ($p_E = p_{O_2} = p_{CO_2} = 1.5\,bar$, $p_{EO} = p_{H_2O} = 0\,bar$) and a wide temperature range. The qualitative trends and the differences between the various reaction rates are similar for other operating conditions.

Since a selective production of ethylene oxide is most important, the selectivity is the major decision criterion. Referring to the comparison shown in Fig. 5.3 the catalyst of Al-Saleh et al. [81] shows by far the highest selectivity and therefore this catalyst is chosen.

5.3.1 Level 1: Optimal integration and enhancement concept

First, each investigated integration and enhancement concept is explained. Each case is a dynamic optimization problem, where the optimal route in state space with respect to the integrated and enhanced fluxes is determined in order to maximize the selectivity. Afterwards, the required model equations are presented and the arising optimization problems are stated. At the end of this section, the results of level 1 are discussed and a promising reaction concept is identified.

On the first level, the potential of different integration and enhancement concepts is investigated. For this purpose, a reference case must be specified, which is a tube bundle reactor with constant cooling temperature as used in the industrial process. For the investigated catalyst, the temperature profile in the reactor for a constant cooling temperature is nearly uniform since the selectivity is high (as discussed in Section 5.1) and the reaction rates are relatively low. Hence, the temperature and pressure for a fluid element with fixed inlet composition ($y_E = y_{O_2} = y_{CO_2} = 0.075$, $y_{EO} = y_{H_2O} = 0$) are directly optimized. The inlet mole fractions are the mean values of the industrial process range [71]. For this study, a STY of 0.27 $\frac{mol}{m^3 s}$ within a residence time of $30\,s$ for all investigated reaction concepts is chosen. Specifying the STY and the residence time is better suited than comparing different integration concepts for a fixed conversion since the amount of reactants can vary depending on the initial composition and on the dosing of reactants. The optimal operation parameters for the reference reactor are $T = 625.7\,K$ and $p = 20\,bar$, which is the upper limit for the pressure. With this reactor a selectivity of up to 79.10% can be achieved.

Investigated integration and enhancement concepts

For the EO production process, controlling the heat flux and applying dosing and removal strategies are of great interest to increase the EO selectivity. The different integration and enhancement concepts which are investigated are shown in Fig. 5.4. Here, all investigated cases from level 1 to level 3 are shown. In all cases the inlet composition and the system pressure are degrees of freedom for the optimization. All investigated cases are referred to as intensified air based processes even though ethylene or oxygen is dosed individually to the reaction mixture since the concentration range, the inert gas, the conversion, and the space time yield are chosen in the range of the industrial air based process. Enrichment in oxygen (assist oxygen) is an important process intensification option in oder to enhance processes for which air is used as oxidizing agent.

For safety reasons, the ethylene and oxygen concentration must not exceed the explosion limit. From the technical range of the ethylene and oxygen concentrations given in Tab. 5.1 simplified upper boundaries for ethylene and oxygen mole fractions are derived, which are in good agreement with the explosive region indicated in Fig. 5.2. The concentration limit of each component is considered as an intrinsic bound and hence considered directly on level 1 (and all subsequent levels) in the followed approach.

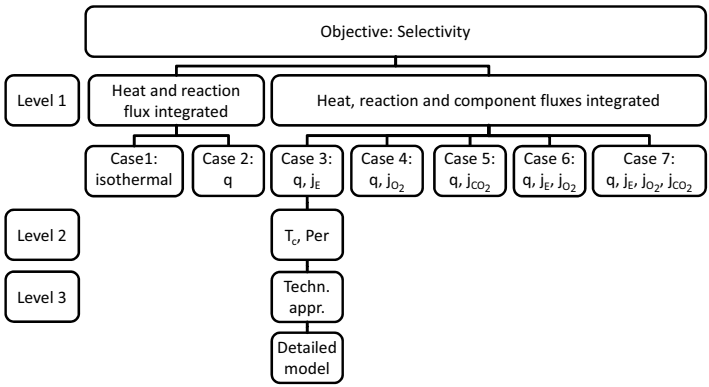

Figure 5.4: Decision structure for the development of an optimal EO reactor

Case 1: Optimized inlet composition, isothermal. This case is similar to the reference case except that the inlet composition is optimized. This does not affect the reactor itself. However, the technical process must be adjusted to meet the optimal inlet conditions and hence this case is regarded as an intensified concept.

Case 2: Inlet composition and heat flux optimized (q). In addition to the optimization parameters of case 1, the heat flux is adjusted along the reaction coordinate in order to obtain an optimal temperature profile. This case yields the potential of an advanced heat flux profile.

Case 3: Inlet composition, heat and ethylene flux optimized (q, j_E). Besides the optimal heat flux profile, an optimal ethylene dosing profile is calculated. This case quantifies the potential of an advanced heat flux profile combined with an ethylene dosing strategy.

Case 4: Inlet composition, heat and oxygen flux optimized (q, j_{O_2}). This case is similar to case 3, but here an optimal oxygen dosing strategy instead of an ethylene dosing strategy is applied.

Case 5: Inlet composition, heat and CO_2 flux optimized (q, j_{CO_2}). Here, an optimal removal strategy for CO_2 is calculated combined with an advanced heat flux

profile. Although CO_2 in principle reduces both reaction rates owing to the adsorption term, the CO_2 partial pressure has a large influence on the selectivity in case the STY is fixed. Due to the STY constraint the reaction temperature must be increased in case of a higher CO_2 partial pressure. This reduces the selectivity due to the higher activation energy of r_2 compared to r_1.
Other removal strategies will not be investigated in this contribution, even though the in situ removal of EO is of great interest, since the consecutive oxidation of EO and the downstream absorption can be avoided. The influence of the EO removal on the selectivity cannot be investigated with the chosen reaction rate laws [81] since EO does not affect r_1 and r_2, and r_3 was neither observed nor determined for this catalyst. The removal of CO_2 can be considered as a general show case to exemplify the proposed methodology for product removal.

Case 6: Inlet composition, heat, ethylene, and oxygen flux optimized (q, j_E, j_{O_2}). This case investigates the potential of an optimal ethylene and oxygen dosing strategy combined with an optimal heat flux profile.

Case 7: Inlet composition, heat, ethylene, oxygen, and CO_2 flux optimized (q, j_E, j_{O_2}, j_{CO_2}). Heat, ethylene, oxygen, and CO_2 flux are optimized in addition to the inlet composition for this case. This concept yields an upper bound for all intensified reaction concepts since all factors influencing the reaction rates, namely the mole fractions of E, O_2, CO_2, the pressure, and the temperature, are optimally manipulated. All degrees of freedom of case 1 to case 6 are included in this case. Nevertheless, case 1 to case 6 are of great interest since it may be sufficient to influence only a certain set of the mole fractions in addition to the temperature. Hence, the potential of each set must be known in order to decide which concept should be further investigated. In addition, the results of this case answer the question whether a reactor with CSTR characteristics can approximate the optimal profiles.

In principle, optimal pressure profiles and apparent catalyst density profiles, which can be obtained by catalyst dilution or by realizing different void fractions using different catalyst packings, are of interest for the optimal reactor design. In case of EO, the optimal pressure is always at the upper boundary since a high pressure helps to fulfill the required STY and increases the selectivity. In addition, the apparent catalyst density is also always at its upper limit specified by the lower limit for the void fraction since the heat flux can be ideally controlled, and hence a high catalyst density helps to fulfill the required STY.

Model equations of level 1

The component mole balance for every component is given by eq. (5.3.1).

$$\frac{\mathrm{d}n_i}{\mathrm{d}t} = s_i \cdot j_{tot} + \rho_p \cdot \frac{1-\epsilon}{\epsilon} \cdot V_g \cdot \sum_{j \in RE} \nu_{i,j} \cdot r_j \tag{5.3.1}$$

The case selection variables s_i are used in order to obtain a comprehensive and clear representation in the balance equation. The value of s_i depends on the investigated case explained before, and it can either be zero if the flux is not considered or one if the flux is considered as optimization function.

The void fraction depends on the catalyst packing and may vary in a wide range depending on the type and shape of the catalyst support. On the first level a constant void fraction is assumed ($\epsilon = 0.4$). The chosen value represents a typical technical void fraction in case of a randomly packed bed with uniform spheres.

The reaction rates [81] along with the reaction rate constants and adsorption constants are given by eq. (5.3.2) – eq. (5.3.4) and the parameters are summarized in Tab. 5.2. In order to apply this catalyst in the design approach, the CO_2 mole fraction of the reactor must be limited by a lower bound (here: $y^L_{CO_2} = 0.05$). Otherwise, the model is not reliable and the extrapolation error might become large due to the high sensitivity of the reaction rates towards low CO_2 mole fractions.

$$r_j = \frac{k_j p_E^{n_{E,j}} p_{O_2}^{n_{O_2,j}}}{1 + K_j p_{CO_2}} \quad j = 1,2 \tag{5.3.2}$$

$$k_j = k_{0,j} \exp\left(-\frac{E_{A,j}}{RT}\right) \quad j = 1,2 \tag{5.3.3}$$

$$K_j = K_{0,j} \exp\left(\frac{T_{ads,j}}{T}\right) \quad j = 1,2 \tag{5.3.4}$$

Table 5.2: Model parameters of the reaction rates [81]

Parameter	Reaction 1	Reaction 2
$k_{0,j}$	$6.275 \cdot 10^6 \left[\frac{mol}{kg_{cat} \cdot s \cdot Pa^{1.1}}\right]$	$1.206 \cdot 10^7 \left[\frac{mol}{kg_{cat} \cdot s \cdot Pa}\right]$
$E_{A,j}$	$74.9 \left[\frac{kJ}{mol}\right]$	$89.8 \left[\frac{kJ}{mol}\right]$
$n_{E,j}$	0.6	0.5
$n_{O_2,j}$	0.5	0.5
$K_{0,j}$	$1.985 \cdot 10^2 \left[Pa^{-1}\right]$	$1.08 \cdot 10^2 \left[Pa^{-1}\right]$
$T_{ads,j}$	2400 $[K]$	1530 $[K]$

The energy balance is written in terms of temperature and is simplified by assuming no technical work, negligible influence of the pressure change and of the dosed components on the temperature change (refer to eq. (5.3.5)). The heat flux into and out of the fluid element q_{tot} is the total heat flux. While the second term on the right hand side is bounded, q_{tot} is assumed to be an unrestricted control function. Hence, every temperature profile can be obtained on level 1 and the temperature profile can directly be taken as an optimization function without solving the energy balance on this level.

$$(n \cdot c_p) \cdot \frac{\mathrm{d}T}{\mathrm{d}t} = -\left(q_{tot} + V_g \cdot \rho_p \cdot \frac{1-\epsilon}{\epsilon} \cdot \sum_{i \in COM} \left(h_i \sum_{j \in RE} \nu_{i,j} \cdot r_j\right)\right) \tag{5.3.5}$$

The gas volume is described by the ideal gas law. This yields the total gas volume and the components partial pressures using the definition for the total amount of substance and the component mole fractions.

$$V_g = \frac{n \cdot R \cdot T}{p} \tag{5.3.6}$$

$$p_i = y_i \cdot p \tag{5.3.7}$$

$$n = \sum_{i \in COM} n_i \tag{5.3.8}$$

$$y_i = \frac{n_i}{n} \tag{5.3.9}$$

The initial conditions are chosen to be in the typical range for the air based ethylene oxide process according to Tab. 5.3. In addition to E, O_2, CO_2, and N_2, some small amounts of EO, H_2O, and CH_4 are present. The upper and lower mole fraction of each component used for the optimization are also given in Tab. 5.3. The inlet mole fractions of E, O_2, and CO_2, as well as the inlet pressure, and the inlet temperature are optimization variables in all calculations. Due to numerical reasons during the optimization calculations, a lower limit on the ethylene and oxygen mole fraction has to be assigned. The inlet mole fractions of EO and H_2O are set to zero and the inlet mole fraction of the N_2 is calculated from the summation constraint.

Table 5.3: Limits for the mole fractions used for optimization, and typical inlet conditions of the air based process [71]

Component	y^L	y^U	**typical inlet conditions** $[vol.-\%]$
E	10^{-5}	0.1	2 – 10
O_2	10^{-5}	0.08	4 – 8
EO	0	0.1	≈ 0
CO_2	0.05	0.1	5 – 10
H_2O	0	0.1	≈ 0
N_2	0	1	72 – 89

The space time yield is related to the catalytic channel and is given by eq. (5.3.10).

$$\mathrm{STY} = \frac{n_{\mathrm{EO},f} - n_{\mathrm{EO},0}}{\int_{t_0}^{t_f} \frac{V_g}{\epsilon} \mathrm{d}t} = 0.27 \, \frac{mol}{m^3 \mathrm{s}} \tag{5.3.10}$$

A general formulation of the selectivity considering ethylene dosing is used as objective function (eq. (5.3.11)).

$$S = \frac{n_{\mathrm{EO},f} - n_{\mathrm{EO},0}}{\left(n_{\mathrm{E},0} + \int_{t_0}^{t_f} j_{tot,\mathrm{E}} \mathrm{d}t \right) - n_{\mathrm{E},f}} \tag{5.3.11}$$

Optimization problems of level 1

The full optimization problems which must be solved on level 1 are stated in (DOP1). In order to compare the cases stated above in a comprehensive manner, the optimization functions, the optimization parameters (together referred to as degree of freedom (DoF)), and the integrated component fluxes are summarized in Tab. 5.4.

$$\text{Obj} = \max_{\text{DoF}} S \tag{DOP1}$$

s.t.

Component balances: eq. (5.3.1)

Reaction kinetics: eq. (5.3.2) – eq. (5.3.4)

Thermodynamic relations: eq. (5.3.6) – eq. (5.3.7)

Further constitutive equations: eq. (5.3.8) – eq. (5.3.9)

Initial conditions: $y_i\,(t=0) = y_{i,0}$

Residence time: $\tau = 30\,s$

STY: eq. (5.3.10)

Intrinsic bounds: $T^L \leq T \leq T^U$, $p^L \leq p \leq p^U$, $y_i^L \leq y_i \leq y_i^U \quad \forall i \in COM$

Case selection: s_i according to Tab. 5.4

Table 5.4: Attributes and selectivity of each reaction concept investigated on level 1

Case	Attributes (DoF)	Decision variables	S [%]
Reference	T, p	$s_i = 0\,\forall i \in COM$	79.10
Case 1	T, p, $y_{i,0}$	$s_i = 0\,\forall i \in COM$	81.35
Case 2	$T\,(t)$, p, $y_{i,0}$	$s_i = 0\,\forall i \in COM$	81.48
Case 3	$T\,(t)$, p, $y_{i,0}$, $j_{tot,\mathrm{E}}\,(t)$	$s_i = 0\,\forall i \in COM \setminus \{\mathrm{E}\}$, $s_{\mathrm{E}} = 1$	82.35
Case 4	$T\,(t)$, p, $y_{i,0}$, $j_{tot,\mathrm{O_2}}\,(t)$	$s_i = 0\,\forall i \in COM \setminus \{\mathrm{O_2}\}$, $s_{\mathrm{O_2}} = 1$	81.73
Case 5	$T\,(t)$, p, $y_{i,0}$, $j_{tot,\mathrm{CO_2}}\,(t)$	$s_i = 0\,\forall i \in COM \setminus \{\mathrm{CO_2}\}$, $s_{\mathrm{CO_2}} = 1$	81.99
Case 6	$T\,(t)$, p, $y_{i,0}$ $j_{tot,\mathrm{E}}\,(t)$, $j_{tot,\mathrm{O_2}}\,(t)$	$s_i = 0\,\forall i \in COM \setminus \{\mathrm{E}, \mathrm{O_2}\}$, $s_{\mathrm{E}} = s_{\mathrm{O_2}} = 1$	82.71
Case 7	$T\,(t)$, p, $y_{i,0}$, $j_{tot,\mathrm{E}}\,(t)$, $j_{tot,\mathrm{O_2}}\,(t)$, $j_{tot,\mathrm{CO_2}}\,(t)$	$s_i = 0\,\forall i \in COM \setminus \{\mathrm{E}, \mathrm{O_2}, \mathrm{CO_2}\}$, $s_{\mathrm{E}} = s_{\mathrm{O_2}} = s_{\mathrm{CO_2}} = 1$	82.84

The total pressure is in the range of $10\,bar$ – $20\,bar$ and the temperature range is $550\,K$ – $630\,K$. The bounds for the composition are given in Tab. 5.3 and the parameters of the reaction rates in Tab. 5.2.

Results

The results for all investigated reaction concepts of level 1 are presented in Fig. 5.5 and the selectivities are summarized in Tab. 5.4.

The optimal temperature of the isothermal case with optimized inlet composition (case 1) is 592.7 K. In this case, the ethylene and oxygen inlet mole fractions are at their upper bound ($y_{E,0} = y_E^U = 0.1$, $y_{O_2,0} = y_{O_2}^U = 0.08$) while the CO_2 inlet mole fraction is at its lower bound ($y_{CO_2,0} = y_{CO_2}^L = 0.05$). The high inlet fractions of ethylene and oxygen in combination with the low inlet fraction of CO_2 enable a lower temperature level compared to the reference case. This reduced temperature level and the direct influence of the higher ethylene mole fraction increase the selectivity by 2.25% compared to the reference case.

In Fig. 5.5(a) the temperature profiles of selected cases where the heat flux is optimized are shown. For the sake of clarity, the temperature profile of case 4 (q, j_{O_2}) is not shown in Fig. 5.5(a) since it is almost the same as in case 3 (q, j_E). In case 7 (q, j_E, j_{O_2}, j_{CO_2}) the optimal temperature profile is constant at 569.5 K. The optimal temperature of the isothermal case 1 is 592.7 K. Both the temperature profiles of case 1 and case 7 are not shown in Fig. 5.5(a).

For case 2 to case 7, the mole fraction profiles and the flux profiles of the manipulated components are presented in Fig. 5.5(c) to Fig. 5.5(h). In addition, the selectivity of each case is given in the caption of the individual figures.

Referring to case 2, it can be concluded that an optimal, non-constant temperature profile exists for the conventional EO reactor. The optimal temperature profile increases continuously starting from 570.1 K to 616.7 K. This temperature rise counterbalances the lower reaction rates due the decreasing ethylene and oxygen partial pressure and the increasing CO_2 partial pressure with increasing residence time. However, the selectivity increases only by 0.13% comparing case 1 to case 2. Hence, it can be concluded that realizing a temperature profile in the reactor is probably not worthwhile if additional investment costs arise.

The optimal ethylene dosing profile with the resulting component mole fraction profiles of case 3 are shown in Fig. 5.5(d). The ethylene dosage makes up for the consumed ethylene so that the ethylene mole fraction is always at its upper bound. The temperature profile is similar to case 2 except that the temperature level is lower. Besides the direct influence of ethylene on the selectivity (compare exponential order of ethylene in r_1 and r_2), the lower temperature level contributes to the selectivity increase of 3.25% compared to the reference case.

Referring to Fig. 5.5(e) belonging to case 4, the optimal oxygen dosing strategy keeps oxygen at its upper boundary. The optimal temperature profile is almost the same as in case 3. The selectivity improvement is lower than in the ethylene dosing case. Hence, dosing ethylene is more worthwhile to investigate than dosing oxygen.

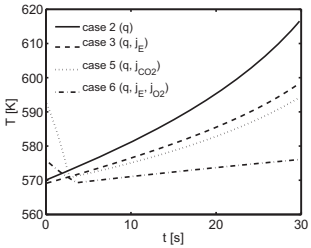

(a) Temperature profiles

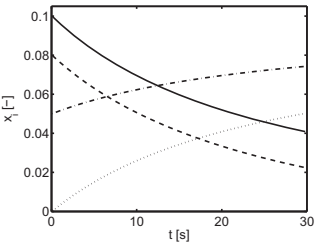

(b) Case 1: isothermal. $S = 81.35\%$

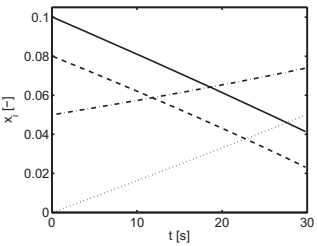

(c) Case 2: q. $S = 81.48\%$

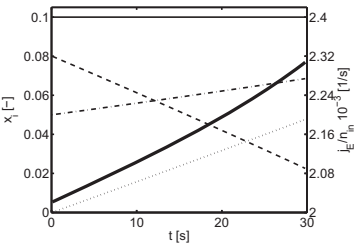

(d) Case 3: q, j_E. $S = 82.35\%$

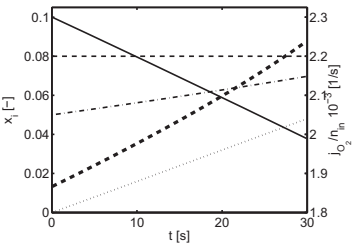

(e) Case 4: q, j_{O_2}. $S = 81.73\%$

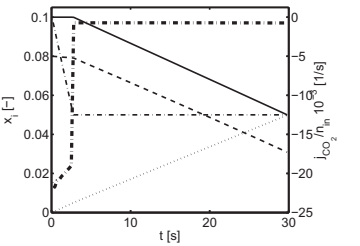

(f) Case 5: q, j_{CO_2}. $S = 81.99\%$

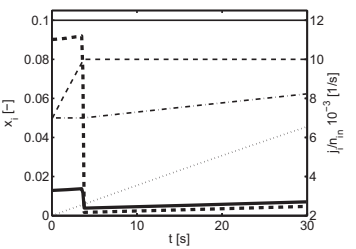

(g) Case 6: q, j_E, j_{O_2}. $S = 82.71\%$

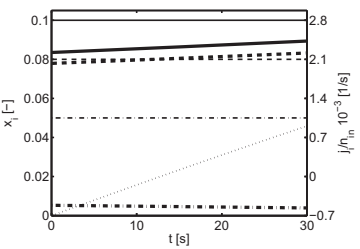

(h) Case 7: q, j_E, j_{O_2}, j_{CO_2}. $S = 82.84\%$

Figure 5.5: (a) Temperature profiles. (b)–(h) Mole fraction and dosing profiles (E: ——, O_2: — —, EO: ···, CO_2: - · -, thin lines: mole fractions, thick lines: dosing profiles)

In case the produced CO_2 can be removed from the reaction mixture in situ (case 5), the selectivity can be increased by 2.89%. Due to the inhibiting effect of CO_2 on the catalyst, a lower CO_2 partial pressure allows a temperature reduction while still matching the required STY. As shown in Fig. 5.5(f), the optimal CO_2 removal strategy starts with a high CO_2 inlet mole fraction and continuously removes CO_2 from the reaction mixture until the lower CO_2 limit is reached. Afterwards, CO_2 is kept at its lower limit. This strategy is advantageous over starting with a CO_2 inlet mole fraction at its lower limit and keeping the CO_2 mole fraction constant at its lower limit, since the former strategy keeps the mole fractions of ethylene and oxygen high up to a residence time of $3\,s$. This effect increases the selectivity more than always staying at the lower limit for the CO_2 mole fraction, which would yield a selectivity 0.10% lower. Such a result can hardly be obtained by intuition or heuristics, which demonstrates that the proposed model based approach is advantageous for the design of optimal reactors.

If optimal ethylene, oxygen and heat fluxes are provided (case 6), the ethylene mole fraction is always kept at its upper boundary while the oxygen mole fraction is increased from $y_{O2}(t_0) = 0.05$ to its upper boundary in the first $4\,s$ (refer to Fig. 5.5(g)). Such a strategy keeps the CO_2 mole fraction low at the beginning and is advantageous over a strategy where both the ethylene mole fraction and the oxygen mole fraction are constant at their upper boundaries.

In case 7 (q, j_E, j_{O_2}, j_{CO_2}) the ethylene and oxygen mole fractions are always kept at their upper bound, while the CO_2 mole fraction is kept at its lower bound (refer to Fig. 5.5(h)). Since these mole fractions are all constant, the optimal temperature is also constant ($T = 596.5\,K$). The selectivity gain compared to the reference case is 3.74%. In case the profiles for the temperature and all influenced mole fractions are constant, these profiles could be approximated by a completely back-mixed reactor. However, the reactant mole fraction profiles must not be at their upper boundaries since the ethylene and oxygen concentration in the feed must be even higher, which is not allowed due to the explosion hazard. In addition, the CO_2 mole fraction profile should not be at its lower boundary since the feed would have to contain even less CO_2 in this case and that contradicts the assumed concentration bounds.

Case 7 has the highest potential for the selectivity increase, but it is also most complicated to realize. The removal of CO_2 could in principle be realized by absorption with an amine solution or a potassium carbonate solution. However, these solvents are not in liquid state at reaction conditions, which makes an in situ absorption impossible with these solvents. Hence, either intermediate absorption must be applied or other solvents (such as ionic liquids) allowing an in situ absorption at the reaction conditions must be used. A detailed investigation which solvent may be used at the reaction temperature and designing a reactor with integrated extraction of CO_2 exceeds the scope of this paper and hence all cases including CO_2 removal are not further investigated in this thesis. Nevertheless, the methodology identifies the upper limit for the selectivity which can be obtained by such a reaction concept.

From the results of level 1 it can be observed that the exact knowledge of the explosive range is very important for the optimal operation of the reactor. The optimal operation conditions are often at the upper boundaries for the ethylene and oxygen mole fractions defined by the explosion limit and this indicates that higher ethylene and oxygen mole fractions will further increase the overall EO selectivity. In addition, decreasing the CO_2 mole fraction will increase the selectivity for the same STY and

residence time. However, the rate law is not applicable at CO_2 levels below the chosen limit and hence the lower bound on the CO_2 mole fraction is necessary to obtain reliable results.

Summing up, it can be concluded that applying advanced concentration and temperature control strategies has high potential for improving the EO selectivity. Hence, it is interesting to investigate if this potential can also be exploited in case the optimal flux profiles are approximated in a technical reactor. Taking the explosion limits into account, ethylene and oxygen must be dosed using separate channels. Hence, the dosing of only one of the components is much easier. In this work, case 3 (q, j_E) will be further investigated since it seems to be the most promising case from a selectivity and a reaction engineering point of view.

5.3.2 Level 2: Principle reactor set-up, transport mechanisms, and control variables

Based on the case studies of level 1, only the most promising cases are further investigated. It is determined which transport mechanisms and control variables are suited to make the desired flux profiles attainable. For this purpose, a schematic reactor design is proposed and control variables which can be changed by the reactor design are identified. The losses due to the limited mass and energy transport are quantified by comparing the results of level 1 and level 2.

In principle, several mechanisms for the realization of heat and component fluxes exist. Here, for the sake of simplicity the heat flux is controlled by changing the cooling temperature along the reaction coordinate and the distributed dosing of ethylene is provided via a membrane. At constant pressure on the ethylene supply side the permeance of the membrane is adjusted along the reaction coordinate in order to control the ethylene flux in an optimal manner. Alternatively, the exchange areas for both fluxes or the pressure on the ethylene supply side could be controlled. It should be noted that the cooling temperature and the permeance of the membrane can still be ideally manipulated within the specified bounds on the second level. The proposed schematic reactor design is shown in Fig. 5.6.

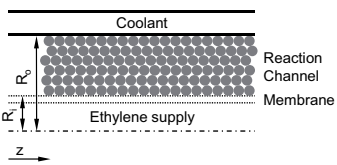

Figure 5.6: Reactor design for case 3 (q, j_E) (longitudinal section view)

At this point, the choice of the schematic reactor set-up includes the choice of the catalyst support. Here, a fixed bed reactor with a randomly packed bed is chosen since it offers the highest catalyst density compared to other catalyst support concepts. A high catalyst density is required in order to meet the required STY – a result which can already be obtained by a sensitivity analysis on the first level.

The design is optimized in a wide design range for all optimization variables, such as the inlet temperatures and exchanges areas. Meaningful bounds for the inner and outer tube diameter (here: $0.5\,cm \leq D_i \leq 3\,cm$, $4\,cm \leq D_o \leq 10\,cm$) yield the bounds for the specific exchange areas for heat and mass transfer. In case of a fixed bed reactor with a conventional catalyst packing, an average void fraction dependent on the inner and outer tube diameter and on the catalyst particle diameter (here: $2\,mm \leq D_p \leq 10\,mm$) must be specified. If additional catalyst supports and reactor concepts, for example coated wall catalyst and micro reactors, should be investigated, the void fraction correlation and the bounds for the geometric design variables must be adjusted. However, including different catalyst supports would only make sense in case higher exchange area to catalyst volume ratios are required.

In order to describe the heat transport, a suited heat transport coefficient model for the one-dimensional heat transfer is used [85]. Ethylene is provided via a porous stainless steel membrane with a wide permeance range (here: $0\,\frac{mol}{Pa \cdot s \cdot m^2} \leq Per \leq 10^{-2}\,\frac{mol}{Pa \cdot s \cdot m^2}$). Such a membrane was successfully used for EO reactors in a previous work reported in the literature [86]. It is assumed that the ethylene flow through the porous membrane is purely convective and hence driven by the pressure difference of both sides.

Criteria for external heat and mass transfer (Mears criteria) [87, 88] as well as for internal heat transfer (Anderson criterion) [89] and mass transfer (expressed by the Thiele modulus [90] or the Damköhler number (e.g. [23])) are considered. These criteria must be applied in order to ensure a reasonable reactor design and the validity of the used pseudo-homogeneous model with a high catalyst efficiency. In addition, a maximal temperature difference between the cooling media and the fluid and a maximum pressure difference between the ethylene dosing side and the fluid are enforced. These criteria limit the mechanical and thermal stress on the construction material and hence are important for safety reasons.

In the next section, the model equations are presented and the arising optimization problem is stated. Afterwards, the results are discussed and the idea for a technical approximation is derived.

Additional model equations of level 2

In addition to the equations of level 1, the energy balance, the momentum balance, the transport equations, and the equations describing the specific exchange areas are required on this level. The model is kept in the substantial formulation, however, the local form of the balance equations can also be used if desired.

For the energy balance the same assumptions are taken as on level 1, but heat exchange with the cooling side is considered. Since it is not obvious that the desired heat flux is attainable, the transport kinetics for the heat fluxes are included and the heat exchange with the cooling side is controlled via the cooling temperature profile.

$$\frac{n \cdot c_p}{V_g} \cdot \frac{\mathrm{d}T}{\mathrm{d}t} = -\left(a_o \cdot q_o + \rho_p \cdot \frac{1-\epsilon}{\epsilon} \cdot \sum_{i \in COM}\left(h_i \sum_{j \in RE} \nu_{i,j} \cdot r_j\right)\right) \tag{5.3.13}$$

The specific exchange areas based on the gas volume for the exchange with the cooling channel and the exchange with the ethylene supply channel are referred to as a_o and a_i, respectively.

$$a_o = \frac{4}{\epsilon} \cdot \frac{D_o}{D_o^2 - D_i^2} \tag{5.3.14}$$

$$a_i = \frac{4}{\epsilon} \cdot \frac{D_i}{D_o^2 - D_i^2} \tag{5.3.15}$$

The heat capacity of the mixture is modeled assuming a linear mixing rule and individual heat capacities depending linearly on the temperature according to eq. (5.3.16). The coefficients $A_{cp,i}$ and $B_{cp,i}$ are fitted to the higher polynomial functions (Shomate Equation) from NIST chemical web book [91], since a linear function is by far easier to handle for the optimization solver than higher order polynomials. In addition, the component heat capacities depend almost perfectly linear on the temperature in the investigated temperature range.

$$c_{p,i} = A_{cp,i} + B_{cp,i} \cdot T^* \tag{5.3.16}$$

The individual component enthalpies are calculated using eq. (5.3.17), where F_i is also fitted to the values given in the literature [91] ($T^* = \frac{T}{1000}$, $T_{ref} = 298.15\,K$).

$$h_i(T) = A_{cp,i} \cdot T^* + \frac{B_{cp,i}}{2} \cdot (T^*)^2 + F_i \tag{5.3.17}$$

Table 5.5: Heat capacity coefficients

Component	$A_{cp,i}\ \left[\frac{J}{mol \cdot K}\right]$	$B_{cp,i}\ \left[\frac{J}{mol \cdot K^2}\right]$	$F_i\ \left[\frac{J}{mol}\right]$
E	21.07	82.76	42.26
O_2	27.73	7.68	−8.70
EO	20.14	110.45	−63.98
CO_2	31.01	27.27	−404.13
H_2O	29.74	10.95	−251.14
N_2	27.08	5.65	−8.33

In case of a randomly packed fixed bed reactor with spherical particles of uniform size, the Ergun equation with the coefficients stated in eq. (5.3.19) can be used to approximates the pressure drop [67]. Under steady state conditions, the operator equation eq. (5.3.18) can be used to convert the Ergun equation into the substantial formulation as shown in eq. (5.3.19).

$$\frac{\mathrm{d}p}{\mathrm{d}t} = v_i \frac{\partial p}{\partial z} \tag{5.3.18}$$

$$\frac{\mathrm{d}p}{\mathrm{d}t} = -\left(150 \frac{\mu\,(1-\bar{\epsilon})^2}{D_p^2 \bar{\epsilon}^3} + 1.75 \frac{v_s \rho\,(1-\bar{\epsilon})}{D_p \bar{\epsilon}^3}\right) \frac{v_s^2}{\bar{\epsilon}} \tag{5.3.19}$$

$$v_s = v_{s,0} \frac{A_0 \cdot p_0 \cdot T \cdot n}{A \cdot p \cdot T_0 \cdot n_0} \tag{5.3.20}$$

The inlet velocity $v_{s,0}$ is chosen as degree of freedom. The dynamic viscosity is assumed to be constant $\left(\mu = 2.52 \cdot 10^{-5} \frac{kg}{m \cdot s}\right)$. This value was calculated for a typical inlet mixture at 500 K and 20 bar using Aspen Plus.

The heat transport between the reaction channel and the cooling channel is described by an one-dimensional model [85] according to eq. (5.3.21) and eq. (5.3.23). It is assumed that the heat transfer resistance is completely on the reaction channel side.

$$q_o = \alpha_o \cdot (T - T_c) \tag{5.3.21}$$

$$\alpha_o = 2.03 \cdot \mathrm{Re}_{D_p}^{0.8} \cdot \frac{\lambda}{D_o} \cdot \exp\left(-\frac{6 \cdot D_p}{D_o}\right) \tag{5.3.22}$$

$$\text{with} \quad 20 \leq \mathrm{Re}_{D_p} = \frac{\rho \cdot v_s \cdot D_p}{\mu} \leq 7600 \tag{5.3.23}$$

The heat conductivity of the mixture is assumed to be constant for all calculations $\left(\lambda = 3.91 \cdot 10^{-2} \frac{W}{m \cdot K}\right)$ and was obtained using Aspen Plus for a typical inlet composition at 500 K and 20 bar.

The mass transport through the membrane is assumed to be purely convective and is described by eq. (5.3.24). Based on the work of Lafarga et al. [73], Al-Juaied et al. [86] investigated the transport kinetics for the flux across the membrane using the dusty gas model. Their results fit qualitatively to the experimental observations, but a simpler model for the cross-membrane transport yields similar results, too. This observation justified the simple transport kinetics assumed in this work.

$$j_{tot,\mathrm{E}} = V_g \cdot a_i \cdot Per \cdot (p_M - p) \tag{5.3.24}$$

In case of an annular tube with randomly packed spherical catalyst particles of uniform size the average void fraction depends on the outer tube diameter, on the inner tube diameter, and on the particle diameter according to eq. (5.3.25). Here, the radius dependent void fraction $\epsilon(r)$ is defined in eq. (A.1.51).

$$\bar{\epsilon} = \frac{2 \int_{R_i}^{R_o} r\epsilon(r)\,\mathrm{d}r}{\left(R_o^2 - R_i^2\right)} \tag{5.3.25}$$

In order to ensure a reasonable reactor design and to be able to use the proposed pseudo-homogeneous model with a high catalyst efficiency, reactor design criteria for the external and internal heat and mass transfer have to considered in the design stage. All criteria are tracked over the whole reaction coordinate and must be fulfilled at all times.

The criteria defined by Mears for external heat [87] and mass [88] transfer are taken into account according to eq. (5.3.26) and eq. (5.3.27), respectively.

$$\frac{0.3 \cdot \beta_i \cdot C_{i,s}}{\sum_{j \in RE}\left(-\nu_{i,j} \cdot n_{i,j} \cdot r_j\right) \cdot \rho_p \cdot D_p} \geq 1, \quad i = \mathrm{E}, \mathrm{O_2} \tag{5.3.26}$$

$$\frac{0.3 \cdot R \cdot T^2 \cdot \alpha}{\bar{E}_A \cdot \sum_{j \in RE} \left(-\Delta H_{r,j} \cdot r_j\right) \cdot \rho_p \cdot D_p} \geq 1 \tag{5.3.27}$$

The criteria for internal and external mass transfer must be checked for both reactants ethylene and oxygen. In eq. (5.3.26), $C_{i,s}$ is the surface concentration of the component calculated from the ideal gas law and $n_{i,j}$ is the reaction order. To calculate the transport coefficient β_i the correlation from Thoenes and Kramers [92] for a packed bed of spherical particles is used (eq. (5.3.28)).

$$\beta_i = \frac{1.9 \cdot D_{m,i}}{D_p} \left(\frac{v_s \cdot D_p \cdot \rho}{\mu}\right)^{0.5} \left(\frac{\mu}{\rho \cdot D_{m,i}}\right)^{0.33} \tag{5.3.28}$$

It is assumed that the molecular diffusion coefficients $D_{m,i}$ can be described by the method of Wilke and Lee [93] assuming binary diffusion in nitrogen. Since the temperature dependence of the reaction rate is by far more pronounced than the temperature dependency of the diffusion coefficients, mean values of the diffusion coefficients in the temperature range of $500\,K$ – $600\,K$ at $20\,bar$ are used ($D_{m,\mathrm{E}} = 2.49 \cdot 10^{-6}\ \frac{m^2}{s}$, $D_{m,\mathrm{O_2}} = 3.15 \cdot 10^{-6}\ \frac{m^2}{s}$). The heat transfer coefficient α is related to the mass transfer coefficient β by eq. (5.3.29) [94] assuming a Lewis number close to unity. Here, the lower β value is chosen in order to ensure a conservative design.

$$\frac{\beta}{\alpha} = \frac{0.7 \cdot M}{\rho \cdot c_p} \geq 1 \quad \text{with } \beta = \min_{i=\mathrm{E,\,O_2}} \beta_i \tag{5.3.29}$$

The Anderson criterion [89] (eq. (5.3.30)) is considered to ensure isothermal catalyst pellets. For the heat transfer criteria the arithmetic mean value of both activation energies $\bar{E}_A$ is used.

$$\frac{3 \cdot R \cdot T^2 \cdot \lambda_p}{\bar{E}_A \cdot \sum_{j \in RE} \left(-\Delta H_{r,j} \cdot r_j\right) \cdot \rho_p \cdot D_p^2} \geq 1 \tag{5.3.30}$$

In order to ensure a catalyst efficiency above 95% the Damköhler criterion (e.g. [23]) is applied according to eq. (5.3.31).

$$\sqrt{\mathrm{Da}_{\mathrm{II},i}} = \left(\frac{\sum_{j \in RE} \left(-\nu_{i,j} \cdot r_j\right) \cdot \rho_p \cdot D_p^2}{4 \cdot D_{ef,i} \cdot C_{i,s}}\right)^{0.5} \leq 1 \quad i = \mathrm{E, O_2} \tag{5.3.31}$$

Here, the effective diffusion coefficient inside the pellet $D_{ef,i}$ is calculated assuming no Knudsen diffusion influence, an inner void fraction of 0.44, and a tortuosity of 3.

To limit the mechanical and thermal stress, criteria for a maximum temperature difference $\left(\Delta T^U = 20\,K\right)$ (eq. (5.3.32)) between the cooling and the fluid side and for a maximum pressure difference $\left(\Delta p^U = 1\,bar\right)$ between both sides of the membrane (eq. (5.3.33)) are applied.

$$T(t) - T_c(t) \leq \Delta T^U \tag{5.3.32}$$

$$p_{M,0} - p_0 \leq \Delta p^U \tag{5.3.33}$$

Optimization problem of level 2

The full optimization problem which must be solved on level 2 is stated in (DOP2). For temperature, pressure, composition, and STY the same bounds apply as on level 1. The substance properties required for the calculation of $c_{p,i}$ and h_i are given in Tab. 5.5.

$$\text{Obj} = \max_{\substack{T_c(t),Per(t),y_{i,0},p,\\ D_o,D_i,D_p,T_0,v_{s,0}}} S \tag{DOP2}$$

s.t.

Component balances: eq. (5.3.1)

Reaction kinetics: eq. (5.3.2) – eq. (5.3.4)

Energy balance: eq. (5.3.13) – eq. (5.3.17)

Momentum balance: eq. (5.3.18) – eq. (5.3.20)

Transport kinetics: eq. (5.3.21) – eq. (5.3.24)

Catalyst support: eq. (5.3.25)

Design criteria: eq. (5.3.26) – eq. (5.3.33)

Thermodynamic relations: eq. (5.3.6) – eq. (5.3.7)

Further constitutive equations: eq. (5.3.8) – eq. (5.3.9)

Initial conditions: $y_i\,(t=0) = y_{i,0}, p\,(t=0) = p_0, T\,(t=0) = T_0$

Residence time: $\tau = 30\,s$

STY: eq. (5.3.10)

Intrinsic bounds: $T^L \leq T \leq T^U$, $p^L \leq p \leq p^U$, $y_i^L \leq y_i \leq y_i^U \quad \forall i \in COM$

Design bounds: $Per^L \leq Per \leq Per^U$, $D_k^L \leq D_k \leq D_k^U$ for $k = i, o, p$

Case selection: $s_i = 0\,\forall i \in COM \setminus \{\text{E}\}$, $s_{\text{E}} = 1$

Results

In Fig. 5.7 the optimal permeance and optimal cooling profile as well as the resulting temperature, reactor design criteria, ethylene flux, and mole fraction profiles are summarized. Referring to Fig. 5.7(b) the temperature increases from $T = 570.4\,K$ to $T = 597.6\,K$ which is qualitatively the same profile as in case 3 on level 1. The temperature difference between the fluid and the coolant is always below the maximum allowed temperature difference of $20\,K$. The optimal outer tube diameter is $D_o = 4.07\,cm$.

Referring to Fig. 5.7(c) the ethylene and oxygen inlet mole fractions are at their upper bound, while the CO_2 inlet mole fraction is at its lower bound. Due to the optimal permeance profile (refer to Fig. 5.7(a)) the ethylene mole fraction is always kept at its upper boundary. The optimal ethylene pressure on the membrane side is $p_{\text{E,M}} = 20.78\,bar$ and the inner tube diameter is at its lower bound $(D_i = 0.5\,cm)$.

The particle diameter is at its lower bound $\left(D_p = 2\,mm\right)$, which is the optimal trade-off between the pressure drop, the void fraction and the catalyst efficiency. The combination of the inner and outer tube as well as particle diameter yields a void fraction of $\epsilon = 0.424$, which is slightly higher than the assumed void fraction on

level 1. At the inlet the velocity is $0.085\,\frac{m}{s}$, which gives rise to a small and almost linear pressure drop of $\Delta p = 0.06\,bar$.

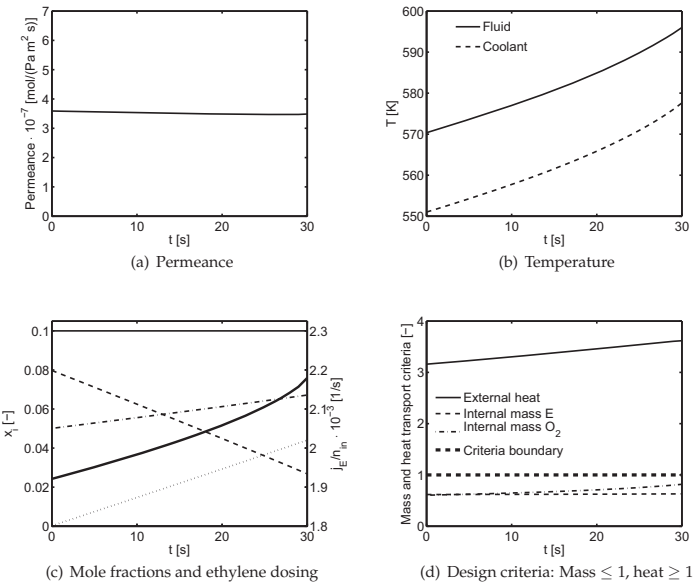

(a) Permeance

(b) Temperature

(c) Mole fractions and ethylene dosing

(d) Design criteria: Mass ≤ 1, heat ≥ 1

Figure 5.7: Results level 2 (Fig. 5.7(a)E: ——, O_2: — —, EO: · · · ·, CO_2: - · -, thin lines: mole fractions, thick line: dosing profile)

Referring to Tab. 5.6, the optimal reactor design never reaches the reactor design bounds. The minimal values for the external heat and mass transfer as well as for the internal heat transfer are always above their minimal value of 1. The maximum value for the internal mass transfer criterion is always below the value where pore diffusion becomes limiting. Here, oxygen is the more limiting component since it depletes along the reaction coordinate. The profiles of the reactor design criteria, which are close to their bounds, are shown in Fig. 5.7(d). The internal heat and the external mass transfer are far away from being limiting, and hence the according criteria are not shown.

The maximum selectivity of such a reactor set-up is 82.33%. In case a degree of freedom is at its bound (e.g. the particle diameter), a sensitivity analysis can be used to investigate whether it is worthwhile to relax this bound. The relaxation of such a bound refers to a different reactor concept or to the shift of the design space, for example by advanced materials or miniaturization. Since the difference in the selectivity between level 2 and level 1 is merely 0.01%, it can be concluded that the cooling temperature and the permeance of the membrane are suitable control variables to obtain the desired fluxes and no design bounds need to be shifted.

In addition, the chosen catalyst packing is optimal since it features the highest catalyst density compared with wall coated reactors, monolithic reactors or foam like catalyst support structures, and no limitations on the overall heat and mass transport occur. In case severe heat and mass transport limitations can be observed, a reactor design with higher specific exchange areas is required. However, such a reactor design will suffer from lower catalyst densities; in order to achieve the desired STY and residence time at a lower catalyst density, the reaction temperature must be increased and thereby the selectivity will decrease. Therefore, it can be concluded that alternative catalyst supports and/or a micro reactor concept is not necessary for the selective production of EO with the chosen catalyst.

5.3.3 Level 3: Best technical reactor

Derivation of a technical approximation

On the third level, technical approximations based on the profiles of the best control variables are developed. In case different ways how to approximate the control variables are derived, the different set-ups are compared using simple models before a chosen set-up is further investigated using more detailed models.

In the investigated case, a technical approximation of the control variable profiles based on existing apparatuses can directly be proposed. The cooling temperature profile can be approximated using a co-current heat exchanger. How the permeance profile can be approximated depends strongly on the manufacturing technology of the porous membrane used. However, a membrane with a constant permeance is a reasonable approximation since the optimal permeance profile on level 2 varies by less than 3.4 %.

On this level, the change in the cooling temperature is determined in a rigorous manner by solving the energy balance for the coolant. On the ethylene supply side, the mass, energy, and momentum balances are solved. The heat transport between the reaction channel and the cooling channel is determined by the heat transfer resistance on the gas side. In case of the heat transfer between the ethylene supply side and reaction channel, the heat transfer resistance of both sides are considered.

Due to the additional balance equations for the coolant and for the ethylene supply side, the degrees of freedom of the optimization problem are reduced. On this level, the flux profiles cannot be optimized anymore. Now, only the design variables which are listed with their according optimal values in Tab. 5.6 are degrees of freedom. Hence, the solution of the optimization problem of level 3 cannot be better – with respect to local optimality – than the solution of (DOP2). On level 3, the balance equations are written in the local formulation and are listed in Appendix A.1. The according optimization problem (DOP3-1D) is stated below.

$$\text{Obj} = \max_{\text{DoF refer to Tab. 5.6}} \frac{\dot{n}_{\text{EO},f} - \dot{n}_{\text{EO},0}}{\dot{n}_{\text{E},0} - \dot{n}_{\text{E},f} + \int_{z=0}^{L} \pi D_i j_{\text{E}} \mathrm{d}z} \tag{DOP3-1D}$$

s.t.

Component balances: eq. (A.1.1)

Reaction kinetics: eq. (5.3.2) – eq. (5.3.4)

Energy balance: eq. (A.1.2)

Momentum balance: eq. (A.1.3)

Transport kinetics: eq. (5.3.21) – eq. (5.3.23), eq. (A.1.16) – eq. (A.1.18)

Catalyst support: eq. (5.3.25)

Design criteria: eq. (5.3.26) – eq. (5.3.33)

Thermodynamic relations: eq. (5.3.7)

Further constitutive equations: eq. (A.1.4) – eq. (A.1.6)

Initial conditions: $y_i\,(t=0) = y_{i,0}$, $p\,(t=0) = p_0$, $T\,(t=0) = T_0$, $T_c\,(t=0) = T_{c,0}$, $p_M\,(t=0) = p_{M,0}$, $T_M\,(t=0) = T_{M,0}$, $\dot{n}_M\,(t=0) = \dot{n}_{M,0}$

Residence time: $\tau = \bar{\epsilon} \int_{z=0}^{L} \frac{1}{v_s} \mathrm{d}z = 30\,s$

STY: $\frac{\dot{n}_{\mathrm{EO},f} - \dot{n}_{\mathrm{EO},0}}{\pi\left(R_o^2 - R_i^2\right) L} = 0.27\,\frac{mol}{m^3 s}$

Intrinsic bounds: $T^L \leq T \leq T^U$, $p^L \leq p \leq p^U$, $y_i^L \leq y_i \leq y_i^U \quad \forall i \in COM$

Design bounds: $Per^L \leq Per \leq Per^U$, $D_k^L \leq D_k \leq D_k^U$ for $k = i, o, p$

Case selection: $s_i = 0\,\forall i \in COM \setminus \{\mathrm{E}\}$, $s_{\mathrm{E}} = 1$

Coolant side: eq. (A.1.7), eq. (A.1.8)

Membrane side: eq. (A.1.9) – eq. (A.1.15)

For temperature, pressure, composition, STY, and permeance the same bounds apply as on the previous levels. The bounds for the coolant constant and all additional required substance properties are stated in the model description. The heat capacity and enthalpy of the ethylene on the membrane side are calculated with the same models and parameters as before.

The selectivity is 82.32% and it is still much higher than the selectivity of the reference case. The difference in the objective between level 2 and level 3 are the losses caused by the non-ideal control variable profiles. Since the difference between level 2 and level 3 is only 0.1%, the technical approximation is reasonable. In case the losses due to the non-ideal control profiles are severe, a different technical approximation should be developed. The results of the derived technical approximation are shown in Fig. 5.8(a) to Fig. 5.8(c).

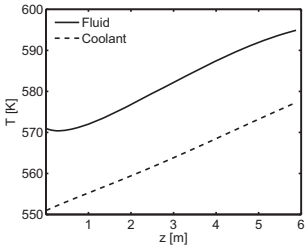

(a) 1D: Temperature

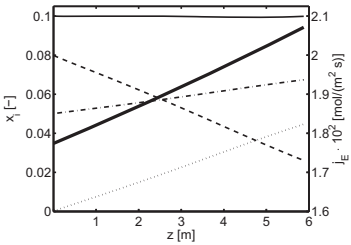

(b) 1D: Mole fractions and dosing

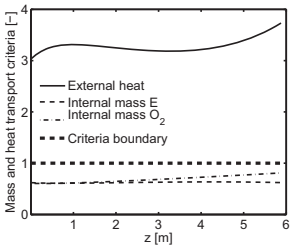

(c) 1D: Design criteria: Mass ≤ 1, heat ≥ 1

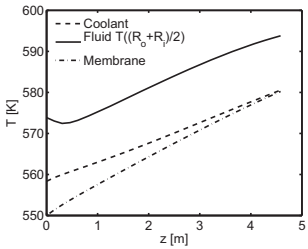

(d) 2D: Temperature

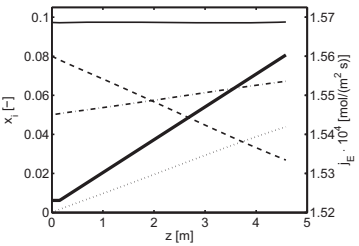

(e) 2D: Mole fractions and dosing

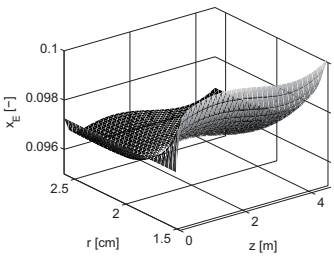

(f) 2D: Ethylene mole fraction

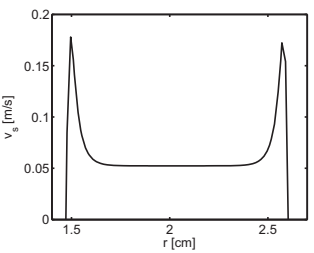

(g) 2D: Inlet velocity profile

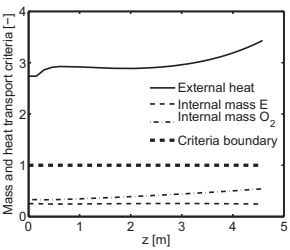

(h) 2D: Design criteria: Mass ≤ 1, heat ≥ 1

Figure 5.8: Results level 3 (Fig. 5.8(b), Fig. 5.8(e): E: ——, O_2: — —, EO: ····, CO_2: –·–, thin lines: mole fractions, thick line: dosing profile)

In order to validate the results obtained by the one-dimensional model on level 3, a more detailed reactor model accounting for radial temperature, concentration, and porosity profiles is derived and used for optimization in the next step.

Detailed investigation of the proposed reactor design

For the detailed investigation of the chosen reactor set-up a two-dimensional, pseudo-homogeneous model is used (refer to Appendix A.1). The model accounts for a radial temperature, concentration, and porosity profile. In order to investigate if a non-ideal temperature profile has a severe effect on the selectivity, the radial temperature distribution needs to be considered. The radial porosity profile results in a radial distribution of the axial velocity, which allows to investigate the effect of by-passing of the dosed ethylene. Since the dosing of ethylene and the radial distribution of the axial velocity give rise to a non plug flow like profile of ethylene, also radial mole fraction profiles need to be considered to ensure a non explosive composition everywhere in the reactor. The optimization model has the same degrees of freedom as the 1D reactor model and is stated in (DOP3-2D).

The equations describing the ethylene supply side and the coolant side are kept one-dimensional since only the radial concentration and temperature gradients as well as the radial velocity distribution in the reaction channel are important to validate the results obtained with the one-dimensional model. All balance equations of the reaction channel are written in cylindrical coordinates.

$$\text{Obj} = \max_{\text{DoF refer to Tab. 5.6}} S_{2D} \qquad \text{(DOP3-2D)}$$

s.t.

Component balances: eq. (A.1.19) – eq. (A.1.28)

Reaction kinetics: eq. (5.3.2) – eq. (5.3.4)

Energy balances: eq. (A.1.29) – eq. (A.1.44)

Momentum balances: eq. (A.1.45) – eq. (A.1.50)

Catalyst support: eq. (A.1.51)

Design criteria: eq. (5.3.26) – eq. (5.3.33)

Thermodynamic relations: eq. (5.3.7)

Initial conditions: $y_i\,(t=0) = y_{i,0}$, $T_c\,(t=0) = T_{c,0}$,

$T_M\,(t=0) = T_{M,0}$, $p_M\,(t=0) = p_{M,0}$, $\dot{n}_M\,(t=0) = \dot{n}_{M,0}$

Residence time: eq. (A.1.53)

STY: eq. (A.1.54)

Intrinsic bounds: $T^L \leq T \leq T^U$, $p^L \leq p \leq p^U$, $y_i^L \leq y_i \leq y_i^U \quad \forall i \in COM$

Design bounds: $Per^L \leq Per \leq Per^U$, $D_k^L \leq D_k \leq D_k^U$ for $k = i, o, p$

Coolant side: eq. (A.1.7), eq. (A.1.8)

Membrane side: eq. (A.1.9) – eq. (A.1.15)

The equations for the case selections are directly implemented in the mass balance of the reaction channel (refer to eq. (A.1.21)), and hence do not appear separately in

(DOP3-2D). The equations of the heat and mass transport kinetics are given together with the component balances and energy balance, respectively.

Referring to the results presented in Tab. 5.6, it can be observed that the inlet temperatures of the reaction, cooling, and membrane channel are very close to the temperatures predicted by the 1D model. Also, the pellet diameter, the coolant constant, and the ethylene flux of the membrane side are in accordance with the 1D model. However, the diameters of the inner and outer tubes vary significantly from the results obtained with the simpler model. The different channel design results in different values for the reactor length, inlet mole flow, and permeance.

Table 5.6: Results comparison between level 2 and level 3

Decision variables	**Level 2**	**Level 3 (1D)**	**Level 3 (2D)**
$D_o\ [cm]$	4.07	4.37	5.21
$D_i\ [cm]$	0.5	0.84	2.94
$D_p\ [mm]$	2	2	2
$L\ [m]$	-	5.88	4.58
$T_0\ [K]$	570.4	570.9	573.9
$T_{c,0}\ [K]$	551.1	550.9	558.3
$K_c\ \left[\frac{m \cdot K}{W}\right]$	-	$5.5 \cdot 10^{-3}$	$7.7 \cdot 10^{-3}$
$T_{M,0}\ [K]$	-	550.9	550.0
$\dot{n}_0\ \left[\frac{mol}{s}\right]$	-	$4.9 \cdot 10^{-2}$	$3.9 \cdot 10^{-2}$
$Per\ \left[\frac{mol}{Pa \cdot m^2 \cdot s}\right]$	-	$8.95 \cdot 10^{-7}$	$5.42 \cdot 10^{-8}$
$\dot{n}_{M,0}\ \left[\frac{mol}{s}\right]$	-	0.1	0.1
Inlet composition (y_E, y_{O_2}, y_{CO_2}, y_{N_2})	0.1, 0.08, 0.05, 0.77	0.1, 0.08, 0.05, 0.77	0.0973, 0.08, 0.05, 0.7727
Design criteria			
External heat (min)	3.16	3.03	2.56
External mass (min)	132.8	140.5	41.5
Internal heat (min)	658.9	650.6	613.7
Internal mass (max)	0.83	0.81	0.57
Selectivity [%]	82.33	82.32	82.26

In Fig. 5.8(d) the profiles for the fluid temperature in the middle of the reaction channel, the cooling temperature, and the membrane temperature are shown. The profiles are similar to the 1D case and the maximum radial hot spot in the fluid is $\Delta T_{radial,max} = 8.2\ K$.

Fig. 5.8(e) shows the average mole fraction profiles of all components. These profiles are very similar to the results obtained by the 1D model, however, the inlet mole

fraction of ethylene is only 9.73%. Due to the dosing of ethylene, the ethylene mole fraction shows a strong radial distribution with a maximum of 10% at the inner tube wall (refer to Fig. 5.8(f)). This underlines the necessity of more detailed models especially when safety constraints have to be met.

The by-pass flow is significant as can be observed from the radial velocity profile shown in Fig. 5.8(g). Similar as in the 1D model the reactor design criteria are not critical and never exceeded along the reaction channel (refer to Fig. 5.8(h) calculated with radially averaged values and to Tab. 5.6 where the extreme values of the design criteria are given considering the radial and axial profiles).

From a reaction engineering point of view, the difference in selectivity between the one-dimensional and the two-dimensional model are due to the non-ideal temperature and concentration distribution as well as the non-ideal flow field. However, since both models are different, a monotonic decrease in the objective function cannot necessarily be expected from a mathematical point of view.

In case the non-ideal radial profiles cause a large decrease in the objective function, a different catalyst packing which yields a better radial heat and mass transport as well as a lower amount of by-passing might improve the reactor performance. Such effects can be realized for example by foam like catalyst packings.

Beside the radial hot spots and the high amount of by-passing, the selectivity calculated with the optimized 2D model is still 82.26%, and hence a technical realization of the proposed reactor design seems to be worthwhile.

Comparison to the technical reactors and current developments

The derived reactor design can be compared to the technically used reactor and recently proposed concepts from literature [73, 75, 95]. A comparison to the industrially used reactor set-up using the same catalyst was already done by the optimized reference case and it is shown that a selectivity increase of 3.3% is possible. The selectivity values reported in the literature for the industrial air based EO process are approximately 80% [71]. This indicates that the considered catalyst is comparable to the industrially used catalysts and the increase in selectivity is realistic.

In comparison to other reactor configurations published in the literature, the obtained selectivity with the derived reactor concept is much higher. Lafarga et al. [73] investigated different fixed bed membrane reactors. In agreement with the current work, they found that dosing ethylene yields the highest selectivity increase, however, the obtained selectivity is only 67%. Kestenbaum et al. [75] achieved a selectivity of up to 69% using a micro reactor set-up. The large discrepancy in the selectivities between Lafarga's [73] and Kestenbaum's [75] works on the one hand and the here calculated values on the other hand is partly due to the fact that the former works were performed with highly active, but less selective catalysts. Zhou and Yuan [95] optimized a conventional fixed bed reactor with a highly selective catalyst and obtained a selectivity up to 80.5%.

Since the oxygen based process offers even higher selectivities (compare Tab. 5.1), it is of interest how the best reaction concept of the air based process compares to the optimal reaction concept of the oxygen based process, which is determined in the next chapter.

5.4 Oxygen based EO process – Optimal reaction concept and plant wide optimization

In this example, the optimal reaction concept for the oxygen based EO process from a process point of view is determined. For this purpose, an overall process model is developed with an intensified functional reaction module taking the interaction between reactor performance and process into account. With such a model, the reaction route and the plant operation are simultaneously optimized giving rise to an overall optimal process.

At the beginning of the example, the overall process is described and the objective function is formulated in Section 5.4.1. In Section 5.4.2, the model of the reaction system including catalyst selection and explosion limits is explained. Afterwards, the downstream process model is discussed.

In Section 5.4.4, the optimization problem is stated and in Section 5.4.5 the results are discussed. In the results section, all investigated cases are compared and a promising case is identified. Afterwards, a detailed comparison of the most promising case to the reference case is performed. At the end, a sensitivity analysis is performed investigating the influence of critical model parameters and assumptions.

After discussing the results of this example, a summary of the air based and oxygen based process is given in Section 5.5.

5.4.1 Process description and objective

The flowsheet of the oxygen based EO process is shown in Fig. 5.9. For an easier process description and naming of units and streams, the process is decomposed into sections, which are classified according to:

- Section 0: Make up section
- Section 1: Reaction section
- Section 2: EO absorption section
- Section 3: CO_2 absorption by-pass, purge, and recompression section
- Section 4: CO_2 absorption section

Regarding the nomenclature, every unit is named according to the following code {Type of unit, section number, unit number in the according section}, e.g. R101 refers to reactor 01 in section 1. The following units are defined: reactor R), column (C), mixer (M), splitter (S), heat exchanger (H), condenser (Cond), reboiler (Reb), pump (P), compressor (CP), and valve (V). Every stream is named according to the following code {section number, stream in the according section}, e.g. 102 refers to stream number 02 in section 1, which is the reactor inlet stream.

Referring to Fig. 5.9, the mixing section consists of ethylene, oxygen, and methane feed streams. In this process, methane is used as inert gas to affect the explosion limit within the reactor and the heat capacity of the fluid.

The reaction section consists of the heat exchangers $H101$, $H102$, $H103$, and the reaction module $R101$. While $H101$ heats up the fluid to the reactor inlet temperature, $H102$ recovers heat from the reactor outlet streams at low pressure steam temperature T_{LPS}, and $H103$ removes additional heat using cooling water (CW) down to absorber

inlet temperature. The reaction module is described with the fluid element approach and different integration and enhancement options are investigated.

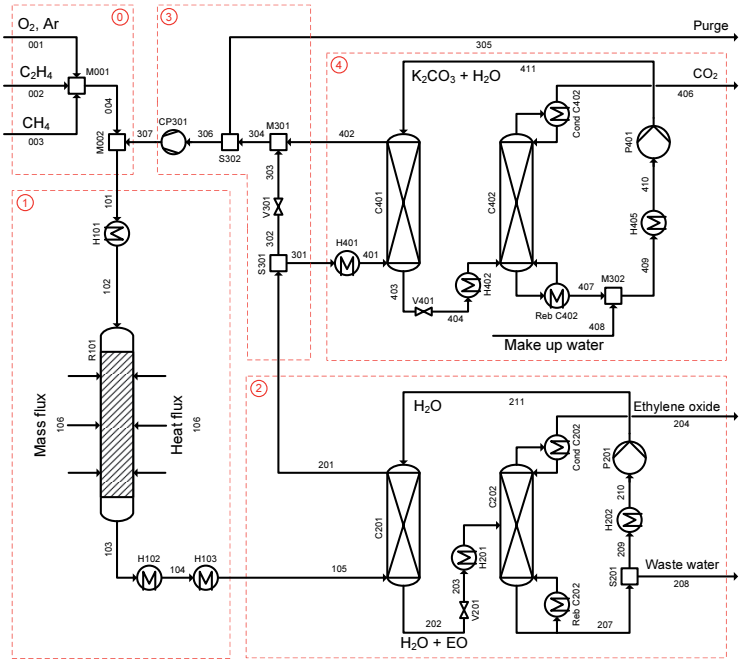

Figure 5.9: Flowsheet of the oxygen based ethylene oxide process

The EO absorption section consists of absorption column *C*201 and regeneration column *C*202. EO is removed from the other gases by physical absorption using water. The absorbent is regenerated at lower pressure and higher temperature. The waste water stream $\dot{n}_{208}$ removes additional water and glycols from the recycled absorbent stream. The water is formed by the combustion to CO_2 in the reactor and the glycols arise from the consecutive reaction of EO with water.

CO_2 is removed from the recycle gas by chemical absorption with hot potassium carbonate solution in the absorption column *C*401. The carbonate solution is regeneration at lower pressure and higher temperature in a second column *C*402. By setting the split fraction *S*301 it is determined which part of the recycle stream is sent to the CO_2 absorption column.

The purge $\dot{n}_{305}$ is required to remove inert gases such as argon, which are part of the feed streams, from the recycle gas. In addition, a compressor *CP*301 is necessary due to pressure losses in the reactor and absorbers.

The focus of this example is to account for the interaction between the intensified reaction module and the downstream process. Hence, adequate models are used to

describe the downstream process and the fluid element approach is used to identify the best reaction concept.

In the next sections, the objective function is discussed. Afterwards, the models of the reaction section and of the downstream process are explained. Within the discussion of the model of the reaction section special emphasis is put on the description of the explosive region. In order to present the model of the downstream section in a clear and comprehensive manner, the principle modeling approach and the assumptions are presented in Section 5.4.3, while the equations are given in Appendix A.2.

Objective

The objective is to minimize the total running expenses of the process for a fixed product stream $\left(\dot{n}_{\mathrm{EO},204} = 1\,\frac{mol}{s}\right)$. Referring to Tab. 5.7, the costs for the individual reactants and utilities are obtained from the literature [96] and converted to $\frac{\$}{kmol}$ and $\frac{\$}{MJ}$, respectively. For this calculation a constant enthalpy of evaporation of water at low pressure steam conditions $\left(\Delta h_{v,\mathrm{H_2O}} = 40.65\,\frac{kJ}{mol}\right)$ is used. In addition, the heat capacity of cooling water is taken as $c_{p,\mathrm{H_2O}} = 75.6\,\frac{J}{mol \cdot K}$ and a temperature rise of the cooling water of $\Delta T_{CW} = 10\,K$ is assumed.

Table 5.7: Prizes for reactants and utilities

Reactant	Costs $\left[\frac{\$}{kmol}\right]$	Utility	Costs $\left[\frac{\$}{MJ}\right]$
Ethylene (C_{E})	21.10	Low pressure steam (C_{LPS})	$7.97 \cdot 10^{-6}$
Oxygen ($C_{\mathrm{O_2}}$)	1.90	Electricity (C_{El})	$1.24 \cdot 10^{-3}$
Methane ($C_{\mathrm{CH_4}}$)	3.80	Cooling water (C_{CW})	$6.25 \cdot 10^{-7}$

The costs of the reactants and utilities are given by eq. (5.4.1) and eq. (5.4.2), respectively. The stream $\dot{n}_{106}$ is the total dosing stream of a reactant according to eq. (A.2.4). The costs for cooling water need to be accounted as negative, since all heat fluxes associated with cooling are negative. In case a heat flux associated with LPS is negative, it is assumed that the heat can be used in the plant and hence it is accounted as credit. Since the water make-up stream $\dot{n}_{408}$ is very small and water is inexpensive, the costs of the make-up water are neglected. Furthermore, the costs associated with the catalyst and other running expenses are not accounted for in the model since these costs are always approximately the same regardless of the reaction concept.

$$\begin{aligned} C_{reactants} =& C_{\mathrm{E}}\left(\dot{n}_{\mathrm{E},002} + \dot{n}_{\mathrm{E},106}\right) + C_{\mathrm{O_2}}\left(\dot{n}_{\mathrm{O_2},001} + \dot{n}_{\mathrm{O_2},106}\right) \cdot \left(1 + F_{\mathrm{Ar}}\right) \\ &+ C_{\mathrm{CH_4}} \cdot \dot{n}_{\mathrm{CH_4},003} \end{aligned} \tag{5.4.1}$$

$$\begin{aligned} C_{utilities} =& C_{LPS}\left(\dot{Q}_{H101} + \dot{Q}_{H102} + \dot{Q}_{R101} + \dot{Q}_{RebC202} + \dot{Q}_{H401} + \dot{Q}_{RebC402}\right) \\ &- C_{CW}\left(\dot{Q}_{CondC202} + \dot{Q}_{CondC402} + \dot{Q}_{H103} + \dot{Q}_{H202} + \dot{Q}_{H405}\right) \\ &+ C_{El}\left(P_{P201} + P_{P401} + P_{CP301}\right) \end{aligned} \tag{5.4.2}$$

The total production costs based on the amount of produced ethylene oxide are given by eq. (5.4.3).

$$C = \frac{C_{reactants} + C_{utilities}}{\dot{n}_{\mathrm{EO},204}} \tag{5.4.3}$$

The composition of the feed streams are restricted by eq. (5.4.4) - eq. (5.4.7). Here, it is assumed that argon accounts for all inert components in the feed streams. Therefore, argon can be regarded as a kind of pseudo component and the argon level in the oxygen feed is chosen much higher than obtained by conventional air separation. Argon is assumed to be proportional to the oxygen feed stream by a factor of $F_{\mathrm{Ar}} = 0.01$.

$$\dot{n}_{i,001} = 0 \quad \forall\, i \in COM \setminus \{\mathrm{O_2}, \mathrm{Ar}\} \tag{5.4.4}$$
$$\dot{n}_{\mathrm{Ar},001} = F_{\mathrm{Ar}} \cdot \dot{n}_{\mathrm{O_2},001} \tag{5.4.5}$$
$$\dot{n}_{i,002} = 0 \quad \forall\, i \in COM \setminus \{\mathrm{E}\} \tag{5.4.6}$$
$$\dot{n}_{i,003} = 0 \quad \forall\, i \in COM \setminus \{\mathrm{CH_4}\} \tag{5.4.7}$$

5.4.2 Reaction system

In this section, the model of the reaction system is explained. Besides the balance equations, the catalyst selection, and a rigorous model for the explosion limits are required.

Balance equations of the reaction system

The reaction section is modeled according to the elementary process functions approach for a fluid element (Fig. 5.10). The different integration and enhancement concepts in the reaction module will be discussed together with the arising optimization problems in Section 5.4.4.

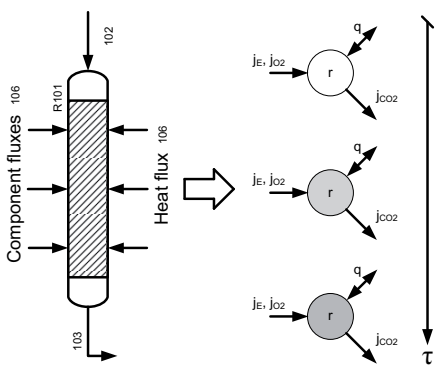

Figure 5.10: Fluid element model for the reaction section

In accordance to the air based process, the component mass balances are given by eq. (5.3.1). The density, partial pressure, including the definitions of the total molar amount and mole fractions are given by eq. (5.3.8) – eq. (5.3.7) (already presented in Section 5.3.1). The space time yield (defined in eq. (5.3.10)) which must be achieved in the oxygen based process is assumed to be 1 $\frac{mol}{m^3 s}$.

The heat removed from the reactor is calculated using an overall energy balance according to eq. (5.4.8). The enthalpy of the dosed components is calculated at ambient temperature, which refers to the condition of the feed streams. If the temperature inside the reactor is always above T_{LPS}, the total heat removed is used to produce steam.

$$\dot{Q}_{R101} = \sum_{i \in COM} \left(\dot{n}_{i,102} \cdot h_{i,102} + \dot{n}_{i,106} \cdot h_{i,106} - \dot{n}_{i,103} \cdot h_{i,103} \right) \tag{5.4.8}$$

All required connectivity equations to link the steady state process model to the reaction module are summarized in Appendix A.2.1.

Catalyst selection

Since the catalyst of Al-Saleh et al. [81] was not investigated at reaction conditions of the oxygen based process, the reaction rate laws are not applicable here. The only available reaction rate laws determined at reaction conditions of the oxygen based process are the reaction rates of Gan et al. [97], and hence this catalyst is used for the further investigations. The rate models derived by Al-Saleh et al. [81] and Gan et al. [97] and the according experimental conditions are given in Tab. 5.8 for comparison.

Table 5.8: Rate expressions and experimental conditions for the catalyst of the air and oxygen based EO process

Model	Experimental conditions	Source
	$p = 21.7\,bar$	
$r_1 = \frac{k_1(T) p_E^{0.6} p_{O_2}^{0.5}}{1+K_1(T) p_{CO_2}}$	$513\,K \leq T \leq 593\,K$	
	$0.03 \leq y_{E,0} \leq 0.065$	
	$0.18 \leq y_{O_2,0} \leq 0.195$	[81]
$r_2 = \frac{k_2(T) p_E^{0.5} p_{O_2}^{0.5}}{1+K_2(T) p_{CO_2}}$	$y_{CO_2,0}$, $y_{EO,0}$,	
	$y_{W,0}$, DCE level: not stated	
	Inert gas: N_2	
	$p = 22\,bar$	
$r_1 = \frac{k_1(T) p_E p_{O_2}}{1+K_1(T) p_{O_2}+K_2(T) p_{O_2}^{0.5} p_{CO_2}}$	$405\,K \leq T \leq 530\,K$	
	$0.27 \leq y_{E,0} \leq 0.36$	
	$0.054 \leq y_{O_2,0} \leq 0.076$	[97]
$r_2 = \frac{k_2(T) p_E p_{O_2}^{0.5}}{1+K_1(T) p_{O_2}+K_2(T) p_{O_2}^{0.5} p_{CO_2}}$	$0.053 \leq y_{CO_2,0} \leq 0.091$	
	$y_{EO,0}$, $y_{W,0}$, DCE level: not stated	
	Inert gas: Methane	

The reaction rate coefficients of the model of Gan et al. [97] are given in eq. (5.4.9) – eq. (5.4.12).

$$k_1(T) = \exp\left(-4.087 - \frac{43585.7}{RT}\right) \tag{5.4.9}$$

$$k_2(T) = \exp\left(3.503 - \frac{77763.2}{RT}\right) \tag{5.4.10}$$

$$K_1(T) = \exp\left(\frac{18321.0}{RT} - 16.644\right) \tag{5.4.11}$$

$$K_2(T) = \exp\left(\frac{34660.6}{RT} - 14.823\right) \tag{5.4.12}$$

From the experimental conditions and the general process window (according to Tab. 5.1) the following limits for temperature, pressure, and CO_2 mole fraction are derived.

$$405\,K \leq T \leq 530\,K \tag{5.4.13}$$

$$10\,bar \leq p \leq 22\,bar \tag{5.4.14}$$

$$y^L_{CO_2} \geq 0.05 \tag{5.4.15}$$

The limit of the lower CO_2 mole fraction is important since the reaction rate and the selectivity are very sensitive on the CO_2 partial pressure. Hence, the reaction rate law cannot be extended to lower CO_2 mole fractions without significant loss in reliability.

Within these limits the catalyst of Gan et al. [97] yields a slightly higher selectivity at low temperature. However, at higher temperature the selectivity of this catalyst is below the selectivity of the catalyst investigated by Al-Saleh et al. [81].

No direct bounds for the ethylene and oxygen mole fraction are specified, but the overall composition is limited by the explosion limits over the entire residence time.

Explosion limits

The typical operation window of the oxygen based EO process and the explosive region (E, O_2, N_2, $20°C$, $1\,atm$) was shown in Fig. 5.2. The oxygen based process operates at high ethylene concentrations and always above the UEL (rich mixture). For the air based process, it was assumed that the mixture must not exceed a critical oxygen and ethylene concentration. This assumption is not valid for the oxygen based process and the UEL of the mixture must be rigorously modeled. For this purpose, a model describing the UEL taking the influence of temperature, pressure, and composition into account is derived in this thesis.

Data on the explosion limits of the pure components (E, EO, CH_4) was experimentally determined by many authors and is available in the literature [98]. The pure component data must be extended to match the reaction conditions with respect to temperature and pressure. In principle, the explosive range increases with temperature and the LEL and the UEL depend linearly on temperature (e.g. [99]). The pressure dependency of the UEL is investigated in the literature and is different for each component [100, 101].

The explosive region of the mixture can be calculated using the rule of Le Chatelier (e.g. [99]). However, this rule applies only to substances with similar properties and

most often the UEL cannot be predicted accurately with this equation. In addition, the cool flame phenomenon might occur and has to be considered within the modeling of the explosion region. Therefore, the rule of Le Chatelier is adapted taking the relative combustion rates of each explosive into account in order to describe the upper flammability limits correctly. For the investigated systems (ethylene, methane, air) this adaption was performed by Klaubert [102].

The influence of different inerts (CO_2, N_2) and of CH_4 on the explosion limit (at 250°C and 20 atm) was experimentally studied by Crescitelli et al. [103]. They found that methane is better suited as inert gas compared to CO_2 and N_2. The difference between CO_2 and N_2 is small and can be explained with the higher heat capacity of CO_2 compared to N_2. The influence of CH_4 on the UEL must be considered rigorously in the model of the explosive region.

The model of the explosive region is completely based on literature data and the UEL is predicted as follows:

1. The UEL of the individual flammable gases UEL_i are calculated using eq. (5.4.16). Each UEL_i depends on the inert to oxygen ratio R_{inert}. At the investigated operation conditions, pure EO can explode and hence the UEL of EO was fixed to be $\mathrm{UEL}_{\mathrm{EO}} = 1$. The models of the individual upper explosion limits in dependence of R_{inert} are based on the data given in the literature [98]. The parameters were obtained by regression and are given in Tab. 5.9.
2. The individual UEL_i of all flammable components are extended to the reaction temperature using eq. (5.4.18).
3. The UEL_is are extended to the reaction pressure by eq. (5.4.19) and eq. (5.4.20), respectively. This model is based on the data of Van den Schoor and Verplaetsen [100, 101], where the parameters are obtained by regression and given in Tab. 5.9.
4. The UEL of the mixture UEL_{mix} is calculated using eq. (5.4.22) (set of flammable components: FG={E, EO, CH_4}). This equation and the according correction factors κ_i are based on the model of Klaubert [102]. The model is extended towards a mixture of three explosives assuming $\kappa_{\mathrm{EO}} = \kappa_{\mathrm{E}}$. This assumption is investigated in detail using a sensitivity study in Chapter 5.4.5. In addition, the temperature dependency of the correction factor κ_{E} is taken into account using eq. (5.4.25). The parameters to describe κ_{E} are obtained by regression of the data published by Klaubert [102] ($A_\kappa = 4.5033 \cdot 10^{-5}$, $B_\kappa = -0.0051$, $C_\kappa = 2.0043$).

All model fits for the individual upper explosion limits are dependent on the inert to oxygen ratio, the pressure dependency of the individual explosion limits, and the temperature dependency of κ_{E} are summarized in Appendix A.2.1.

$$\mathrm{UEL}_i = \left[A_{\mathrm{UEL},i} R_{\mathrm{inert}}^3 + B_{\mathrm{UEL},i} R_{\mathrm{inert}}^2 + C_{\mathrm{UEL},i} R_{\mathrm{inert}} + D_{\mathrm{UEL},i}\right] \cdot f(\Theta) \cdot f(p) \quad \text{for } i = \mathrm{CH_4}, \mathrm{E} \tag{5.4.16}$$

$$R_{\mathrm{inert}} = \frac{y_{\mathrm{H_2O}} + y_{\mathrm{CO_2}} + y_{\mathrm{Ar}}}{y_{\mathrm{O_2}}} \tag{5.4.17}$$

$$f(\Theta) = \left[1 + \frac{1}{891 + \Theta^\circ}\left(\Theta - \Theta^\circ\right)\right] \tag{5.4.18}$$

$$f(p) = \left[1 + A_{p,\mathrm{E}} \ln\left(\frac{p}{p^\circ}\right)\right] \quad \text{for ethylene} \tag{5.4.19}$$

$$f(p) = \left[1 + A_{p,\mathrm{CH_4}} \left(\frac{p - p^\circ}{p^\circ}\right)\right] \quad \text{for methane} \tag{5.4.20}$$

$$\mathrm{UEL_{EO}} = 1 \tag{5.4.21}$$

Table 5.9: Parameters of the UEL of the individual flammable gases

Component	$A_{\mathrm{UEL},i}$	$B_{\mathrm{UEL},i}$	$C_{\mathrm{UEL},i}$	$D_{\mathrm{UEL},i}$	Θ°	p°	$A_{p,i}$
Ethylene	$4.16 \cdot 10^{-4}$	-0.0047	-0.0761	0.8972	$100^\circ C$	$10\,bar$	0.2586
Methane	-0.0015	0.0270	-0.2087	0.7204	$20^\circ C$	$10\,bar$	0.0428

$$\mathrm{UEL}_{mix} = \frac{1}{\sum_{i \in \mathrm{FG}} \frac{\tilde{y}_i^*}{\mathrm{UEL}_i}} \tag{5.4.22}$$

$$\tilde{y}_i^* = \frac{\tilde{y}_i \kappa_i}{\sum_{i \in \mathrm{FG}} \tilde{y}_i \kappa_i} \quad \text{for } i \in \mathrm{FG} \tag{5.4.23}$$

$$\tilde{y}_i = \frac{y_i}{\sum_{i \in \mathrm{FG}} y_i} \quad \text{for } i \in \mathrm{FG} \tag{5.4.24}$$

$$\kappa_\mathrm{E} = A_\kappa \Theta^2 + B_\kappa \Theta + C_\kappa \tag{5.4.25}$$

$$\kappa_{\mathrm{CH_4}} = 1 \tag{5.4.26}$$

$$\kappa_\mathrm{EO} = \kappa_\mathrm{E} \tag{5.4.27}$$

In order to stay out of the explosive region, eq. (5.4.28) must hold over the entire residence time in the reaction module. Furthermore, it should be noted that the derived model for the explosion limit needs experimental validation before it can be safely used in practice.

$$\sum_{i \in \mathrm{FG}} y_{i,R101} \geq \mathrm{UEL}_{mix} \tag{5.4.28}$$

5.4.3 Downstream process

At the beginning of the downstream process description, the EO absorption section will be explained. Afterwards, a model for the CO_2 absorption using hot potassium carbonate solution is derived. At the end, the models of the additional process units are stated.

5.4.3.1 EO absorption section

Ethylene oxide is very efficiently separated from the gas mixture by physical absorption into water. The EO absorption is performed in an adiabatic counter-current flow column C201 at high pressure. In order to model the absorption column, the Kremser equation is used. This equations is modified in order to account for saturation of water in the gaseous outlet stream according to the saturation pressure of water at

the outlet conditions. The vapor-liquid equilibrium of the gaseous components in the absorbent are modeled using Henry's law.

The produced EO is recovered in a second column *C*202, which operates at lower pressure and higher temperatures. Due to the very high separation factors, only two theoretical separation trays are used to model the EO desorption column. Similar to the EO absorber, the Henry solubilities of all gases in water are used to calculate the vapor-liquid equilibrium and the mole fraction of water in the gas phase is calculated by the saturation pressure of water. The outlet mole flow of EO is fixed at 1 $\frac{mol}{s}$ (refer to eq. (A.2.31)) and the purity of the produced EO is enforced to be above 95% before fine purification.

The model assumptions and all model equations both for the EO absorption column as well as for the regeneration column are stated in Appendix A.2.2.1.

5.4.3.2 CO_2 absorption section

The absorption of CO_2 is performed by chemical absorption in hot potassium carbonate solution similar to the Benfield process [104]. In order to enhance the separation efficiency of the potassium carbonate solution for CO_2, piperazine is used as a promoter. The model of the CO_2 absorption section fully accounts for the physical absorption of all gases in the solution exemplified for CO_2 by

$$CO_{2,g} \rightleftharpoons CO_{2,aq} \tag{5.4.29}$$

and for the chemical reactions in the hot potassium carbonate solution given by eq. (5.4.30) – eq. (5.4.35).

$$CO_{2,aq} + 2 \cdot H_2O \overset{K_1}{\rightleftharpoons} HCO_3^- + H_3O^+ \tag{5.4.30}$$

$$HCO_3^- + H_2O \overset{K_2}{\rightleftharpoons} CO_3^{2-} + H_3O^+ \tag{5.4.31}$$

$$PZ + H_2O + CO_{2,aq} \overset{K_3}{\rightleftharpoons} PZCOO^- + H_3O^+ \tag{5.4.32}$$

$$PZH^+ + H_2O \overset{K_4}{\rightleftharpoons} PZ + H_3O^+ \tag{5.4.33}$$

$$PZCOO^- + H_2O + CO_{2,aq} \overset{K_5}{\rightleftharpoons} PZ(COO^-)_2 + H_3O^+ \tag{5.4.34}$$

$$H^+PZCOO^- + H_2O \overset{K_6}{\rightleftharpoons} PZCOO^- + H_3O^+ \tag{5.4.35}$$

The physical absorption of all gas phase components except CO_2 is modeled similar as in the EO absorption section using Henry's law and the saturation pressure of water. The CO_2 solubility in aqueous potassium carbonate solution must be calculated more accurately using the similarity of CO_2 to N_2O as proposed by Danckwerts [105]. N_2O has approximately the same molecular weight as CO_2 and a similar electron configuration, but does not react in the aqueous potassium carbonate solution, and hence its physical solubility can be measured more accurately. The physical solubility of CO_2 is then correlated to the solubility of N_2O.

Due to the high separation efficiency of the chemical absorption of CO_2 in hot potassium carbonate solution, the CO_2 absorption column C401 is modeled using one adiabatic equilibrium stage for the physical absorption and chemical equilibrium. The CO_2 is regenerated at lower pressure in a second column C402, which is approximated by two theoretical separation trays. The purity of the separated CO_2 is enforced to be above 95% to limit water losses.

The derived model is discussed in detail and all model equations are given in Appendix A.2.2.2.

5.4.3.3 Additional process units

In addition to the absorption and regeneration columns for EO and CO_2, additional process units are required in order to model the overall oxygen based EO process. These additional units are

- mixers and splitters,
- compressors, pumps, and valves,
- heat exchangers.

All of these units are described with component mole flow balances and energy balances. Furthermore, the enthalpy of the individual streams need to be calculated in order to solve the energy balances of all units. All model assumptions and model equations for the additional process units and for the enthalpy of the individual streams are presented in Appendix A.2.2.3.

5.4.4 Problem statement

In this section the investigated integration and enhancement concepts are introduced and the arising optimization problem is stated (refer to eq. (DOP1)). For the oxygen based process, advanced cooling and dosing of ethylene and oxygen as well as in situ removal of CO_2 is investigated. The reference case is an isothermal operated PFTR, which is a good approximation of the industrially used reactor. All considered combinations of heat, dosing and removal fluxes are listed in Tab. 5.10 and presented together with the results in Fig. 5.11.

$$\text{Obj} = \min_{\text{DoF}} C \tag{DOP1}$$

s.t.

Reactor section:

Component balances: eq. (5.3.1)

Case selection: s_i according to Tab. 5.10

Reaction kinetics: Tab. 5.8 with eq. (5.4.9) – eq. (5.4.12)

Energy balance: eq. (5.4.8)

Explosion limits: eq. (5.4.16) – eq. (5.4.28)

Intrinsic bounds: eq. (5.4.13) – eq. (5.4.15)

Reaction engineering bounds: $STY \geq 1 \frac{mol}{m^3 s}$

Connectivity equations: eq. (A.2.1) – eq. (A.2.4)

Further constitutive equations: eq. (5.3.6) – eq. (5.3.9)

Process model:

Feed section: eq. (5.4.4) – eq. (5.4.7)

EO absorption section: eq. (A.2.8) – eq. (A.2.33)

CO_2 absorption section: eq. (A.2.34) – eq. (A.2.80)

Additional process units: eq. (A.2.81) – eq. (A.2.100)

Further constitutive equations: eq. (A.2.5) – eq. (A.2.6)

In general, the degrees of freedom are the reaction pressure p_{R101}, the residence time in the reaction module τ, the feed and make-up streams ($\dot{n}_{001,O_2}$, $\dot{n}_{002,E}$, $\dot{n}_{003,CH_4}$, $\dot{n}_{408,H_2O}$), the reactor inlet temperature T_{102}, the temperatures of the absorbers and regenerators (T_{C201}, $T_{C202,Cond}$, $T_{C202,Reb}$, T_{C401}, $T_{C402,Cond}$, $T_{C402,Reb}$), and the split fractions (ξ_{S201}, ξ_{S301}, ξ_{S302}). Additional degrees of freedom arise in the reaction section depending on the investigated case (refer to Tab. 5.10). The number of degrees of freedom reduce if the explosion limit, the minimum CO_2 mole fraction in the reactor, the minimum EO outlet mole fraction of stream $\dot{n}_{204}$, and the minimum CO_2 outlet mole fraction of $\dot{n}_{406}$ are active constraints. In case of in situ CO_2 removal (case 7 – case 9), the CO_2 absorption section is not considered in the model and the associated split fraction is fixed ($\xi_{S301} = 0$).

Table 5.10: Attributes and degrees of freedom of each investigated reaction concept

Case	Additional DoF in the reaction section	Decision variables (s_i)
Case 1 (Reference)	T_{R101}	$s_i = 0 \, \forall i \in COM$
Case 2	$T_{R101}(t)$	$s_i = 0 \, \forall i \in COM$
Case 3	$T_{R101}(t)$, $j_{tot,E}(t)$	$s_i = 0 \, \forall i \in COM \setminus \{E\}$, $s_E = 1$
Case 4	$T_{R101}(t)$, $j_{tot,O_2}(t)$	$s_i = 0 \, \forall i \in COM \setminus \{O_2\}$, $s_{O_2} = 1$
Case 5	$T_{R101}(t)$, $j_{tot,CO_2}(t)$	$s_i = 0 \, \forall i \in COM \setminus \{CO_2\}$, $s_{CO_2} = 1$
Case 6	$T_{R101}(t)$, $j_{tot,E}(t)$, $j_{tot,O_2}(t)$	$s_i = 0 \, \forall i \in COM \setminus \{E, O_2\}$, $s_E = s_{O_2} = 1$
Case 7	$T_{R101}(t)$, $j_{tot,E}(t)$, $j_{tot,CO_2}(t)$	$s_i = 0 \, \forall i \in COM \setminus \{E, CO_2\}$, $s_E = s_{CO_2} = 1$
Case 8	$T_{R101}(t)$, $j_{tot,O_2}(t)$, $j_{tot,CO_2}(t)$	$s_i = 0 \, \forall i \in COM \setminus \{O_2, CO_2\}$, $s_{O_2} = s_{CO_2} = 1$
Case 9	$T_{R101}(t)$, $j_{tot,E}(t)$, $j_{tot,O_2}(t)$, $j_{tot,CO_2}(t)$	$s_i = 0 \, \forall i \in COM \setminus \{E, O_2, CO_2\}$, $s_E = s_{O_2} = s_{CO_2} = 1$

5.4.5 Results and discussion

In this section, the results of the optimization calculations will be presented and discussed. First of all, a general overview on results of all investigated cases is given. This allows to identify the most promising case for a technical realization later on. Afterwards, a detailed comparison of the chosen case and the reference case is performed. At the end of the section, the results of the sensitivity study are explained and important conclusions regarding the potential of the optimal case in practice are drawn.

5.4.5.1 Comparison of all investigated cases

As reference case (case 1) an optimal operated EO plant with an isothermal tube bundle reactor is chosen. This reference case is optimized using the same process model as the intensified cases except that the reaction module is operated isothermally and no component dosing flux exist in the reaction module. Therefore, all improvements in the running expenses are due to the intensified reaction module. The operating costs of all investigated cases are summarized in Fig. 5.11.

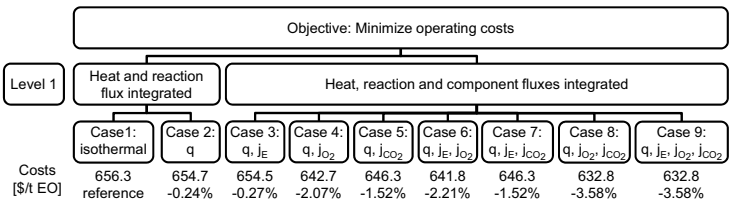

Figure 5.11: Results overview

In the reference case the production costs are 656.3 $\frac{\$}{t_{EO}}$, which is very close to the data presented in the literature [96] for the state-of-the-art process based on the same reactant and utility costs. From this results, it can be concluded that the EO process and reactor model are well suited to represent the state-of-the-art industrial EO process. However, no further conclusions can be drawn since the type of catalyst and the obtained STY are not stated in the cited work [96].

As can be seen by comparing case 2 and case 3 to the reference case, an optimal heat flux profile alone or in combination with distributed dosing of ethylene has small potential to reduce the EO production costs. The reasons for this are that the optimal temperature profile is only slightly increasing (almost isothermal) and ethylene has no direct influence on the selectivity (refer to reaction rates of Gan et al. [97]). In addition, ethylene is abundant during the reaction and therefore dosing ethylene hardly affects the reaction.

A maximum reduction of the running expenses of 3.58% is possible by providing an optimal heat flux profile, dosing ethylene and oxygen, and removing CO_2 in situ from the reactor (case 9). This includes the degrees of freedom of every other cases and hence case 9 states an upper limit for all investigated integration and enhancement

concepts. However, it should be noted that it is still unknown by which technology CO_2 can be removed in situ from the reactor. In addition, no costs are associated with the in situ removal of CO_2 so far. Hence, all cases with CO_2 are only taken as an assessment of these reaction concepts with regard to their economic potential and are not further investigated.

Referring to Fig. 5.11, almost the full cost saving potential is exploited by case 4 and case 6 and working on a technical realization for the in situ CO_2 removal does not seem to be worthwhile. Case 4 refers to a concept with advanced cooling and distributed oxygen dosing. In the reaction concept of case 6, ethylene is dosed in addition to oxygen and advanced cooling. Since the additional maximum cost savings, which are determined by comparing case 6 and case 4, are only 0.24% and simultaneous dosing of ethylene and oxygen might be difficult with respect to the explosion limits in the gas supply channel, case 4 seems to be more attractive from a technical and economical point of view. Hence, oxygen dosing with advanced cooling (case 4) is determined as the most promising concept from a technical and economic point of view and will be investigated in more detail.

5.4.5.2 Detailed comparison of chosen case with the reference case

Within this section, the results of case 4 (oxygen dosing and advanced cooling) will be compared to the reference case (case 1) in detail. At first, the obtained profiles during the reaction will be explained. Afterwards, the total costs will be analyzed in terms of costs for the individual feedstocks and utilities. Thereafter, the main results for optimal operation of the downstream process with special focus on the EO and CO_2 absorption sections are discussed.

In Fig. 5.12, the concentration, temperature, dosing, and UEL profiles of the reference case (left hand side) and the intensified case (right hand side) are shown.

By comparing the concentration profiles of both cases (Fig. 5.12(a) and Fig. 5.12(b)), it can be noted that the ethylene level in reactor of the intensified case is considerably higher (approximately $+8\%$). In addition, no methane is used in the intensified case, while the methane concentration in the reference case is about 8%. In the reference case, the methane is required to keep the reaction mixture out of the explosive region. If no methane would be used in the reference case, either the CO_2 level, the oxygen level, the reaction temperature, or the reaction pressure need to be changed in order to avoid explosion hazards. All of these options will increase the running expenses of the process more than adding methane. In the intensified case, the reaction temperature and the oxygen level can be adopted along the reaction coordinate in such a manner that the reaction mixture is always out of the explosive region even without adding methane to the feed.

By taking a closer look at the concentration profiles of oxygen and ethylene oxide (Fig. 5.12(c) and Fig. 5.12(d)), it can be observed that the EO outlet mole fraction of the intensified case is considerably higher (3% compared to 1.5%). In the intensified case, the optimal dosing flux of oxygen is almost constant and the oxygen mole fraction is kept at approximately 7.4%.

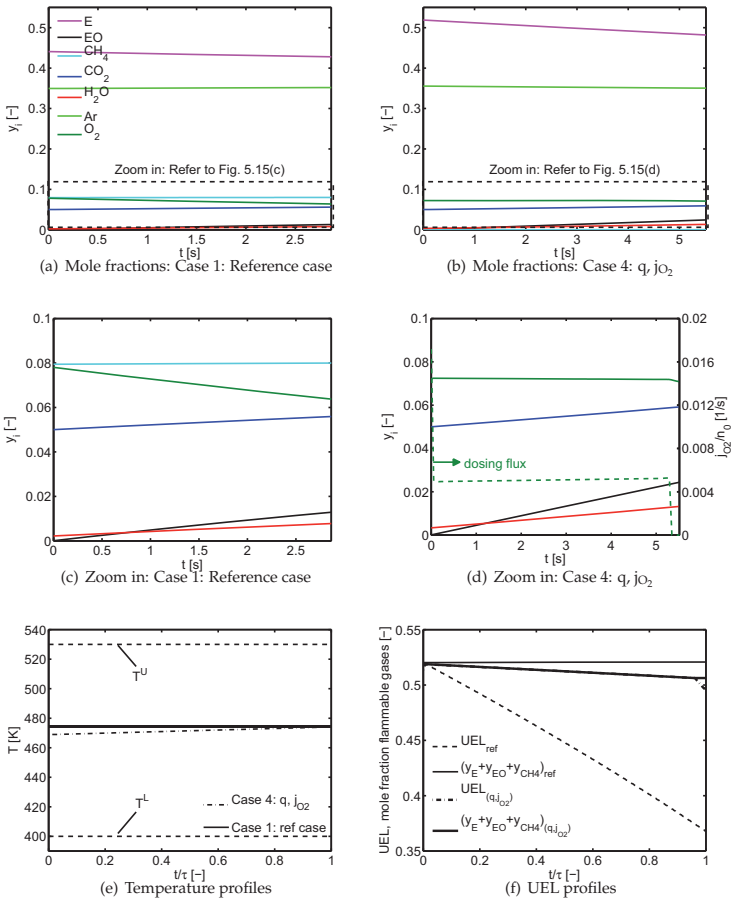

(a) Mole fractions: Case 1: Reference case
(b) Mole fractions: Case 4: q, j_{O_2}
(c) Zoom in: Case 1: Reference case
(d) Zoom in: Case 4: q, j_{O_2}
(e) Temperature profiles
(f) UEL profiles

Figure 5.12: Profiles in the reaction module: Reference and intensified case

The optimal temperature profile of the intensified case (shown in Fig. 5.12(e)) is slightly increasing (from 470 K to 475 K) and very close to the optimal reaction temperature of the isothermal case. In the intensified case, the optimal temperature profile and the optimal oxygen dosing profile keep the reaction mixture always at the UEL (refer to Fig. 5.12(f)). In the reference case, the mixture is at the explosion limit only at the start of the reaction. At higher conversions, oxygen depletes and the margin from the explosive region increases.

Therefore, it can be concluded that the largest decrease in the operation costs is obtained in the reactor by dosing oxygen in such a way that the reaction mixture is always at the UEL. This enhances the selectivity and gives rise to a higher EO outlet

concentration, which allows for a smaller reactor outlet and recycle stream (reference case: $\dot{n}_{103} = 77.9\,\frac{mol}{s}$, case 4: $\dot{n}_{103} = 41.0\,\frac{mol}{s}$). The lower recycle stream and the higher selectivity give rise to savings in the reactant costs and in the utility costs of the downstream process as will be explained below.

As shown in Fig. 5.11, the total cost saving potential of case 4 is 2.06%. The individual raw material and utility costs as well as the CO_2 emissions of both case are summarized Tab. 5.11.

Table 5.11: Feedstock and utility costs

Raw material, utility	**Reference case Costs** [%]	**Case 4:** q, j_{O_2} **Costs** [%]	**Reduction by** [%]
Ethylene	91.26	91.85	1.4
Oxygen	7.67	7.55	3.5
Methane	$3.45 \cdot 10^{-2}$	0	100
Electricity	$9.66 \cdot 10^{-1}$	$5.29 \cdot 10^{-1}$	46.3
Steam	$6.05 \cdot 10^{-2}$	$5.75 \cdot 10^{-2}$	7.0
Cooling water	$5.74 \cdot 10^{-3}$	$5.45 \cdot 10^{-3}$	6.9
Direct CO_2 emissions	0.50 $\left[\frac{mol_{CO_2}}{mol_{EO}}\right]$	0.46 $\left[\frac{mol_{CO_2}}{mol_{EO}}\right]$	7.2
Indirect CO_2 emissions	2.78 $\left[\frac{mol_{CO_2}}{mol_{EO}}\right]$	2.56 $\left[\frac{mol_{CO_2}}{mol_{EO}}\right]$	7.9

In both cases, ethylene causes the main costs (above 91%), and hence a higher selectivity in the reactor yields directly lower operating costs. In the intensified case, no methane is used giving rise to a simpler process design and additional savings. For example, the direct CO_2 emissions[1] arising partly from the methane consumption are decreased by 7.2%. Furthermore, the utility costs of the intensified case are much lower compared to the reference case due to the smaller recycle stream and the higher EO outlet concentration. Here, 46.3% electricity, 7.0% steam, and 9.1% cooling water are saved. Thereby, the associated indirect CO_2 emissions[2] of these utilities are reduced by 7.9%. Both, reducing the direct CO_2 emissions and the emissions associated with the utility consumption gives rise to a more sustainable and greener ethylene oxide process.

The streams of the EO absorption section of both cases and the according operation conditions are summarized in Tab. 5.12. Since the gas recycle stream of the intensified case is much lower, the required absorbent stream is also much lower (compare $\dot{n}_{207}$) giving rise to a smaller absorption column. The ethylene oxide in the reactor outlet stream $\dot{n}_{EO,105}$ is completely absorbed and no ethylene oxide is left in the gaseous outlet stream of the absorber $\dot{n}_{201}$. The absorption efficiency of water is very good and almost no other gases are absorbed. This allows for the production of very pure ethylene oxide ($y_{EO,204} = 0.95$) before the produced EO is sent to the fine purification.

[1] The direct CO_2 emissions are calculated as CO_2 equivalent assuming that all hydrocarbons in the purge stream, in the CO_2 stream $\dot{n}_{406}$, and in the waste water stream, as well as all hydrocarbons which are impurities of the ethylene oxide product stream are completely combusted to CO_2.

[2] The indirect CO_2 emissions of the used electricity are calculated assuming the average CO_2 emissions for electricity consumed in Germany in 2010 [106]. For the CO_2 emissions associated with steam consumption, it is assumed that the surplus of required steam is produced from methane with a thermal efficiency of 100% at its lower heating value calculated with the stated enthalpy values at the steam temperature. No CO_2 emissions associated with the consumption of cooling water are assumed.

Table 5.12: Comprehensive results of the EO absorption section

	Reference	Case 4		Reference	Case 4
$y_{E,105}$	0.428	0.482	$y_{E,204}$	0.014	0.008
$y_{EO,105}$	0.013	0.024	$y_{EO,204}$	0.950	0.950
$y_{O_2,105}$	0.064	0.071	$y_{O_2,204}$	$0.52 \cdot 10^{-3}$	$0.30 \cdot 10^{-3}$
$y_{CH_4,105}$	0.080	0	$y_{CH_4,204}$	$0.72 \cdot 10^{-3}$	0
$y_{CO_2,105}$	0.056	0.059	$y_{CO_2,204}$	0.013	0.007
$y_{H_2O,105}$	0.008	0.013	$y_{H_2O,204}$	0.018	0.032
$y_{Ar,105}$	0.352	0.350	$y_{Ar,204}$	0.003	0.002
$\dot{n}_{105}\ \left[\frac{mol}{s}\right]$	77.88	41.04	$\dot{n}_{204}\ \left[\frac{mol}{s}\right]$	1.05	1.05
$y_{E,201}$	0.436	0.500	$y_{E,207}$	0	0
$y_{EO,201}$	0	0	$y_{EO,207}$	0.006	0.004
$y_{O_2,201}$	0.065	0.073	$y_{O_2,207}$	0	0
$y_{CH_4,201}$	0.082	0	$y_{CH_4,207}$	0	0
$y_{CO_2,201}$	0.057	0.061	$y_{CO_2,207}$	$0.2 \cdot 10^{-6}$	$0.1 \cdot 10^{-6}$
$y_{H_2O,201}$	0.002	0.002	$y_{H_2O,207}$	0.994	0.996
$y_{Ar,201}$	0.359	0.364	$y_{Ar,207}$	0	0
$\dot{n}_{201}\ \left[\frac{mol}{s}\right]$	76.34	39.54	$\dot{n}_{207}\ \left[\frac{mol}{s}\right]$	18.59	10.00
$y_{E,203}$	$0.74 \cdot 10^{-3}$	$0.78 \cdot 10^{-3}$	$T_{204}\ [K]$	305.2	315.7
$y_{EO,203}$	0.057	0.094	$p_{204}\ [bar]$	2.6	2.6
$y_{O_2,203}$	$0.28 \cdot 10^{-4}$	$0.29 \cdot 10^{-4}$	$T_{207}\ [K]$	390.9	394.2
$y_{CH_4,203}$	$0.39 \cdot 10^{-4}$	0	$p_{207}\ [bar]$	2.6	2.6
$y_{CO_2,203}$	$0.72 \cdot 10^{-3}$	$0.71 \cdot 10^{-3}$	$\dot{n}_{205}\ \left[\frac{mol}{s}\right]$	34.70	32.35
$y_{H_2O,203}$	0.941	0.904	$\dot{n}_{206}\ \left[\frac{mol}{s}\right]$	33.65	31.29
$y_{Ar,203}$	$0.17 \cdot 10^{-3}$	$0.16 \cdot 10^{-3}$	$\dot{n}_{208}\ \left[\frac{mol}{s}\right]$	0.47	0.45
$\dot{n}_{203}\ \left[\frac{mol}{s}\right]$	19.64	11.05			

The operating conditions of the EO absorber are the same in the reference and intensified case ($T = 298\,K$, $p = 21\,bar$, not additionally given in Tab. 5.12). With respect to the temperature level of the EO desorption column, the operating conditions differ slightly between the reference and intensified case. Here, the intensified case operates at higher temperature both in the condenser and reboiler. The internal streams of the desorption column $\dot{n}_{205}$ and $\dot{n}_{206}$ are reduced in the intensified case leading to a slightly smaller desorption column.

The lower gas recycle stream leads to a higher purge fraction in the intensified case since the amount of inerts arising from the feed streams must be removed as in the reference case (0.024% in the reference case, 0.054% in case 4). In general, the purge fractions are very low since the ethylene costs dominate the production costs and otherwise ethylene which is present in the purge gas is sent to the flare system. These low purge fractions lead to the high argon concentrations in the reactor. However, these high argon fractions are also necessary to stay out of the explosive region.

The split fraction ξ_{S301} specifies the amount of recycle gas which is sent to the CO_2 absorption section. It is optimal to send only a specific split of the recycle gas to the CO_2 absorption section (30.8% in the reference case, 53.3% in case 4), even though the minimum allowed CO_2 mole fraction at the reactor inlet ($y_{CO_2} \geq 0.05$) is met in

both cases. In the CO_2 absorption, the outlet mole fraction of CO_2 in the recycle gas is even below 5% and by mixing this gas stream with the by-passed stream and the fresh feed stream, the reactor inlet constraint for the minimum CO_2 mole fraction is met.

This result can be explained with the complex interaction of CO_2 absorption and purge. It is more worthwhile to send only a part of the recycle gas stream to the CO_2 absorption, reduce its CO_2 content below 5%, and purge afterwards than send all the recycle gas stream to the CO_2 absorption and reduce its CO_2 mole fraction only to 5%. In the latter case, more ethylene will be lost in the CO_2 absorption and purge and hence this option does not pay off. Due to the higher fraction of the recycle stream which is sent to the CO_2 absorption in the intensified case, the gas stream in the CO_2 absorption ($\dot{n}_{401}$) is almost the same in the reference and intensified case (refer to Tab. 5.13). Hence, the CO_2 absorbent stream ($\dot{n}_{407}$) is also very similar.

Table 5.13: Comprehensive results of the CO_2 absorption section

	Reference	**Case 4**		**Reference**	**Case 4**
$y_{E,401}$	0.436	0.450	$y_{E,406}$	0.016	0.017
$y_{EO,401}$	0	0	$y_{EO,406}$	0	0
$y_{O_2,401}$	0.065	0.073	$y_{O_2,406}$	$0.68 \cdot 10^{-3}$	$0.73 \cdot 10^{-3}$
$y_{CH_4,401}$	0.082	0	$y_{CH_4,406}$	$0.90 \cdot 10^{-3}$	0
$y_{CO_2,401}$	0.057	0.061	$y_{CO_2,406}$	0.950	0.950
$y_{H_2O,401}$	0.002	0.002	$y_{H_2O,406}$	0.029	0.029
$y_{Ar,401}$	0.359	0.364	$y_{Ar,406}$	0.004	0.004
$\dot{n}_{401}$ $\left[\frac{mol}{s}\right]$	23.52	21.07	$\dot{n}_{406}$	0.44	0.42
$y_{E,402}$	0.443	0.508	$y_{E,407}$	0	0
$y_{EO,402}$	0	0	$y_{EO,407}$	0	0
$y_{O_2,402}$	0.066	0.075	$y_{O_2,407}$	0	0
$y_{CH_4,402}$	0.083	0	$y_{CH_4,407}$	0	0
$y_{CO_2,402}$	0.040	0.043	$y_{CO_2,407}$	0.006	0.006
$y_{H_2O,402}$	0.004	0.005	$y_{H_2O,407}$	0.994	0.994
$y_{Ar,402}$	0.365	0.370	$y_{Ar,407}$	0	0
$\dot{n}_{402}$ $\left[\frac{mol}{s}\right]$	23.14	20.73	$\dot{n}_{pseudo,H_2O,407}$ $\left[\frac{mol}{s}\right]$	12.66	12.17
$y_{E,403}$	$0.53 \cdot 10^{-3}$	$0.56 \cdot 10^{-3}$	T_{406} $[K]$	299.3	299.3
$y_{EO,403}$	0	0	p_{406} $[bar]$	1.2	1.2
$y_{O_2,403}$	$0.23 \cdot 10^{-4}$	$0.24 \cdot 10^{-4}$	$\dot{n}_{406}$	0.44	0.42
$y_{CH_4,403}$	$0.30 \cdot 10^{-4}$	0	T_{407} $[K]$	376.1	376.1
$y_{CO_2,403}$	0.038	0.038	p_{407} $[bar]$	1.2	1.2
$y_{H_2O,402}$	0.961	0.961	$\dot{n}_{408}$	0.06	0.08
$y_{Ar,403}$	$0.14 \cdot 10^{-3}$	$0.13 \cdot 10^{-3}$	$\dot{n}_{pseudo,K_2CO_3}$ $\left[\frac{mol}{s}\right]$	0.71	0.68
$\dot{n}_{pseudo,H_2O,403}$ $\left[\frac{mol}{s}\right]$	12.67	12.18	$\dot{n}_{pseudo,Pip}$ $\left[\frac{mol}{s}\right]$	0.14	0.13
T $[K]$	313.7	319.4	$\dot{n}_{412}$ $\left[\frac{mol}{s}\right]$	26.16	25.94
p $[bar]$	20	20	$\dot{n}_{413}$ $\left[\frac{mol}{s}\right]$	25.72	25.52

The absorption with a hot potassium carbonate solution is very selective and almost no losses in ethylene and oxygen (refer to $\dot{n}_{406}$, $y_{E,406}$, and $y_{O_2,406}$) occur. The CO_2 outlet concentration of the exhaust gas is 95% and the CO_2 outlet fraction of the recycle gas is well below 5% in both cases. The ethylene losses due to the CO_2 absorption are approximately the same (refer to stream $\dot{n}_{406}$ and $y_{E,406}$). In the intensified case the absorption temperature is slightly higher than in the reference case ($+5\,K$). The operating conditions of the CO_2 desorption column are almost the same in both cases.

The make-up water stream ($\dot{n}_{408}$) is very small and hence it can be neglected for the overall cost estimation.

The compositions of the streams $\dot{n}_{403}$ and $\dot{n}_{407}$ are calculated with the pseudo stream of water and CO_2. Thereby, the total loading of the potassium carbonate solution with CO_2 after the absorber can be identified to be about 3.8%.

Summing up, a cost reduction of 2.06% compared to the optimized reference case is possible by applying advanced cooling and oxygen dosing. In addition, further reductions of the consumed utilities and the CO_2 are obtained.

5.4.5.3 Sensitivity analysis

In this section, a sensitivity analysis is performed to investigate the influence of the model assumptions taken so far. This analysis answers the questions whether the objective function is sensitive to a change in these model parameters and how the cost reduction potential (difference between reference case and intensified case) behaves with respect to the investigated parameters, which are

- the safety margin with respect to the UEL in the reaction module,
- the κ_{EO}/κ_E-ratio,
- the inert fraction in the feed streams,
- the minimum CO_2 fraction during the reaction,
- the minimum space time yield.

For this analysis, the influence of each parameter on the objective function is analyzed in a wide range in order to obtain much more information than by determining only the local sensitivity. The impact of each parameter is determined individually keeping the other parameters constant at their reference values. For each parameter variation the optimization problem is solved anew, determining optimal operation conditions for the new set of parameters. The results of the sensitivity analysis for each parameter are presented in Fig. 5.13.

Due to the safety hazard, a safety margin (ΔEx, defined according to eq. (5.4.37)) need to be enforced in the reaction module. Here, it is investigated how the objective function value change with respect to this safety margin varied in the range of 0% (reference value) to 10%.

$$\sum_{i \in \mathrm{FG}} y_{i,R101} \geq \mathrm{UEL}_{mix} + \Delta\mathrm{Ex} \tag{5.4.37}$$

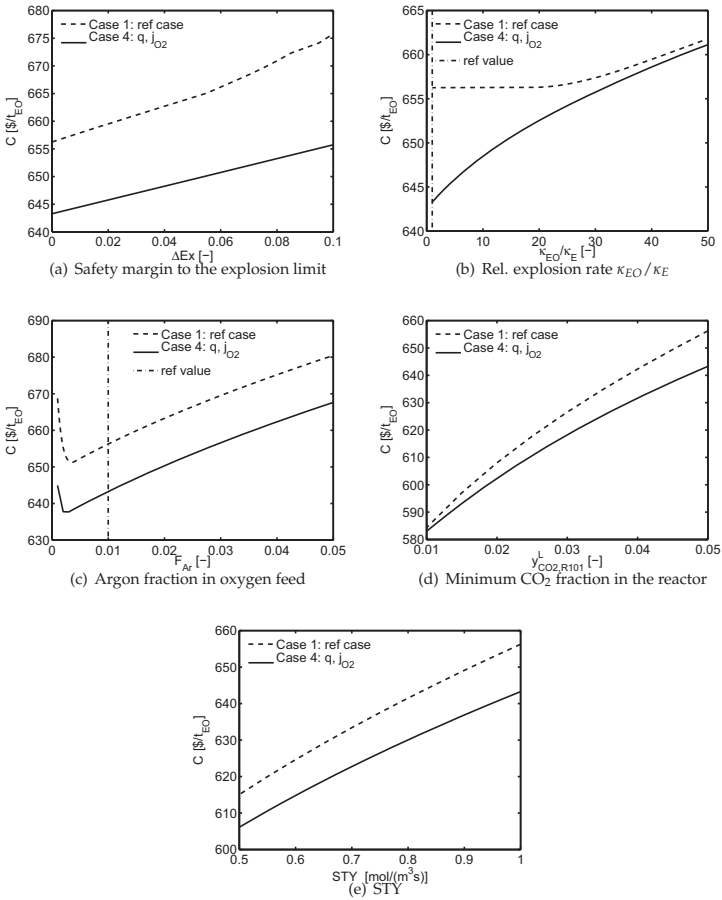

(a) Safety margin to the explosion limit
(b) Rel. explosion rate κ_{EO}/κ_E
(c) Argon fraction in oxygen feed
(d) Minimum CO_2 fraction in the reactor
(e) STY

Figure 5.13: Results of the sensitivity analysis

According to Fig. 5.13(a), a safety margin of up to 10% increases the production costs of the intensified case approximately linear. In the reference, the production costs are more sensitive to the safety margin. Hence, the difference in the operating costs between the reference case and the intensified case increases for a higher safety margin. Therefore, the intensified reaction concept becomes even more worthwhile when a safety margin is enforced in the reactor.

Beside the safety margin, the sensitivity of the production costs with respect to the κ_{EO}/κ_E-ratio is studied. The κ_{EO}/κ_E-ratio refers to the relative combustion rate of ethylene oxide compared to ethylene. Since the influence of EO was not investigated by Klaubert [102], the exact value is not known, and hence a sensitivity study is performed to investigate the impact of this parameter (reference value $\kappa_{EO}/\kappa_E = 1$).

In Fig. 5.13(b) the production costs of both the reference and the intensified case for a κ_{EO}/κ_E-ratio between 1 and 50 are shown. While the reference case is insensitive to the κ_{EO}/κ_E-ratio for $\kappa_{EO}/\kappa_E \leq 20$ (and hardly sensitive for $\kappa_{EO}/\kappa_E > 20$), the performance of the intensified case is more sensitive to the κ_{EO}/κ_E-ratio. This result can be explained by considering that the κ_{EO}/κ_E-ratio becomes important only for high EO mole fractions. At low ethylene oxide concentrations, the presence of EO does hardly affect the UEL, and hence the κ_{EO}/κ_E-ratio has no influence on the performance of the reaction module at low EO mole fractions.

In the reference case, the UEL is only important at the start of the reaction and with ongoing reaction the reaction mixture withdraws from the explosion limit. Hence, the κ_{EO}/κ_E-ratio has no effect on the reactor performance of the reference case as long as $\kappa_{EO}/\kappa_E \leq 20$. For $\kappa_{EO}/\kappa_E > 20$ the reactor inlet conditions must not match the UEL anymore since the explosion limits are exceeded for increasing EO mole fractions otherwise. At this point, κ_{EO}/κ_E-ratio has an impact on the performance of the reaction module and thereby increases the EO production costs.

In the intensified case, the oxygen is dosed in such a way that the reaction mixture is always at its explosion limit. Hence, any $\kappa_{EO}/\kappa_E > 1$ has a direct influence on the allowed composition during the reaction and thereby the performance of the reaction module is decreased for increasing κ_{EO}/κ_E-ratio. However, at low κ_{EO}/κ_E-ratios the economic potential of the intensified case is still worthwhile. In addition, ensuring a safety margin during the reaction seems to be sufficient and for that case the economic potential of the intensified case increases.

With respect to the plant operations, fluctuations in the feed streams might occur. In addition, it is important to know how the process performance depends on the feed composition and what the optimal inert fraction in the feed is. Here, two competing effects are important: On the one hand, the inerts must be removed from the recycle stream resulting in an ethylene loss in the purge stream. On the other hand, argon is used as inert gas in the reaction module. In case no argon is present during the reaction, more methane or CO_2 must be used to stay out of the explosive region resulting in additional methane costs or in a reduced performance of the reaction module due to the higher CO_2 level, respectively. Hence, it is to be expected that a minimum in the production costs with respect to F_{Ar} exists.

Referring to Fig. 5.13(c), the lowest EO production costs for the intensified case are $637 \frac{\$}{kg_{\mathrm{EO}}}$ for an argon fraction in the feed stream of $F_{\mathrm{Ar}} = 0.002$. For $F_{\mathrm{Ar}} \leq 0.002$ the production cost increase rapidly for decreasing inert fraction in the feed; the argon supply by the feed streams is not sufficient to keep the desired inert level during the reaction. For $F_{\mathrm{Ar}} > 0.002$ the production cost increase moderately for an increasing inert fraction; the purge stream need to be increased to keep the desired argon level in the reaction module giving rise to higher ethylene losses in the purge.

The difference in the production costs between the reference and the intensified case are insensitive to the inert fraction of the feed. Hence, it can be concluded that the overall plant performance is sensitive to the inert fraction, but the economic potential

of the intensified reaction concept is independent of the chosen inert fraction in the investigated range.

Since the reaction kinetics are only valid for a CO_2 mole fraction above 5%, this value was enforced in the optimization as a lower limit during the reaction so far. Referring to the results of the reference and intensified case presented in Section 5.4.5, the CO_2 inlet mole fraction was always chosen at its constrained minimum value at the reactor inlet. Hence, reducing the production costs by decreasing the CO_2 inlet mole fraction seems possible. The effect of a minimum CO_2 mole fraction in the reactor down to $y^L_{CO_2} = 0.01$ is investigated and the results are summarized in Fig. 5.13(d). There seems to be a large potential for further savings, e.g. at $y^L_{CO_2} = 0.01$ the production costs for both the reference as well as the intensified reaction concept are predicted to be less than $585 \frac{\$}{t_{EO}}$. These savings are much higher than the additional production costs which might arise from enforcing a safety margin or operating the plant with a higher inert load in the feed streams. However, to investigate if these savings can be realized, the reaction kinetics must be validated in this concentration region by additional experiments. This result underlines the necessity of simultaneous optimization of the reaction system and experimental validation of the reaction kinetics in order to match the experimental conditions to the optimal operating conditions.

In addition to a lower limit for the CO_2 mole fraction in the reactor, the effect of the STY limit is investigated. Referring to Fig. 5.13(e), the process can be operated at much lower running expenses by reducing the STY of the reactor. For example, by decreasing the required STY down to $STY^L = 0.5 \frac{mol}{m^3 \cdot s}$, the production costs are reduced to $607 \frac{\$}{t_{EO}}$ for the intensified reaction concept. However, the cost reduction potential of the intensified case slightly decreases for lower space time yields.

This result can also be used for the revamp of existing plants. In case the existing reactor are replaced with two reactors in parallel operating at 50% of the original STY, the running expenses can be strongly decreased. Since reducing the STY causes higher investment cost for the reactors, this trade-off need to be taken into account when the overall life-cycle costs of the plant is optimized by maximizing the net present value of the plant.

From the sensitivity analysis presented in the section, it can be concluded that the production costs increase slightly by enforcing a safety margin during the reaction or by operating the plant with a higher inert load in the feed streams. However, by reducing the minimum CO_2 mole fraction in the reactor or the STY, the operating costs can drastically be decreased. Except for the κ_{EO}/κ_E-ratio, the cost reduction potential of the intensified case is approximately constant for small changes in all investigated parameters.

5.5 Summary

Regarding the methodological approach, it was shown how

1. dosing and removal concepts can be included in the methodological framework,
2. the catalyst support is adequately chosen using reactor design criteria,
3. the derived technical approximations can be validated using detailed reactor models,
4. the optimal reaction concept from a process point of view can be obtained,
5. complex intrinsic bounds such as explosion limits can be considered,
6. a sensitivity analysis can be used on an early design stage.

Regarding the first aspect, removal concepts for specific components independent of the existence of a technical solution can be efficiently investigated giving rise to the maximum potential of this process intensification measure. Determining the maximum potential is important in order to evaluate if further research on these concepts is worthwhile at an early stage in the process design.

Following the design approach, the best technical reactor is derived from a sequence of models and decisions. The second level, where the principle reactor set-up and catalyst support are chosen, was exemplified with the air based process. In order to avoid external and internal heat and mass transport limitations for the catalyst, reactor design criteria were directly included on this level avoiding unsuited catalyst support geometries.

Furthermore, this approach yields an optimal reactor design without tedious comparison of every possible reactor set-up, and therefore the method saves much effort with respect to computational and model building aspects. In addition, the derived design can always be rated to the optimum case obtained on the previous levels. For the air based process, a two-dimensional reactor model for a tube-in-tube reactor with ethylene dosing and cooling was adjusted for optimization purposes taking a radial dependent void fraction, radial distribution of the axial velocity, the temperature, and the composition into account.

It was shown with the oxygen based EO process how the reaction concept and the plant operation can be optimized simultaneously. Thereby, the optimal reaction concept from a process point of view can be obtained. Here, a complete process model was developed considering the EO absorption in water as well as CO_2 absorption in hot potassium carbonate solution in order to describe the interactions between reaction module and process.

In addition, complex intrinsic bounds can be included on the first level. For the oxygen based process, a model for the explosive region was derived based on literature data.

Furthermore, a sensitivity study with respect to the critical model assumptions was performed for the oxygen based process. This sensitivity analysis allows one to investigate the robustness of the cost reduction potential and gives rise to further process improvements on an early design stage.

Regarding the obtained results of the air based and oxygen based EO processes, it can be concluded that intensified reaction concepts can increase the selectivity and reduce the running expenses of the process. Depending on the catalyst and the concentration range, either ethylene dosing (air based process) or oxygen dosing (oxygen based process) is more worthwhile. It should be noted that all improvements are solely due to the intensified reaction concept since the comparisons are performed based on an optimized reference case using the same basic conditions and model.

In the air based process, a selectivity increase of 3.25% can be obtained, which is quite significant remembering the relatively low conversion. These savings can also be realized by an appropriate technical approximation of the optimal reaction route as was shown by the validation of the results using a more detailed reactor model.

In case of the oxygen based process, a reduction of the running expenses by 2.06% was achieved. For an average plant capacity of $10^5 \frac{t_{EO}}{yr}$ this refers to savings in the order of $1.35 \frac{Mio.\$}{yr}$. Furthermore, the gas recycle stream was significantly reduced leading to smaller apparatuses in the downstream process. In addition, the utility consumption was strongly reduced and the total green house gas emission shortened by $2.6 \cdot 10^4 \frac{t_{CO_2}}{yr}$ for an average EO plant giving rise to a more sustainable and greener process.

Summing up, the method proved to be able to design optimal reactors for complex reaction systems. The approach is very useful for investigating the potential of dosing and removal of certain components and yields the best suited integration and enhancement concept for the investigated reaction system. Complex intrinsic bounds such as explosion limits can be directly considered on level 1, yielding an accurate model from the thermodynamic point of view. In addition, the interactions between the process and the reaction module are included on level 1, yielding an optimized process. The obtained results indicate significant potential for cost reductions, selectivity increases, and CO_2 emission reductions giving rise to a new generation of more economical and sustainable partial oxidation processes.

Chapter 6

Hydroformylation of long chain alkenes

The hydroformylation is one of the industrially most important homogeneously catalyzed reactions. The aldehydes with a chain length above C4 are used for plasticizers, detergents, and surfactants. Due to the good biodegradability of unbranched surfactants, the market for linear long chain aldehydes strongly rises, and hence linear aldehydes are more valuable than iso-aldehydes. Since the separation of n- and iso-aldehydes is very energy intensive and requires also high capital investment, a high n/iso-ratio within the aldehyde production is very important. Beside a high selectivity towards the linear aldehyde, the recovery of the expensive Rh catalyst is of major importance for the economics of the process.

In Section 6.1 different hydroformylation process technologies with special focus on the production of long chain aldehydes are shortly introduced. In addition, different process intensification approaches to overcome the reactant solubility and catalyst recycling limitations recently proposed in the literature are discussed.

Afterwards, existing design approaches for multiphase reactors and new reactor designs for hydroformylation are reviewed in Section 6.2.

In Section 6.3 an optimal reactor design for the hydroformylation of 1-octene within a multiphase system is derived applying the proposed methodology [107]. Here, the special focus is on the extension of the design approach towards multiphase systems and gas-liquid mass transfer. As long as the reaction only takes place in one phase, the other phases such as the gas phase are regarded as service phases, which are used to manipulate the reaction phase in an optimal manner.

Section 6.4 provides a short summary of the obtained results for the hydroformylation.

6.1 Process description

In case of the hydroformylation, different process technologies depending on the chain length of the reactant exist. In principle, short chain alkenes are produced very efficiently using a Rh-based catalyst. For the long chain alkenes, mostly Co-based processes are applied suffering from a lower selectivity towards the linear aldehyde and lower activity.

The state-of-the-art hydroformylation process for short chain aldehydes ($\leq$ C4), namely the Ruhrchemie-Rhône Poulenc process, cannot be applied to long chain alkenes since the alkenes are not soluble in the aqueous catalyst phase (e.g. [108]). The other prevalent process for short chain aldehydes, the low pressure UCC process [109], was adapted for higher alkenes. In this process, solvent and catalyst are mainly recovered by extraction, which requires energy intensive recovery of the catalyst from the extracting phase and involves high investment costs [110, 111]. Due to the catalyst separation problem, industrial processes for the production of long chain aldehydes are still mainly based on Co-systems as catalysts. Here, the catalyst is much cheaper and higher catalyst losses can be accepted. In addition, the Co-based catalysts are more robust allowing catalyst recovery at higher temperatures. Since Rh-based catalyst systems with state-of-the-art ligands provide much higher selectivities and space time yields, large efforts are put into the development of Rh-based processes for the hydroformylation of long chain alkenes.

In order to overcome the catalyst recycle and reactant solubility problem and obtain an energetically efficient process, several innovative concepts are currently under investigation in academia. Those are thermomorphic solvent systems (e.g. [112]), micellar solvent systems (e.g. [113, 114]), perfluorinated solvents (e.g. [115]), biphasic ionic liquid (IL) systems (e.g. [116, 117]), supported ionic liquid phase catalysts (e.g. [118]), supported aqueous phase catalysts (e.g. [119, 120]), and polymer attached ligands where the catalyst is retarded by a membrane [121]. In addition, the solvent-free hydroformylation [122] and the hydroformylation using $scCO_2$ [123] are current research topics.

The objective of this example is the design of an optimal reactor for the hydroformylation of long chain alkenes. For this purpose, a biphasic ionic liquid (IL) system with TPPTS modified Rh as catalyst as investigated by Sharma et al. [117] is chosen. The catalyst is present in an IL phase, while reactants and products are present in the organic phase. The IL system ensures a simple and efficient catalyst recycling and the octene solubility in the catalyst phase is significantly improved compared to aqueous systems [117, 124]. The choice of the example system is mainly due to the availability of reaction kinetics. The other systems mentioned before are also promising approaches for better hydroformylation process, but no reaction kinetics describing the complete reaction network of the hydroformylation are published so far. Hence, a model-based reactor design for these systems is not yet possible.

Before the methodology is extended towards multiphase systems and applied to the hydroformylation, existing optimal design strategies for multiphase reactors are discussed in the next section.

6.2 Optimal design of multiphase reactors

Most of the existing reactor design approaches discussed in Section 2.3 have been developed for homogeneous systems.

In the field of multiphase reactor design methodologies, only few approaches are published [125–127]. Krishna and Sie [125] developed a strategy for the selection of multiphase reactors. It is intended to choose from a set of suited reactors from a multitude of existing apparatuses depending on the existing phases (gas/solid, gas/liquid,

gas/liquid/solid) and the specific requirements of the investigated reaction system. Mehta and Kokossis [126] proposed reactor configurations for non-isothermal, multiphase systems. The flow pattern (ideally distributed or ideally back-mixed) for the gas and liquid phase can be chosen, and in each reactor segment the phases are in equilibrium. Kelkar and Ng [127] proposed a screening method for non-isothermal, multiphase reactors. It is based on a generic reactor model, a sensitivity analysis, and knowledge based heuristics. Despite the fact that these approaches can support the decision of the contacting pattern, exchange area, and at the end the choice of reactor, they can hardly give rise to new apparatuses since the methods are intended to choose from existing reactors [125], are based on ideal PFTR and CSTR reactors [126], or use a construction set of different reactor parts [127].

As stated in Chapter 3, a reactor can be regarded as optimal if the reactant concentrations, temperature, and pressure follow their optimal profiles along the entire reaction coordinate. For single phase systems the design methodology based on this idea was presented in the previous examples.

In this chapter, the method is extended for the design of optimal multiphase reactors. Here, the main focus is on the optimal concentration and temperature profiles in the gas and liquid phase, and on the optimal exchange for the gas-liquid heat and mass transfer. Since the reactions occur in the liquid phase, the gas phase is considered as service phase which can be manipulated in order to provide optimal gas component fluxes into the reactive liquid phase.

As for the single phase system, the methodology consists of three design levels where technical restrictions are added on each level. On the first level, the optimal route in state space is calculated for the reaction phase. Again, this route is obtained by optimal manipulation of a fluid element via energy and material fluxes (refer to Fig. 6.1).

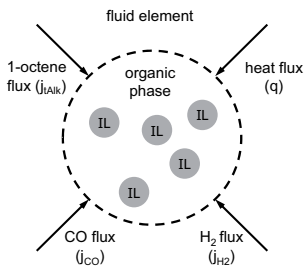

Figure 6.1: Material and energy envelope of the balanced fluid element

On the second level, the influence of limited mass and energy transport is investigated. In a gas-liquid system the mass transport between the gas-liquid phase must be optimized. Here, only maximizing the gas-liquid mass transfer leads to suboptimal solutions since the costs for high mass transfer rates, for example in terms of pressure drop, must also be taken into account. In addition, a multitude of contact apparatuses exist and all have different mass transfer characteristics and it is not reasonable to compare all possible apparatuses. Hence, the inverse problem is solved; a sensitivity study with respect to the ($k_L a$)-value is performed and thereby the optimal

(k_La)-value with respect to reactor performance and costs is chosen. In accordance to the approach for single phase systems, it is also investigated if the desired flux profiles are attainable by identifying control variables which can be manipulated by the reactor design and solving the according optimization problems.

On the third level, the best possible technical reactor is derived based on the results of level 2. The control variable profiles are approximated and the desired (k_La)-value is realized by the choice of the gas-liquid mixing strategy.

With regard to the hydroformylation, two earlier publications demonstrate the potential of innovative reactor concepts. Wiese et al. [128] showed that the STY of the biphasic Ruhrchemie-Rhône Poulenc process for short chain alkenes can be significantly increased by applying a reactor which provides higher gas-liquid mass transfer rates compared to the industrial predominant bubble column reactors. Enache et al. [122] compared a stirred tank batch reactor to a capillary flow reactor with sophisticated temperature control. Here, the reaction rate was increased by a factor of 10, and also the selectivity was slightly increased. Although, these two examples demonstrate the potential of an innovative reactor design for the hydroformylation, the rigorous design of optimal hydroformylation reactors is still an open question to be adressed.

6.3 Design of an optimal hydroformylation reactor

6.3.1 Level 1: Integration and enhancement concepts

6.3.1.1 Reaction system

In order to exemplify the design method for multiphase reactors, the biphasic IL hydroformylation system investigated by Sharma et al. [117] is chosen.

The product spectrum of the hydroformylation consists of the n- and iso-aldehydes, the n- and iso-alcohols, the alkane, internal alkenes, and high boiling components. The extent of the occurrence of the side reactions depends on the catalyst (Rh or Co), the ligand, the solvent, and the reaction conditions.

The macroscopic reaction network considered in this work is based on the simplified reaction network reported by Sharma et al. [117] for the investigated biphasic IL hydroformylation system and extended by the consecutive reactions of the aldehydes. Beside the hydroformylation reactions towards the linear and branched aldehyde, also the isomerization reaction, and the consecutive reactions towards the alcohols are considered (refer to Fig. 6.2). The hydrogenation reactions of the terminal and internal alkenes are not included in the reaction network since they were not observed for the investigated biphasic IL hydroformylation system.

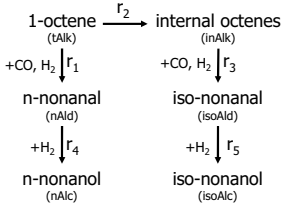

Figure 6.2: Simplified reaction network of the hydroformylation

The catalyst is present in several modifications (refer to Fig. 6.3), where each species has a different selectivity and activity. In order to obtain high amounts of n-aldehyde, the $HRh(CO)L_2$ species is desired. The mono-substituted and unmodified species are considered to be highly active, but unselective with regard to the n/iso-ratio and the hydrogenation and isomerization reaction. The tri-substituted and $HRh(CO)_2L_2$ species are regarded as inactive. The catalyst equilibrium depends on the reaction conditions (T, C_{H_2}, C_{CO}), and hence the selectivity depends on these conditions, too. In addition to the catalyst equilibrium shown in Fig. 6.3, the catalyst agglomerates if the hydrogen concentration is too low.

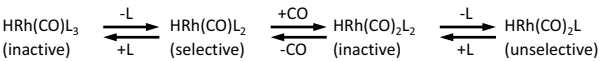

Figure 6.3: Catalyst equilibrium of the TPPTS modified Rh catalyst

According to the Wilkinson cycle [129], a high CO concentration leads to the formation of an inactive species in the catalytic cycle. Therefore, a high CO concentration will reduce the activity of the hydroformylation system. Contrarily, hydrogen is most often assumed to have a linear influence on the reaction rate. Hence, a high H_2:CO-ratio will increase the activity of the hydroformylation system, which was also shown experimentally for $CO:H_2$ ratios between 0.8 and 1.2 by Haumann et al. [114]. However, if the hydrogen concentration is too high, the hydrogenation of the reactants and products will be promoted. Despite these promising findings, controlling the H_2:CO-ratio in the design of hydroformylation reactors has not been considered so far.

The isomerization reaction indirectly promotes the reaction to the iso-aldehyde via the formation of internal alkenes. Based on the experimental results of Sharma et al. [117] it can be concluded that hardly any iso-aldehyde is directly formed from the terminal alkene in the investigated hydroformylation system. Since the isomerization depends on the 1-octene concentration, controlling the reactant concentration is of major importance for minimization of the iso-aldehyde formation.

The discussed dependencies can also be observed in the reaction kinetics given by eq. (6.3.5) – eq. (6.3.9). Referring to eq. (6.3.5), CO has an inhibiting effect on the formation of the linear aldehyde and the optimal CO concentration depends on the alkene concentration. Hydrogen has a positive influence on the formation of the linear aldehyde since the isomerization reaction is not promoted by hydrogen. How-

ever, a high hydrogen concentration will also lead to the increased formation of alcohols.

The reaction rates are obtained from Sharma et al. [117] and are extended by the temperature dependencies using additional information from the literature [110, 117, 120, 130]. In case the consecutive reactions of the aldehydes are not modeled, the optimal reaction concept can be efficiently approximated by a CSTR as was shown in [131]. However, such a model does not adequately describe the reaction network present during hydroformylation since it neglects the consecutive reaction which might significantly reduce the selectivity.

In order to describe the conditions in the hydroformylation reaction system more realistically, the consecutive formation of alcohols is taken into account since alcohols are observed in the product spectrum of the adapted UCC process for higher alkenes [110]. With respect to the consecutive reactions this work should be regarded as a case study since no kinetics of the alcohol formation are available in the open literature and therefore several assumptions had to be made.

6.3.1.2 Model equations

Sharma et al. [132] showed that the direct transport from the gas phase into the dispersed IL phase can be neglected compared to the transport from the gas phase into the continuous organic phase and subsequently into the IL phase. In addition, the transport of gas and 1-octene from the organic phase into the IL phase is much faster than the reaction [132]. Hence, a pseudo-homogeneous model of the liquid phase is used where the organic phase and the IL phase are in equilibrium. However, between the gas and liquid phase the mass transport is rigorously considered.

In order to reduce the model complexity, the temperature profile is directly taken as an optimization profile for the intensified case of level 1. Since the heat flux is unrestricted, any possible temperature profile is attainable.

Component mass balance and org/IL phase distribution The mass balance for each component is given by eq. (6.3.1). It is assumed that decane is not soluble in the IL phase and vice versa, which is in good agreement with the experimental findings [117]. On level 1, eq. (6.3.1) has only to be solved for liquid phase components ($i \in COML$) since the concentrations of the gas phase components are directly calculated using the according solubility. On level 2, eq. (6.3.1) for H_2 and CO in the liquid phase is additionally required ($i \in COM$).

$$\frac{\mathrm{d}n_{i,liq}}{\mathrm{d}t} = j_{tot,i} + \sum_{j=1}^{NR} \nu_{i,j} \cdot r_j \cdot V_{IL} \tag{6.3.1}$$

The distribution of the liquid phase components between organic and IL phase are calculated using eq. (6.3.2) combined with eq. (6.3.4). The phase equilibrium can only be approximated since equilibrium data is hardly available and no parameters for activity coefficient models or equation of state models are available. For alkenes and aldehydes the K-values are mean values obtained from the literature [117] ($K_{tAlk} = K_{inAlk} = 1.00 \cdot 10^{-2}$, $K_{nAld} = K_{isoAld} = 1.61 \cdot 10^{-3}$). It is assumed that the alcohols can

be described with the K-values of the aldehydes. The K-values of the gas components are considered to behave like the inverse of the Henry coefficients stated in eq. (6.3.3).

$$K_i = \frac{w_{i,IL}}{w_{i,org}}, \quad i = tAlk\,, inAlk\,, nAld\,, isoAld\,, nAlc\,, isoAlc \tag{6.3.2}$$

$$K_i = \frac{x_{i,IL} \cdot C_{tot,IL}}{x_{i,org}} = \frac{H_{i,IL}^{-1}}{H_{i,org}^{-1}}, \quad i \in COMG \tag{6.3.3}$$

$$n_{i,liq} = n_{i,IL} + n_{i,org}, \quad i \in COML \tag{6.3.4}$$

Reaction rates The reaction rates for the hydroformylation of the terminal and internal alkene, and for the isomerization are obtained from Sharma et al. [117]. The model is extended by taking the temperature dependency of the reaction rates into account. The activation energy of r_1 is taken from Sharma et al. [117], while the activation energy of the isomerization reaction is obtained by regression of data from Disser et al. [120]. The activation energy of the formation of isomeric aldehyde is assumed to be the same as for the n-aldehyde formation, which is based on the observations of Bernas et al. [130] for short chain aldehydes.

In order to model the hydrogenation of the aldehydes, several assumptions need to be taken. Based on first principles, the alcohol formation is assumed to depend linearly on the aldehyde, the H_2, and the catalyst concentration in the IL phase. The hydrogenation of the n- and iso-aldehyde are assumed to have an identical activation energy and frequency factor. Based on the selectivity towards the aldehydes of the adapted UCC process for higher alkenes ($S = 95\%$) [110], it is assumed that 5% of the converted alkene reacts to alcohols. The frequency factor of the alcohol formation was estimated by taking the reference case stated in Peschel et al. [131] and assuming an activation energy of half of that of the n-aldehyde formation.

$$r_1 = k_{0,1} \cdot \exp\left(\frac{-E_{A,1}}{R \cdot T}\right) \cdot \frac{C_{tAlk,IL} \cdot C_{H_2,IL} \cdot C_{CO,IL} \cdot C_{cat,IL}}{1 + K_{CO} \cdot C_{CO,IL}^3 \cdot C_{tAlk,IL}} \tag{6.3.5}$$

$$r_2 = k_{0,2} \cdot \exp\left(\frac{-E_{A,2}}{R \cdot T}\right) \cdot C_{tAlk,IL} \cdot C_{cat,IL} \tag{6.3.6}$$

$$r_3 = k_{0,3} \cdot \exp\left(\frac{-E_{A,3}}{R \cdot T}\right) \cdot C_{inAlk,IL} \cdot C_{H_2,IL} \cdot C_{CO,IL} \cdot C_{cat,IL} \tag{6.3.7}$$

$$r_4 = k_{0,4} \cdot \exp\left(\frac{-E_{A,4}}{R \cdot T}\right) \cdot C_{nAld,IL} \cdot C_{H_2,IL} \cdot C_{cat,IL} \tag{6.3.8}$$

$$r_5 = k_{0,5} \cdot \exp\left(\frac{-E_{A,5}}{R \cdot T}\right) \cdot C_{isoAld,IL} \cdot C_{H_2,IL} \cdot C_{cat,IL} \tag{6.3.9}$$

All reaction rate parameters are summarized in Tab. 6.1. The catalyst concentration in the IL phase is chosen constant $C_{cat,IL} = 5 \cdot 10^{-2}\ \frac{kmol}{m_{IL}^3}$. The CO adsorption constant is $K_{CO} = 1.023 \cdot 10^{-6} \left(\frac{mol}{m^3}\right)^{-4}$ [117].

Table 6.1: Kinetic parameters of the reaction rates

Reaction	$E_A \left[\frac{J}{mol}\right]$	$k_0 \left[\left(\frac{mol}{m^3}\right)^{-n}\right]$
1: Hydroformylation of terminal alkene	$107.9 \cdot 10^3$	$40.65 \cdot 10^9, n = 3$
2: Isomerization of terminal alkene	$43.6 \cdot 10^3$	$11.16 \cdot 10^3, n = 1$
3: Hydroformylation of internal alkene	$107.9 \cdot 10^3$	$33.51 \cdot 10^9, n = 3$
4: Alcohol formation from n-Aldehyde	$53.95 \cdot 10^3$	$1.233 \cdot 10^2, n = 2$
5: Alcohol formation from iso-Aldehyde	$53.95 \cdot 10^3$	$1.233 \cdot 10^2, n = 2$

Further constitutive equations The volume of the organic phase and IL phase are each calculated using a linear mixing rule and neglecting the influence of the gases and the catalyst (refer to eq. (6.3.10)). The densities of all liquid phase components are considered to temperature dependent and are given by eq. (6.3.11). The sets of gas components $(COMG)$ and liquid components $(COML)$ are defined according to the reference state of each species as given in Tab. 6.4. The parameters are fitted in the range $353\,K \leq T \leq 373\,K$ to data given in the literature [133, 134].

$$V_k = \sum_{i \in COML} \frac{n_{i,k} \cdot M_i}{\rho_i}, \quad k = IL, org \tag{6.3.10}$$

$$\rho_i = A_{\rho,i} \cdot T + B_{\rho,i}, \quad i \in COML \tag{6.3.11}$$

Table 6.2: Parameters for density calculation

Component	$A_{\rho,i} \left[\frac{kg}{m^3 \cdot K}\right]$	$B_{\rho,i} \left[\frac{kg}{m^3}\right]$
Decane	-0.8597	990.1
1-Octene	-1.0240	1025.3
2-Octene	-0.9869	1022.6
n-Nonanal	-0.7925	1061.0
iso-Nonanal	-0.9777	1165.0
n-Nonanol	-0.7610	1055.4
iso-Nonanol	-0.9704	1125.4
[bmim] [PF_6]	-0.8052	1604.2

Solubility The concentration of H_2 and CO in the IL and in the organic phase are limited by their solubility, which depends on the temperature and the according partial pressure. The solubility is modeled using Henry's law based on the experimental data given by Sharma et al. [117], Srivatsan et al. [135], and Park et al. [136] and the parameters are summarized in Tab. 6.3.

$$C^s_{i,IL} = H^{-1}_{i,IL} \cdot p_i, \quad i \in COMG \tag{6.3.12}$$
$$x^s_{i,org} = H^{-1}_{i,org} \cdot p_i, \quad i \in COMG \tag{6.3.13}$$
$$H^{-1}_{i,k} = A_{H,i,k} + B_{H,i,k} \cdot T, \quad i \in COMG \tag{6.3.14}$$
$$p_{\mathrm{H_2}} + p_{\mathrm{CO}} = p \tag{6.3.15}$$

Table 6.3: Parameters of Henry coefficients

Component	$A_{H,i,IL}\ \left[\frac{mol}{m^3 \cdot Pa}\right]$	$B_{H,i,IL}\ \left[\frac{mol}{m^3 \cdot Pa \cdot K}\right]$
CO	$4.6936 \cdot 10^{-5}$	$-8.6482 \cdot 10^{-8}$
H_2	$1.076 \cdot 10^{-5}$	$2.645921 \cdot 10^{-9}$
Component	$A_{H,i,org}\ \left[\frac{1}{Pa}\right]$	$B_{H,i,org}\ \left[\frac{1}{Pa \cdot K}\right]$
CO	$6.3853 \cdot 10^{-9}$	$2.4456 \cdot 10^{-11}$
H_2	$-7.8249 \cdot 10^{-9}$	$4.3979 \cdot 10^{-11}$

Intrinsic bounds On all levels, bounds on the pressure and temperature range are enforced in order to ensure the validity of the reaction kinetics and the solubility model.

$$353\,K \leq T \leq 373\,K \tag{6.3.16}$$
$$1\,bar \leq p \leq 60\,bar \tag{6.3.17}$$

System bounds The total amount of terminal octene ($n_{tAlk,tot}$) must be the same for all cases and is chosen as scaling variable for the optimization. The initial amount of 1-octene ($n_{tAlk,0}$) in addition to the amount added along the reaction coordinate must match the total amount, which is the same for all calculations.

$$n_{tAlk,tot} = n_{tAlk,0} + \int_{t_0}^{t_f} j_{tot,tAlk} \mathrm{d}t \tag{6.3.18}$$

In the investigated system, decane is present as solvent in the organic phase. In order to ensure conditions comparable to the conditions at which the experiments for the reaction kinetics where conducted [117], the amount of decane with respect to the total amount of octene is specified according to eq. (6.3.19).

$$C_{tAlk} = \frac{n_{tAlk,tot}}{\frac{n_{tAlk,tot} \cdot M_{tAlk}}{\rho_{tAlk}(373\,K)} + \frac{n_{Dec} \cdot M_{Dec}}{\rho_{Dec}(373\,K)}} = 2 \cdot 10^3\,\frac{mol}{m^3} \tag{6.3.19}$$

The volume of organic solvent compared to the volume of IL is restricted to be within certain limits (eq. (6.3.20), $V_{frac}^{L} = 1.5$, $V_{frac}^{U} = 5$, calculated at 373 K) in order to ensure that the IL phase is dispersed within the organic phase.

$$V_{frac}^{L} \leq \frac{V_{Dec}}{V_{IL}} \leq V_{frac}^{U} \tag{6.3.20}$$

Recycle condition In order to model the recycling of the solvent and unreacted alkene, the initial amount of terminal alkene ($n_{tAlk,0}$) must be greater than or equal to the amount of terminal alkene at the end of the reaction ($n_{tAlk,f}$) (refer to the separation scheme shown in Fig. 6.9).

$$n_{tAlk,0} \geq n_{tAlk,f} \tag{6.3.21}$$

STY, X, and S In order to compare all investigated cases on a fair basis, a minimum space time yield depending on the conversion is defined. Here, the STY with respect to the liquid phase of the reference case is used as a lower bound for all intensified cases (refer to Fig. 6.5(b)). The conversion of 1-octene is given by eq. (6.3.23).

$$STY\,(X) = \frac{n_{nAld,f} - n_{nAld,0}}{\int_{t_0}^{t_f} \left(V_{IL} + V_{org}\right) \mathrm{d}t} \geq STY^{L}\,(X) \tag{6.3.22}$$

$$X = \frac{n_{tAlk,tot} - n_{tAlk,f}}{n_{tAlk,tot}} \tag{6.3.23}$$

$$S = \frac{n_{nAld,f} - n_{nAld,0}}{n_{tAlk,tot} - n_{tAlk,f}} \tag{6.3.24}$$

6.3.1.3 Investigated reaction concepts and problem statements

In order to calculate the optimal route in state space, a dynamic optimization problem must be solved. The problem is subject to the component mass balances, the energy balance, the reaction kinetics, thermodynamic relationships such as the solubility of the reactants in the IL, and bounds on temperature, pressure, STY, and conversion. The objective is to maximize the n-aldehyde selectivity since it is the desired product. The investigated reaction concepts are summarized in Fig. 6.4 and the according optimization problems (DOP1 ref), (DOP1 int), and (DOP1 CSTR) are stated below.

Since the best conversion for the reaction system is not known, a conversion study is performed on this level. In order to have comparable conditions for all investigated set-ups, the same total amount of 1-octene $n_{tAlk,tot}$ must be present in each case.

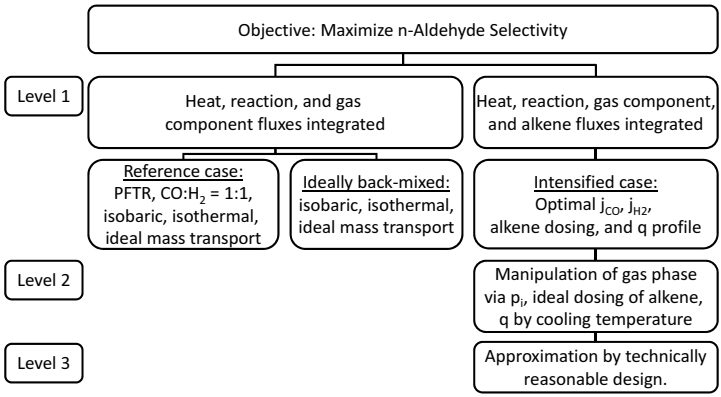

Figure 6.4: Decision structure for the development of an optimal hydroformylation reactor

Reference case As reference case an isothermal and isobaric batch reactor, which corresponds to a continuously operated reactor with plug flow characteristics in steady state, is chosen. It is assumed that the system operates with synthesis gas ($p_{\mathrm{H_2}} : p_{\mathrm{CO}} = 1$) and that the gas concentration in the liquid is defined by its saturation limit. The total pressure is a degree of freedom, but it is bounded by an upper limit.

$$\mathrm{Obj} = \max_{T,p,V_{frac},\tau} S \qquad \text{(DOP1 ref)}$$

s.t.

Component balances and phase distribution: eq. (6.3.1) – eq. (6.3.4)

Reaction kinetics: eq. (6.3.5) – eq. (6.3.9)

Further constitutive equations: eq. (6.3.10) – eq. (6.3.11)

Solubility and gas composition: eq. (6.3.12) – eq. (6.3.15), $p_{\mathrm{H_2}} = p_{\mathrm{CO}}$

Intrinsic bounds: eq. (6.3.16) – eq. (6.3.17)

System bounds: eq. (6.3.18) – eq. (6.3.20)

Recycle condition: eq. (6.3.21)

Conversion: eq. (6.3.23)

Ideally back-mixed In order to compare the results obtained for the intensified case to an ideally back-mixed system, a CSTR model is formulated and optimized additionally. The characteristics of such a back-mixed system can also be obtained using the dynamic optimization of the fluid element; the flux profiles over the entire reaction coordinate might be chosen by the optimizer in such a way that the state variables are constant. It was already shown that if no consecutive reactions occur, a CSTR is a well suited approximation of the dosing profiles obtained in the intensified case [131]. Considering consecutive reactions, however, the CSTR will perform worse compared to the intensified case.

The CSTR operates at the outlet conditions and hence the balance equations simplify. All additional required equations are given in Appendix A.3.2. The inlet concentration of 1-octene is defined by eq. (6.3.19). The temperature, the volume fraction of the IL, and the partial pressures of H_2 and CO are degrees of freedom. In contrast to the reference case, it is assumed that the partial pressures of the gases (i.e. H_2 and CO) can be adjusted individually.

$$\text{Obj} = \max_{T,p,V_{frac},\tau} S_{CSTR} \qquad \text{(DOP1 CSTR)}$$

s.t.

Component balances and phase distribution: eq. (A.3.8), eq. (6.3.2) – eq. (6.3.4)

Reaction kinetics: eq. (6.3.5) – eq. (6.3.9)

Further constitutive equations: eq. (A.3.9) – eq. (A.3.11), eq. (6.3.11)

Solubility: eq. (6.3.12) – eq. (6.3.15)

Intrinsic bounds: eq. (6.3.16) – eq. (6.3.17)

System bounds: eq. (A.3.12), eq. (A.3.13)

Recycle condition: eq. (A.3.14)

Conversion: eq. (A.3.15)

Intensified case In the intensified case, an optimal heat flux profile as well as optimal H_2, CO, and 1-octene flux profiles into the fluid element are calculated in order to maintain the optimal reaction conditions in terms of T, C_{H_2}, C_{CO}, and C_{tAlk} over the entire reaction coordinate. Controlling the 1-octene flux is meaningful due to the isomerization reaction, which reduces the selectivity towards the linear aldehyde significantly at high 1-octene concentrations. In addition, the optimal gas phase composition will change along the reaction coordinate and hence the fluxes of H_2 and CO should be controlled. The upper limits for the gas and octene concentrations in the IL are still defined by the solubility. In addition, a minimum STY for each conversion is enforced, which is defined by the according STY of the reference case (refer to Fig. 6.5(b)).

$$\text{Obj} = \max_{\substack{T(t),p_{H_2}(t),p_{CO}(t),\dot{n}_{tAlk}(t),\\ n_{tAlk,0},V_{frac},\tau}} S \qquad \text{(DOP1 int)}$$

s.t.

Component balances and phase distribution: eq. (6.3.1) – eq. (6.3.4)

Reaction kinetics: eq. (6.3.5) – eq. (6.3.9)

Further constitutive equations: eq. (6.3.10) – eq. (6.3.11)

Solubility: eq. (6.3.12) – eq. (6.3.15)

Intrinsic bounds: eq. (6.3.16) – eq. (6.3.17)

System bounds: eq. (6.3.18) – eq. (6.3.20)

Recycle condition: eq. (6.3.21)

STY: eq. (6.3.22)

Conversion: eq. (6.3.23)

6.3.1.4 Results

The results of the calculations of level 1 are summarized in Fig. 6.5. The attainable selectivities (Fig. 6.5(a)) and the according STY (Fig. 6.5(b)) for each reaction concept depending on the conversion are shown.

For the reference case, the selectivity reaches a maximum at a conversion of 90% followed by a rapid decrease for higher conversions. For a decreasing 1-octene concentration the rate of the parallel reaction decreases faster than the rate of the hydroformylation, and hence the selectivity increases up to a certain conversion (refer to Fig. 6.6(c), differential selectivity). However, larger residence times in the reactor, which are necessary to obtain higher conversions, promote the consecutive reaction and thus the selectivity reduces.

In the intensified reaction concept the optimal trade-off between parallel and consecutive reaction is obtained over the entire residence time since the 1-octene concentration, H_2, and CO concentration as well as the temperature are optimally controlled. At low conversions the intensified case and the CSTR yield almost the same selectivity and STY. Due to the minor importance of the consecutive reaction at low residence times, the optimal 1-octene profile matches the characteristics of an ideally back-mixed system, which is in accordance to the results of our earlier studies [131]. At higher conversion, selectivity and STY of the CSTR are significantly reduced, and hence a CSTR is not able to approximate the intensified reaction concept anymore. Applying the intensified reaction concept the selectivity can be maintained close to its maximum up to a conversion of 80%.

For the choice of the desired conversion in the reactor plant wide considerations have to be taken into account. In general, a higher conversion leads to lower separation costs due to reduced recycle flow rates. Hence, there is a trade-off between the selectivity and the conversion. In order to reasonably satisfy this trade-off, a conversion of 80% was chosen for the further investigations.

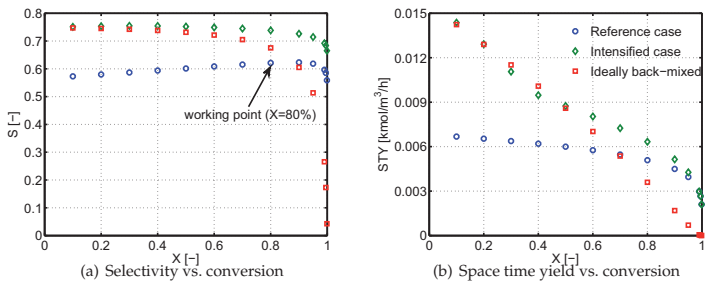

(a) Selectivity vs. conversion (b) Space time yield vs. conversion

Figure 6.5: Results level 1: Space time yield and selectivity

The profiles for the concentration of the liquid components in the pseudo-liquid phase (IL + organic phase), the reaction rates, the differential selectivity S_{diff}, and the

flux profiles are shown in Fig. 6.6 for the reference case (left hand side) and for the intensified case (right hand side). For a better comparison, all fluxes are normalized with their respective maximum values, and the reaction rates are normalized with the maximum rate observed in the discussed case. The definition of the normalized variables and the according reference values are summarized in Appendix A.3.1.

Fig. 6.6(a) illustrates the liquid phase concentration profiles for the reference case. The 1-octene profile is in accordance with a typical reactant profile in a batch process (or reactor with PFTR characteristics). The optimal pressure and temperature are both at their respective maximum value (not shown in figure). In order to obtain saturated conditions for H_2 and CO in the liquid phase and a constant temperature, non trivial flux profiles are required as shown in Fig. 6.6(e).

On the right hand side of Fig. 6.6, the profiles for the intensified case are shown. As can be seen from the comparison of Fig. 6.6(a) and Fig. 6.6(b), both cases differ significantly. The 1-octene concentration starts at the lowest value allowed by the recycling condition (eq. (6.3.21)) and decreases to approximately 0.2 $\frac{kmol}{m^3_{liq}}$ followed by an increase up to 0.75 $\frac{kmol}{m^3_{liq}}$ caused by the dosing of 1-octene (refer to Fig. 6.6(f)). After a residence time of 80 s the 1-octene flux vanishes, and hence 1-octene is consumed to its outlet value defined by the conversion.

It should be noted that the dosing profile of 1-octene is optimized as a continuous and free control function, i.e. any dosing profile of 1-octene is allowed, and is not a priori restricted to three segments as it is done by other design approaches [56]. However, the 1-octene flux is restricted to be positive since a selective withdrawal of 1-octene from the system is not reasonable being a reactant component, and also hardly feasible.

The unconventional dosing profile of 1-octene can be explained with the fact that the same amount of 1-octene must be converted as in the reference case. In the intensified case, the reactant can be present at the beginning and in addition it can be dosed over the residence time. The minimum amount of 1-octene present at the beginning is defined by the recycle condition eq. (6.3.21), which defines that the unconverted amount of 1-octene is recycled with the organic solvent (refer to Fig. 6.9).

At the beginning of the reaction, the optimal alkene dosing profile increases the selectivity of r_1 over r_2 since r_2 has a higher order dependency on the 1-octene concentration than r_1 (compare eq. (6.3.5) and eq. (6.3.6)). However, 1-octene is not kept at a low concentration all the time since the consecutive reactions become increasingly important for longer residence times and higher n-aldehyde concentrations.

The dosing profile of 1-octene causes kinks in the 1-octene concentration and subsequently in all other fluxes. Since the optimal heat flux profile aims to maintain the temperature at its upper limit, it is approximately proportional to the rate of the dominant reaction (r_1), which depends on the 1-octene concentration. The optimal CO concentration is inversely proportional to the 1-octene concentration (refer to eq. (6.3.5)), and hence CO is adjusted accordingly. Since H_2 is correlated to CO by the maximum pressure constraint (eq. (6.3.17)), the H_2 flux is also linked to the CO flux. The realization of the optimal CO and H_2 fluxes will probably require a varying H_2:CO-ratio in the gas phase, which is part of the investigations on level 2.

The optimal temperature and pressure of the system are always at their respective upper boundaries stated in eq. (6.3.16) and eq. (6.3.17), respectively. Regarding the

ionic liquid phase, the optimal H_2 concentration is much higher than the optimal CO concentration even though the fluxes are almost the same (refer to the equilibrium concentration in Fig. 6.7(c) for level 2). This leads to the conclusion that the selectivity can be enhanced further by a higher temperature and H_2 concentration in the ionic liquid phase. The potential of a temperature and pressure increase can be evaluated by a sensitivity analysis shifting these bounds. However, in order to obtain reliable results the model validity range must be extended by further experiments. How a sensitivity analysis can be used in order to investigate the influence of critical assumptions and to shift the system constraints was already demonstrated in the ethylene oxide process in Section 5.4.5.3. In this example, the focus lies on multiphase aspects arising on the design levels 2 and 3 discussed in the next sections.

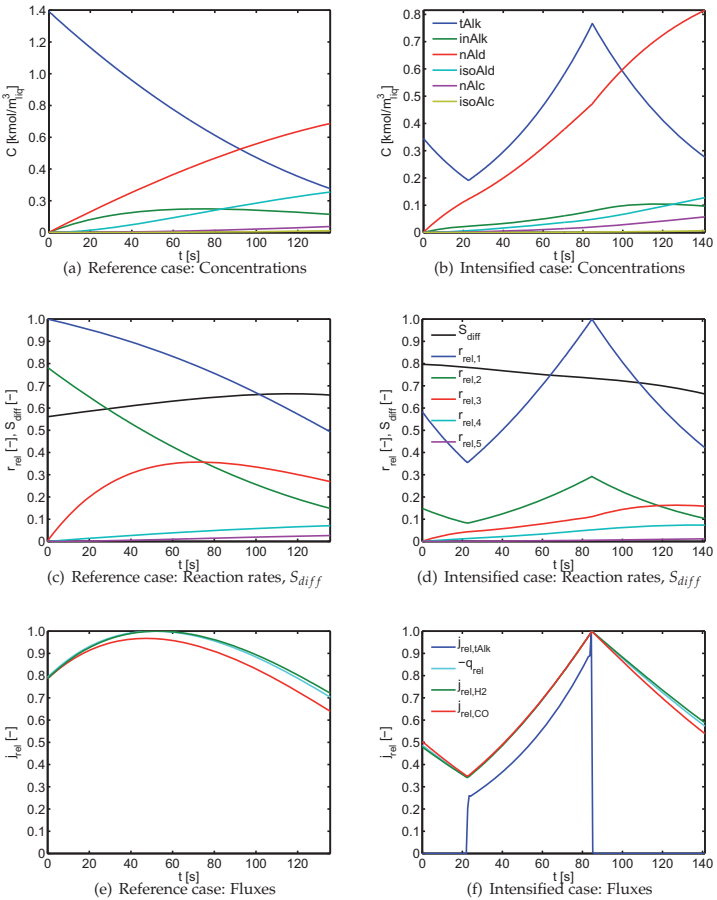

(a) Reference case: Concentrations
(b) Intensified case: Concentrations
(c) Reference case: Reaction rates, S_{diff}
(d) Intensified case: Reaction rates, S_{diff}
(e) Reference case: Fluxes
(f) Intensified case: Fluxes

Figure 6.6: Results level 1: Reference (l.h.s.) and intensified case (r.h.s.) ($X = 0.8$)

6.3.2 Level 2: Heat and mass transport

On level 2, the influence of heat and mass transport is studied and suited transport mechanisms and control variables, which make the desired fluxes attainable, are identified.

The heat flux is realized by indirect cooling and it is controlled by adapting the cooling temperature T_c along the reaction coordinate. The 1-octene flux is provided by ideal dosing into the liquid phase. Later, this can be approximated by a membrane, by a perforated tube, or by discrete dosing points.

The H_2 and CO fluxes into the liquid phase depend on the (k_La)-value and the respective partial pressure. In order to control the individual gas component fluxes, the partial pressures are controlled by ideal manipulation of the gas phase. A mass balance for the gas phase is not solved on this level, instead the gas phase is considered as ideal service phase and the partial pressure profiles in the gas phase are directly optimized. This ideal treatment of the gas phase is chosen in order to reduce the model complexity and to focus on the gas-liquid mass transfer. By performing a (k_La)-study, the influence of limited mass transfer between the gas and the liquid phase is investigated and a minimum desired (k_La)-value is identified.

In order to find the best reactor set-up for the gas-liquid mass transfer, an inverse problem is solved; instead of choosing a reactor and calculating the according (k_La)-value, the minimum desired (k_La)-value is obtained from calculating the dependence of the objective function on the mass transport resistance and then choosing a reactor which can achieve this (k_La)-value.

6.3.2.1 Additional model equations of level 2

Energy balance The energy balance is formulated in terms of temperature assuming no technical work, and negligible influence of the pressure change on the temperature (refer to eq. (6.3.28)). The total heat flux q_{tot} in eq. (6.3.28) accounts for the sensitive heat flux times the exchange area and for the enthalpy flux caused by the dosed components. In this energy balance, the contribution of the dissolved H_2 and CO is neglected.

$$\sum_{i \in COML} \left(n_{i,liq} \cdot c_{p,i} \right) \frac{\mathrm{d}T}{\mathrm{d}t} = - \left(q_{tot} + V_{IL} \sum_{i \in COM} \left(h_i \sum_{j}^{NR} \nu_{i,j} \cdot r_j \right) \right) \tag{6.3.28}$$

The heat capacity and enthalpy of each component are calculated using the correlations given in eq. (6.3.29) and eq. (6.3.30), respectively. The parameters were fitted in the investigated temperature range to data given in the literature [133, 137] and are presented in Tab. 6.4. The heat capacity correlation for the used IL is directly obtained from the literature [134].

$$c_{p,i} = A_{cp,i} + B_{cp,i} \cdot T + C_{cp,i} \cdot T^2, \quad i \in COM \tag{6.3.29}$$

$$h_i = A_{cp,i} \cdot T + \frac{B_{cp,i}}{2} \cdot T^2 + \frac{C_{cp,i}}{3} \cdot T^3 + F_i, \quad i \in COM \tag{6.3.30}$$

Table 6.4: Heat capacity parameters

Component	$A_{cp,i}\ \left[\frac{J}{mol \cdot K}\right]$	$B_{cp,i}\ \left[\frac{J}{mol \cdot K^2}\right]$	$C_{cp,i}\ \left[\frac{J}{mol \cdot K^3}\right]$	$F_i\ \left[\frac{J}{mol}\right]$
Decane (l)	$2.00 \cdot 10^2$	$3.72 \cdot 10^{-1}$	-	-
1-Octene (l)	$1.21 \cdot 10^2$	$3.69 \cdot 10^{-1}$	-	$-2.17 \cdot 10^5$
2-Octene (l)	$1.34 \cdot 10^2$	$3.60 \cdot 10^{-1}$	-	$-2.21 \cdot 10^5$
n-Nonanal (l)	$2.25 \cdot 10^2$	$2.89 \cdot 10^{-1}$	-	$-4.68 \cdot 10^5$
iso-Nonanal (l)	$2.25 \cdot 10^2$	$2.89 \cdot 10^{-1}$	-	$-4.68 \cdot 10^5$
n-Nonanol (l)	$2.78 \cdot 10^2$	$3.43 \cdot 10^{-1}$	-	$-5.66 \cdot 10^5$
iso-Nonanol (l)	$2.32 \cdot 10^2$	$3.77 \cdot 10^{-1}$	-	$-5.54 \cdot 10^5$
[bmim] [PF_6] (l)	$3.88 \cdot 10^2$	$-4.02 \cdot 10^{-1}$	$1.57 \cdot 10^{-3}$	-
H_2 (g)	$2.79 \cdot 10^1$	$3.12 \cdot 10^{-3}$	-	$-8.45 \cdot 10^3$
CO (g)	$2.80 \cdot 10^1$	$3.63 \cdot 10^{-3}$	-	$-1.19 \cdot 10^5$

Heat and mass transport The transfer of the gas phase components into the liquid phase is described by eq. (6.3.31). Since the flux j_i is the total flux into the fluid element (refer to eq. (6.3.1)), it has to be scaled by the liquid volume V_{liq}.

$$j_i = (k_L a)_{liq} \cdot \left(C^s_{i,org} - C_{i,org}\right) \cdot V_{liq}, \quad i \in COMG \tag{6.3.31}$$

$$V_{liq} = V_{IL} + V_{org} \tag{6.3.32}$$

In accordance to the equilibrium assumption of the film model, the surface concentration C^s_i depends on the partial pressure of the gas and its Henry coefficient in the organic phase according to eq. (6.3.33).

$$C^s_i = H^{-1}_{i,org} \cdot C_{tot,org} \cdot p_i, \quad i \in COMG \tag{6.3.33}$$

The heat transport coefficient between the fluid and the cooling media is assumed to be constant. Here, a mean value for a similar fluid system (organic solvent – water, $\alpha_{liq} = 0.5 \cdot 10^3\ \frac{W}{m^2 \cdot K}$) is taken from the literature [138]. In case heat transfer problems occur, the exchange area is a degree of freedom to investigate whether reactors with high heat exchange areas will improve the reactor performance [57, 69].

$$q_{tot} = (a \cdot V \cdot \alpha)_{liq} \cdot (T - T_c) \tag{6.3.34}$$

6.3.2.2 Problem statement

The optimization problem arising of level 2 is stated in a comprehensive manner below in (DOP2). The profiles of the cooling temperature, of the partial pressures of the gases, and of the alkene dosing flux are the control functions. In addition, the initial temperature, initial amount of terminal alkene, the volume fraction of the IL phase, and the residence time are degrees of freedom. The inlet amount of H_2 and CO ($n_{H_2,liq,0}$, $n_{CO,liq,0}$) in the liquid phase are calculated from saturation conditions at the inlet. The (k_La)-value is fixed according to the investigated case, giving rise to the dependence of the selectivity and STY on the gas-liquid mass transport.

$$\text{Obj} = \max_{\substack{T_c(t),T_o,p_{H_2}(t),p_{CO}(t),\\ j_{tAlk}(t),n_{tAlk,0},V_{frac},\tau}} S \tag{DOP2}$$

s.t.

Component balances and phase distribution: eq. (6.3.1) – eq. (6.3.4)

Energy balances: eq. (6.3.28) – eq. (6.3.30)

Reaction kinetics: eq. (6.3.5) – eq. (6.3.9)

Transport kinetics: eq. (6.3.31) – eq. (6.3.34)

Further constitutive equations: eq. (6.3.10) – eq. (6.3.11)

Solubility: eq. (6.3.12) – eq. (6.3.15)

Intrinsic bounds: eq. (6.3.16) – eq. (6.3.17)

System bounds: eq. (6.3.18) – eq. (6.3.20)

Recycle condition: eq. (6.3.21)

STY: eq. (6.3.22)

Conversion: $X = 0.8$

G/L mass transfer: k_La according to investigated case

6.3.2.3 Results

In Fig. 6.7(a) the concentration profiles of the liquid phase are shown. The concentration profiles look qualitatively similar to the profiles of level 1, but due to the limited gas-liquid mass transfer the residence time increased slightly and the maximum and minimum concentration of 1-octene slightly shifted as well.

The control variables for the fluxes, namely the cooling temperature, the partial pressure of H_2 and CO, and the dosing flux of 1-octene are presented in Fig. 6.7(b). All normalized variables and the according reference values are given in Appendix A.3.1.

The optimal cooling temperature profile (refer to Fig. 6.7(b)) provides the optimal fluid temperature (constant upper limit) over the entire residence time, and hence the required heat flux is completely attainable. The heat flux profile is calculated for a specific heat exchange area based on the liquid phase volume of $a_{liq} = 20\,m^{-1}$. For this exchange area a maximum temperature difference between cooling and fluid temperature of 18.8 K arises. From this result it can be concluded that there is no need to investigate reactor concepts with a very high heat exchange area (for example a micro reactor) for this reaction system.

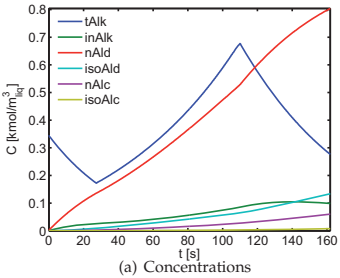

(a) Concentrations

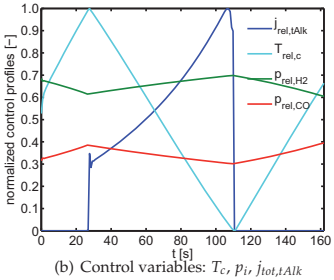

(b) Control variables: T_c, p_i, $j_{tot,tAlk}$

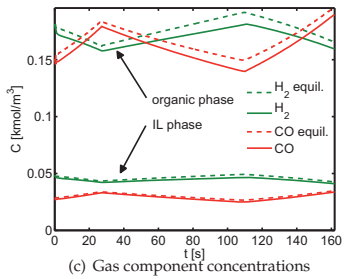

(c) Gas component concentrations

Figure 6.7: Results level 2 ($X = 0.8$, $(k_La)_{liq} = 1\,s^{-1}$)

The total gas pressure is always at its maximum. In Fig. 6.7(c) the concentration of the gas phase components in the organic phase and in the ionic liquid are shown for $(k_La)_{liq} = 1\,s^{-1}$. The equilibrium concentrations depend on the temperature and the individual gas pressures and are also plotted in the figure. Since the partial pressures of the gases are not constant, the equilibrium concentrations are also not constant. Even for this high $(k_La)_{liq}$-value, it can be observed that the gas concentrations in the liquid are still not at their equilibrium values.

Fig. 6.8 illustrates how selectivity and STY depend on the gas-liquid mass transfer. For high $(k_La)_{liq}$-values ($\approx 10\,s^{-1}$) almost the maximum potential of the reaction system with respect to selectivity and STY identified in level 1 can be achieved. At a $(k_La)_{liq}$ of $0.6\,s^{-1}$, the minimum required STY defined by the reference case of level 1 (refer to Fig. 6.8(b)) is reached. For lower $(k_La)_{liq}$-values the required STY can only be obtained by higher 1-octene concentrations in the reactor. The selectivity decreases significantly already for $(k_La)_{liq} \leq 1\,s^{-1}$. Assuming a maximum acceptable selectivity loss of 1%, the $(k_La)_{liq}$-value should be above $1\,s^{-1}$ as indicated in Fig. 6.8(a).

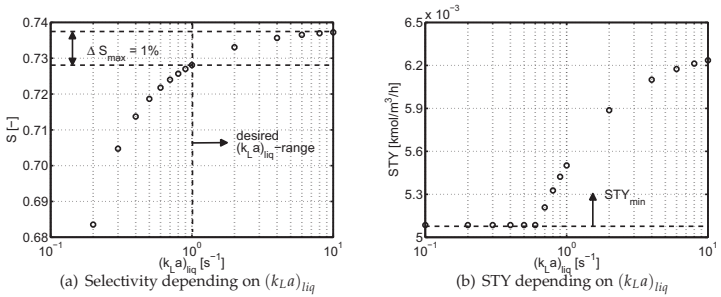

(a) Selectivity depending on $(k_La)_{liq}$ (b) STY depending on $(k_La)_{liq}$

Figure 6.8: Results (k_La)-study on level 2 ($X = 0.8$)

From the results of level 2 it can be concluded that the chosen control variables (T_c, p_i, direct dosing) are suited to attain the optimal profiles and that high gas-liquid mass transfer rates ($(k_La)_{liq} \geq 1\,s^{-1}$) are required for a good performance of the investigated hydroformylation reaction system.

6.3.3 Level 3: Technical approximation

In order to obtain the best technical reactor, the optimal control variable profiles of level 2 have to be approximated by a technically feasible design. In addition, a gas-liquid mixing strategy has to be chosen which can provide the desired (k_La)-value and plug flow characteristics. In summary, the catalog of requirements for the best technical hydroformylation reactor for long chain alkenes is given by:

1. The gas-liquid mass transfer rates must be high.
2. The reactor design must be able to approximate the optimal control variable profiles.
3. The reactor should have plug flow characteristics.

For the investigated system, bubble columns are not a promising option due to the low gas-liquid mass transfer rates. However, it should be noted that the design of bubble columns is very flexible, and therefore they are still attractive for gas-liquid systems with lower reaction rates.

Since several mixing strategies exist which fulfill the defined catalog of requirements, the gas-liquid mixing strategy with the lowest energy consumption with respect to the provided (k_La)-value is the preferred reactor concept. For this purpose, Nagel et al. [139, 140] derived correlations for the required energy in dependence of the (k_La)-value for several gas-liquid reactors. Grosz-Röll et al. [141] compared the energy demand of stirred tank reactors, jet loop reactors, and static mixers and found that static mixers offer the highest (k_La)-value for a given energy demand. Furthermore, it was shown that the residence time behavior of static mixers is approximately plug flow like (e.g. [142]) and that static mixers can be used for gas-liquid-liquid systems [128].

Other concepts such as the capillary flow reactor, which was successfully demonstrated for gas/liquid/solid reactions [143] and also for the hydroformylation [122], are not taken into account for the technical realization since the energy demand in dependence of the (k_La)-value is not known. Hence, these reactor types can hardly be compared. In addition, it was shown on level 2 that the required heat exchange area is small and hence no reactor concept with high heat exchange areas is required.

From the control function profiles of level 2 (refer to Fig. 6.7(b)) it is evident that a reactor with three segments seems to be adequate to approximate the desired profiles. In the first segment, additional gas is dosed into the reactor at three discrete dosing points. Since H_2 and CO are approximately equally consumed, synthesis gas (H_2:CO=1) can be used to maintain the H_2:CO-partial pressure ratio approximately constant. By using perforated pipe distributors (as shown in [144]) the gas is equally distributed over the pipe radius. The cooling temperature is approximated using a co-current heat exchanger since the optimal cooling temperature rises almost linearly.

The optimal profiles in the second segment are approximated by dosing additional synthesis gas (H_2:CO=1) and 1-octene in combination with a counter-current heat exchanger. Here, 20 discrete dosing points are used for the gas as well as for the 1-octene. Again perforated pipe distributors are used to obtain a good radial mixing at the dosing points.

The third segment features the same principle design as the first segment, except that 8 dosing points are selected. The number of dosing points is chosen in order to provide nearly equidistantly spaced dosing over the entire reactor length.

The proposed reactor configuration is shown in Fig. 6.9. The dosing of gas and 1-octene is only shown symbolically and the static mixer elements are represented by crossed boxes.

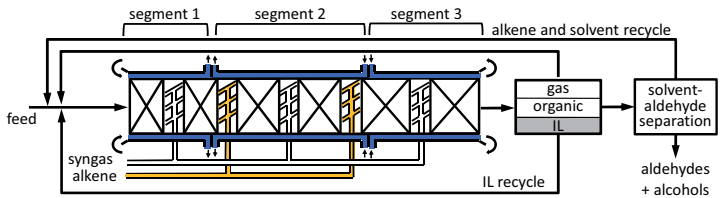

Figure 6.9: Best technical hydroformylation reactor configuration

To model the shown reactor set-up, additional balance equations for the gas and coolant phase as well as for the dosing points are required. The static mixer investigated by Heyouni et al. [145] is selected since correlations to calculate the local (k_La)-value and pressure drop for these static mixers are available. Here, the local formulation of the balance equations is used since the local velocities of the gas and liquid phase are required to calculate the (k_La)-value and pressure drop, and also the dimensions of the reactor are of interest.

6.3.3.1 Problem statement

In contrast to the previous levels where optimal control problems were solved, in level 3 a parameter optimization problem, which is dynamically constrained, must be solved. Since all phases (liquid, gas, coolant) and all fluxes are rigorously modeled, no control functions can be optimized anymore. The according optimization problem is formulated in (DOP3). The design variables of the reactor (length, radius), the inlet conditions of the reactant, gas, and cooling phase, as well as the cooling side heat capacity flowrate, the volume fraction of the IL, and the amount of gas and liquid dosing at each dosing point are the degrees of freedom. All required equations are presented in Appendix A.3.3. The inlet streams of H_2 and CO ($\dot{n}_{H_2,liq,0}$, $\dot{n}_{CO,liq,0}$) in the liquid phase are calculated from saturation conditions at the inlet.

$$\text{Obj} = \max_{\substack{R_h, L_h, T_{c,0,h}, K_{c,0,h}, T_o, \\ \dot{n}_{liq,0}, \dot{n}_{gas,0}, \dot{n}_{tAlk,liq,0}, \\ \dot{n}_{tAlk,liq,d}, \dot{n}_{syngas,g,d}, \\ p_{H_2,0}, p_{CO,0}, \dot{V}_{frac}}} S \tag{DOP3}$$

s.t.

Component balances: eq. (A.3.17) – eq. (A.3.22)

Phase distribution: eq. (6.3.2) – eq. (6.3.3)

Component balances distributor: eq. (A.3.23) – eq. (A.3.24)

Energy balances: eq. (A.3.25) – eq. (A.3.31), eq. (6.3.29) – eq. (6.3.30)

Energy balances distributor: eq. (A.3.32)

Momentum balances: eq. (A.3.34) – eq. (A.3.36)

Reaction kinetics: eq. (6.3.5) – eq. (6.3.9)

G/L mass transport: eq. (A.3.33)

Further constitutive equations: eq. (A.3.38) – eq. (A.3.45), eq. (6.3.11)

Solubility: eq. (6.3.12) – eq. (6.3.15)

Intrinsic bounds: eq. (6.3.16) – eq. (6.3.17)

System bounds: eq. (A.3.46) – eq. (A.3.48)

Recycle condition: eq. (A.3.49)

STY: eq. (A.3.50)

Conversion: eq. (A.3.51)

Coolant side: eq. (A.3.52)

6.3.3.2 Results

The selectivity of the optimized reactor set-up is 71.2 %. Due to the non-ideal approximation of the control profiles and the pressure drop considered on this level, the objective value is slightly below the selectivity of level 2. However, it is remarkably higher than the selectivity which can be obtained with the reference reactor set-up or a CSTR on level 1 (refer to Fig. 6.5(a)). In addition, it should be noted that the reference case and the CSTR are calculated with ideal gas-liquid mass transfer and the losses due to the limited ($k_L a$)-value are not yet considered.

The results for the concentration profiles, the amount of dosed 1-octene and synthesis gas, the fluid and cooling temperature, the total pressure, and the gas composition for the optimized reactor are shown in Fig. 6.10, and the definitions of the normalized variables are given in Appendix A.3.1.

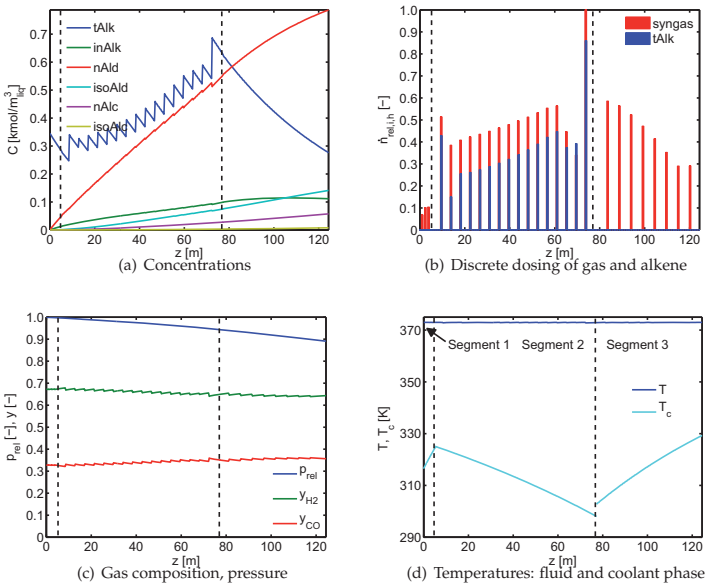

Figure 6.10: Results level 3 ($X = 0.8$)

In Fig. 6.10(a), the profiles for the liquid phase concentrations are given. Due to the discrete dosing of 1-octene (refer to Fig. 6.10(b)), the concentration of 1-octene occurs as zig-zag profile in segment 2. More discrete dosing points will smooth this profile and will also improve the reactor performance since the ideal profile can be better approximated. However, the qualitative trend is in accordance to level 1 and 2.

As shown in Fig. 6.10(c), the gas composition cannot be ideally controlled using synthesis gas with a composition of H_2:CO=1. However, the dosing of synthesis gas can keep the gas phase composition almost constant. Using another gas composition will improve the H_2:CO-profile in the gas phase and hence the reactor performance, but from an economic point of view this does not seem to be worthwhile. In addition, the gas dosing maintains the volumetric gas fraction high, which improves the gas-liquid mass transfer. At the inlet the gas fraction is at its maximum, which was defined based on the values given in the literature [144] for static mixers.

The pressure drop, which was neglected on level 1 and 2 so far, is relatively high (refer to Fig. 6.10(c)). It reduces the STY and selectivity of the system and can also be regarded as a loss caused by the technical realization. The mean $(k_L a)_{liq}$-value obtained in the technical reactor is 0.75, which is below the desired value of 1. The $(k_L a)$-value

can be further enhanced by a higher fluid velocity, however, in this case the pressure drop will also increase. Since the superficial fluid velocity ($v_{g,s,0} = 0.25\,\frac{m}{s}$) is not at its bounds, the (k_La)-value and pressure drop are balanced in an optimal manner.

The approximation of the cooling profile is very good and almost the optimal temperature profile is obtained (refer to Fig. 6.10(d)). Hence, the chosen cooling strategy is absolutely appropriate for the temperature control.

The optimization results for the decision variables which cannot be obtained from Fig. 6.10 are given in Table 6.5.

Table 6.5: Optimized design and operating variables

Decision variable	Segment	Value
Tube radius, $R\ [m]$	$S1 - S3$	0.11, 0.11, 0.10
Segment length, $L\ [m]$	$S1 - S3$	5.28, 71.99, 47.14
Inlet cooling temperatures, $T_{c,0}\ [K]$	$S1 - S3$	316.4, 298.4, 302.6
Coolant constant, $K_c\ \left[\frac{m \cdot K}{W}\right]$	$S1 - S3$	$1.03 \cdot 10^{-4}$, $-2.19 \cdot 10^{-5}$, $3.45 \cdot 10^{-5}$
Inlet temperature, $T_0\ [K]$	$S1$	373.0
Total liquid inlet flowrate, $\dot{n}_{liq,0}\ \left[\frac{mol}{s}\right]$	$S1$	50.1
Total gas inlet flowrate, $\dot{n}_{gas,0}\ \left[\frac{mol}{s}\right]$	$S1$	19.6
$V_{frac}\ [-]$	$S1$	1.5

6.4 Summary

In Table 6.6 the attainable selectivities and the main characteristics of each level are summarized.

Table 6.6: Result comparison level 1 – 3

Level	Characteristics and insight gained	S [%]
Reference	Defines technical reference reactor, determines maximum potential of intensified concepts	62.1
Level 1	All fluxes are required, C_{tAlk} defines optimal value C_{CO}, best conversion from overall process point of view	73.8
Level 2	$(k_La)_{liq} \geq 1\,s^{-1}$ desired, $p_{\mathrm{H_2}} : p_{\mathrm{CO}} \approx 2$	72.8
Level 3	3 segments are adequate to approximate the profiles, static mixers are well suited to provide (k_La)-value	71.2

On the first level, it was shown that an intensified reaction concept can improve the selectivity compared to an optimized reference case by 11.7%. The best reaction concept shows a complex dosing profile of the 1-octene. In addition, the optimal concentration profiles of H_2 and CO in the liquid phase are non-trivial and depend on the octene concentration profile.

On the second level, the minimum required $(k_L a)$-value was determined by specifying a maximum selectivity loss of 1%. It was shown that the selectivity and the STY depend strongly on the gas-liquid mass transfer velocity.

Using this information about the desired $(k_L a)$-value and the optimal profiles for the control variables, a technical approximation was derived on level 3. The best technical reactor consists of three segments with advanced cooling and distributed dosing of synthesis gas and 1-octene. In order to obtain high gas-liquid mass transfer, static mixers were applied. This technical approximation still shows a selectivity increase of 9% compared to the idealized and optimized technical reference.

In addition, the losses due to limited mass and energy transport (compare level 1 and 2) and due to non-ideal control profiles (compare level 2 and 3) are quantified. However, the overall losses due to the non-ideal control profiles, the limited gas-liquid transfer, and the pressure drop are small and sum up to only 2.6% (compare level 1 and 3). Therefore, it can be concluded that the proposed reactor design using three segments is well suited and can only be slightly improved, for example by an increasing number of dosing points and a flexible gas composition of the dosed gas.

Summing up, the proposed reactor design approach is suited to design multiphase reactors with complex reaction networks. The approach is superior to conventional reactor selection heuristics since it is able to yield non-intuitive results which originate from the strongly coupled nonlinear interaction of complex multiphase reaction systems. In general, the method can be applied to all gas-liquid systems where the gas phase is considered to be a service phase. By using the proposed $(k_L a)$-study, the influence of limited gas-liquid mass transfer can be investigated and a detailed catalog of requirements for the selection of the best suited gas-liquid reactor is obtained.

Chapter 7
Summary and outlook

In the first part of this thesis, a new reactor design method based on the elementary process functions concept was proposed. This methodology focuses on the model-based calculation of the optimal reaction route and its technical realization by an appropriate reactor design.

On its first level, the design methodology enables the calculation of the optimal route in state space independent of existing apparatuses. The optimal route is rigorously based on the equations of change, thermodynamic relationships, reaction kinetics, and further intrinsic bounds of the investigated system and is determined by solving a dynamic optimization problem. In addition, different integration and enhancement concepts are compared to an optimized technical reference reactor and the best concept defines a benchmark for any technical realization. This model-based approach considers process intensification options by modeling the according physical and chemical principles on the phase level.

The second level of the methodology yields the best suited principle reactor set-up including the service phases and the catalyst support geometry. Here, the best set of control variables, which can be manipulated by the reactor design, is identified in order to obtain the desired flux profiles. On this level, reactor design criteria ensure the validity of the model regarding external and internal mass and heat transfer limitations.

On the third level, a technical approximation of the optimal control variable profiles is derived. In addition, the developed technical reactor is analyzed in detail using a model accounting for the non-idealities in the flow, concentration, and temperature field.

In the second part of the work, several industrially important processes were considered in order to prove the wide applicability and potential of the method. The examples represent different classes of processes and reactions. The SO_2 oxidation as an exothermic equilibrium reaction, the ethylene oxide synthesis as partial oxidation with a parallel reaction network, and the hydroformylation as a homogeneously catalyzed multiphase process with parallel and consecutive reactions were investigated. The processes were chosen with increasing difficulty with respect to the number and complexity of the reactions, the fluxes, and the considered phases.

The SO_2 oxidation [57] was chosen in order to illustrate the method. Here, a residence time reduction of 69% compared to an optimized adiabatic reaction concept with intermediate cooling was achieved by an advanced cooling concept.

In the case of the air based ethylene oxide process [69], the selectivity was increased by 3.13% compared to an optimized isothermal plug flow reactor using the derived ethylene dosing concept.

For the oxygen based ethylene oxide process, the determination of the optimal reaction module and the optimization of the overall process parameters were performed simultaneously. Thereby, the interaction between the reaction module and the process was fully taken into account and plant wide process intensification was achieved. Here, an oxygen dosing concept shows a cost reduction potential of 2.4%, which refers to savings in the order of $1.35 \cdot 10^6 \frac{\$}{yr}$ for a plant capacity of $10^5 \frac{t_{EO}}{yr}$. Besides the reduction of the running expenses, the recycle stream is decreased by about 40% leading to smaller apparatuses and hence to further intensification of the process. In addition, the utility consumption is reduced by up to 46% and the total CO_2 emissions of the processes are shortened by around $2.6 \cdot 10^4 \frac{t_{CO_2}}{yr}$ for an average sized plant giving rise to a greener and more sustainable EO process. For this process a first-principle model of the explosive region suitable for optimization was developed. Furthermore, a sensitivity analysis of the critical model assumptions was performed in order to determine the robustness of the economical potential of the intensified reaction concept.

In the case of the hydroformylation of long chain aldehydes [107, 131], the method was extended for multiphase systems. For this purpose, a (k_La)-study was used on the second level in order to determine the influence of gas-liquid mass transfer limitations. Thereby, the inverse problem to find the best suited principle reactor set-up was solved. Instead of choosing a principle set-up and evaluating its heat and mass transport characteristics, the necessary (k_La)-value is determined and a suitable device for gas-liquid contact strategy is chosen. It turned out that the process selectivity can be increased by at least 9.1% by applying a dedicated dosing strategy for all reactants in combination with static mixers ensuring adequate gas-liquid mass transfer.

Outlook

Regarding the process hierarchy discussed in the introduction, the design approach for optimal chemical processes can be extended on each level as shown in Fig. 7.1.

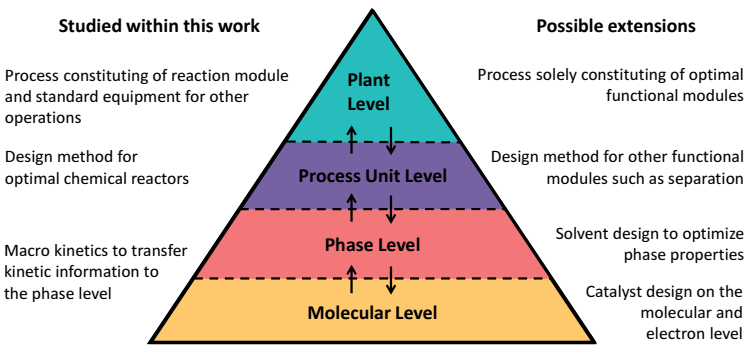

Figure 7.1: Possible extensions of the design framework (adapted from [3])

Within this work, macro kinetics are used to transfer the reaction kinetic information from the molecular to the phase level. In order to overcome the limited predictability of macro kinetics and to gain more insights on the physical and chemical processes on the catalyst surface, micro kinetics can be used for the reactor design. In addition, solvents can be designed to optimize the phase properties, for example to achieve a homogeneous liquid phase at reaction conditions and to induce a phase split at separation conditions as it is obtained by thermomorphic solvent systems [112]. Furthermore, the design method can be extended towards the design of other functional modules such as separation devices. This allows one to construct the overall process as a combination of functional modules in order to obtain the optimal route of the fluid element over the entire process coordinate.

In order to extend the method to all kinds of functional modules, the rigorous treatment of multiphase systems by considering the relative velocities between the phases is necessary. Such an extension will require a different model formulation in addition to the rigorous consideration of the mass and heat transport between all phases which are not service phases already on the first level. Within the modeling approach used in this work, the reactive phase consists of a pseudo-homogeneous phase (either in case of heterogeneous catalysis or in case of the hydroformylation of long chain alkenes in a biphasic IL system) and the non-reactive phases were treated as service phases. Further possible extensions of the method on each design level are summarized in Fig. 7.2.

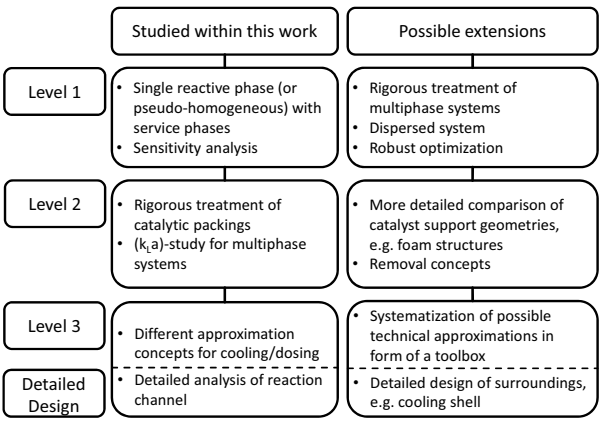

Figure 7.2: Possible extensions of the design method

Processes such as polymerization or crystallization constitute dispersed systems. The method can be extended to deal with these property distributed processes by including population balances of the individual species on the first design level. Furthermore, the method can be extended towards the robust optimization of the optimal route in order to handle uncertainties in the model. In case of the oxygen based EO process, a sensitivity study with respect to the critical model assumptions revealed the high potential of such considerations.

The second design level can be further concretized by a more detailed treatment of the possible catalyst support geometries such as foam structures and monolithic honeycombs. These foam like catalyst support geometries will become more important for reactions with very high heat production, but so far no limitations from packed beds arose for the considered examples. Furthermore, the realization of a removal concept needs to be exemplified on this design level.

In order to simplify the derivation of the technical approximation on the third design level, a toolbox for possible technical approximations of some typical control variable profiles can be derived – as it was exemplified for the heat capacity flowrate for the cooling phase. Such a toolbox limits the possible technical approximations, but might give rise to a faster application in industry and may constitute the interface to equipment based systematization approaches. In addition, a detailed design of the surroundings such as the cooling shell need be taken into account, similar to detailed analysis of the reaction channel in case of the air based EO process, in order to build the proposed reactors.

Beside these extensions of the method, an experimental validation of the calculated optimal reaction route needs to be done. In addition, the planning and design of reaction kinetic experiments should be linked to the optimal reaction route in order to ensure that the experimental range with respect to temperature, pressure, and concentrations fit to the conditions dominant for the optimal route.

Conclusion

The proposed reactor design approach is suited to design innovative reactors based on the optimal route in state space. The multi-level approach is based on the realization of the optimal fluxes by a suitable technical reactor. The method considers process intensification options based on the according physical and chemical principles. As it was shown for the investigated examples, the derivation of already existing reactors (if these are optimal) as well as of innovative reactors is possible. The approach is superior to conventional reactor selection heuristics since it is able to yield non-intuitive results which originate from the strongly coupled nonlinear interactions of complex systems. The different example processes proved the applicability of the method for a wide field of chemical processes. In addition, the design approach was extended towards multiphase systems and process wide optimization giving rise to a deeper understanding of these highly complex systems.

To sum up, the method enables the design of tailor-made reactors which is the first step on the way towards more economical as well as greener and more sustainable chemical processes.

Chapter A
Appendix

A.1 Air based ethylene oxide process

A.1.1 Model equations of level 3: One-dimensional analysis

The one-dimensional equations of change for the reaction channel under steady state conditions are given by eq. (A.1.1) – eq. (A.1.3).

Component balances

$$\frac{\mathrm{d}\dot{n}_i}{\mathrm{d}z} = 2\pi R_i s_i j_i + \pi \left(R_o^2 - R_i^2\right) \cdot (1-\bar{\varepsilon}) \cdot \rho_p \cdot \sum_{j \in RE} \nu_{i,j} \cdot r_j \tag{A.1.1}$$

Energy balance

$$\sum_{i \in COM} \left(\dot{n}_i \cdot c_{p,i}\right) \frac{\mathrm{d}T}{\mathrm{d}z} = \tag{A.1.2}$$
$$- \left(2\pi \left(R_o q_o + R_i q_i\right) + \pi \left(R_o^2 - R_i^2\right) (1-\bar{\varepsilon}) \rho_p \sum_{i \in COM} \left(h_i \sum_{j \in RE} \nu_{i,j} \cdot r_j\right)\right)$$

Momentum balance

$$\frac{\mathrm{d}p}{\mathrm{d}z} = -\left(150 \frac{\mu (1-\bar{\varepsilon})^2}{D_p^2 \bar{\varepsilon}^3} + 1.75 \frac{v_s \rho (1-\bar{\varepsilon})}{D_p \bar{\varepsilon}^3}\right) v_s \tag{A.1.3}$$

Constitutive equations

$$v_s = \frac{\dot{n} \cdot R \cdot T}{p \cdot \pi \left(R_o^2 - R_i^2\right)} \tag{A.1.4}$$

$$\dot{n} = \sum_{i \in COM} \dot{n}_i \tag{A.1.5}$$

$$y_i = \frac{\dot{n}_i}{\dot{n}} \tag{A.1.6}$$

Energy balance coolant side The energy balance on the coolant side (Index c) is written in temperature form and simplified so that the change in the coolant temperature is proportional to the heat flux. The introduced coolant constant is chosen within

meaningful bounds $\left(-0.314\,\frac{m \cdot K}{W} \leq K_c \leq 0.314\,\frac{K}{W}\right)$. A value of K_c smaller than zero accounts for the possibility of counter-current cooling, a value larger than zero for co-current cooling, and $K_c = 0$ accounts for isothermal cooling, for example by an evaporating fluid.

$$\frac{\mathrm{d}T_c}{\mathrm{d}z} = K_c \cdot q_o \tag{A.1.7}$$

$$K_c^L \leq K_c \leq K_c^U \tag{A.1.8}$$

Mass balance membrane side The mass balance on the membrane side (Index M) only has to account for an ethylene flow through the membrane and is written in terms of the molar ethylene flux. The membrane side consists of pure ethylene and the inlet mole flow through the membrane channel is bounded according to eq. (A.1.10) with $\dot{n}_{M,0}^L = 0.01\,\frac{mol}{s}$ and $\dot{n}_{M,0}^U = 1\,\frac{mol}{s}$.

$$\frac{\mathrm{d}\dot{n}_M}{\mathrm{d}z} = -\pi \cdot D_i \cdot j_\mathrm{E} \tag{A.1.9}$$

$$\dot{n}_{M,0}^L \leq \dot{n}_{M,0} \leq \dot{n}_{M,0}^U \tag{A.1.10}$$

Energy balance membrane side The energy balance on the membrane side is simplified so that it only accounts for the heat exchange between ethylene supply channel and reaction channel. Bounds on the temperature of the membrane side are given by eq. (A.1.12) with $T_M^L = 490\,K$ and $T_M^U = 600\,K$.

$$\dot{n}_M c_{p,M} \frac{\mathrm{d}T_M}{\mathrm{d}z} = \pi \cdot D_i \cdot q_i \tag{A.1.11}$$

$$T_M^L \leq T_M \leq T_M^U \tag{A.1.12}$$

Momentum balance membrane side For the momentum balance on the ethylene supply side, the pressure drop correlation for the flow through an empty pipe is used with the friction factor c_w (eq. (A.1.13) and eq. (A.1.14)) [146].

$$\frac{\mathrm{d}p_M}{\mathrm{d}z} = -\frac{c_w \cdot \rho_M \cdot v_M^2}{2 \cdot D_i} \tag{A.1.13}$$

$$c_w = \frac{0.3164}{\mathrm{Re}_M^{0.25}} \quad \text{for} \quad 3000 \leq \mathrm{Re}_M = \frac{\rho_M \cdot v_M \cdot D_i}{\mu_M} \leq 10^5 \tag{A.1.14}$$

Constitutive equations membrane side The velocity on the membrane side v_M is calculated from the volume flow using the ideal gas law and the cross sectional area of the ethylene supply channel according to eq. (A.1.15).

$$v_M = \frac{4 \cdot \dot{n}_M \cdot R \cdot T_M}{p_M \cdot \pi \cdot D_i^2} \tag{A.1.15}$$

Transport kinetics The heat transfer between ethylene supply channel and reaction channel depends on the heat transfer resistance on both sides and is given by eq. (A.1.16).

$$q_i = \frac{\alpha_i \cdot \alpha_M}{\alpha_i + \alpha_M} \cdot (T - T_M) \tag{A.1.16}$$

On the ethylene side, the heat transfer coefficient is determined according to the turbulent flow through an empty pipe by eq. (A.1.17) [147].

$$\alpha_M = 0.0214 \cdot \frac{\lambda_M}{D_i} \cdot \left(\mathrm{Re}_M^{4/5} - 110 \right) \cdot \mathrm{Pr}_M^{1/4} \tag{A.1.17}$$

The heat conductivity and the viscosity of ethylene are assumed to be constant ($\lambda_M = 5.86 \cdot 10^{-2} \frac{W}{m \cdot K}$, $\mu_M = 1.75 \cdot 10^{-5} \frac{kg}{m \cdot s}$) and are obtained from Aspen Plus at $T = 550\,K$ and $p = 20\,bar$. The Prandtl number is also assumed to be constant ($\mathrm{Pr}_M = 0.724$).

On the reaction side the heat transfer coefficient is calculated using eq. (5.3.23) with D_i instead of D_o.

The ethylene supply flux through the membrane is given by eq. (A.1.18).

$$j_\mathrm{E} = Per \cdot (p_M - p) \tag{A.1.18}$$

A.1.2 Model equations of level 3: Two-dimensional analysis

2D component mass balance The component mass balances are simplified by assuming no axial dispersion, no radial convection, and steady state conditions (refer to eq. (A.1.19)).

$$\frac{\partial (\rho_i v_s)}{\partial z} = -\frac{1}{r} \frac{\partial}{\partial r} (r \cdot M_i \cdot j_{r,i}) + \rho_p \cdot (1 - \epsilon) \cdot M_i \cdot \sum_{j \in RE} \nu_{i,j} \cdot r_j \tag{A.1.19}$$

$$M_i \cdot j_{r,i} = -D_{r,i} \frac{\partial \rho_i}{\partial r} \tag{A.1.20}$$

$$j_{r,i}|_{r=R_i} = \begin{cases} Per \cdot (p_M - p) & i = \mathrm{E} \\ 0 & \text{else} \end{cases} \tag{A.1.21}$$

$$j_{r,i}|_{r=R_o} = 0 \tag{A.1.22}$$

$$y_i = \frac{\frac{\dot{m}_i}{M_i}}{\sum_{i \in COM} \left(\frac{\dot{m}_i}{M_i} \right)} \tag{A.1.23}$$

The initial mass flow distribution $(\rho_{i,0} v_{s,0})$ is calculated solving eq. (A.1.45) for the velocity distribution at the inlet. The component densities $\rho_{i,0}$ and the total density ρ_0

at the inlet are calculated from the inlet conditions (T_0, p_0) and the inlet composition ($x_{i,0}$). The dispersion coefficient (eq. (A.1.24) – eq. (A.1.27)) are calculated in accordance to the models published in the literature (e.g. [148, 149]). In order to estimate the dispersion coefficient, the diffusion coefficient of ethylene in nitrogen is used for all components in eq. (A.1.25). To simplify the calculations, the Peclet number is calculated with the average inlet velocity.

$$D_r = D_{bed} + K_1 \cdot \mathrm{Pe}_m \cdot D_m \cdot f_D(r) \cdot \frac{\overline{v}_{s,0}}{v_s(r)} \tag{A.1.24}$$

$$D_{bed} = D_m \cdot \left(1 - \sqrt{1 - \epsilon(r)}\right) \tag{A.1.25}$$

$$\mathrm{Pe}_m = \frac{\overline{v}_{s,0} \cdot D_p}{D_m} \tag{A.1.26}$$

$$K_1 = \frac{1}{8}\left(1 + \frac{3}{\mathrm{Pe}_m^{0.5}}\right)^{-1} \tag{A.1.27}$$

$$f_D(r) = \begin{cases} \left(\frac{R_o - r}{0.44 \cdot D_p}\right)^2 & \text{if } R_o - r < 0.44 \cdot D_p \\ 1 & \text{if } R_o - r \geq 0.44 \cdot D_p \end{cases} \tag{A.1.28}$$

2D energy balance The energy balance is simplified using the assumptions of the $\Lambda(r)$-model resulting in eq. (A.1.29) to eq. (A.1.32).

$$\frac{\rho \cdot c_p \cdot v_s}{M}\frac{\partial T}{\partial z} = -\rho_p \cdot (1-\epsilon) \cdot \sum_{i \in COM}\left(h_i \sum_{j \in RE} \nu_{i,j} \cdot r_j\right) + \frac{1}{r}\frac{\partial}{\partial r}\left(r \cdot \Lambda \cdot \frac{\partial T}{\partial r}\right) \tag{A.1.29}$$

$$T(z=0) = T_0 \tag{A.1.30}$$

$$\Lambda \cdot \left.\frac{\partial T}{\partial r}\right|_{r=R_i} = \frac{k_i \cdot \alpha_M}{k_i + \alpha_M}\left(T_M - T(R_i)\right) \tag{A.1.31}$$

$$\Lambda \cdot \left.\frac{\partial T}{\partial r}\right|_{r=R_o} = k_o \cdot \left(T(R_o) - T_c\right) \tag{A.1.32}$$

The heat flux is calculated using the effective radial conductivity in the packed bed (eq. (A.1.33)) as summarized by [149]. The average velocity ($\overline{v}_{s,0}$) and all properties depending on the fluid state are calculated at the inlet conditions for the $\Lambda(r)$-model. The heat conductivity of the particles $\left(\lambda_p = 17.75 \frac{W}{m \cdot K}\right)$ is assumed to be constant and calculated at 550 K [133].

$$\Lambda = \lambda_{bed} + \frac{1}{8} \cdot \mathrm{Pe} \cdot \lambda \cdot f_\Lambda(r) \cdot \frac{\overline{v}_{s,0}}{v_s(r)} \tag{A.1.33}$$

$$\lambda_{bed} = \lambda \cdot k_{bed} \tag{A.1.34}$$

$$k_{bed} = 1 - \sqrt{1 - \epsilon(r)} + \sqrt{1 - \epsilon(r)} \cdot k_c \tag{A.1.35}$$

$$k_c = \frac{2}{N}\left(\frac{B}{N^2}\frac{k_p - 1}{k_p}\ln\left(\frac{k_p}{B}\right) - \frac{B+1}{2} - \frac{B-1}{N}\right) \tag{A.1.36}$$

$$N = 1 - \frac{B}{k_p} \tag{A.1.37}$$

$$k_p = \frac{\lambda_p}{\lambda} \tag{A.1.38}$$

$$B = 1.25 \left(\frac{1 - \epsilon\,(r)}{\epsilon\,(r)} \right)^{10/9} \tag{A.1.39}$$

$$\mathrm{Pe} = \frac{\overline{v}_{s,0} \cdot \rho \cdot D_p \cdot c_p}{\lambda \cdot M} \tag{A.1.40}$$

$$f_\Lambda\,(r) = \begin{cases} \left(\frac{R_o - r}{K_2 \cdot D_p} \right)^2 & \text{if } R_o - r < K_2 \cdot D_p \\ 1 & \text{if } R_o - r \geq K_2 \cdot D_p \end{cases} \tag{A.1.41}$$

$$K_2 = 0.44 + 4 \cdot \exp\left(-\frac{\mathrm{Re}}{70} \right) \tag{A.1.42}$$

$$\mathrm{Re} = \frac{\dot{m}_0 \cdot D_p}{\pi \left(R_o^2 - R_i^2 \right) \mu} \tag{A.1.43}$$

At the boundaries ($r = R_i$ and $r = R_o$) the fluid heat conductivity is used, which is in agreement to the $\Lambda(r)$–model. For the heat transport coefficients on the reaction channel side the according correlations for a 2D model must be used according to eq. (A.1.44) [85].

$$k_i = k_o = 0.17 \frac{\lambda}{D_p} \left(\mathrm{Re}_{D_p} \right)^{0.79} \text{for} \quad 20 \leq \mathrm{Re}_{D_p} = \frac{D_p \cdot \rho \cdot \overline{v}_{s,0}}{\mu} \leq 7600 \tag{A.1.44}$$

2D momentum balance The Brinkman equation eq. (A.1.45) is used to calculate the radial profile of the axial velocity for the inlet conditions. In order to reduce the model complexity so that it can be handled by the optimization solver, the radial velocity distribution is only calculated for the inlet since the radial concentration and temperature gradients do not strongly influence the velocity distribution along the channel. The Reynolds number is defined in eq. (A.1.43) and the void fraction profile in eq. (A.1.51). To calculate the pressure drop from the Brinkman equation, the total mass balance according to eq. (A.1.50) is required. The pressure gradient is assumed to be constant over the reactor length, which is in good agreement with the results of the 1D model.

$$\left. \frac{\partial p}{\partial z} \right|_{z=0} = -f_1 \cdot v_{s,0}(r) - f_2 \cdot v_{s,0}(r)^2 + \frac{\mu_{eff}}{r} \cdot \frac{\partial}{\partial r} \left(r \frac{\partial v_{s,0}(r)}{\partial r} \right) \tag{A.1.45}$$

$$f_1 = 150 \cdot \frac{(1 - \epsilon(r))^2 \cdot \mu}{\epsilon(r)^3 \cdot D_p^2} \tag{A.1.46}$$

$$f_2 = 1.75 \cdot \frac{(1 - \epsilon(r)) \cdot \rho_0}{\epsilon(r)^3 \cdot D_p} \tag{A.1.47}$$

$$p(z = 0) = p_0, \quad v_{s,0}(r = R_i) = 0, \quad v_{s,0}(r = R_o) = 0 \tag{A.1.48}$$

$$\mu_{eff} = 2 \cdot \mu \cdot \exp\left(2 \cdot 10^{-3} \cdot \mathrm{Re} \right) \tag{A.1.49}$$

$$\dot{m}_0 = 2\pi \int_{r=R_i}^{R_o} v_{s,0}(r) \cdot \rho_0 \cdot r \, \mathrm{d}r \tag{A.1.50}$$

Radial void fraction profile The radial void fraction for imperfect spherical particles is usually described using exponential functions. Here, a modified correlation for the void fraction distribution of an annular tube obtained from the literature [148] is used (eq. (A.1.51)).

$$\epsilon(r) = \begin{cases} 0.4 \cdot \left(1 + 1.36 \cdot \exp\left(\frac{-5 \cdot (r - R_i)}{D_p}\right)\right), & R_i \leq r < \frac{R_o + R_i}{2} \\ 0.4 \cdot \left(1 + 1.36 \cdot \exp\left(\frac{-5 \cdot (R_o - r)}{D_p}\right)\right), & \frac{R_o + R_i}{2} \leq r \leq R_o \end{cases} \tag{A.1.51}$$

Selectivity, total residence time, and STY for the 2D case The selectivity, residence time, and STY for the 2D case are given by eq. (A.1.52), eq. (A.1.53), and eq. (A.1.54), respectively.

$$S_{2D} = \frac{\int_{r=R_i}^{R_o} \left(v_{s,f}\rho_{\mathrm{EO},f} - v_{s,0}\rho_{\mathrm{EO},0}\right) r \,\mathrm{d}r}{\int_{r=R_i}^{R_o} \left(v_{s,0}\rho_{\mathrm{E},0} - v_{s,f}\rho_{\mathrm{E},f}\right) r \,\mathrm{d}r + R_i M_{\mathrm{E}} \int_{z=0}^{L} j_{\mathrm{E}}(r = R_i) \,\mathrm{d}z} \cdot \frac{M_{\mathrm{E}}}{M_{\mathrm{EO}}} \tag{A.1.52}$$

$$\tau_{2D} = \int_{z=0}^{L} \frac{\left(R_o^2 - R_i^2\right)}{\int_{r=R_i}^{R_o} v_s r \,\mathrm{d}r} \mathrm{d}z = 30\,\mathrm{s} \tag{A.1.53}$$

$$STY_{2D} = \frac{\int_{r=R_i}^{R_o} \left(v_{s,f}\rho_{\mathrm{EO},f} - v_{s,0}\rho_{\mathrm{EO},0}\right) r \,\mathrm{d}r}{\left(R_o^2 - R_i^2\right) L \cdot M_{\mathrm{EO}}} = 0.27 \,\frac{mol}{m^3 s} \tag{A.1.54}$$

A.2 Oxygen based ethylene oxide process

A.2.1 Reaction section: Additional model equations and data fits

Data fits for the description of the upper explosion limit

In Fig. A.1 the fits of the individual UEL in dependence of R_{inert}, of the pressure dependency of the individual UEL, and of the temperature dependence of κ are presented. For temperature dependence of κ the second order model was chosen since it is able to fit the data points better compared to the exponential model.

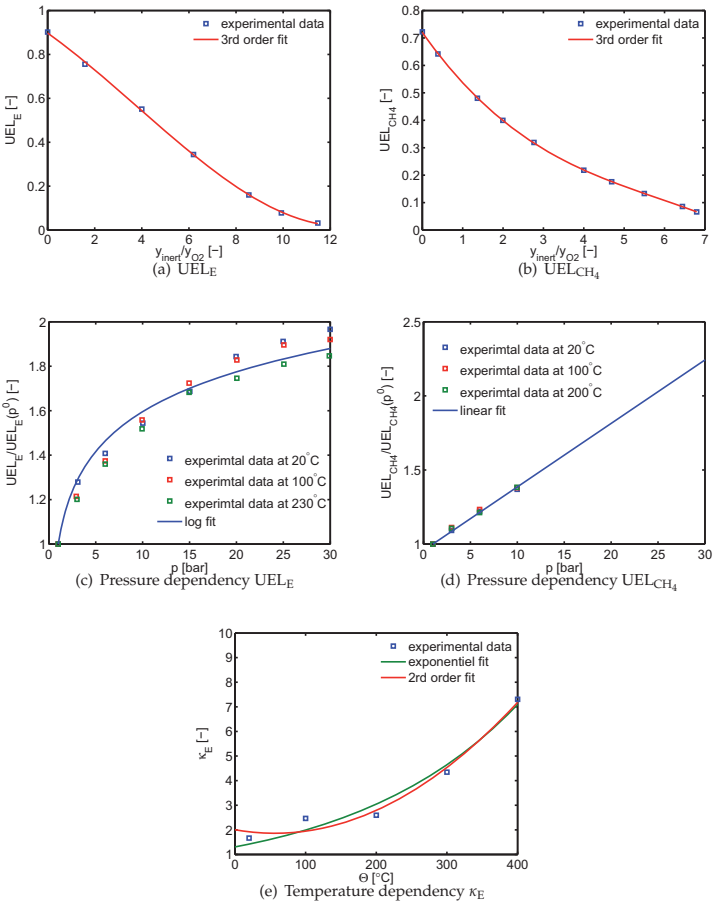

Figure A.1: Required submodels and fits for the description of the explosive region

Connection of reaction system and downstream process

Since the overall process is modeled in steady state, the reaction module must be connected to the overall process using eq. (A.2.1) – eq. (A.2.4) with n_{R101} as total molar amount in the fluid element.

$$y_{i,R101,0} = y_{i,102} \qquad \forall i \in COM \tag{A.2.1}$$

$$y_{i,103} = y_{i,R101,f} \qquad \forall i \in COM \tag{A.2.2}$$

$$\dot{n}_{103} = \dot{n}_{102} \cdot \frac{n_{R101,f}}{n_{R101,0}} \tag{A.2.3}$$

$$\dot{n}_{i,106} = \frac{\int_{t_0}^{t_f} j_{tot,i} \mathrm{d}t}{n_{R101,0}} \cdot \dot{n}_{102} \qquad \forall i \in COM \tag{A.2.4}$$

The initial amount of the fluid element can be chosen in order to adequately scale the volume and molar amount of the fluid element for the numeric calculations (here, $n_{R101,0} = 1\,mol$).

In general, the mole fraction of component i in stream s is referred to as $y_{i,s}$. The mole fractions inside the reaction module are referred to as $y_{i,R101}$. The set of streams, which are required to describe the process (refer to Fig. 5.9), are called STR. The definition of the total streams and its molar composition is given in eq. (A.2.5) and eq. (A.2.6).

$$\dot{n}_s = \sum_{i \in COM} \dot{n}_{i,s} \quad s \in STR \tag{A.2.5}$$

$$y_{i,s} = \frac{\dot{n}_{i,s}}{\dot{n}_s} \quad s \in STR \tag{A.2.6}$$

A.2.2 Downstream process: Model description

A.2.2.1 EO absorption section

EO absorber

The EO absorption column C201 is modeled using an adiabatic counter-current flow column using the following assumptions to derive an efficient model which considers the main aspects of the EO absorption:

- Isobaric operation: The absorption column is operated isobaric at elevated pressure. For the pressure a conservative estimation according to eq. (A.2.16) is used with assumed pressure drops in the reaction module and absorptions columns ($\Delta p_{R101} = 1\,bar$, $\Delta p_{C201} = \Delta p_{C401} = 0.5\,bar$).
- Isothermal operation: The temperature change of the gas and liquid phase are neglected according to eq. (A.2.14). This assumption is in good agreement to the technical operating conditions, the typical adiabatic temperature rise is around $10\,K$. The required cooling to balance the heat of absorption is neglected.
- The gas phase behaves like an ideal gas.

- The solubility of the gases in water can be described using Henry's law with temperature dependent parameters given in Tab. A.1. In the investigated temperature range, the Henry coefficients are described using a second order polynomial and the parameters were fitted to data available in the literature [71, 150].
- The temperature operation window is chosen according to the industrial range (refer to eq. (A.2.15)).
- Phase equilibrium is obtained at every separation tray.

With these assumptions, the Kremser equation (eq. (A.2.8)) can be used to describe the absorption column. Since the investment costs for the absorber are not considered, the number of absorption trays is fixed ($N = 5$).

The mole fraction of water in the gaseous outlet stream is defined by the saturation pressure of water at the according temperature, which is given by eq. (A.2.7) [151].

$$\log\left(p^{\mathrm{s}}_{\mathrm{H_2O}}(T)\right) = 11.210 - (2354.731/(T + 7.559)) \tag{A.2.7}$$

In order to calculate the outlet stream of the liquid phase, the overall component balances are used (refer to eq. (A.2.19)). In eq. (A.2.8), the mole fractions $\hat{y}_{i,201}$ are based on the gaseous inlet stream $\dot{n}_{105}$. Since the gas flow is not constant, the real outlet composition must be calculated according to eq. (A.2.17). Then, the overall gaseous outlet flow is given by eq. (A.2.18).

The complete model for the EO absorber is given by eq. (A.2.8) – eq. (A.2.19).

$$N_{C201} = -\frac{\ln\left[\frac{y_{i,105}-y^*_{i,105}}{\hat{y}_{i,201}-y^*_{i,105}}(1-\lambda_i)+\lambda_i\right]}{\ln(\lambda_i)} \tag{A.2.8}$$

$$\lambda_i = \frac{\dot{n}_{105}}{\dot{n}_{211}} K_i \tag{A.2.9}$$

$$y^*_{i,105} = K_i y_{i,211} \tag{A.2.10}$$

$$K_i = \frac{H_i}{p_{C201}} \qquad \forall i \in COM \setminus \mathrm{H_2O} \tag{A.2.11}$$

$$H_i(T_{C201}) = A_{H,i} T^2_{C201} + B_{H,i} T_{C201} + C_{H,i} \qquad \forall i \in COM \setminus \mathrm{H_2O} \tag{A.2.12}$$

$$K_{\mathrm{H_2O}} = \frac{p^s_{\mathrm{H_2O}}(T_{C201})}{p_{C201}} \tag{A.2.13}$$

$$T_{105} = T_{201} = T_{202} = T_{211} = T_{C201} \tag{A.2.14}$$

$$298\mathrm{K} \leq T_{C201} \leq 413\mathrm{K} \tag{A.2.15}$$

$$p_{C201} = p_{R101} - \Delta p_{R101} - \Delta p_{C201} \tag{A.2.16}$$

$$y_{i,201} = \frac{\dot{n}_{i,201}}{\sum\limits_{i \in COM} \dot{n}_{i,201}} = \frac{\hat{y}_{i,201}\dot{n}_{105}}{\sum\limits_{i \in COM} \hat{y}_{i,201}\dot{n}_{105}} = \frac{\hat{y}_{i,201}}{\sum\limits_{i \in COM} \hat{y}_{i,201}} \tag{A.2.17}$$

$$\dot{n}_{201} = \dot{n}_{105} \sum_{i \in COM} \hat{y}_{i,201} \tag{A.2.18}$$

$$\dot{n}_{i,105} + \dot{n}_{i,214} = \dot{n}_{i,201} + \dot{n}_{i,202} \qquad \forall i \in COM \tag{A.2.19}$$

Table A.1: Parameters of the Henry coefficients

Component	$A_{H,i}\ \left[bar^{-1}K^{-2}\right]$	$B_{H,i}\ \left[bar^{-1}K^{-1}\right]$	$C_{H,i}\ \left[bar^{-1}\right]$
E	-1.689	1319	$-2.318 \cdot 10^5$
EO	0	0.9515	-18.76
O_2	-6.013	4332	$-7.126 \cdot 10^5$
CH_4	-6.138	4508	$-7.583 \cdot 10^5$
CO_2	-0.244	210.7	$-3.961 \cdot 10^4$
Ar	-5.073	3755	$-6.284 \cdot 10^5$

EO desorber

The absorbent is regenerated by distillation at lower pressure and higher temperature. Since the regeneration is very effective, only two theoretical separation trays (partial reboiler and partial condenser) are used to model the EO desorption column (refer to Fig. A.2). The Henry solubilities of all gases in water are used to calculate the vapor-liquid equilibrium. In order to determine the mole fraction of water in the gas phase, it is assumed that the outlet gas stream is saturated with water.

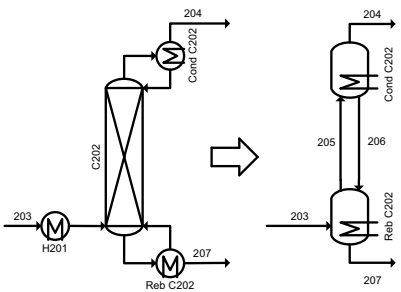

Figure A.2: EO desorption column

The component balances for the reboiler are given by eq. (A.2.20) with the equilibrium conditions stated in eq. (A.2.21) – eq. (A.2.23). The operation window for the temperature is chosen according to the technical operation conditions (refer to eq. (A.2.24)). The pressure of the EO desorber is fixed at $p_{C202} = 1.2\,bar$.

$$\dot{n}_{i,203} = \dot{n}_{i,205} + \dot{n}_{i,207} \qquad \forall i \in COM \tag{A.2.20}$$

$$y_{i,205} \cdot H_{i,205} = y_{i,207} \cdot p_{C202} \qquad \forall i \in COM \setminus \{H_2O\} \tag{A.2.21}$$

$$y_{H_2O,205} \cdot p_{C202} = p^s_{H_2O}\left(T_{C202,Reb}\right) \tag{A.2.22}$$

$$T_{205} = T_{207} = T_{C202,Reb} \tag{A.2.23}$$

$$298\,K \leq T_{C202,Reb} \leq 410\,K \tag{A.2.24}$$

The model for the condenser is given by eq. (A.2.25) – eq. (A.2.31). Here, the EO purity is constrained by eq. (A.2.30) and the EO outlet stream is fixed according to eq. (A.2.31).

$$\dot{n}_{i,205} = \dot{n}_{i,204} + \dot{n}_{i,206} \qquad \forall i \in COM \tag{A.2.25}$$

$$y_{i,204} \cdot H_{i,204} = y_{206} \cdot p_{C202} \qquad \forall i \in COM \setminus \{H_2O\} \tag{A.2.26}$$

$$y_{H_2O,204} \cdot p_{C202} = p^s_{H_2O}\left(T_{C202,Cond}\right) \tag{A.2.27}$$

$$T_{204} = T_{206} = T_{C202,Cond} \tag{A.2.28}$$

$$298\,K \leq T_{C202,Cond} \leq 410\,K \tag{A.2.29}$$

$$y_{EO,204} \geq 0.95 \tag{A.2.30}$$

$$\dot{n}_{EO,204} = 1\,\frac{mol}{s} \tag{A.2.31}$$

The required amount of cooling and heating are approximated by eq. (A.2.32) and eq. (A.2.33), respectively. The heat duties associated with the sensitive heat change in the condenser and the desorption of the gases are neglected since both heat duties are much smaller than the heat duty associated with the evaporation and condensation of water.

$$\dot{Q}_{C202,Reb} = \dot{n}_{H_2O,202} \cdot c_{p,H_2O,l} \cdot \left(T_{205} - T_{202}\right) + \dot{n}_{H_2O,206} \cdot \Delta h_{v,H_2O} \tag{A.2.32}$$

$$\dot{Q}_{C202,Cond} = \dot{n}_{H_2O,206} \cdot \Delta h_{v,H_2O} \tag{A.2.33}$$

A.2.2.2 CO_2 absorption section

The chemical equilibrium of the CO_2 absorption in hot potassium carbonate solution is modeled according to the reactions eq. (5.4.30) – eq. (5.4.35). The equilibrium constants for these reactions are published individually by several authors [152–155] and summarized by eq. (A.2.34) – eq. (A.2.40). Cullinane and Rochelle [156] proposed a model for the chemical equilibrium of the CO_2 absorption based on the published equilibrium constants [152–155], where they fitted the pre-factors in eq. (A.2.34) – eq. (A.2.36) and eq. (A.2.39) to experimental data ($T = 60°C$, molality of piperazine (PZ) of 0.6, weight fraction of K_2CO_3 between 0.2 and 0.3). These pre-factors account for the complex interplay of the chemical reactions. Since the model is based on first principles, it can be extended towards the conditions of the CO_2 absorption and desorption with respect to the temperature and CO_2 partial pressure. However, the loadings of piperazine and K_2CO_3 will be fixed in the optimization to the experimental conditions in order to limit the extrapolation error (refer to eq. (A.2.58) and eq. (A.2.59)).

$$K_1 = 0.31 \cdot \frac{HCO_3^- \cdot H_3O^+}{CO_{2,aq} \cdot H_2O^2} \tag{A.2.34}$$

$$K_2 = 0.0961 \cdot \frac{CO_3^{2-} \cdot H_3O^+}{HCO_3^- \cdot H_2O} \tag{A.2.35}$$

$$K_3 = 0.75 \cdot \frac{\mathrm{PZCOO^-} \cdot \mathrm{H_3O^+}}{\mathrm{PZ} \cdot \mathrm{H_2O} \cdot \mathrm{CO_{2,aq}}} \tag{A.2.36}$$

$$K_4 = \frac{\mathrm{PZ} \cdot \mathrm{H_3O^+}}{\mathrm{PZH^+} \cdot \mathrm{H_2O}} \tag{A.2.37}$$

$$K_5 = 0.7 \cdot \frac{\mathrm{PZ(COO^-)_2} \cdot \mathrm{H_3O^+}}{\mathrm{PZCOO^-} \cdot \mathrm{H_2O} \cdot \mathrm{CO_{2,aq}}} \tag{A.2.38}$$

$$K_6 = \frac{\mathrm{PZCOO^-} \cdot \mathrm{H_3O^+}}{\mathrm{H^+PZCOO^-} \cdot \mathrm{H_2O}} \tag{A.2.39}$$

$$\ln K_j = A_j + B_j/T + C_j \ln T \tag{A.2.40}$$

Table A.2: Equilibrium constants (mole fractions)

Equil. reaction	A_j	B_j	C_j
1	231.1	-12092	-36.78
2	216.0	-12432	-35.48
3	-29.31	5615	0
4	-11.91	-4351	0
5	-30.78	5615	0
6	-8.21	-5286	0

In order to reduce the dimension of the overall process model, the chemical equilibrium of the CO_2 absorption must only be solved for the following set of streams $STR_{CO_2} \in \{403, 407, 411\}$. For the component mass balances of all reacting species of the CO_2 a set of intermediate species ISC is defined according to:

$$ISC = \left\{\mathrm{HCO_3^-}, \mathrm{H_3O^+}, \mathrm{CO_3^{2-}}, \mathrm{PZ}, \mathrm{PZCOO^-}, \mathrm{PZH^+}, \mathrm{PZ(COO^-)_2}, \mathrm{H^+PZCOO^-}, \mathrm{H_2O}, \mathrm{CO_{2,aq}}\right\}$$

The reacting species and the gas phase components are partly decoupled by using the following definitions for the mole fractions of the reacting species and the mole fractions the gas phase components in the streams with CO_2 equilibrium. Since the total amount of gases (except of CO_2) dissolved in the carbonate solution is very small, the dissolved gases hardly affect the chemical equilibrium. Hence, this assumption reflects the real conditions quite well.

$$y_{i,s} = \frac{\dot{n}_{i,s}}{\sum_{i \in ISC} \dot{n}_{i,s}} \quad \forall i \in ISC,\, s \in STR_{\mathrm{CO_2}} \tag{A.2.41}$$

$$y_{i,s} = \frac{\dot{n}_{i,s}}{\dot{n}_{\mathrm{H_2O},s}} \quad \forall i \in COM \setminus \{\mathrm{H_2O}, \mathrm{CO_2}, s \in STR_{\mathrm{CO_2}}\} \tag{A.2.42}$$

CO_2 absorber

Since the chemical absorption of CO_2 in the potassium solution is very efficient, the absorption column is modeled with one equilibrium stage (refer to Fig. A.3). The

performed flash calculation takes the chemical absorption of CO_2 and the physical absorption of the other components into account.

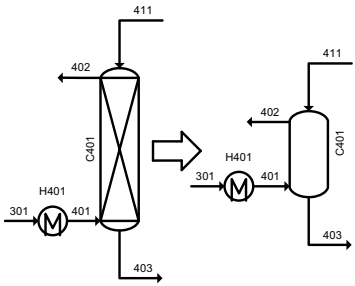

Figure A.3: CO_2 absorption column

The component balances for the flash tank are given by eq. (A.2.43) – eq. (A.2.47). For all components which do not take part in the chemical reaction a conventional component balance is formulated. For the reacting species the chemical equilibrium together with atom balances for carbon, nitrogen, oxygen, and hydrogen have to be solved. The according stoichiometric coefficients for the atom balances are given in Tab. A.3.

$$\dot{n}_{i,401} + \dot{n}_{i,411} = \dot{n}_{i,402} + \dot{n}_{i,403} \qquad \forall i \in COM \setminus \{H_2O, CO_2\} \tag{A.2.43}$$

$$\sum_{i \in ISC} (\dot{n}_{i,411} \cdot \nu_{C,i}) + \dot{n}_{CO_2,401} = \sum_{i \in ISC} (\dot{n}_{i,403} \cdot \nu_{C,i}) + \dot{n}_{CO_2,402} \tag{A.2.44}$$

$$\sum_{i \in ISC} (\dot{n}_{i,411} \cdot \nu_{N,i}) = \sum_{i \in ISC} (\dot{n}_{i,403} \cdot \nu_{N,i}) \tag{A.2.45}$$

$$\begin{aligned} &\sum_{i \in ISC} (\dot{n}_{i,411} \cdot \nu_{O,i}) + 2 \cdot \dot{n}_{CO_2,401} + \dot{n}_{H_2O,401} \\ &= \sum_{i \in ISC} (\dot{n}_{i,403} \cdot \nu_{O,i}) + 2 \cdot \dot{n}_{CO_2,402} + \dot{n}_{H_2O,402} \end{aligned} \tag{A.2.46}$$

$$\sum_{i \in ISC} (\dot{n}_{i,411} \cdot \nu_{H,i}) + 2 \cdot \dot{n}_{H_2O,401} = \sum_{i \in ISC} (\dot{n}_{i,403} \cdot \nu_{H,i}) + 2 \cdot \dot{n}_{H_2O,402} \tag{A.2.47}$$

Table A.3: Stoichiometric coefficients of the reactions within the CO_2 absorption

Reacting species of the CO_2 absorption	$\nu_{N,i}$	$\nu_{C,i}$	$\nu_{O,i}$	$\nu_{H,i}$
HCO_3^-	0	1	3	1
H_3O^+	0	0	1	3
CO_3^{2-}	0	1	3	0
PZ	1	0	0	2
$PZCOO^-$	1	1	2	1
PZH^+	1	0	0	3
$PZ(COO^-)_2$	1	2	4	0
H^+PZCOO^-	1	1	2	2
H_2O	0	0	1	2
$CO_{2,aq}$	0	1	2	0

The solubility of the gases (except CO_2) in the liquid phase is estimated using Henry's law for water as absorbent (refer to eq. (A.2.48)). The mole fraction of water in the gaseous outlet stream is defined by its saturation pressure according to eq. (A.2.50).

$$y_{i,403} \cdot H_{i,403} = p_{C401} \cdot y_{i,402} \qquad \forall i \in COM \setminus \{H_2O, CO_2\} \tag{A.2.48}$$

$$y_{CO_2,403} \cdot H^*_{CO_2,403} = p_{C401} \cdot y_{CO_2,402} \tag{A.2.49}$$

$$y_{H_2O,402} \cdot p_{C401} = p^s_{H_2O}(T_{C401}) \tag{A.2.50}$$

Since the solubility of CO_2 in aqueous potassium carbonate solution cannot be measured directly, the similarity of CO_2 to N_2O is exploited [105]. N_2O has approximately the same molecular weight as CO_2 and a similar electron configuration, but does not react in the aqueous potassium carbonate solution and hence, its physical solubility can be measured more accurately. The solubility of CO_2 is correlated to the solubility of N_2O according to eq. (A.2.51). Here, H_i is the Henry coefficient of component i in water and $H^*_{CO_2}$ is the Henry coefficient of CO_2 in aqueous potassium carbonate solution.

$$H^*_{CO_2} = H^*_{N_2O} \frac{H_{CO_2}}{H_{N_2O}} \qquad s \in STR_{CO_2} \tag{A.2.51}$$

The temperature dependence of the CO_2 solubility is determined by using the Henry coefficients of CO_2 and N_2O in water from the literature [157]. This yields the Henry coefficient of CO_2 in the potassium carbonate solution $H^*_{CO_2}$ as defined in eq. (A.2.52).

$$H^*_{CO_2,s} = \left(-2.0998 \cdot 10^9 + 7.8892 \cdot 10^6 \cdot T_s\right) \cdot \exp\left(\frac{240}{T_s}\right) \qquad s \in STR_{CO_2} \tag{A.2.52}$$

Cullinane [158] showed that piperazine has little effect on the physical solubility of CO_2 in aqueous potassium carbonate solution. Hence, the used model accurately describes the physical solubility of CO_2 in the used aqueous potassium carbonate solution.

Since the model for the chemical equilibrium in the CO_2 absorption is only valid for a specific molality of piperazine ($m_{PZ} = 0.6 \frac{mol_{PZ}}{kg_{H_2O}}$) and a specific weight fraction of K_2CO_3 ($w_{K_2CO_3} = 0.3$) in the aqueous solution, the stream of piperazine and K_2CO_3 are coupled to the water stream. For this purpose, a set of pseudo components is defined according to:

$$COM_{pseudo} = \{\mathrm{PZ}, \mathrm{K_2CO_3}, \mathrm{H_2O}, \mathrm{CO_2}\}$$

For these pseudo components, the according pseudo streams are calculated by solving the following set of equations (for $s \in STR_{CO_2}$):

$$\dot{n}_{pseudo,\mathrm{PZ},s} = \sum_{i \in ISC} (\dot{n}_{i,s} \cdot \nu_{N,i}) \tag{A.2.53}$$

$$2 \cdot \dot{n}_{pseudo,\mathrm{H_2O},s} + \dot{n}_{pseudo,PZ,s} = \sum_{i \in ISC} (\dot{n}_{i,s} \cdot \nu_{H,i}) \tag{A.2.54}$$

$$\dot{n}_{pseudo,\mathrm{K_2CO_3},s} + \dot{n}_{pseudo,\mathrm{CO_2},s} = \sum_{i \in ISC} (\dot{n}_{i,s} \cdot \nu_{C,i}) \tag{A.2.55}$$

$$3 \cdot \dot{n}_{pseudo,\mathrm{K_2CO_3},s} + 2 \cdot \dot{n}_{pseudo,\mathrm{CO_2},s} + \dot{n}_{pseudo,\mathrm{H_2O},s} = \sum_{i \in ISC} (\dot{n}_{i,s} \cdot \nu_{O,i}) \tag{A.2.56}$$

In order to calculate the amount of K_2CO_3 from the composition of the liquid phase, complete dissociation of K_2CO_3 is assumed (refer to eq. (A.2.57)).

$$\mathrm{K_2CO_3} \leftharpoons 2\mathrm{K^+} + \mathrm{CO_3^{2-}} \tag{A.2.57}$$

The constraints which couple the pseudo streams of piperazine and K_2CO_3 to the water stream are stated in eq. (A.2.58) and eq. (A.2.59).

$$\dot{n}_{pseudo,\mathrm{PZ},411} = M_{\mathrm{H_2O}} \cdot m_{\mathrm{PZ}} \cdot \dot{n}_{pseudo,\mathrm{H_2O},411} \tag{A.2.58}$$

$$\dot{n}_{pseudo,\mathrm{K_2CO_3},411} = \frac{w_{\mathrm{K_2CO_3}}}{1 - w_{\mathrm{K_2CO_3}}} \cdot \frac{M_{\mathrm{H_2O}}}{M_{\mathrm{K_2CO_3}}} \cdot \dot{n}_{pseudo,\mathrm{H_2O},411} \tag{A.2.59}$$

It is assumed that the absorber can be operated isothermally and the heat of absorption is neglected. This assumption gives rise to the isothermality condition according to eq. (A.2.60). The adiabatic temperature rise associated with the chemical absorption of CO_2 and the evaporation of water was estimated a priori to be in the range of $18\,K$. Due to the small adiabatic temperature rise, the absorber can be operated isothermally by external cooling if desired. The associated heat duty is small and since cooling water costs are low, the costs for cooling the absorber are neglected. The column temperature T_{C401} is a degree of freedom within the typical operation conditions stated in eq. (A.2.61). The desired absorption temperature is obtained by adjusting the heat duty of $H401$.

$$T_{401} = T_{402} = T_{403} = T_{411} = T_{C401} \tag{A.2.60}$$

$$298\,K \leq T_{C401} \leq 410\,K \tag{A.2.61}$$

The operating pressure of the CO_2 absorber is defined by the reactor pressure and the pressure loss of the EO and CO_2 absorbers. As a conservative guess, the column is operated at constant outlet pressure according to eq. (A.2.62).

$$p_{C401} = p_{R101} - \Delta p_{R101} - \Delta p_{C201} - \Delta p_{C401} \tag{A.2.62}$$

CO_2 desorber

The potassium carbonate solution is recovered using a CO_2 desorption column operated at lower pressure ($p_{C402} = 1.2\,bar$). The regeneration column is approximated using two equilibrium stages according to Fig. A.4. Since it is assumed that all species arising from potassium carbonate and piperazine have a negligible vapor pressure, the chemical equilibrium has only to be solved for the reboiler. The condenser is described by a conventional flash calculation.

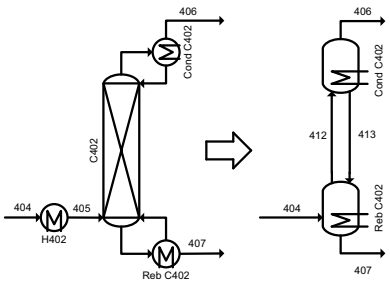

Figure A.4: CO_2 desorption column

Similar to the CO_2 absorber, the reboiler of the CO_2 regeneration column is described by eq. (A.2.63) – eq. (A.2.71). The operating temperature is a degree of freedom and is constrained by the operating window stated in eq. (A.2.72).

$$\dot{n}_{i,404} + \dot{n}_{i,413} = \dot{n}_{i,412} + \dot{n}_{i,407} \qquad \forall i \in COM \setminus \{H_2O, CO_2\} \tag{A.2.63}$$

$$\sum_{i \in ISC} (\dot{n}_{i,413} \cdot \nu_{C,i}) + \dot{n}_{CO_2,404} = \sum_{i \in ISC} (\dot{n}_{i,407} \cdot \nu_{C,i}) + \dot{n}_{CO_2,412} \tag{A.2.64}$$

$$\sum_{i \in ISC} (\dot{n}_{i,413} \cdot \nu_{N,i}) = \sum_{i \in ISC} (\dot{n}_{i,407} \cdot \nu_{N,i}) \tag{A.2.65}$$

$$\sum_{i \in ISC} (\dot{n}_{i,413} \cdot \nu_{O,i}) + 2 \cdot \dot{n}_{CO_2,404} + \dot{n}_{H_2O,404} = \sum_{i \in ISC} (\dot{n}_{i,407} \cdot \nu_{O,i}) + 2 \cdot \dot{n}_{CO_2,412} + \dot{n}_{H_2O,412} \tag{A.2.66}$$

$$\sum_{i \in ISC} (\dot{n}_{i,413} \cdot \nu_{H,i}) + 2 \cdot \dot{n}_{H_2O,404} = \sum_{i \in ISC} (\dot{n}_{i,407} \cdot \nu_{H,i}) + 2 \cdot \dot{n}_{H_2O,412} \tag{A.2.67}$$

$$y_{i,407} \cdot H_{i,407} = p_{C402} \cdot y_{i,412} \qquad \forall i \in COM \setminus \{H_2O, CO_2\} \tag{A.2.68}$$

$$y_{CO_2,407} \cdot H^*_{CO_2,407} = p_{C402} \cdot y_{CO_2,412} \tag{A.2.69}$$

$$y_{H_2O,412} \cdot p_{C402} = p^s_{H_2O}(T_{C402,Reb}) \tag{A.2.70}$$

$$T_{407} = T_{412} = T_{C402,Reb} \tag{A.2.71}$$
$$298\,K \leq T_{C402,Reb} \leq 410\,K \tag{A.2.72}$$

The condenser is described by eq. (A.2.73) – eq. (A.2.78) similar to the condenser of the EO desorber. The thermal equilibrium is given by eq. (A.2.76). The condenser temperature is a degree of freedom within its typical operating window (refer to eq. (A.2.77)). In addition, the purity of CO_2 in the outlet stream is restricted by eq. (A.2.78).

$$\dot{n}_{412} = \dot{n}_{406} + \dot{n}_{413} \tag{A.2.73}$$
$$y_{i,406} \cdot H_{i,406} = y_{413} \cdot p_{C402} \tag{A.2.74}$$
$$y_{H_2O,406} \cdot p_{C402} = p^s_{H_2O}\left(T_{C402,Cond}\right) \tag{A.2.75}$$
$$T_{406} = T_{413} = T_{C402,Cond} \tag{A.2.76}$$
$$298\,K \leq T_{C402,Reb} \leq 410\,K \tag{A.2.77}$$
$$y_{CO_2,406} \geq 0.95 \tag{A.2.78}$$

The heat duties of the condenser and reboiler are estimated using the same simplifications as in the EO absorption section (refer to eq. (A.2.79) and eq. (A.2.80)).

$$\dot{Q}_{C402,Cond} = \dot{n}_{H_2O,404} \cdot c_{pl,H_2O} \cdot (T_{412} - T_{404}) + \dot{n}_{H_2O,412} \cdot \Delta h_{v,H_2O} \tag{A.2.79}$$
$$\dot{Q}_{C402,Reb} = \dot{n}_{H_2O,413} \cdot \Delta h_{v,H_2O} \tag{A.2.80}$$

A.2.2.3 Additional process units

Mixers and splitters

The general component balances of the mixers are given in eq. (A.2.81). The set of inlet streams IN_u of each mixer u is defined in Tab. A.4.

$$\dot{n}_{i,out_u} = \sum_{s \in IN_u} \dot{n}_{i,s} \quad \text{for } u = M001,\ M001,\ M301 \tag{A.2.81}$$

The mixing temperature is calculated from the energy balance of an adiabatic system without phase change and neglecting the heat of mixing (refer to eq. (A.2.82)).

$$\sum_{i \in COM} \dot{n}_{i,out_u} \cdot h_{i,out_u} = \sum_{i \in COM} \sum_{s \in IN_u} \dot{n}_{i,s} \cdot h_{i,s} \quad \text{for } u = M001,\ M001,\ M301 \tag{A.2.82}$$

The general component balances of the splitters with the according split fraction ξ_u are given in eq. (A.2.83) – eq. (A.2.85). The outlet streams of each splitter are defined in Tab. A.4.

$$\dot{n}_{i,out_{1,u}} = \xi_u \cdot \dot{n}_{i,in_u} \quad \text{for } u = S201,\ S301,\ S303 \tag{A.2.83}$$

$$\dot{n}_{i,out_{2,u}} = (1 - \xi_u) \cdot \dot{n}_{i,in_u} \quad \text{for } u = S201,\ S301,\ S303 \tag{A.2.84}$$

$$0 \leq \xi_u \leq 1 \quad \text{for } u = S201,\ S301,\ S303 \tag{A.2.85}$$

By assuming adiabatic splitters, the energy balances for the splitters simplify to eq. (A.2.86).

$$T_{out_{1,u}} = T_{out_{2,u}} = T_{in_u} \quad \text{for } u = S201,\ S301,\ S303 \tag{A.2.86}$$

Table A.4: Inlet and outlet streams of mixers and splitters

Unit	Outlet streams	Inlet streams
$M001$	$out_u = 004$	$IN_{M001} = \{001, 002, 003\}$
$M002$	$out_u = 101$	$IN_{M002} = \{004, 307\}$
$M301$	$out_u = 304$	$IN_{M301} = \{303, 402\}$
$M302$	$out_u = 409$	$IN_{M302} = \{407, 408\}$
$S201$	$out_{1,u} = 211$ $out_{2,u} = 212$	$in_u = 210$
$S301$	$out_{1,u} = 301$ $out_{2,u} = 302$	$in_u = 201$
$S303$	$out_{1,u} = 305$ $out_{2,u} = 306$	$in_u = 304$

Compressors, pumps, and valves

The ideal component balances for each compressor, pump, and valve are given by eq. (A.2.87).

$$\dot{n}_{i,out} = \dot{n}_{i,in} \quad \text{for } u = C301,\ P201,\ P401,\ V201,\ V301,\ V401 \tag{A.2.87}$$

Assuming an isentropic compressor, the outlet temperature of the compressor is given by eq. (A.2.88). The energy requirement is calculated using eq. (A.2.89). For the compressors and the pumps, a compression efficiency of $\eta = 100\%$ is assumed in oder to calculate the lowest possible energy consumption. Since the compression ratio $\frac{p_{307}}{p_{306}}$ is low, no staged compressors with intermediate cooling are required. Assuming an ideal system, a constant isentropic exponent of $\kappa = 1.4$ can be taken [138].

$$T_{307} = T_{306} \left(\frac{p_{307}}{p_{306}} \right)^{\frac{\kappa-1}{\kappa}} \tag{A.2.88}$$

$$P_{CP301} = \dot{n}_{306} \frac{\kappa}{\kappa - 1} R T_{306} \left[\left(\frac{p_{307}}{p_{306}} \right)^{\frac{\kappa-1}{\kappa}} - 1 \right] \tag{A.2.89}$$

The energy requirement of each pump is estimated by eq. (A.2.90). The volume flow in each pump is calculated using the inlet streams and assuming pure water (refer to eq. (A.2.91) with $M_{H_2O} = 18\,\frac{kg}{kmol}$ and $\rho_{H_2O} = 1000\,\frac{kg}{m^3}$). Since the potassium carbonate solution has a density very close to the density of water [158], this assumption can also be used within the CO_2 absorption section. Here, isothermal operation of the pumps is assumed (refer to eq. (A.2.92)) and the required cooling duty is neglected since it is very small.

$$P_u = \dot{V}_u \left(p_{out,u} - p_{in,u}\right) \quad \text{for } u = P201,\ P401 \tag{A.2.90}$$

$$\dot{V}_u = \frac{\dot{n}_{H_2O,in_u} M_{H_2O}}{\rho_{H_2O}} \quad \text{for } u = P201,\ P401 \tag{A.2.91}$$

$$T_{out,u} = T_{in,u} \quad \text{for } u = P201,\ P401 \tag{A.2.92}$$

For the valves, isothermal operation is assumed (refer to eq. (A.2.93)) and the associated heat duty is neglected.

$$T_{out,u} = T_{in,u} \quad \text{for } u = S201,\ S301,\ S303 \tag{A.2.93}$$

Heat exchangers

The component balances for each heat exchanger are given in eq. (A.2.94) with the according in and outlet stream defined in Tab. A.5.

$$\dot{n}_{i,out_u} = \dot{n}_{i,in_u} \tag{A.2.94}$$
$$\text{for } u = H101,\ H102,\ H103,\ H201,\ H202,\ H401,\ H402,\ H405$$

Table A.5: Inlet and outlet streams of the heat exchanger

Unit	Inlet stream (in_u)	Outlet stream (out_u)	Utility
$H101$	101	102	LPS
$H102$	103	104	LPS
$H103$	104	105	CW
$H201$	203	204	LPS
$H202$	212	213	CW
$H401$	301	401	CW
$H402$	404	405	LPS
$H405$	409	410	CW

The heat duty for each heat exchanger cooling down or heating up a gas stream is defined by eq. (A.2.95) and the used utility is given in Tab. A.5.

$$\dot{Q}_u = \sum_{i \in COM} \left(\dot{n}_{i,in_u} \left(h_{i,out_u} - h_{i,in_u}\right)\right) \quad \text{for } u = H101,\ H102,\ H103,\ H201 \tag{A.2.95}$$

The gas phase enthalpy of each component is calculated by eq. (A.2.96) and the heat capacity is calculated as stated in eq. (A.2.97). The required parameters are given in Tab. A.6 and are obtained by regression from data given in the literature [65].

$$h_i(T) = A_{cp,i}T^* + \frac{B_{cp,i}}{2}(T^*)^2 + F_{cp,i} \tag{A.2.96}$$

$$c_p(T) = A_{cp,i} + B_{cp,i}T^* \tag{A.2.97}$$

$$T^* = \frac{T}{1000} \tag{A.2.98}$$

Table A.6: Heat capacity parameters and standard enthalpy (gas phase)

Component	$A_{cp,i}\left[\frac{J}{mol\cdot K}\right]$	$B_{cp,i}\left[\frac{J}{mol\cdot K^2}\right]$	$F_{cp,i}\left[\frac{J}{mol}\right]$
E	14.5491	95.9198	$4.3864 \cdot 10^4$
EO	8.5836	133.8392	$-6.1146 \cdot 10^4$
O_2	25.6178	12.0468	$-8.1927 \cdot 10^3$
CH_4	18.6258	55.1964	$-8.2879 \cdot 10^4$
CO_2	26.8792	35.6990	$-4.0313 \cdot 10^5$
H_2O	30.8928	8.5749	$-2.5142 \cdot 10^5$
Ar	20.8	0	0

The heat exchanger $H202$ and $H405$ cool down the EO absorbent and the CO_2 absorbent stream, respectively. Since these streams are composed of almost pure water the heat duties are approximated using eq. (A.2.99) and eq. (A.2.100).

$$\dot{Q}_{H202} = \dot{n}_{H_2O,209} \cdot c_{p,H_2O} \cdot (T_{210} - T_{209}) \tag{A.2.99}$$

$$\dot{Q}_{H405} = \dot{n}_{H_2O,409} \cdot c_{p,H_2O} \cdot (T_{410} - T_{409}) \tag{A.2.100}$$

A.3 Hydroformylation of long chain alkenes

A.3.1 Definition of normalized variables for graphical display

The definition of all normalized variables used in Chapter 6 are given in eq. (A.3.1) – eq. (A.3.7). The according reference values are summarized in Tab. A.7.

$$r_{rel,j} = \frac{r_j}{r_{ref}} \tag{A.3.1}$$

$$j_{rel,i} = \frac{j_{tot,i}}{j_{ref,i}} \tag{A.3.2}$$

$$q_{rel} = \frac{q_{tot}}{q_{ref}} \tag{A.3.3}$$

$$T_{rel,c} = \frac{T_c - \min\left(T_c\right)}{\Delta T_{ref}} \tag{A.3.4}$$

$$p_{rel} = \frac{p}{p_{ref}} \tag{A.3.5}$$

$$p_{rel,i} = \frac{p_i}{p_{ref}} \tag{A.3.6}$$

$$\dot{n}_{rel,i,h} = \frac{\dot{n}_{i,h,k,add}}{n_{ref,i}} \tag{A.3.7}$$

Table A.7: Reference values used for scaling

Figure	Reference variable	Reference value	Unit
Fig. 6.6(c)	r_{ref}	21.9	$\left[\frac{mol}{m_{IL}^3 \cdot s}\right]$
Fig. 6.6(d)	r_{ref}	31.4	$\left[\frac{mol}{m_{IL}^3 \cdot s}\right]$
Fig. 6.6(e)	$j_{ref,\mathrm{H_2}}$, $j_{ref,\mathrm{CO}}$	6.1	$\left[\frac{mol}{s}\right]$
	q_{ref}	661.7	$[W]$
Fig. 6.6(f)	$j_{ref,tAlk}$	24.8	$\left[\frac{mol}{s}\right]$
	$j_{ref,\mathrm{H_2}}$	8.3	$\left[\frac{mol}{s}\right]$
	$j_{ref,\mathrm{CO}}$	7.9	$\left[\frac{mol}{s}\right]$
	q_{ref}	898.6	$[W]$
Fig. 6.7(b)	$\min\left(T_c\right)$	354.18	$[K]$
	ΔT_{ref}	10.35	$[K]$
	$j_{ref,tAlk}$	16.0	$\left[\frac{mol}{s}\right]$
Fig. 6.7(b), Fig. 6.10(c)	p_{ref}	60	$[bar]$
Fig. 6.10(b)	$\dot{n}_{ref,tAlk}$, $\dot{n}_{ref,syngas}$	2.4	$\left[\frac{mol}{s}\right]$

A.3.2 Additional model equations of level 1

CSTR model The equations describing the CSTR are summarized in a comprehensive manner below.

$$\dot{n}_{i,f} - \dot{n}_{i,0} = \epsilon_{IL} V_R \sum_{j=1}^{NR} \nu_{i,j} \cdot r_j, \quad i \in COML \tag{A.3.8}$$

The fraction of IL is calculated using eq. (A.3.9), and V_R is the total liquid volume inside the reactor.

$$\epsilon_{IL} = \frac{\dot{V}_{IL}}{\dot{V}_{IL} + \dot{V}_{org}} \tag{A.3.9}$$

$$V_R = \left(\dot{V}_{IL} + \dot{V}_{org}\right) \tau \tag{A.3.10}$$

The volume flow of IL and organic phase is calculated by eq. (A.3.11).

$$\dot{V}_k = \sum_{i \in COML} \frac{\dot{n}_{i,k} \cdot M_i}{\rho_i}, \quad k = IL, org \tag{A.3.11}$$

For comparison, the amount of solvent is connected to the amount of terminal alkene as in the reference case (eq. (A.3.12)). The volume fraction of IL and organic phase at the inlet are also restricted by the same bounds as before (eq. (A.3.13)).

$$C_{tAlk} = \frac{\dot{n}_{tAlk,0}}{\frac{\dot{n}_{tAlk,0} \cdot M_{tAlk}}{\rho_{tAlk}(373\,K)} + \frac{\dot{n}_{Dec} \cdot M_{Dec}}{\rho_{Dec}(373\,K)}} = 2 \cdot 10^3 \, \frac{mol}{m^3} \tag{A.3.12}$$

$$V_{frac}^{L} \leq \frac{\dot{V}_{Dec}}{\dot{V}_{IL}} \leq V_{frac}^{U} \tag{A.3.13}$$

In case of a CSTR, the conversion and the selectivity are given by eq. (A.3.14), eq. (A.3.15), and eq. (A.3.16), respectively.

$$\dot{n}_{tAlk,0} \geq \dot{n}_{tAlk,f} \tag{A.3.14}$$

$$X = \frac{\dot{n}_{tAlk,0} - \dot{n}_{tAlk,f}}{\dot{n}_{tAlk,0}} \tag{A.3.15}$$

$$S_{CSTR} = \frac{\dot{n}_{nAld,f} - \dot{n}_{nAld,0}}{\dot{n}_{tAlk,0} - \dot{n}_{tAlk,f}} \tag{A.3.16}$$

A.3.3 Model equations of level 3

On this level, a reactor with static mixer elements and distributors for additional gas and alkene feed is modeled. The distributors are designed such that gas and liquid is added over the entire cross sectional area in order to avoid radial concentration gradients due to discrete dosing. In accordance to the literature, the flow characteristics

are plug flow like when using static mixers [142]. Furthermore, for the investigated static mixers, no slip velocity between gas and liquid phase was observed [145].

Component balances for each segment The component balances in each segment (set of segments $SEG = \{1,2,3\}$) are given by eq. (A.3.17) for the gas phase and for the liquid phase by eq. (A.3.18). For the sake of simplicity, the segment index s is only used where it is absolutely necessary. The handover conditions from one segment to the other are defined by eq. (A.3.19). Further constitutive equations for the mass balances are given by eq. (A.3.21) – eq. (A.3.22).

$$\frac{\mathrm{d}\dot{n}_{i,g,s}}{\mathrm{d}z} = -\left(k_L a\right) \cdot \left(C_i^* - C_{i,org}\right) \pi R^2, \quad i \in COMG,\, s \in SEG \tag{A.3.17}$$

$$\frac{\mathrm{d}\dot{n}_{i,liq,s}}{\mathrm{d}z} = \begin{cases} \left(k_L a\right) \cdot \left(C_i^* - C_{i,org}\right) \pi R^2 + A_{IL} \cdot \sum_{j=1}^{NR} \nu_{i,j} \cdot r_j, & i \in COMG,\, s \in SEG \\ A_{IL} \cdot \sum_{j=1}^{NR} \nu_{i,j} \cdot r_j & i = \text{else},\, s \in SEG \end{cases} \tag{A.3.18}$$

$$\dot{n}_{i,s,0} = \dot{n}_{i,s-1,f}, \quad i \in COM,\, s \in SEG \setminus \{1\} \tag{A.3.19}$$

$$\dot{n}_{i,1,0} = \dot{n}_{i,0}, \quad i \in COM \tag{A.3.20}$$

$$A_{IL} = \frac{\dot{V}_{IL}}{v_i} \tag{A.3.21}$$

$$\dot{n}_{i,liq} = \dot{n}_{i,IL} + \dot{n}_{i,org}, \quad i \in COM \tag{A.3.22}$$

Mass balance for each distributor For each gas and liquid distributor ($h \in DIS = \{1,\ldots,31\}$ with set of distributors DIS), eq. (A.3.23) need to be solved for each component, respectively. Fig. A.5 illustrates the balance envelope for a distributor. The added streams of substances $\dot{n}_{i,h,k,add}$ are degrees of freedom for the optimization.

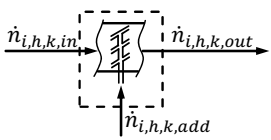

Figure A.5: Balance envelope for each distributor

$$\dot{n}_{i,h,k,out} = \begin{cases} \dot{n}_{i,h,k,in} + \dot{n}_{i,h,k,add}, \text{ for } \begin{cases} h = 1,\, k = g,\, i \in COMG \\ h = 2,\, (k = g,\, i \in COMG)\,,\, (k = liq,\, i = tAlk) \\ h = 3,\, k = g,\, i \in COMG \end{cases} \\ \dot{n}_{i,h,k,in}, \text{ else} \end{cases} \tag{A.3.23}$$

In case synthesis gas with a composition of H_2:CO=1 is used, eq. (A.3.24) must be fulfilled for each distributor.

$$\dot{n}_{\mathrm{H_2},h,g,add} = \dot{n}_{\mathrm{CO},h,g,add},\ h \in DIS \tag{A.3.24}$$

Energy balance for each segment With respect to temperature a pseudo-homogeneous gas liquid system is assumed and the energy balance for each segment is given by eq. (A.3.25). Here, the contribution of the dissolved H_2 and CO in the liquid phase is neglected while the general contribution of the gas phase to the heat capacity flowrate is considered.

$$\left(\sum_{i\in COML} \dot{n}_{i,liq,s}\cdot c_{p,i} + \sum_{i\in COMG} \dot{n}_{i,g,s}\cdot c_{p,i}\right)\frac{\mathrm{d}T_s}{\mathrm{d}z} = \tag{A.3.25}$$
$$-\left(2\cdot\pi\cdot R\cdot q_s + A_{IL}\cdot\sum_{i\in COM} h_i\cdot\sum_{j\in RE}\nu_{i,j}\cdot r_j\right),\ s\in SEG$$

$$T_{s,0} = T_{s,f},\ s\in SEG\setminus\{1\} \tag{A.3.26}$$

$$T_{1,0} = T_0 \tag{A.3.27}$$

$$q_s = \alpha\cdot(T_s - T_{c,s}),\ s\in SEG \tag{A.3.28}$$

The overall heat transport coefficient α is modeled assuming a linear contribution of the gas and liquid phase. Here, α_g is obtained from a mean value for a comparable system (water - compressed gas, $\alpha_g = 0.17\cdot 10^3\ \frac{\mathrm{W}}{m^2\cdot K}$) [138] and α_l as in level 2. The contribution of the solid phase is neglected due to its small volume fraction (for the chosen mixer $\epsilon_s = 0.13$ [145]).

$$\alpha = \epsilon_{liq}\cdot\alpha_{liq} + \epsilon_g\cdot\alpha_g \tag{A.3.29}$$

$$\frac{\epsilon_g}{\epsilon_{liq}} = \frac{\dot{V}_g}{\dot{V}_{liq}} \tag{A.3.30}$$

$$1 = \epsilon_{liq} + \epsilon_g + \epsilon_s \tag{A.3.31}$$

Energy balance for each distributor In order to calculate the mixing temperature at each distributor outlet, an energy balance (eq. (A.3.32)) has to be solved at each distributor. The temperature of the dosed alkene (373 K) and synthesis gas (298 K) is fixed.

$$\sum_{i\in COM}\dot{n}_{i,h,out}\cdot h_{i,h,out} = \sum_{i\in COM}\dot{n}_{i,h,in}\cdot h_{i,h,in} + \sum_{i\in COM}\dot{n}_{i,h,add}\cdot h_{i,h,add},\ h\in DIS \tag{A.3.32}$$

G/L mass transfer and momentum balance For the calculation of the (k_La)-value and the pressure drop, correlations from the literature [145] are used ($K_1 = 3.45$, $K_2 = 1.5$, $K_3 = 0.64$, $K_4 = 0.346$, $K_5 = 1.71$, $K_6 = 0.070$). In the context of velocity, the subscript s refers to superficial.

$$(k_L a)_s = K_1 \cdot v_{liq,s}^{K_2} \cdot v_{g,s}^{K_3} \tag{A.3.33}$$

$$\frac{\mathrm{d}p_s}{\mathrm{d}z} = -K_4 \cdot v_{liq,s}^{K_5} \cdot v_{g,s}^{K_6},\ s \in SEG \tag{A.3.34}$$

$$p_{s,0} = p_{s,f},\ s \in SEG \setminus \{1\} \tag{A.3.35}$$

$$p_{1,0} = p_0 \tag{A.3.36}$$

The validity range of the correlations is $0 \leq v_{g,s} \leq 0.5\,\frac{m}{s}$ and $0.1 \leq v_{liq,s} \leq 2\,\frac{m}{s}$ [145], and these ranges are used as bounds in the optimization. The superficial gas and liquid velocities are calculated according to eq. (A.3.38) – eq. (A.3.41).

On level 3, the $(k_L a)$-value and exchange area are based on the total reactor volume, while these values are based on the liquid volume on level 2. The values can be converted according to eq. (A.3.37).

$$(k_L a) = (k_L a)_{liq} \cdot \epsilon_{liq} \tag{A.3.37}$$

Further constitutive equations In order to calculate the interstitial velocity and the superficial velocities of gas and liquid eq. (A.3.38) – eq. (A.3.43) are required.

$$\dot{V}_g = \frac{R \cdot T}{p} \cdot \sum_{i \in COMG} \dot{n}_{g,i} \tag{A.3.38}$$

$$\dot{V}_{liq} = \sum_{i \in COML} \frac{\dot{n}_{liq,i} \cdot M_i}{\rho_i} \tag{A.3.39}$$

$$v_{g,s} = \frac{\dot{V}_g}{A} \tag{A.3.40}$$

$$v_{liq,s} = \frac{\dot{V}_{liq}}{A} \tag{A.3.41}$$

The interstitial velocity is calculated assuming no slip velocity between the phases and considering the solid fraction of the investigated mixers and the cross sectional area of the tube.

$$v_i = \frac{\dot{V}_{liq} + \dot{V}_g}{A \cdot \epsilon_s} \tag{A.3.42}$$

$$A = \pi \cdot R^2 \tag{A.3.43}$$

Assuming ideal gas behavior the partial pressure of each gas is calculated using eq. (A.3.44) and eq. (A.3.45).

$$p_i = p \cdot y_i, \quad i \in COMG \tag{A.3.44}$$

$$y_i = \frac{\dot{n}_{g,i}}{\sum_{i \in COMG} \dot{n}_{g,i}}, \quad i \in COMG \tag{A.3.45}$$

System bounds The total alkene stream is calculated from the inlet alkene stream and the added alkene at each liquid distributor according to eq. (A.3.46).

$$\dot{n}_{tAlk,tot} = \dot{n}_{tAlk,0} + \sum_{d \in DIS} \dot{n}_{tAlk,add,d} \tag{A.3.46}$$

In accordance to the previous levels, the solvent stream is connected to the reactant stream at the inlet of the first segment by eq. (A.3.47) and the volume fractions of organic and IL phase are restricted by eq. (A.3.48).

$$C_{tAlk} = \frac{\dot{n}_{tAlk,tot}}{\frac{\dot{n}_{tAlk,tot} \cdot M_{tAlk}}{\rho_{tAlk}(373\,K)} + \frac{\dot{n}_{Dec} \cdot M_{Dec}}{\rho_{Dec}(373\,K)}} = 2 \cdot 10^3 \, \frac{mol}{m^3} \tag{A.3.47}$$

$$V^L_{frac} \leq \frac{\dot{V}_{Dec}}{\dot{V}_{IL}} \leq V^U_{frac} \tag{A.3.48}$$

Recycle condition Due to the recycling of the terminal alkene and the solvent, the terminal alkene inlet stream of the first segment $\dot{n}_{tAlk,0}$ is connected to the outlet stream of the last segment $\dot{n}_{tAlk,f}$ according to eq. (A.3.49).

$$\dot{n}_{tAlk,0} \geq \dot{n}_{tAlk,f} \tag{A.3.49}$$

STY and X The space time yield of the technical reactor based on the liquid phase (otherwise not comparable to level 1 and 2) is given by eq. (A.3.50). Within this equation the range of the integral is over all segments of the reactor. The conversion for the continuously operated reactor is fixed according to eq. (A.3.51).

$$STY = \frac{\dot{n}_{nAld,f} - \dot{n}_{nAld,0}}{\pi \int_{z=0}^{L} \epsilon_{liq} \cdot R^2 \mathrm{d}z} \geq 5.09 \, \frac{mol}{m^3 s} \tag{A.3.50}$$

$$X = \frac{\dot{n}_{tAlk,tot} - \dot{n}_{tAlk,f}}{\dot{n}_{tAlk,tot}} = 0.8 \tag{A.3.51}$$

Energy balance for the coolant The energy balance for the coolant in each reactor segment is formulated in temperature form. By applying the same assumption as for the coolant side of the SO_2 and EO reactor, the change in the coolant temperature is proportional to the heat flux according to eq. (A.3.52).

$$\frac{\mathrm{d}T_{c,s}}{\mathrm{d}z} = K_c q_s, \; s \in SEG \tag{A.3.52}$$

A.4 Numerical solution approach

In this section, an overview of established solution approaches for dynamic optimization problems is presented. In addition, the applicability of the methods to the arising optimization problems is discussed. Furthermore, details on the used software, solvers, and challenges within the implementation, as well as on the computing times are given. Last but not least, aspects of local and global optimality of the obtained solutions are considered.

Overview on solution methods for dynamic optimization problems

A classification of the different methods to solve dynamic optimization problems is illustrated in Fig. A.6.

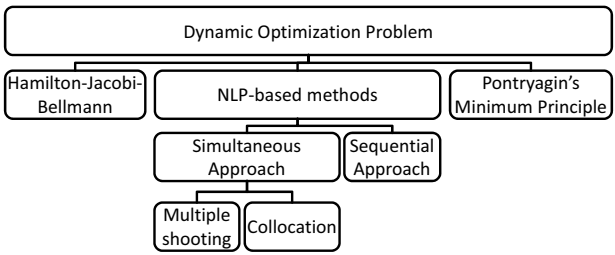

Figure A.6: Solution approaches for dynamic optimization problems

In principle, dynamic optimization problems can be solved using the Hamilton-Jacobi-Bellmann equation, the Pontryagin's minimum principle (PMP) or methods based on nonlinear programming (NLP).

In the Hamilton-Jacobi-Bellmann approach, the optimization problem is transformed into a partial differential equation (PDE) (e.g. [159]). The advantage of this method is that the solution of the derived partial differential equation can be used for both feedback and feed forward control. However, obtaining a solution for the PDE is hard and additional problems arise when the optimization problem is also constrained by algebraic equations.

The Pontryagin's Minimum Principle is based on local considerations around the optimal trajectory. Within this approach, a co-state is associated to each state variable giving rise to a two-point boundary value problem with a dimension two times the original problem size (e.g. [159]). Thereby, the numerical solution might become inefficient due to the very large problem size. Similar to the Hamilton-Jacobi-Bellmann approach, considering algebraic equations in this method is not straight forward.

Within the NLP-based methods, the sequential approach and the simultaneous approach are distinguished [160].

In the sequential approach, an optimization solver is coupled to a subjacent ODE solver. This approach is especially efficient if no control functions but only parameters are optimized and the sensitivity of the ODE system with respect to the optimization parameters can be computed. However, numerous and time consuming calculations of the subjacent ODE system might be necessary. Furthermore, algebraic

constraints often cause additional difficulties by transforming the ODE subsystem into a system of differential algebraic equations (DAE). In case control functions exist, these functions are often optimized as polynomials. The so-called control vector approach reduces the degrees of freedom and enhances the calculation efficiency, but is inadequate if the optimal profile is discontinuous.

Within the simultaneous approach the states and the control functions are discretized yielding a large scale NLP problem (state and control vector discretization). This approach converts the infinite dimensional optimal control problem to a finite dimensional optimization problem. Here, mainly the multiple shooting approach (e.g. [161]) or the orthogonal collocation on finite elements method (e.g. [162, 163]) are used. Since all ODEs are converted to algebraic equations, integrating further algebraic constraints is straight forward. In addition, state-of-the art NLP solvers can be used enabling the efficient numerical computation.

Advantages and disadvantages of the simultaneous approach

In order to solve the optimization problems of the considered processes, numerical schemes must be applied regardless which solution method is used due to the complexity and nonlinearity of the problems. Since the optimization problems of the proposed methodology are constrained by a DAE system, the simultaneous approach is the best suited method. In case of first order ODEs, further advantages arise using orthogonal collocation on finite elements, in particular

1. the starting values can easily be guessed since they correspond to the physical states,

2. the collocation matrix can be calculated a priori and the number of finite elements can be easily adapted in order to limit the numerical discretization error,

3. the method proved to be much faster than other discretization techniques for the same numerical discretization error for the considered examples [164].

A comparison of orthogonal collocation on finite elements to the finite volume method was performed within a study research project [164] supervised in the course of this thesis. If the number of supporting points was chosen large enough the mean relative deviation from the analytical solution became much smaller than 1% for both methods. Here, a simplified problem of the SO_2 oxidation for which an analytical solution could be derived was investigated in order to determine the numerical discretization error. It turned out that orthogonal collocation is much faster (factor 2.3) compared to the finite volume method for the same level of accuracy. These differences become more severe with increasing problem size.

The disadvantages arising with orthogonal collocation are mainly that

1. the constraints are only enforced at the collocation points,

2. the profiles of the control variables are only approximated,

3. oscillation in the solution of singular problems might arise since the Hamiltonian is not very sensitive to the individual values of the control variables on the

finite elements,

4. the number of finite elements is not known a priori and must be determined for each example in order to ensure a physical meaningful solution.

In case of sufficient supporting points, it is of no practical relevance that the constraints are only enforced at the collocation points since the solution in between the supporting points is smooth and does not greatly vary from the solution at the adjacent points. In addition, the profiles of the control variables are very well approximated as long as the number of finite elements is large. Oscillations in the solution are easy to determine, and in this case the model formulation and the number of supporting points can be changed in order to reduce this problem.

In order to determine an adequate number of finite elements, a heuristic approach is applied. In case a change in the number of finite elements yields a noteworthy divergence in the solution for the control functions, the state profiles, or objective, the number of supporting points is not adequate and must be increased. In general, the number of finite elements can be increased as long as no oscillations occur and the computation time stays acceptable. To ensure physical meaningful solutions, the global mass balance and energy balance can be checked.

Following the above arguments, orthogonal collocation on finite elements is the method of choice for the arising optimization problems. However, finding an adequate number of supporting points needs some experience and depends greatly on the problem.

Implementation issues and computational effort

All problems are solved using *CONOPT 3.14 G* under *AMPL* on a PC with an Intel(R)Core(TM)2 Duo CPU E6850 with 3.00 GHz (calculation on a single CPU), a cache size of 4096 KB, a memory of 2 GB, and a Linux operating system. *CONOPT* is a generalized reduced-gradient solver based on sequential quadratic programming designed for large scale NLP problems. Details of *CONOPT* as it is implemented in *AMPL* are given by Drud [165, 166].

In the following paragraphs, details of the applied numerical solution approach and the computational effort for each example process are shortly discussed. In general, the complexity of the problem is hard to define and it depends on the number of equations, the degrees of freedom, the nonlinearity of the model equations, and the model formulation itself. Besides these factors, the interconnection arising from recycles or a two-dimensional model affects the sparsity of the Hamiltonian matrix and thereby the computing efficiency. In addition, the computing times depend strongly on the starting values. Due to these many influencing factors, the given numbers for the computing times should only be considered for orientation purposes.

A graphical overview on the complexity of selected optimization problems and the associated computing times (*CONOPT* times) is given in Fig. A.7. Here, the optimization problems of the selected intensified cases of the SO_2 oxidation, the air and oxygen based EO processes, and the hydroformylation process are shown. In addition, the computation times, number of variables, constraints, and finite elements are listed for the same optimization problems in Tab. A.8. In this table, the number of variables and number of constraints refer to the values given by *AMPL*. Since not all

constraints are active, the difference between these values do not directly yield the number of degrees of freedom.

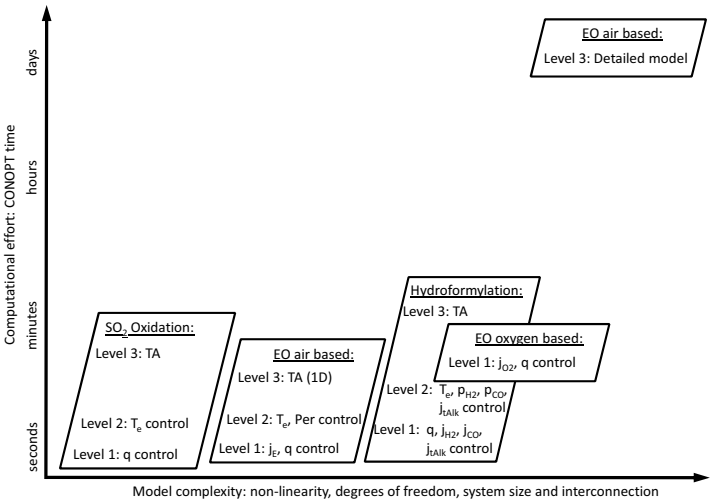

Figure A.7: Overview on the computational effort and complexity of selected optimization problems

In case of the SO_2 oxidation, the computing time is very short for all models, since the model formulation in terms of elementary process functions is very efficient. For example, the *CONOPT* time for 200 equally distributed finite elements and three collocation points per finite element is 13.2 *s* for the optimal heat flux case on level 1. On the third level, the computation takes about 113.3 *s* for the investigated reactor set-up.

In case of the air based ethylene oxide process, the computing times differ in a wide range depending on the design level and the investigated case. For the one-dimensional problems orthogonal collocation on finite elements is used as discretization method. On the first level, the computing times are short since the model formulation is efficient. However, the computing time increases drastically for increasing degrees of freedom. For example the *CONOPT* time for the chosen case is 16.8 *s*, while the *CONOPT* time for case 7 (control of q, j_E, j_{O_2}, and j_{CO_2}) is 2824 *s* on the first level. The computing time for the one-dimensional model on level 3 is in the range of 92 *s*. In this case, the number of equations is high due to the additional balance equations, but only few degrees of freedom exist.

For the two-dimensional reactor model on level 3, the axial coordinate is discretized using orthogonal collocation on finite elements, while the radial coordinate is discretized using the finite volume method with constant profiles on each finite volume. This approach proved to be more robust in the optimization especially with respect to mass balance errors. In order to find feasible starting points for the two-dimensional reactor model, an advanced convergence strategy is necessary where single blocks of equality constraints defined by the balance and flux equations are added to the op-

timization problem step-by-step. In case of the two-dimensional reactor model, the calculation times are in the range of 80 h, where most of the time is required for the pre-processing to obtain a feasible point. Here, a sensitivity analysis can also be used in order to reduce the degree of freedom and help the optimizer to converge.

In the oxygen based ethylene oxide process, the calculation times on level 1 were longer compared to the equivalent case of the air based EO process due to strong coupling of reaction module and the process. In addition, reformulations of the equilibrium constants arising in the CO_2 absorption were necessary using logarithmic scaling in order to avoid numerical difficulties associated with the very small numerical values of these constants. Similar to the two-dimensional reactor model, an advanced convergence strategy is necessary in order to obtain feasible solutions.

Table A.8: Overview on the computing time, the number of variables, constraints, and finite elements of selected optimization problems

Process and case	Solver time $[s]$	# variables	# constraints	# FE
SO_2 oxidation				
Level 1	13.2	10804	10603	200
Level 2	30.8	21908	22507	300
Level 3	113.3	35567	36908	450
EO air based				
Level 1	16.8	9708	13105	100
Level 2	40.1	6618	8438	30
Level 3 (1D)	92.3	13401	16190	50
Level 3 (2D)	$2.9 \cdot 10^5$	180408	213063	30×30
EO oxygen based				
Level 1	96.2	16297	15887	100
Hydroformylation				
Level 1	16.2	31944	29605	200
Level 2	16.9	47458	46004	200
Level 3	133.4	60775	61164	151

In case of the hydroformylation, the temperature, hydrogen, carbon monoxide, and octene profile were simultaneously optimized causing a large number of degrees of freedom. In addition, the reaction network is complex giving rise to additional challenges to obtain feasible solutions. In all considered processes, the computational effort rises with an increasing number of model equations arising from the technical constraints. Hence, the computing time increases from level 1 to level 3 in all examples.

Local and global optimality of the obtained solutions

In principle, this solution approach can only yield locally optimal solutions, and hence even better solutions might exist. In order to ensure the global optimality of a solution, criteria such as defined by Mangasarian [167] and Arrow [168] can be

applied. Similar to the sufficient KKT conditions for NLP problems, the dynamic optimization problem needs to be convex in the objective functions and the system equations on the whole feasible solution space spanned by the control functions and states. However, the applicability of these criteria is very limited due to the complexity of the models.

In addition, global optimization solvers such as *BARON* [169] can be used to directly determine the global optimum. However, the considered optimization problems cannot be solved with *BARON* due to the very high computational effort of this solver even for much smaller and simpler problems.

In order to examine if different local solutions occur, each problem was solved several times using different starting values. For all optimization problems no other feasible local optima apart from the stated solutions were obtained indicating that the found local optima are probably also the global optimum of the problem.

Conclusion

It can be concluded that adequate solutions with respect to computation times and the numerical discretization error were obtained in all cases. All arising optimization problems can be solved on a desktop computer giving rise to the direct applicability of the method in practice. In addition, the proposed hierarchy of optimization problems significantly reduces the reactor design task with respect to computational effort compared to a brute force approach where the results of detailed reactor models of every reactor set-up need to be calculated. In the proposed methodology, only the most promising reactor set-ups are modeled in detail.

Bibliography

[1] H. Freund and K. Sundmacher. Towards a Methodology for the Systematic Analysis and Design of Efficient Chemical Processes. Part 1. From Unit Operations to Elementary Process Functions. *Chem. Eng. Process.*, 47(12):2051–2060, 2008.

[2] K. Sundmacher and H. Freund. Chemical Process Design: Moving Matter Elements Along Optimal Travel Routes in the Thermodynamic State Space. *The 5th International Symposium on Design, Operation and Control of Chemical Processes*, 2010.

[3] H. Freund and K. Sundmacher. Process Intensification, 1. Fundamentals and Molecular Level. In *Ullmann's Encyclopedia of Industrial Chemistry. Online Edition.* Wiley-VCH, Weinheim, 2011.

[4] H. Freund and K. Sundmacher. Process Intensification, 2. Phase Level. In *Ullmann's Encyclopedia of Industrial Chemistry. Online Edition.* Wiley-VCH, Weinheim, 2011.

[5] H. Freund and K. Sundmacher. Process Intensification, 3. Process Unit Level. In *Ullmann's Encyclopedia of Industrial Chemistry. Online Edition.* Wiley-VCH, Weinheim, 2011.

[6] H. Freund and K. Sundmacher. Process Intensification, 4. Plant Level. In *Ullmann's Encyclopedia of Industrial Chemistry. Online Edition.* Wiley-VCH, Weinheim, 2011.

[7] C. Ramshaw. Higee Distillation - An Example of Process Intensification. *Chem. Eng.-London*, 389(Feb.):13–14, 1983.

[8] F. M. Dautzenberg and M. Mukherjee. Process Intensification Using Multifunctional Reactors. *Chem. Eng. Sci.*, 56(17):251–267, 2001.

[9] J. J. Lerou and K. M. Ng. Chemical Reaction Engineering: A Multiscale Approach to a Multiobjective Task. *Chem. Eng. Sci.*, 51(10):1595–1614, 1996.

[10] E. D. Gilles. Network Theory for Chemical Processes. *Chem. Eng. Technol.*, 21(2):121–132, 1998.

[11] M. Mangold, S. Motz, and E. D. Gilles. A Network Theory for the Structured Modelling of Chemical Processes. *Chem. Eng. Sci.*, 57(19):4099–4116, 2002.

[12] A. Gerstlauer, M. Hierlemann, and W. Marquardt. On the Representation of Balance Equations in Knowledge-Based Process Modeling Tool. *11th Congress on Chemical Engineering, Chemical Equipments, Design and Automation.*, 1993.

[13] W. Marquardt. Trends in Computer-Aided Process Modeling. *Comput. Chem. Eng.*, 20(6–7):591–609, 1996.

[14] M. Strohrmann. Prozessintensivierung – Gibt es etwas Neues? Prozessintensivierung: Ansichten der Industrie, DECHEMA Infotag, Frankfurt am Main, Germany, 2006.

[15] A. I. Stankiewicz and J. A. Moulijn. Process Intensification: Transforming Chemical Engineering. *Chem. Eng. Process.*, 96(1):22–34, 2000.

[16] T. van Gerven and A. I. Stankiewicz. Structure, Energy, Synergy, Times – The Fundamentals of Process Intensification. *Ind. Eng. Chem. Res.*, 48(5):2465–2474, 2009.

[17] B. G. Rong, E. Kolehmainen, and I. Turunen. Methodology of Conceptual Process Synthesis for Process Intensification. *Comp. Aid. Ch.*, 25:283–288, 2008.

[18] P. Lutze, R. Gani, and J. M. Woodley. Process Intensification: A Perspective on Process Synthesis. *Chem. Eng. Process.*, 49(6):547–558, 2010.

[19] J. A. Arizmendi-Sánchez and P. N. Sharratt. Phenomena-Based Modularisation of Chemical Process Models to Approach Intensive Options. *Chem. Eng. J.*, 135(1–2):83–94, 2010.

[20] A. R. Menon, A. A. Pande, H. J. M. Kramer, P. J. Jansens, and J. Grievink. A Task-Based Synthesis Approach toward the Design of Industrial Crystallization Process Units. *Ind. Eng. Chem. Res.*, 46(12):3979–3996, 2007.

[21] R. Lakerveld, H. J. M. Kramer, A. I. Stankiewicz, and J. Grievink. Application of Generic Principles of Process Intensification to Solution Crystallization Enabled by a Task-Based Design Approach. *Chem. Eng. Process.*, 49(9):979–991, 2010.

[22] G. F. Froment and K. B. Bischoff. *Chemical Reactor Analysis and Design*. John Wiley and Sons, New York, 1990.

[23] G. Emig and E. Klemm. *Technische Chemie*. Springer Verlag, Heidelberg, 2005.

[24] G. Schembecker, T. Dröge, U. Westhaus, and K. H. Simmrock. Readpert - Development, Selection and Design of Chemical Reactors. *Chem. Eng. Process.*, 34(3):317–322, 1995.

[25] J. Till, G. Sand, S. Engell, T. von Trotha, and G. Schembecker. ReadOpt - Reactor Design Optimization by Heuristic MINLP Methods. *Chem. Ing. Tech.*, 76(8):1105–1110, 2004.

[26] F. Horn. Attainable Regions in Chemical Reaction Techniques. In *The Third European Symposium on Chemical Reaction Eng.* Pergamon, London, 1964.

[27] D. Glasser, D. Hildebrandt, and C. M. Crowe. A Geometric Approach to Steady Flow Reactors – The Attainable Region and Optimization in Concentration Space. *Ind. Eng. Chem. Res.*, 26(9):1803–1810, 1987.

[28] D. Hildebrandt and D. Glasser. The Attainable Region and Optimal Reactor Structures. *Chem. Eng. Sci.*, 45(8):2161–2168, 1990.

[29] D. Hildebrandt, D. Glasser, and C. M. Crowe. Geometry of the Attainable Region Generated by Reaction and Mixing - with and without Constraints. *Ind. Eng. Chem. Res.*, 29(1):49–58, 1990.

[30] M. Feinberg and D. Hildebrandt. Optimal Reactor Design from a Geometric Viewpoint – I. Universal Properties of the Attainable Region. *Chem. Eng. Sci.*, 52(10):1637–1665, 1997.

[31] W. C. Rooney, B. P. Hausberger, L. T. Biegler, and D. Glasser. Convex Attainable Region Projections for Reactor Network Synthesis. *Comput. Chem. Eng.*, 24(2–7):225–229, 2000.

[32] S. Balakrishna and L. T. Biegler. Constructive Targeting Approaches for the Synthesis of Chemical Reactor Networks. *Ind. Eng. Chem. Res.*, 31(1):300–312, 1992.

[33] S. Balakrishna and L. T. Biegler. Targeting Strategies for the Synthesis and Energy Integration of Nonisothermal Reactor Networks. *Ind. Eng. Chem. Res.*, 31(9):2152–2164, 1992.

[34] S. Balakrishna and L. T. Biegler. A Unified Approach for the Simultaneous Synthesis of Reaction, Energy, and Separation Systems. *Ind. Eng. Chem. Res.*, 32(7):1372–1382, 1993.

[35] A. Lakshmanan and L. T. Biegler. Synthesis of Optimal Chemical Reactor Networks. *Ind. Eng. Chem. Res.*, 35(4):1344–1353, 1996.

[36] A. Nisoli, M. F. Malone, and M. F. Doherty. Attainable Regions for Reaction with Separation. *AIChE J.*, 43(2):374–387, 1997.

[37] M. Feinberg and P. Ellison. General Kinetic Bounds on Productivity and Selectivity in Reactor-Separator Systems of Arbitrary Design: Principles. *Ind. Eng. Chem. Res.*, 40(14):3181–3194, 2001.

[38] V. Agarwal, S. Thotla, and S. M. Mahajani. Attainable Regions of Reactive Distillation. Part I. Single Reactant Non-Azeotropic Systems. *Chem. Eng. Sci.*, 63(11):2946–2965, 2008.

[39] V. Agarwal, S. Thotla, and S. M. Mahajani. Attainable Regions of Reactive Distillation. Part II. Single Reactant Azeotropic Systems. *Chem. Eng. Sci.*, 63(11):2928–2945, 2008.

[40] L. E. K. Achenie and L. T. Biegler. Algorithmic Synthesis of Chemical Reactor Networks Using Mathematical-Programming. *Ind. Eng. Chem. Fund.*, 25(4):621–627, 1986.

[41] L. E. K. Achenie and L. T. Biegler. A Superstructure Based Approach to Chemical Reactor Network Synthesis. *Comput. Chem. Eng.*, 14(1):23–40, 1990.

[42] A. C. Kokossis and C. A. Floudas. Synthesis of Isothermal Reactor Separator Recycle Systems. *Chem. Eng. Sci.*, 46(5–6):1361–1683, 1991.

[43] A. C. Kokossis and C. A. Floudas. Optimization of Complex Reactor Networks. 2. Nonisothermal Operation. *Chem. Eng. Sci.*, 49(7):1037–1051, 1994.

[44] M. Hillestad. A Systematic Generation of Reactor Designs. II. Non-Isothermal Conditions. *Comput. Chem. Eng.*, 29(5):1101–1112, 2005.

[45] R. Aris. *The Optimal Design of Chemical Reactors – A Study in Dynamic Programming*. Academic Press, New York, 1961.

[46] F. Horn. Optimale Temperatur- und Konzentrationsverläufe. *Chem. Eng. Sci.*, 14(1):77–88, 1961.

[47] O. Bilous and N. R. Amundson. Optimum Temperature Gradients in Tubular Reactors. I: General Theory and Methods. *Chem. Eng. Sci.*, 5(2):81–92, 1956.

[48] O. Bilous and N. R. Amundson. Optimum Temperature Gradients in Tubular Reactors. II: Numerical Study. *Chem. Eng. Sci.*, 5(3):115–126, 1956.

[49] R. Aris. Studies in Optimization. 2. Optimum Temperature Gradients in Tubular Reactors. *Chem. Eng. Sci.*, 13(1):18–29, 1960.

[50] C. D. Siebenthal and R. Aris. Studies in Optimization. 7. The Application of Pontryagins Methods to the Control of Batch and Tubular Reactors. *Chem. Eng. Sci.*, 19(10):747–761, 1964.

[51] Y. D. Lang, A. M. Cervantes, and L. T. Biegler. Dynamic Optimization of a Batch Cooling Crystallization Process. *Ind. Eng. Chem. Res.*, 38(4):1469–1477, 1999.

[52] O. Abel, A. Helbig, W. Marquardt, H. Zwick, and T. Daszkowski. Productivity Optimization of an Industrial Semi-Batch Polymerization Reactor under Safety Constraints. *J. Process Control*, 10(4):351–362, 2000.

[53] E. Johannessen and S. Kjelstrup. Minimum Entropy Production Rate in Plug Flow Reactors: An Optimal Control Problem Solved for SO_2 Oxidation. *Energy*, 29(12–15):2403–2423, 2004.

[54] E. Johannessen and S. Kjelstrup. A Highway in State Space for Reactors with Minimum Entropy Production. *Chem. Eng. Sci.*, 60(12):3347–3361, 2005.

[55] A. Rosjorde, S. Kjelstrup, E. Johannessen, and R. Hansen. Minimizing the Entropy Production in a Chemical Process for Dehydrogenation of Propane. *Energy*, 32(4):335–343, 2007.

[56] M. Hillestad. Systematic Staging in Chemical Reactor Design. *Chem. Eng. Sci.*, 65(10):3301–3312, 2010.

[57] A. Peschel, H. Freund, and K. Sundmacher. Methodology for the Design of Optimal Chemical Reactors Based on the Concept of Elementary Process Functions. *Ind. Eng. Chem. Res.*, 49(21):10535–10548, 2010.

[58] H. Müller. Sulfuric Acid and Sulfur Trioxide. In *Ullmann's Encyclopedia of Industrial Chemistry. Online Edition*. Wiley-VCH, Weinheim, 2011.

[59] R. Eklund. *The Rate of Oxidation of Sulfur Dioxide with a Commerical Vanadium Catalyst*. Almquist & Wiksells Boktryckeri AB, Uppsala, 1956.

[60] D. R. Stull and H. Prophet. *JANAF Thermochemical Tables*. U.S. Dept. of Commerce, National Bureau of Standards, Washington D. C., 1971.

[61] M. Baerns, A. Behr, A. Brehm, J. Gmehling, H. Hofmann, U. Onken, and A. Renken. *Technische Chemie*. Wiley-VCH, Weinheim, 2006.

[62] R. Aris. Studies in Optimization. 1. The Optimum Design of Adiabatic Reactors with Several Beds. *Chem. Eng. Sci.*, 12(4):243–252, 1960.

[63] A. P. de Wasch and G. F. Froment. Heat-Transfer in Packed-Beds. *Chem. Eng. Sci.*, 27(3):567, 1972.

[64] D. Vortmeyer and E. Haidegger. Discrimination of 3 Approaches to Evaluate Heat Fluxes for Wall-Cooled Fixed-Bed Chemical Reactors. *Chem. Eng. Sci.*, 46(10):2651–2660, 1991.

[65] R. C. Reid, J. M. Prausnitz, and B. E. Poling. *The Properties of Gases and Liquids*. McGraw-Hill, New York, 4th edition, 1987.

[66] D. Vortmeyer. Modellierung chemischer Festbettreaktoren. In D. Behrend and G. Kreysa, editors, *Dechema Monographien Bd. 94. Reaktionstechnik chemischer und elektrochemischer Prozesse*. VCH Verlag, Weinheim, 1983.

[67] S. Ergun. Fluid Flow Through Packed Columns. *Chem. Eng. Process.*, 48(2):89–94, 1952.

[68] H. J. Lee, M. Ghanta, D. H. Busch, and B. Subramaniam. Toward a CO_2-free Ethylene Oxide Process: Homogeneous Ethylene Oxide in Gas-Expanded Liquids. *Chem. Eng. Sci.*, 65(1):128–134, 2010.

[69] A. Peschel, F. Karst, H. Freund, and K. Sundmacher. Analysis and Optimal Design of an Ethylene Oxide Reactor. *Chem. Eng. Sci.*, 66(24):6453–6469, 2011.

[70] A. Peschel, A. Jörke, K. Sundmacher, and H. Freund. Optimal Reaction Concept and Plant Wide Optimization of the Ethylene Oxide Process. *Chem. Eng. J.*, submitted.

[71] S. Rebsdat and D. Mayer. Ethylene Oxide. In *Ullmann's Encyclopedia of Industrial Chemistry. Online Edition.* Wiley-VCH, Weinheim, 2011.

[72] A. A. Pekalski, J. F. Zevenbergen, M. Braithwaite, S. M. Lemkowitz, and H. J. Pasman. Explosive Decomposition of Ethylene Oxide at Elevated Condition: Effect of Ignition Energy, Nitrogen Dilution, and Turbulence. *J. Hazard. Mater.*, 118(1–3):19–34, 2005.

[73] D. Lafarga and A. Varma. Ethylene Epoxidation in a Catalytic Packed-Bed Membrane Reactor: Effects of Reactor Configuration and 1,2-Dichloroethane Addition. *Chem. Eng. Sci.*, 55(4):749–758, 2000.

[74] R. Dittmeyer, V. Höllein, P. Quicker, G. Emig, G. Hausinger, and F. Schmidt. Factors Controlling the Performance of Catalytic Dehydrogenation of Ethylbenzene in Palladium Composite Membrane Reactors. *Chem. Eng. Sci.*, 54(10):1431–1439, 1999.

[75] H. Kestenbaum, A. L. de Oliveira, W. Schmidt, F. Schüth, W. Ehrfeld, K. Gebauer, H. Löwe, T. Richter, D. Lebiedz, I. Untiedt, and H. Zuchner. Silver-Catalyzed Oxidation of Ethylene to Ethylene Oxide in a Microreaction System. *Ind. Eng. Chem. Res.*, 41(4):710–719, 2002.

[76] J. Fischer, C. Liebner, H. Hieronymus, and E. Klemm. Maximum Safe Diameters of Microcapillaries for a Stoichiometric Ethene/Oxygen Mixture. *Chem. Eng. Sci.*, 64(12):2951–2956, 2009.

[77] T. Berndt and S. Bräsel. Epoxidation of a Series of C_2 – C_6 Olefins in the Gas Phase. *Chem. Eng. Technol.*, 8(8):1–17, 2009.

[78] K. H. Mueller and W. D. Walters. The Thermal Decomposition of Ethylene Oxide. *J. Am. Chem. Soc.*, 73(4):1458–1461, 1951.

[79] L. Petrov, A. Eliyas, and D. Shopov. Kinetics of Ethylene Oxidation over a Silver Catalyst in the Presence of Dichloroethane. *Appl. Catal.*, 24(1–2):145–161, 1986.

[80] M. Stoukides and S. Pavlou. Ethylene Oxidation on Silver Catalysts. Effect of Ethylene-Oxide and of External Transfer Limitations. *Chem. Eng. Commun.*, 44(1–6):53–74, 1986.

[81] M. A. Al-Saleh, M. S. Al-Ahmadi, and M. A. Shalabi. Kinetic Study of Ethylene Oxidation in a Berty Reactor. *Chem. Eng. J. Bioch. Eng.*, 37(1):35–41, 1988.

[82] P. C. Borman and K. R. Westerterp. An Experimental Study of the Kinetics of the Selective Oxidation of Ethene over a Silver on α-Alumina Catalyst. *Ind. Eng. Chem. Res.*, 34(1):49–58, 1995.

[83] E. P. S. Schouten, P. C. Borman, and K. R. Westerterp. Influence of Reaction Products on the Selective Oxidation of Ethene. *Chem. Eng. Process.*, 35(2):107–120, 1995.

[84] D. Lafarga, M. A. Al-Juaied, C. M. Bondy, and A. Varma. Ethylene Epoxidation on Ag-Cs/α-Al_2O_3 Catalyst: Experimental Results and Strategy for Kinetic Parameter Determination. *Ind. Eng. Chem. Res.*, 39(7):2148–2156, 2000.

[85] C. Li and B. A. Finlayson. Heat-Transfer in Packed Beds – Re-Evaluation. *Chem. Eng. Sci.*, 32(9):1055–1066, 1977.

[86] M. A. Al-Juaied, D. Lafarga, and A. Varma. Ethylene Epoxidation in a Catalytic Packed-Bed Membrane Reactor: Experiments and Model. *Chem. Eng. Sci.*, 56(2):395–402, 2001.

[87] D. E. Mears. Diagnostic Criteria for Heat Transport Limitations in Fixed Bed Reactors. *J. Catal.*, 20(2):127–131, 1971.

[88] D. E. Mears. Tests for Transport Limitations in Experimental Catalytic Reactors. *Ind. Eng. Chem. Proc. Des. Dev.*, 10(4):541–547, 1971.

[89] D. E. Mears. A Criterion for Isothermal Behaviour of a Catalyst Pellet. *Chem. Eng. Sci.*, 18(2):147–148, 1963.

[90] E. W. Thiele. Relation Between Catalytic Activity and Size of Particle. *Ind. Eng. Chem.*, 31(7):916–920, 1939.

[91] P. J. Linstrom and W. G. Mallard (eds.). *NIST Chemistry WebBook, NIST Standard Reference Database Number 69. http://webbook.nist.gov*. National Institute of Standards and Technology, Gaithersburg, MD, USA, retrieved July 16, 2010.

[92] D. Thoenes and H. Kramers. Mass Transfer from Spheres in Various Regular Packings to a Flowing Fluid. *Chem. Eng. Sci.*, 8(3–4):271–283, 1958.

[93] C. R. Wilke and C. Y. Lee. Estimation of Diffusion Coefficients for Gases and Vapors. *Ind. Eng. Chem.*, 47(6):1253–1257, 1955.

[94] J. de Acetis and G. Thodos. Mass and Heat Transfer in Flow of Gases Through Spherical Packings. *Ind. Eng. Chem.*, 52(12):1003–1006, 1960.

[95] X. G. Zhou and W. K. Yuan. Optimization of the Fixed-Bed Reactor for Ethylene Epoxidation. *Chem. Eng. Process.*, 44(10):1098–1107, 2005.

[96] Nexant-Inc. Ethylene Oxide/Ethylene Glycol. PERP Program 04/05-5, 2006.

[97] L. Gan, H. Wang, B. Zhu, S. Xu, and Z. Wang. Global Kinetics and Deactivation of Ag-Catalyst for Ethylene Oxide Synthesis. *Chem. Ind. Eng.*, 52(11):969–972, 2001.

[98] M. Molnárné, T. Schendler, and V. Schröder. *Safety Characteristic Data. Volume 2: Explosion Regions of Gas Mixtures*. Wirtschaftsverlag NW, Bremerhaven, 2008.

[99] W. Bartknecht. *Explosionsschutz*. Springer Verlag, Heidelberg, 1993.

[100] F. van den Schoor and F. Verplaetsen. The Upper Explosion Limit of Lower Alkanes and Alkenes in Air at Elevated Pressures and Temperatures. *J. Hazard.*

Mater., 128(1):1–9, 2006.

[101] F. van den Schoor and F. Verplaetsen. The Upper Flammability Limit of Methane/Hydrogen/Air Mixtures at Elevated Pressures and Temperatures. *Int. J. Hydrogen Energ.*, 32(13):2548–2552, 2007.

[102] M. Klaubert. *Explosionsgrenzen von Brenngasgemischen, die mehrere brennbare Komponenten, Inertgase und Luft enthalten: Experimentelle Bestimmung und Simulation*. PhD thesis, University of Paderborn, Germany, 1998.

[103] S. Crescitelli, G. Russo, and V. Tufano. The Influence of Different Diluents on the Flammability Limits of Ethylene at High Temperatures and Pressures. *J. Hazard. Mater.*, 3(2):167–175, 1979.

[104] A. Kohl and R. Nielsen. *Gas Purification*. Gulf Pub Co., Houston, 1997.

[105] P. V. Danckwerts. *Gas-Liquid Reactions*. McGraw-Hill, New York, 1970.

[106] *Datenerhebung 2010 – Bundesmix 2010 (Stand 06.10.2011). Durchschnittswerte der allgemeinen Stromversorgung in Deutschland*. BDEW Bundesverband der Energie- und Wasserwirtschaft e.V., Berlin, Germany, 2011.

[107] A. Peschel, B. Hentschel, H. Freund, and K. Sundmacher. Design of Optimal Multiphase Reactors Exemplified on the Hydroformylation of Long Chain Alkenes. *Chem. Eng. J.*, 188:126–141, 2012.

[108] B. Cornils. Oxo-Synthese (Hydroformylierung). In R. Dittmeyer, and G. Kreysa W. Keim, and A. Oberholz, editors, *Winnacker–Küchler: Chemische Technik–Prozesse und Produkte. Band 4: Energieträger, Organische Grundstoffe*. Wiley-VCH, Weinheim, 2005.

[109] R. Tudor and M. Ashley. Enhancement of Industrial Hydroformylation Processes by the Adoption of Rhodium-Based Catalyst: Part II. *Platinum Metals Rev.*, 54(4):164–171, 2007.

[110] H. W. Bohnen and B. Cornils. Hydroformylation of Alkenes: An Industrial View of Status and Importance. *Adv. Catal.*, 47:1–64, 2002.

[111] J. Haggin. New Hydroformylation Process Developed. *Chem. Eng. News*, 73(16):25–26, 1995.

[112] A. Behr, D. Obst, and C. Schulte. Kinetik der isomerisierenden Hydroformylierung von trans-4-Octen. *Chem. Ing. Tech.*, 76(7):904–910, 2004.

[113] Y. Q. Zhangand Z. S. Mao and T. Y. Chen. Interfacial Kinetics of Biphasic Hydroformylation of 1-Dodecene Catalyzed by Water-Soluble Rhodium Complex by a Combined Numerical and Experimental Approach. *Ind. Eng. Chem. Res.*, 40(21):4496–4505, 2001.

[114] M. Haumann, H. Koch, P. Hugo, and R. Schomäcker. Hydroformylation of 1-Dodecene Using Rh-TPPTS in a Microemulsion. *Appl. Catal. A - Gen.*, 225(1–2):239–249, 2002.

[115] I. T. Horváth, G. Kiss, R. A. Cook, J. E. Bond, P. A. Stevens, J. Rábai, and E. J. Mozeleski. Molecular Engineering in Homogeneous Catalysis: One-Phase Catalysis Coupled with Biphase Catalyst Separation. The Fluorous-Soluble $HRh(CO)\{P[CH_2CH_2(CF_2)_5CF_3]_3\}_3$ Hydroformylation System. *J. Am. Chem. Soc.*, 120(13):3133–3143, 1998.

[116] C. C. Brasse, U. Englert, A. Salzer, H. Waffenschmidt, and P. Wasserscheid. Ionic Phosphine Ligands with Cobaltocenium Backbone: Novel Ligands for the Highly Selective, Biphasic, Rhodium-Catalyzed Hydroformylation of 1-Octene in Ionic Liquids. *Organometallics*, 19(19):3818–3823, 2000.

[117] A. Sharma, C. Julcour Lebigue, R. M. Deshpande, A. A. Kelkar, and H. Delmas. Hydroformylation of 1-Octene Using [Bmim][PF_6]-Decane Biphasic Media and Rhodium Complex Catalyst: Thermodynamic Properties and Kinetic Study. *Ind. Eng. Chem. Res.*, 49(21):10698–10706, 2010.

[118] A. Riisager, A. Eriksen, P. Wasserscheid, and R. Fehrmann. Propene and 1-Octene Hydroformylation with Silica-Supported, Ionic Liquid-Phase (SILP) Rh-Phosphine Catalysts in Continuous Fixed-Bed Mode. *Catal. Lett.*, 90(3–4):149–153, 2003.

[119] J. P. Arhancet, M. E. Davis, J. S. Merola, and B. E. Hanson. Hydroformylation by Supported Aqueous-Phase Catalysis – A New Class of Heterogeneous Catalysts. *Nature*, 339(6224):454–455, 1989.

[120] C. Disser, C. Muennich, and G. Luft. Hydroformylation of Long-Chain Alkenes with New Supported Aqueous Phase Catalysts. *Appl. Catal. A - Gen*, 296(2):201–208, 2005.

[121] J. Fang. *Towards a Benign and Viable Rhodium Catalyzed Hydroformylation of Higher Olefins: Economic and Environmental Impact Analyses, Solvent Effects and Membrane-Based Catalyst Separation*. PhD thesis, University of Kansas, Lawrence, KS, USA, 2009.

[122] D. I. Enache, W. Thiam, D. Dumas, S. Ellwood, G. J. Hutchings, S. H. Taylor, S. Hawker, and E. H. Stitt. Intensification of the Solvent-Free Catalytic Hydroformylation of Cyclododecatriene: Comparison of a Stirred Batch Reactor and a Heat-Exchange Reactor. *Catal. Today*, 128(1–2):18–25, 2007.

[123] D. Koch and W. Leitner. Rhodium-Catalyzed Hydroformylation in Supercritical Carbon Dioxide. *J. Am. Chem. Soc.*, 120(51):13398–13404, 1998.

[124] O. Wachsen, K. Himmler, and B. Cornils. Aqueous Biphasic Catalysis: Where the Reaction Takes Place. *Catalysis Today*, 42(4):373–379, 1998.

[125] R. Krishna and S. T. Sie. Strategies for Multiphase Reactor Selection. *Chem. Eng. Sci.*, 49(24):4029–4065, 1994.

[126] V. L. Mehta and A. C. Kokossis. Nonisothermal Synthesis of Homogeneous and Multiphase Reactor Networks. *AIChE J.*, 46(11):2256–2273, 2000.

[127] V. V. Kelkar and K. M. Ng. Screening Multiphase Reactors for Nonisothermal Multiple Reactions. *AIChE J.*, 46(2):389–406, 2000.

[128] K. D. Wiese, O. Möller, G. Protzmann, and M. Trocha. A New Reactor Design for Catalytic Fluid–Fluid Multiphase Reactions. *Catalysis Today*, 79(1–4):97–103, 2003.

[129] D. Evans, J. A. Osborn, and G. Wilkinson. Hydroformylation of Alkenes by Use of Rhodium Complex Catalysts. *J. Chem. Soc. A*, 12:3133–3142, 1968.

[130] A. Bernas, P. Mäki-Arvela, J. Lehtonen, T. Salmi, and D. Y. Murzin. Kinetic Modeling of Propene Hydroformylation with Rh/TPP and Rh/CHDPP Catalysts. *Ind. Eng. Chem. Res.*, 47(13):4317–4324, 2008.

[131] A. Peschel, B. Hentschel, H. Freund, and K. Sundmacher. Optimal Reactor Design for the Hydroformylation of Long Chain Alkenes in Biphasic Liquid Systems. *Comp. Aid. Ch.*, 28(B):1246–1250, 2011.

[132] A. Sharma. *Catalytic Reaction Engineering Using Ionic Liquids: Hydroformylation of 1-Octene*. PhD thesis, Université de Tolouse, Tolouse, France, 2009.

[133] C. L. Yaws (Ed.). *Chemical Properties Handbook*. McGraw-Hill, New York, 1999.

[134] J. Troncoso, C. A. Cerdeirin, Y. A. Sanmamed, L. Romaní, and L. P. N. Rebelo. Thermodynamic Properties of Imidazolium-Based Ionic Liquids: Densities, Heat Capacities, and Enthalpies of Fusion of [Bmim][PF_6] and [Bmim][NTf_2]. *J. Chem. Eng. Data*, 51(5):1856–1859, 1996.

[135] S. Srivatsan, X. Yi, R. L. Robinson, and K. A. M. Gasem. Solubilities of Carbon Monoxide in Heavy Normal Paraffins at Temperatures from 311 to 423 K and Pressures to 10.2 MPa. *J. Chem. Eng. Data*, 40(1):237–240, 1995.

[136] J. Park, R. L. Robinson, and K. A. M. Gasem. Solubilities of Hydrogen in Heavy Normal Paraffins at Temperatures from 323.2 to 423.2 K and Pressures to 17.4 MPa. *J. Chem. Eng. Data*, 40(1):241–244, 1995.

[137] A. Vatani, M. Mehrpooya, and F. Gharagheizi. Prediction of Standard Enthalpy of Formation by a QSPR Model. *Int. J. Mol. Sci.*, 8(5):407–432, 2007.

[138] L. T. Biegler, I. E. Grossmann, and A. W. Westerberg. *Systematic Methods of Chemical Process Design*. Prentice Hall, Upper Saddle River, 1999.

[139] O. Nagel, R. Sinn, and H. Kurten. Mass Exchange Surface and Energy Dissipation Density from Selective Criteria for Gas-Fluid Reactors. 1. Mass Exchange Surface in Various Gas-Fluid Reactors as Function of Operation Parameters. *Chem. Ing. Tech.*, 44(6):367–373, 1972.

[140] O. Nagel, R. Sinn, and H. Kurten. Material Exchange Surfaces and Energy Dissipation Densities as Selection Criteria for Gas-Liquid Reactors. 2. Correlation of Material Exchange Surface as a Function of Energy Dissipation Density with Aid of a Model. *Chem. Ing. Tech.*, 44(14):899–902, 1972.

[141] F. Grosz-Röll, J. Battig, and F. Moser. Gas-Flüssig Stoffübergang an statischen Mischern. *Verfahrenstechnik*, 17(12):698–708, 1983.

[142] R. Thakur, C. Vial, K. Nigam, E. Nauman, and G. Djelveh. Static Mixers in the Process Industries–A Review. *Chem. Eng. Res. Des.*, 81(7):787–826, 2007.

[143] D. I. Enache, G. J. Hutchings, S. H. Taylor, R. Natividad, S. Raymahasay, J. M. Winterbottom, and E. H. Stitt. Experimental Evaluation of a Three-Phase Downflow Capillary Reactor. *Ind. Eng. Chem. Res.*, 44(16):6295–6303, 2005.

[144] P. Trambouze and J. P. Euzen. *Chemical Reactors: From Design to Operation*. Editions Technip, Paris, 2004.

[145] A. Heyouni, M. Roustan, and Z. Do-Quang. Hydrodynamics and Mass Transfer in Gas–Liquid Flow Through Static Mixers. *Chem. Eng. Sci.*, 57(16):3325–3333, 2002.

[146] W. Karst. Druckverlust in durchströmten Rohren. In *VDI Wärmeatlas*, pages Lab1–Lab4. Springer Verlag, Heidelberg, 2006.

[147] V. Gnielinski. Wärmeübertragung bei der Strömung durch Rohre. In *VDI Wärmeatlas*, pages Ga1–Ga9. Springer Verlag, Heidelberg, 2006.

[148] E. Tsotsas. Wärmeleitung und Disperion in durchströmten Schüttungen. In *VDI Wärmeatlas*, pages Mh1–Mh15. Springer Verlag, Heidelberg, 2006.

[149] E. Tsotsas. Wärmeleitfähigkeit von Schüttschichten. In *VDI Wärmeatlas*, pages Dee1–Dee9. Springer Verlag, Heidelberg, 2006.

[150] Inc. Aspen Technology. Aspen Plus v.2006.5 Binary Data Bank, 2006.

[151] A. N. Gubkov, N. A. Fermor, and N. I. Smirnov. Vapor Pressure of Mono-Poly Systems. *Zh. Prikl. Khim.*, 37:2204–2210, 1964.

[152] J. M. Pagano, D. E. Goldberg, and W. C. Fernelius. A Thermodynamic Study of Homopiperazine, Piperazine and N-(2aminoethyl)-Piperazine and their Complexes with Copper(II)-Ion. *J. Phys. Chem.-US.*, 65(6):1062–1064, 1961.

[153] T. Edwards, G. Maurer, J. Newman, and J. Prausnitz. Vapor-Liquid Equilibria in Multicomponent Aqueous Solution of Volatile Weak Electrolytes. *AIChE J.*, 24(6):966–976, 1978.

[154] M. L. Posey. *Thermodynamics Model For Acid Gas Loaded Aqueous Alkanolamine Solutions*. PhD thesis, The University of Texas at Austin, Austin, TX, USA, 1996.

[155] S. Bishnoi. *Carbon Dioxide Absorption and Solution Equilibrium in Piperazine Activated Methyldiethanolamine*. PhD thesis, The University of Texas at Austin, Austin, TX, USA, 2000.

[156] J. T. Cullinane and G. T. Rochelle. Carbon Dioxide Absorption with Aqueous Potassium Carbonate Promoted by Piperazine. *Chem. Eng. Sci.*, 59(17):3619–3630, 2004.

[157] G. F. Versteeg and W. P. M. Swaaij. Solubility and Diffusivity of Acid Gases (CO_2, N_2O) in Aqueous Alkanolamine Solutions. *J. Chem. Eng. Data*, 33(1):29–34, 1988.

[158] J. T. Cullinane. *Thermodynamics and Kinetics of Aqueous Piperazine with Potassium Carbonate for Carbon Dioxide Absorption*. PhD thesis, The University of Texas at Austin, Austin, TX, USA, 2005.

[159] D. P. Bertsekas. *Dynamic Programming and Optimal Control. Volumne One.* Athena Scientific Press, Belmont, 2000.

[160] L. T. Biegler. An Overview of Simultaneous Strategies for Dynamic Optimization. *Chem. Eng. Process.*, 46(11):1043–1053, 2007.

[161] A. Schäfer, P. Kühl, M. Diehl, J. Schlöder, and H. Bock. Fast Reduced Multiple Shooting Methods for Nonlinear Model Predictive Control. *Chem. Eng. Process.*, 46(11):1200–1214, 2007.

[162] J. S. Logsdon and L. T. Biegler. Accurate Solution of Differential Algebraic Optimization Problems. *Ind. Eng. Chem. Res.*, 28(11):1628–1639, 1989.

[163] J. E. Cuthrell and L. T. Biegler. Simultaneous-Optimization and Solution Methods for Batch Reactor Control Profiles. *Comput. Chem. Eng.*, 13(1–2):49–62, 1989.

[164] N. Novotny. Analysis and Optimization of a Sulfur Dioxide Reactor with Elementary Process Functions. Study research thesis, Otto-von-Guericke University, Magdeburg, Germany, 2010.

[165] A. Drud. A GRG Code for Large Sparse Dynamic Nonlinear Optimization Problems. *Math. Program.*, 31(2):153–191, 1985.

[166] A. Drud. A Large-Scale GRG Code. *INFORMS J. Comput.*, 6(2):207–216, 1992.

[167] O. L. Mangasarian. Sufficient Conditions for the Optimal Control of Nonlinear Systems. *SIAM J. Control*, 4(1):139–152, 1966.

[168] K. J. Arrow. Applications of Control Theory to Economic Growth. In *Mathematics of the Decision Sciences*. American Mathematical Society, Providence, 1968.

[169] M. Tawarmalani and N. V. Sahinidis. A Polyhedral Branch-And-Cut Approach to Global Optimization. *Math. Program.*, 103(2):225–249, 2005.

List of figures

List of tables